Investigations on neuropeptide Y and histamine receptors by fluorescence-based and radiochemical methods

Dissertation
zur Erlangung des Doktorgrades der Naturwissenschaften
(Dr. rer. nat.)
der Fakultät für Chemie und Pharmazie
der Universität Regensburg

vorgelegt von
Miroslaw Lopuch
aus Prömsel (Przemyśl – Перемишль)
2011

Die vorliegende Arbeit entstand in der Zeit von Mai 2007 bis September 2011 unter der Leitung von Herrn Prof. Dr. A. Buschauer und Herrn Prof. Dr. G. Bernhardt am Institut für Pharmazie der Naturwissenschaftlichen Fakultät IV – Chemie und Pharmazie – der Universität Regensburg.

Das Promotionsgesuch wurde eingereicht im September 2011.

Tag der mündlichen Prüfung: 06.10.2011

Prüfungsausschuß:	Prof. Dr. Dr. Wolfgang Wiegrebe	(Vorsitzender)
	Prof. Dr. Armin Buschauer	(Erstgutachter)
	Prof. Dr. Günther Bernhardt	(Zweitgutachter)
	Prof. Dr. Sigurd Elz	(Drittprüfer)

This work is dedicated to all researchers
who work to save and protect human life as a precious gift from God
– from its beginning at the moment of conception
to its end at the moment of natural death

„Es gibt keine wertfreie Wissenschaft,
denn die Wahrheit ist immer wertvoller als der Irrtum.“

Prof. Dr. Erich Blechschmidt (1904-1992)

Acknowledgements / Danksagung

An dieser Stelle möchte ich mich bedanken bei:

Herrn Prof. Dr. Armin Buschauer, meinem Doktorvater, für die interessante Aufgabenstellung, die Gelegenheit, in seinem Arbeitskreis zu arbeiten und an den Fortbildungsveranstaltungen teilzunehmen, für seine stete Unterstützung und väterliche Geduld sowie seine konstruktive Kritik bei der Durchsicht dieser Arbeit,

Herrn Prof. Dr. Günther Bernhardt, meinem Meister, für die Möglichkeit, eine wissenschaftliche Ehrlichkeit zu erlernen, für seine fachliche Beratung, sein lebendiges Interesse am Fortgang der Experimente sowie seine sorgfältige Rezension dieser Arbeit,

Herrn Prof. Dr. Roland Seifert (Medizinische Hochschule Hannover) und Herrn Prof. Dr. Jens Schlossmann und ihren Mitarbeitern für die Möglichkeit, Radioligandbindungsversuche am Lehrstuhl für Pharmakologie und Toxikologie der Universität Regensburg durchzuführen,

Herrn Prof. Dr. Sigurd Elz für seine fachliche Beratung und Bereitstellung verschiedener Histamin Rezeptorliganden,

Herrn Prof. Dr. Stefan Dove für sein Interesse und die wertvollen Anregungen,

Herrn Prof. Dr. Achim Göpferich und seinen Mitarbeitern für die Bereitstellung des konfokalen Mikroskops,

Frau Prof. Dr. Chiara Cabrele (Ruhruniversität Bochum) für die Synthese der peptidischen NPY-Rezeptoragonisten,

Frau Dr. Oksana Sereda für ihre herzliche Freundschaft, ihre Hilfe bei der Durchführung der radiochemischen Bindungsstudien sowie für ihre stete Unterstützung bei allen möglichen Problemen,

Frau Dr. Nathalie Pop für ihre Freundschaft und großherzige Hilfe, insbesondere für die geduldige Einführung in die Arbeit mit Zellkulturen und in die Benutzung des konfokalen Mikroskops, sowie für ihre kollegiale Zusammenarbeit,

Herrn Dr. Erich Schneider für seine Freundschaft, seine Hilfe beim theoretischen Einarbeiten in das Thema sowie beim Erlernen der radiochemischen Arbeitstechniken,

Herrn Dr. Max Keller für alle guten Anregungen, seine Unterstützung bei der Durchführung der radiochemischen Bindungsstudien sowie für seine Hilfe bei der chromatographischen Reinigung der peptidischen NPY-Rezeptoragonisten und für die Bereitstellung der nichtpeptidischen NPY-Rezeptorantagonisten,

Frau Dr. Daniela Erdmann für ihre Kollegialität, die Bereitstellung der Histamin H_2-Rezeptorliganden, die gute Zusammenarbeit sowie für eine schöne Zeit in Regensburg,

Frau Dr. Heidrun Appl für die freundliche Bereitstellung ihrer Bindungsdaten am humanen Histamin H_2-Rezeptor,

Herrn Dr. Johanes Mosandl und Herrn Dr. David Schnell für ihre Hilfsbereitschaft und guten Ratschläge bei der Durchführung der Radioligandbindungsexperimente,

Herrn Dr. Hans-Joachim Wittmann für die geduldige Erklärung und Hilfe bei der Berechnung der Bindungskinetik,

Herrn Dr. Dietmar Gross, Herrn Dr. Patrick Igel, Herrn Dr. Martin Memminger, Herrn Dr. Matthias Kühnle, Herrn Dr. Peter Höcherl, Herrn Dr. Damir Posavec, Herrn Dr. Shangjun Teng und Herrn Dr. Senthil-Kumar Palaniappan für ihre fachliche Unterstützung und Beratung, interessante Unterhaltungen und ihren Humor,

Herrn Tobias Birnkammer für die Bereitstellung der Histamin H_2-Rezeptorliganden und für die enge Zusammenarbeit bei der Erforschung des Wirkmechanismus der bivalenten Verbindungen,

Frau Irena Brunskole für das gute Einvernehmen, die freundschaftliche Zusammenarbeit sowie das angenehme Klima beim Zusammenschreiben der Doktorarbeit,

Herrn Uwe Nordemann und Herrn Johannes Felixberger für die fachliche Unterstützung und ihre Hilfsbereitschaft sowie die hervorragende Arbeitsatmosphäre in unserem Büro,

Frau Dorina Kaufel (Institut für Pharmazie, Universität Bonn) für die freundliche Bereitstellung der Durchführungsanweisungen zur Bestimmung der Dissoziationskinetik,

Frau Melanie Kaske, Herrn Roland Geyer und Herrn Paul Baumeister für ihre gute Laune sowie die Geduld und Freundlichkeit beim gemeinsamen Benutzen der Laminar-Airflow Werkbank und des Harvesters,

Frau Elvira Schreiber für die fachliche Unterstützung bei der Durchführung der durchflusszytometrischen Bindungsexperimente und der ratiometrischen Calcium-Assays sowie bei der Betreuung der Zellkulturen,

Frau Maria Beer-Krön und Frau Sabine Dirrigl für die Hilfe bei der Durchführung der GTPase-Assays und der radiochemischen Bindungsexperimente,

Frau Gertraud Wilberg für ihre Hilfsbereitschaft und die Vorbereitung der Sf9-Zellen,

Herrn Dr. Max Keller, Frau Irena Brunskole, Herrn Johannes Felixberger, Herrn Stefan Huber und Frau Brigitte Wenzl sowie Frau Dr. Nathalie Pop, Frau Janina Hamberger, Frau Kira Bürger, Frau Stefanie Bauer, Herrn Dr. Peter Höcherl, Herrn Uwe Nordemann und Herrn Martin Rothenhöfer für ihre kräftige Unterstützung bei der Betreuung des Biochemie Praktikums,

Frau Martina Welcher, Frau Silvia Heinrich, Frau Uta Hasselmann und Frau Karin Reindl für ihre Unterstützung bei allen organisatorischen Fragen,

Herrn Peter Richthammer für seine stete Hilfsbereitschaft bei technischen Problemen und die guten Unterhaltungen,

allen Kolleginnen und Kollegen für ihre stete Hilfsbereitschaft und das gute Klima in unserer Arbeitsgruppe,

dem Graduiertenkolleg 760 der Deutschen Forschungsgemeinschaft sowie dem Freistaat Bayern für die wissenschaftliche Förderung und finanzielle Unterstützung.

Außerdem möchte ich herzlich danken:

meinen Lehrern aus Schule und Wissenschaft, die mir geholfen haben meinen Weg zu finden, mir Ziele vor Augen gestellt und durch ihren wissenschaftlichen Rat und ihren Zuspruch geholfen haben, diese Ziele zu erreichen,

meinem Pfarrer Oleksandr Smetanin für die großherzige geistliche Führung,

meinen Eltern Stefania und Zenon, meiner Schwester Maria, meinem Bruder Petro und seiner Frau Olga, meiner Großmutter Helena Lopuch sowie allen anderen Familienmitglieder und Freunden für ihre Liebe und jede nur mögliche Unterstützung

und meinen verstorbenen Großeltern Anna Borys, Iwan Borys und Iwan Lopuch für das unschätzbare Geschenk des Lebens und des Glaubens.

Contents

List of the used abbreviations

7TMR	seven-transmembrane domain receptor (known also as GPCR)
Ar	argon ion laser
ARP	arpromidine
β_2AR	β_2-adrenergic receptor
B_{max}	maximum number of binding sites
BP	band pass filter
bp	base pairs (length of a DNA fragment in base pairs)
Bq	becquerel (SI-derived unit of radioactivity, equivalent to s^{-1})
BRET	bioluminescence resonance energy transfer
BSA	bovine serum albumin
cAMP	cyclic 3',5'-adenosine-monophosphate
CHO	Chinese hamster ovary (cells)
Ci	curie (unit of radioactivity, defined as $3.7 \cdot 10^{10}$ Bq)
CI	confidence interval
CIM	cimetidine
CLSM	confocal laser scanning microscopy
Con A	concanavalin A
DIM	dimaprit
DMEM	Dulbecco's modified eagle medium
DMSO	dimethylsulfoxide
EC_{50}	agonist concentration inducing 50% of the maximum response
ECFP	enhanced cyan fluorescent protein
EDTA	ethylenediaminetetraacetic acid
EMEM	Eagle's minimum essential medium
EYFP	enhanced yellow fluorescent protein
FACS	fluorescence-activated cell sorting
FAM	famotidine
FCS (FBS)	fetal calf serum (fetal bovine serum)
Fl-1, Fl-2, Fl-3, Fl-4	fluorescence channels (flow cytometer)
FLAG	octapeptide protein tag (enabling e.g. recognition by an antibody)
FlAsH	fluorescein arsenical hairpin binder
FRET	fluorescence resonance energy transfer
GAIP	RGS19
GDP	guanosine diphosphate
GFP	green fluorescent protein
gp	guinea-pig (in context with receptor subtypes, e.g. gpH_2R)
GPCR	G-protein-coupled receptor (known also as 7TMR)
Gpp(NH)p	guanosine 5'-[γ-imido]triphosphate
$G_{s\alpha S}$	short splice variant of the $G_{s\alpha}$ protein
GTP	guanosine triphosphate
GTPγS	guanosine 5'-[γ-thio]triphosphate
h	human (in context with receptor subtypes, e.g. hH_2R)
H_2R, H_3R, H_4R	histamine receptor subtypes
HeNe	helium neon ion laser
HEPES	2-[4-(2-hydroxyethyl)piperazin-1-yl]ethanesulfonic acid
HFT	main dichroic beam splitter (Hauptfarbteiler)
HIS	histamine
His_6	hexahistidine tag for labelling and purification of proteins
IAPT	iodoaminopotentidine (used as the H_2R radioligand [^{125}I]APT)

IC_{50}	inhibitor concentration causing 50% inhibition
IMP	impromidine
k_1	(radio)ligand association rate constant (on-rate constant, k_{on})
k_2	(radio)ligand dissociation rate constant (off-rate constant, k_{off})
k_3	ligand association rate constant
k_4	ligand dissociation rate constant
K_b	affinity constant of an antagonist derived from functional assays
K_d	dissociation constant of a labelled ligand from saturation assays
K_i	dissociation constant of an inhibitor from competition assays
k_{obs}	observed (macroscopic) association rate constant
L-15	Leibovitz's medium (without phenol red)
LP	longpass barrier (filter)
M	molar (mol/L)
n.d.	not determined
NFT	secondary dichroic beam splitter (Nebenfarbteiler)
n_H	Hill slope (coefficient)
NMS	N-methylscopolamine
NPY	neuropeptide Y
NPY Y_xR	neuropeptide Y receptor subtypes
p	porcine (in context with ligand, e.g. pNPY)
PBS	phosphate buffered saline
PCR	polymerase chain reaction
PEI	polyethylenimine
PMSF	phenylmethylsulfonyl fluoride
r	rat (in context with receptor subtypes, e.g. rH_2R)
RAN	ranitidine
RGS	regulator of G-protein signalling
ROI	region of interest (of a confocal image)
rpm	rotations (revolutions) per minute
SEM	standard error of the mean
Sf9 cells	insect *Sporodoptera frugiperda* cells
$t_{0.5}$	half-life time of radioligand dissociation
THIO	thioperamide
TIO	tiotidine
Tris	tris(hydroxymethyl)aminoethane

Chapter 1

Introduction

1 Introduction

1.1 G-protein-coupled receptors: structure and function

The G-protein-coupled receptors (GPCR), also called seven-transmembrane domain receptors (7TMR), are shapeshifting signalling proteins involved in responses to hormones and neurotransmitters, such as neuropeptide Y and histamine. 7TMRs are encoded by approx. 800 sequences (including olphactory GPCRs; Bjarnadóttir *et al.*, 2006), which account for only 3% of the human genome (26,383 genes in total; Venter *et al.*, 2001). Nevertheless, GPCRs comprise a significant part of the druggable human genome, representing 30% of the marketed small-molecule drug targets (Hopkins and Groom, 2002). A well known and widely accepted pharmacological paradigm for this class of receptors states that an elementary unit, required for signal transduction, involves a sole receptor molecule, interacting *via* its unique binding site with a single pharmacophoric moiety (Lazareno, 2001). However, this classical model will probably require revision, as a series of experimental data indicate that oligo- or dimerization of the receptors is a quite abundant phenomenon (Ferré *et al.*, 2009). Also the examination of other lively discussed postulates for GPCR pharmacology, including allosterism and functional selectivity, might be advantageous for both, research and clinics.

1.1.1 3D Structures

Class A GPCRs (also referred to as rhodopsin-like family) includes *inter alia* neuropeptide Y Y_1 (NPY Y_1R) as well as histamine H_2 and H_4 receptors (H_2R and H_4R) as representative peptidergic and aminergic GPCRs, respectively. Apart from the typical seven transmembrane domains surrounding a pocket with the recognition site for the endogenous ligand (Fig. 1.1.1), this class of receptors reveals other common features, such as a disulfide bridge between the second (ECL2) and the third extracellular loop (ECL3), a series of highly conserved amino acids (e.g. the DRY motif in the second intracellular loop, ICL2) or a palmitoylated cysteine at the C-terminus (Gether, 2000). The first known 3D models for class A GPCRs were established by means of high-resolution electron crystallography for bacterial and bovine rhodopsins (Kimura *et al.*, 1997; Palczewski *et al.*, 2000). However, the current information on the spatial arrangement of the domains and the shape of the binding pocket is mainly based on the crystal structures of the human β_2-adrenergic receptor (β_2AR,) recently described by Kobilka and colleagues (Rasmussen *et al.*, 2007; Rosenbaum *et al.*, 2007). Using these templates, homology models of the H_2R and H_4R have been derived in our re-

search group (Kraus *et al.*, 2009; Seifert *et al.*, 2011). Whereas the experiments with rhodopsin, an archetypal GPCR, demonstrated the formation of receptor dimers (Fotiadis *et al.*, 2006), the aforementioned studies on the β_2AR revealed rather monomeric state of the receptors. The last finding contradicted the results from earlier studies using BRET and immunoprecipitation (Kroeger *et al.*, 2004). Additionally, both the transmembrane core of the GPCR (containing the orthosteric ligand-binding site) and the cytoplasmic domains (involved in G-protein coupling) were found to be highly conserved. By contrast, the structural diversity of the extracellular domains of GPCRs offers an opportunity for the discovery of subtype-selective drugs. Moreover, the conformational coupling between the extracellular domains and the orthosteric recognition site, shown by means of NMR spectroscopy, suggests that ligands binding to the extracellular domains might function as allosteric modulators (Bokoch *et al.*, 2010).

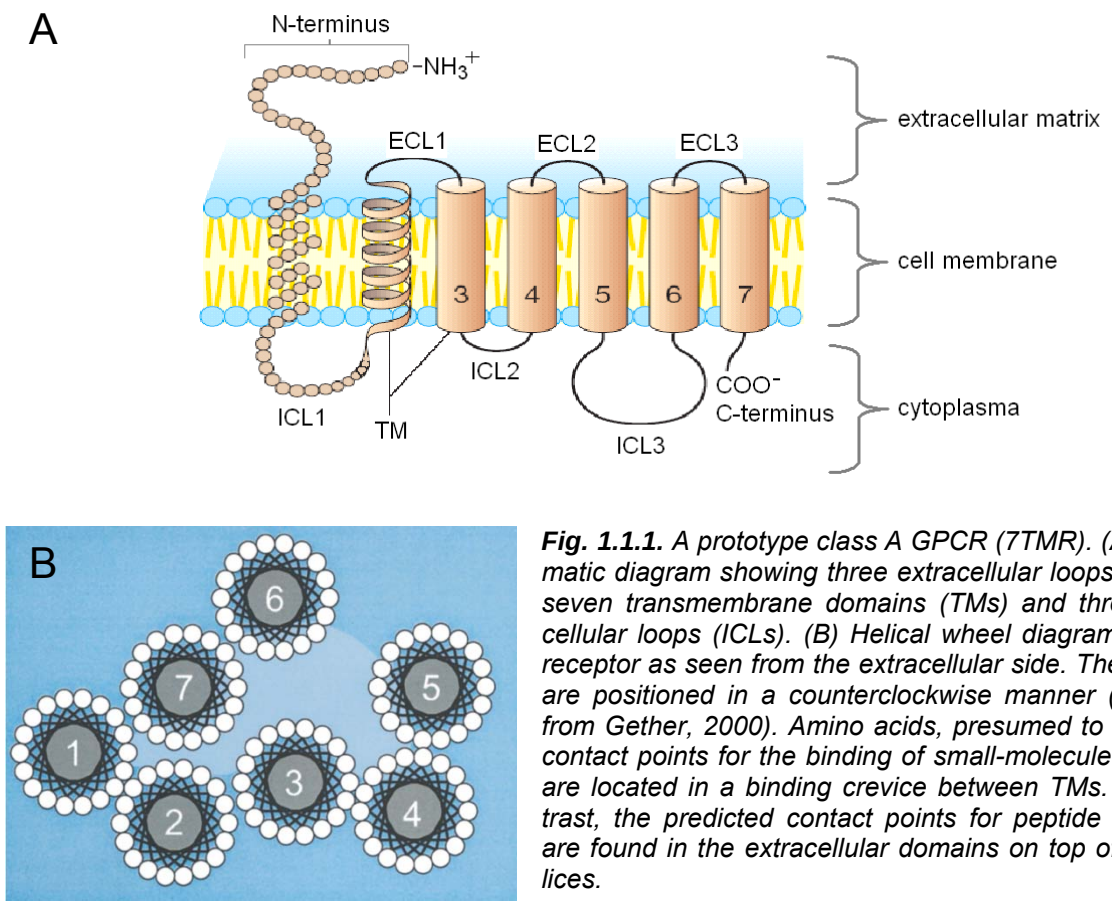

Fig. 1.1.1. *A prototype class A GPCR (7TMR). (A) Schematic diagram showing three extracellular loops (ECLs), seven transmembrane domains (TMs) and three intracellular loops (ICLs). (B) Helical wheel diagrams of the receptor as seen from the extracellular side. The helices are positioned in a counterclockwise manner (adopted from Gether, 2000). Amino acids, presumed to form the contact points for the binding of small-molecule ligands, are located in a binding crevice between TMs. By contrast, the predicted contact points for peptide agonists are found in the extracellular domains on top of the helices.*

1.1.2 Models of ligand-receptor interaction for GPCRs

1.1.2.1 GPCR dimers and bivalent ligands

The phenomenon of dimerization among numerous types of GPCRs has been investigated during the last three decades, significantly contributing to the understanding of intermolecular interactions in cellular signal transduction pathways. For the investigation of GPCR dimers different approaches have been used, such as functional complementation, resonance energy transfer techniques and immunoprecipitation (Gomes *et al.*, 2001; Kroeger *et al.*, 2004; Milligan and Bouvier, 2005). The dimerizing receptor protomers might be of the same or different type (Table 1.1.1, cf. Ferré *et al.*, 2009). For example, the functional H_2R homooligomers have been found in the transfected insect Sf9 (*Sporodoptera frugiperda* cell/baculovirus expression system) and mammalian COS-7 cells (Fukushima, 1997).

Table 1.1.1. *Proposed nomenclature for the oligomeric interactions of GPCRs (cf. Ferré et al., 2009).*

Classification	Definition	Examples
Hetero(di)meric receptor	the minimal functional unit is composed of two or more ***different*** subunits that are ***not functional*** on their own	$GABA_B$ receptor: subunits $GABA_{B1}$ and $GABA_{B2}$ (Marshall *et al.*, 1999)
Homo(di)meric receptor	the minimal functional unit is composed of two or more ***identical*** subunits that are ***not functional*** on their own	-
Receptor homo(di)mer	composed of two or more ***identical functional*** receptor units with biochemical properties that are different from those of its individual components	H_2 recetor (Fukushima, 1997) NPY Y_1 recetor (Dinger *et al.*, 2003)
Receptor hetero(di)mer	composed of two or more ***different functional*** receptor units with biochemical properties that are different from those of its individual components	μ and δ opioid receptors (Daniels *et al.*, 2005)

In addition to that, *bivalent ligands*, composed of two pharmacophoric moieties joined with a linker, have been reported for some GPCRs (5-HT_{1B} receptors: Perez *et al.*, 1998; opioid δ and κ receptors: Bhushan *et al.*, 2004; gonadotropin releasing hormone receptor: Bonger *et al.*, 2008; serotonin 5-HT_4 receptor: Lezoualc'h *et al.*, 2009; other receptors reviewed in: Shonberg *et al.*, 2011). Provided that twin compounds, are capable of addressing two binding sites simultaneously, such bivalent ligands may be valuable tools to investigate whether GPCR dimers are involved in the activation or inhibition of receptor-mediated signal trans-

duction. However, it is still unclear, if binding of bivalent ligands involves bridging of receptor dimers or rather orthosteric/allosteric interaction with a single receptor protein or if these compounds simply bind with high affinity only to a single (orthosteric) receptor binding site (Fig. 1.1.2).

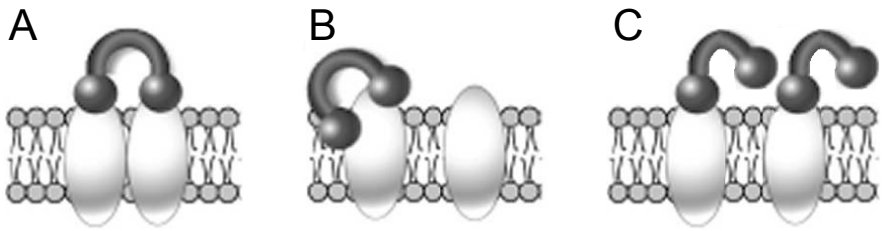

Fig. 1.1.2. *Possible binding modes of bivalent ligands: (A) bridging of a GPCR dimer, (B) dualsteric (simultaneous binding to ortho- and allosteric binding sites at the same GPCR), (C) univalent (adopted from Bonger et al., 2007 with modifications).*

It is worth mentioning that in the case of GPCRs “twin compounds”, supporting the existence of receptor dimers, have only been reported by the group of Portoghese for opioid receptors (μ and δ receptors in mice, Daniels *et al.*, 2005). In order to address both binding pockets of a receptor dimer, the distance between the two pharmacophore moieties in a bivalent compound should be equal to 20–21 carbon atoms (Bhushan *et al.*, 2004). Additionally, the assumed binding mode of a radioactively labelled bivalent ligand should also result in a halved maximal binding (B_{max}) in saturation binding experiments, compared to its monovalent counterpart. Moreover, the binding of one pharmacophore to the first receptor could strengthen the interaction of the other pharmacophore with the second receptor molecule (*positive cooperativity*). In the latter case, the affinity of bivalent compounds should increase and the slope (*Hill coefficient*) of saturation and displacement curves should be greater than unity (chapter 4; cf. Repke and Liebmann, 1987).

1.1.2.2 Allosteric interactions

Bivalent ligands, possessing two pharmacophores, may also bind to two distinct non-interconverting sites on the same receptor molecule, resulting in *dualsteric* (bitopic, orthosteric/allosteric) ligands, as shown for the M_2 muscarinic acetylcholine receptors (Valant *et al.*, 2008). The cooperative interaction between orthosteric (usually occupied by the natural ligand) and allosteric binding sites is reciprocal (conformational linkage). The modulatory effect of allosteric agents on affinity or/and intrinsic activity of natural orthosteric ligands can be positive, neutral or negative. Occupation of an allosteric site does not exclude simultaneous interaction of the orthoster with its receptors. Allosterically acting compounds should not block receptors, as do competitive antagonists, and therefore, might lead to new therapeutic

applications of the former. Moreover, allosteric binding site, being less structurally conserved as the orthosteric one, could be an excellent target for drug design due to its improved selectivity profile (May *et al.*, 2007).

The bitopic binding mode of bivalent compounds can lead to the flattening of saturation and displacement curves. When the Hill coefficient is smaller than unity, *negative cooperativity* may be assumed (the binding to one binding site weakens the interaction with the second binding site). However, this fact may have other reasons than cooperative interaction, e.g. a heterogenic population of the ligand binding sites (Repke and Liebmann, 1987). Allosteric properties of test compounds can be verified using radioligand binding methodology concerning kinetic studies. Simultaneous occupation of ortho- and allosteric binding sites should lead to the formation of a ternary orthoster-receptor-alloster complex with altered dissociation and/or association of an orthosteric radioligand (chapter 5; cf. Kostenis and Mohr, 1996).

1.1.2.3 Ternary complex model

The Hill slopes of ligand binding curves approximating unity are consistent with a competitive ligand-receptor interaction and reflect the presence of homogenic population of ligand binding sites (Repke and Liebmann, 1987). As mentioned above, flattened displacement curves, which are sometimes detected for agonists, may suggest the existence of two binding sites with different affinities for a tested agonist, when using an antagonist radioligand (Fig. 1.1.3). To explain this phenomenon, a ternary complex model has been proposed. According to this model, agonists are believed to bind with a higher affinity to receptors coupled to nucleotide-free G proteins than to unbound receptors, resulting in ternary agonist-receptor-G-protein complexes.

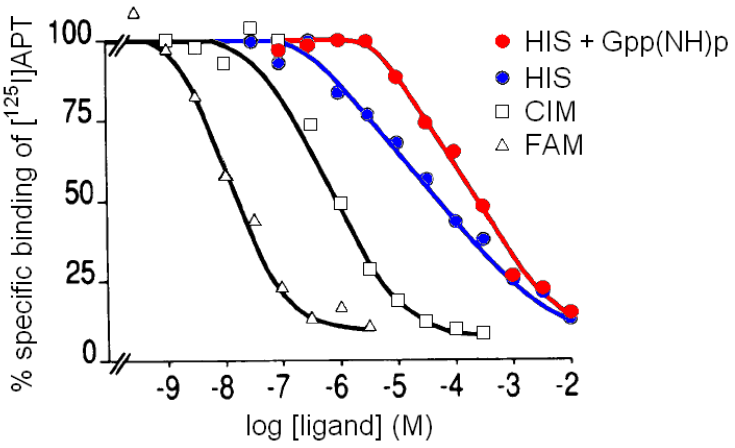

Fig. 1.1.3. *Effect of standard H_2R ligands: histamine (HIS), cimetidine (CIM) and famotidine (FAM) on the binding of 0.3 nM [^{125}I]iodoaminopotentidine ([^{125}I]APT) to membranes prepared from CHO-rH_2 cells. The flat competition curve of histamine (n_H of 0.43) was right-shifted and steepened (n_H of 0.80) in presence of 100 µM Gpp(NH)p (adopted from Traiffort et al., 1992 with modifications).*

Guanine nucleotides (Fig. 1.1.4) such as GTP, being substrates for G proteins, are known to disrupt these complexes (Maguire *et al.*, 1976). Disappearance of a high-affinity binding site and a concomitant decrease in agonist affinity can be observed as a *rightward shift and steepening* of the binding curve after addition of exogenous GTP (Lazareno, 2001). The same effect can be observed in intact cells, where the high intracellular concentration of GTP leads to dissociation of the ternary complex, allowing agonists to bind only to the low-affinity binding site, as it can be deduced from steep binding curves (Kenakin, 2006). Contrary to that, antagonists, which do not change the affinity of receptors to G proteins, are insensitive towards guanine nucleotides. For example, a lacking GTP shift was previously demonstrated for *N*-methylscopolamine, an antagonist of muscarinic receptors in membranes of the rabbit myocardium (Ehlert *et al.*, 1985).

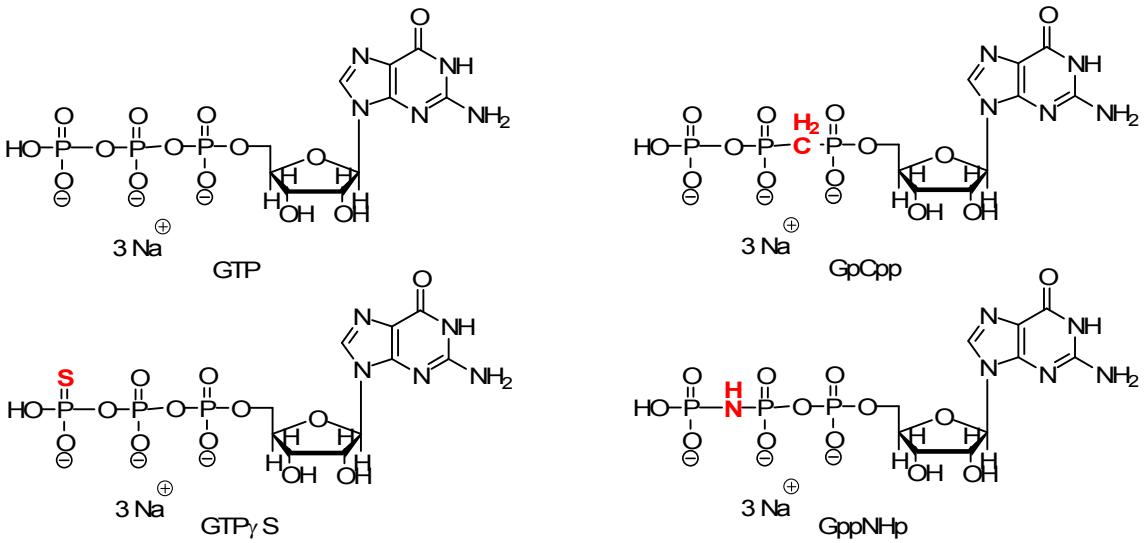

Fig. 1.1.4. *Guanine nucleotides: GTP and its non-hydrolyzable analogues.*

If the number of G proteins significantly exceeds the amount of receptors, agonists would bind mostly to the high-affinity binding site, resulting in left-shifted binding curves with slopes of 1 (Fig. 1.1.5). However, if binding to receptors takes place in the absence of G protein, rightward-shifted and steep curves would be expected, like in the presence of GTP. Finally, by similar *receptor-to-G-protein stoichiometry*, formation of the ternary complexes can lead to a depletion of free G proteins (Kenakin, 2006). In thist case, two binding sites occur and a flat binding curve will be detected.

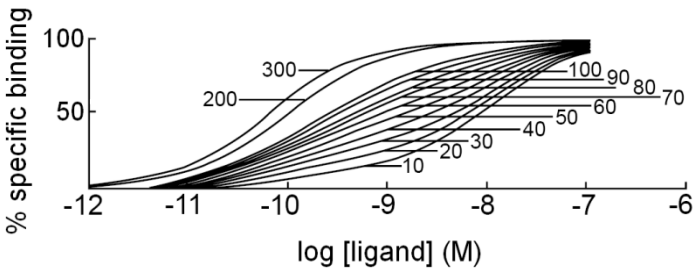

Fig. 1.1.5. *Impact of the G-protein-to-receptor (G/R) stoichiometry on the binding of a radioligand agonist. The binding curves were simulated for the indicated G/R ratios expressed as % (adopted from Kenakin, 1997 with modifications).*

The ratio of high- and low-affinity values in the absence of guanine nucleotides may be used for the prediction of agonist efficacy. Moreover, the estimation of agonist efficacy should also be possible from the GTP shift, defined as the ratio of the IC_{50} values in the presence and absence of GTP (Lazareno, 2001). Provided that an agonist binds to a receptor according to the ternary complex model, the shape of its binding curve reflects both, the proportion of the high-affinity binding site, and the ratio of affinity constants of the two binding sites. However, it seems , easier to identify and interpret such results from a single IC_{50} value and a slope, when the logistic rather than biphasic curve is used to fit the binding data (cf. section 4.3.2; Lazareno, 2001).

1.1.2.4 Extended ternary complex model

Basal activity in the absence of agonists has been already reported for a number of receptor types, for example on Sf9 membranes expressing $hH_2R\text{-}G_{s\alpha S}$ and $gpH_2R\text{-}G_{s\alpha S}$ fusion proteins (Preuss *et al.*, 2007). *Constitutive activity* could be reduced by ligands, known so far as antagonists in other test systems. Such unusual findings can be explained only, when it is assumed that a significant proportion of receptors is precoupled to G proteins (already in the absence of agonists). Then, such ligands, called *inverse agonists*, bind much stronger to free receptors than to receptor-G-protein complexes, reducing the affinity of receptors to the G proteins (Fig. 1.1.6). These assumptions are part of the extended ternary complex model.

According to this model, receptors can isomerize between ground and active states (Lazareno, 2001). Only receptors in the active state are able to form effective ternary complexes. Agonists, possessing higher affinity towards the active conformation of a receptor, induce isomerization of receptors to the active form. This, in turn, increases the affinity of receptors to G proteins and triggers a response of a typical biological system. However, in case of systems with constitutive activity, the equilibrium is already shifted to the active form of receptor. Therefore, inverse agonists, which have higher affinity to the ground state of the receptor, diminish the prevalence of the active form and reduce basal activity. Both, the simple and the extended ternary complex model, are equivalent in terms of equilibrium binding. The simple

model is usually sufficient to fit ligand binding data. However, its extended version allows the interpretation of results from systems with genetically modified receptors (Lazareno, 2001).

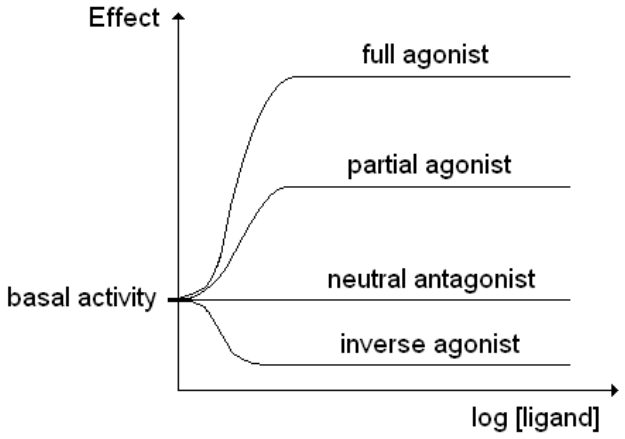

Fig. 1.1.6. *Concentration-response curves of different ligands in a system with constitutive activity as predicted by the extended ternary complex model.*

1.1.3 Signal transduction pathways of GPCRs

1.1.3.1 Mechanisms of receptor activation, endocytosis and resensitization

According to the ternary complex model, binding of an agonist to its GPCR leads to the activation of a trimeric G protein (composed of α, β and γ subunits). As a result, GDP (bound to the G_α subunit) is exchanged for GTP. The G_α subunit dissociates subsequently from the βγ heterodimer, activating or inhibiting appropriate effector proteins. An intracellular signal is mediated by *second messengers* until the G_α-bound GTP is hydrolyzed to GDP. For example, coupling of the receptor to the G_s protein raises the enzymatic activity of adenyl cyclase (AC), which leads to an increase in the intracellular concentration of cAMP. The cAMP-dependent signalling pathway was described previously for the β_2AR and H_2R. The biological effect can be measured at a point more or less distal from the activated receptor, enabling the pharmacological characterization of an agonist (Schneider and Seifert, 2010).

However, the initial stimulus also releases regulatory mechanisms, which silence the signal in order to keep a delicate cellular balance. Otherwise, the cell would be exposed to a permanent triggering and its homeostasis would be at risk. Therefore, an intracellular receptor domain is phosphorylated by GRK (G-protein-coupled receptor kinase). The phosphorylation of the GPCR increases the affinity of cytosolic β-arrestins to the receptor (*β-arrestin recruitment*) and leads to uncoupling of the G-protein α subunit. This, in turn, results in a reduced response to the next agonist exposure. The *desensitization* is accompanied by the interaction of β-arrestin with β2-adaptin (subunit of the AP-2 heterotetrameric adaptor complex) and

the subsequent *internalization* of the receptor into clathrin-coated pits (Fig. 1.1.7; cf. Ferguson, 2001).

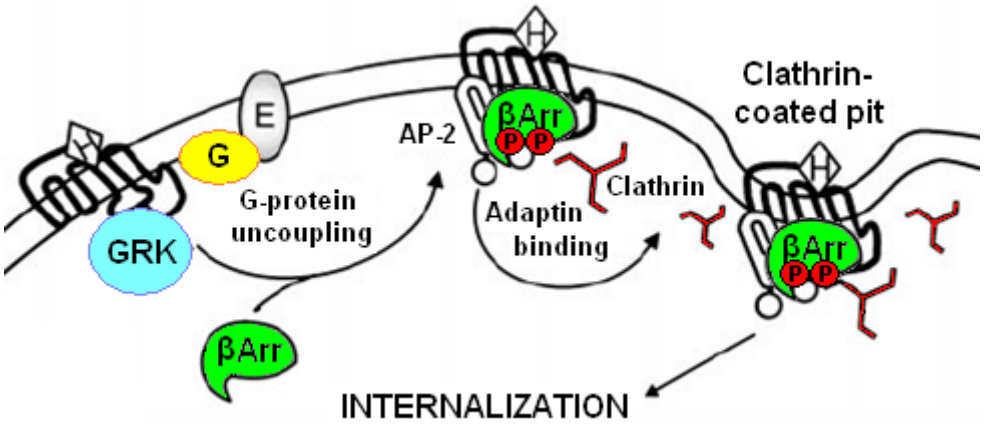

Fig. 1.1.7. *Desensitization and internalization of the phosphorylated (P) receptors upon agonist (hormone, H) stimulation involve interactions with numerous proteins: GRKs (GPCR kinases), β-arrestins (βArr), adaptins (subunits of the AP-2 heterotetrameric adaptor complex) and clathrins (adopted from Ferguson, 2001 with modifications).*

Subsequently, the internalized agonist-receptor complexes dissociate due to the low pH in endosomes, which, in turn, leads to the release of β-arrestins. Then, in the absence of β-arrestins, receptors can be dephosphorylated and rapidly recycled to the cell membrane (*resensitization*). However, after long exposure to an agonist, receptors may undergo the lysosomal degradation pathway also referred to as *down-regulation* (Gurevich and Gurevich, 2006).

1.1.3.2 β-Arrestin-mediated signalling (inclusive biased agonism)

In the classical model of GPCR activation, signalling is exclusively mediated by G proteins. Contrary to that, the current model predicts signal transduction by both G proteins and β-arrestins. This means that β-arrestins are recognized not only as the regulators of receptor desensitization and internalization, but (together with G proteins) also as true adaptor proteins of the heptahelical receptors. β-arrestin-mediated signalling involves multiple mediators: G-protein-coupled receptor kinase (GRK), mitogen-activated protein kinase (MAPK), phosphoinositide 3-kinase (PI3K), etc. The regulation of the kinases may be accompanied by the transactivation of the epidermal growth factor receptor (EGFR), by the control of chemotaxis and apoptotic/anti-apoptotic signaling, as well as by the regulation of mRNA translation and protein synthesis (DeWire *et al.*, 2008; Luttrell and Gesty-Palmer, 2010; Rajagopal *et al.*, 2010).

In a balanced system, after binding of an agonist, the signal is transduced equally by G proteins and β-arrestins (Fig. 1.1.8). However, in systems with *biased agonism (functional selectivity)* the signalling proceeds through one pathway only (β-arrestin- or G-protein-biased systems). Furthermore, bias may also result from the properties of the used ligands (Violin and Lefkowitz, 2007), as in case of the recently discovered first H_4R biased ligand (JNJ7777120, an antagonist with respect to G-protein activation, induced β-arrestin recruitment independently of G proteins; Rosethorne and Charlton, 2011; Seifert *et al.*, 2011). Such biased signalling presumes the existence of different *ligand-induced conformations* of GPCRs. Namely, in the presence of biased ligands, distinct prevailing receptor conformations are assumed to be stabilized, triggering the coupling of receptors to different protein effectors (Kenakin and Miller, 2010).

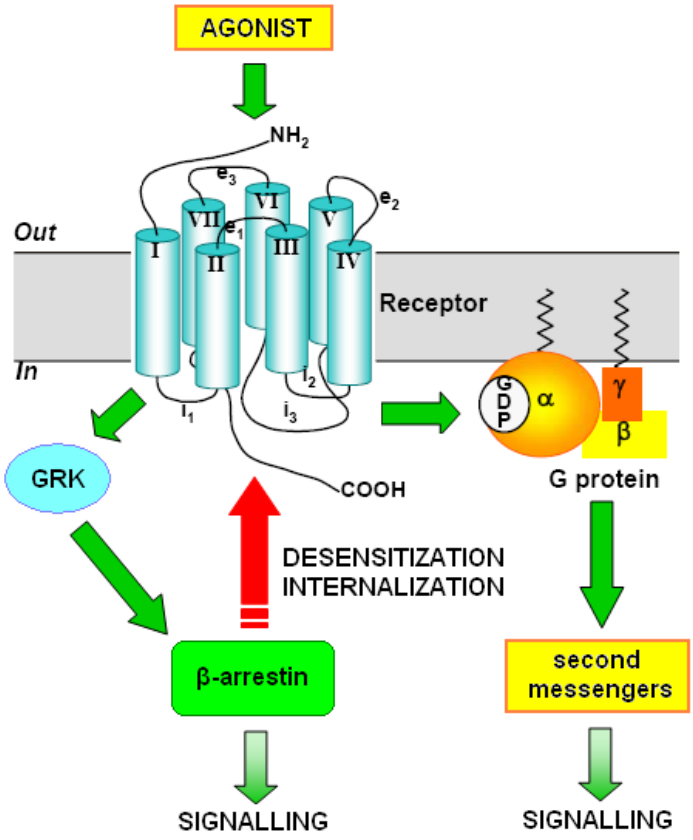

Fig. 1.1.8. *Current model of receptor activation. Signaling is mediated by both G proteins and β-arrestins. Additionally, the latter regulate desensitization and internalization of heptahelical receptors.*

It is widely accepted that conformational changes in proteins are crucial for the signal transduction. They may result either from non-covalent interactions (ligand binding, association of receptors, G-protein coupling) or from covalent modifications (phosphorylation by kinases). Given that each agonist induces/stabilizes a unique receptor conformation, the binding of a

small-molecule ligand at the specific recognition site may affect the shape of other receptor domains due to conformational linkage (allosteric regulation). For example, lateral translocations of helices along the plane of the membrane might result in modified interactions with other membranal proteins (receptor dimerization; chapter 4). Changes induced in the extracellular domains and at the orthosteric binding site can alter the binding affinity towards other ligands (allosterism; cf. chapter 5). Finally, movements of the intracellular loops may imply variable coupling to adaptor proteins like G proteins and β-arrestins. This "vectorial nature" of the allosteric interactions of 7TMRs is depicted in Fig. 1.1.9 (cf. Kenakin and Miller, 2010).

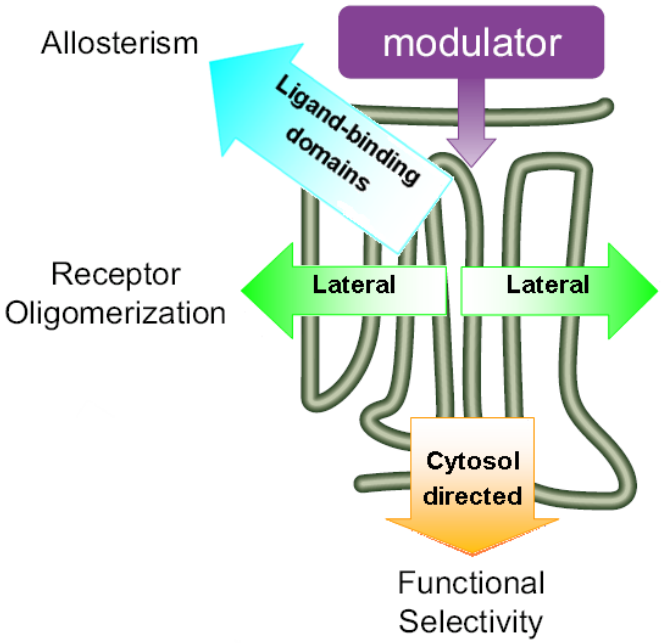

Fig. 1.1.9. *Allosteric interactions of 7TMRs have "vectorial" nature. The existence of ligand-specific receptor conformations may help to explain such complex phenomena as allosterism, receptor dimerization and functional selectivity (adopted from Kenakin and Miller, 2010 with modifications).*

1.2 Neuropeptide Y and histamine receptors: signalling and pharmacology

1.2.1 Neuropeptide Y receptors

Neuropeptide Y is a peptide neurotransmitter involved in numerous behavioral and physiological processes such as the regulation of food intake, energy balance, emotional behavior or stress response. Together with peptide YY (PYY) and pancreatic polypeptide (PP), they comprise the family of pancreatic polypeptides. In humans, the effects of these peptides are mediated *via* four receptor subtypes designated Y_1, Y_2, Y_4 and Y_5, which belong to the rhodopsin-like (class A) GPCRs. All these receptors possess similar signalling patterns. Upon agonist challenge, they couple to the pertussis toxin-sensitive $G_{i/o}$ proteins, reduce subsequently the intracellular level of cAMP and increase the intracellular Ca^{2+} concentration (Michel *et al.*, 1998; Merten and Beck-Sickinger, 2006; MacNeil, 2007).

1.2.1.1 Dimerization of NPY receptors

FRET-based studies performed previously by Beck-Sickinger and coworkers suggested that NPY receptors can oligomerize. The human Y_1R, hY_2R and hY_5R, C-terminally tagged with fluorescent proteins (GFP, DsRed, ECFP and EYFP), were found to bind the natural ligand and to remain functional, as shown by the saturation and competition experiments with [^{3}H]propionyl-NPY and by the inhibition of adenylyl cyclase (Dinger *et al.*, 2003). Additionally, the results of the BRET-based studies on the rhesus Y_4R supported the agonist-induced dissociation of homodimers (Berglund *et al.*, 2003).

In contrast to these earlier findings, the application of the bivalent ligand approach to Y_1R antagonists, pioneered at our department, did not support the hypothesis of receptor dimerization (Keller *et al.*, 2009).

1.2.1.2 Pharmacological tools for the NPY Y_1 receptor

Stimulation of NPY Y_1 receptors by the natural agonist changes the intracellular concentrations of second messengers, which can be measured either in the cAMP assays or in the ratiometric calcium assays with fura-2 (cf. subsection 3.2.6). Additionally, agonist-

stimulated internalization may be visualized by confocal microscopy, as shown previously for the NPY Y_1 receptor tagged with the green fluorescent protein (Gicquiaux *et al.*, 2002). In order to obtain pharmacological tools for flow cytometry and confocal microscopy, the ε-amino group of Lys^4 of pNPY has been coupled to different dyes, resulting in far-red fluorescent Y_1R agonists with significantly reduced autofluorescence (Fig. 1.2.1; Schneider, 2005; Schneider *et al.*, 2006).

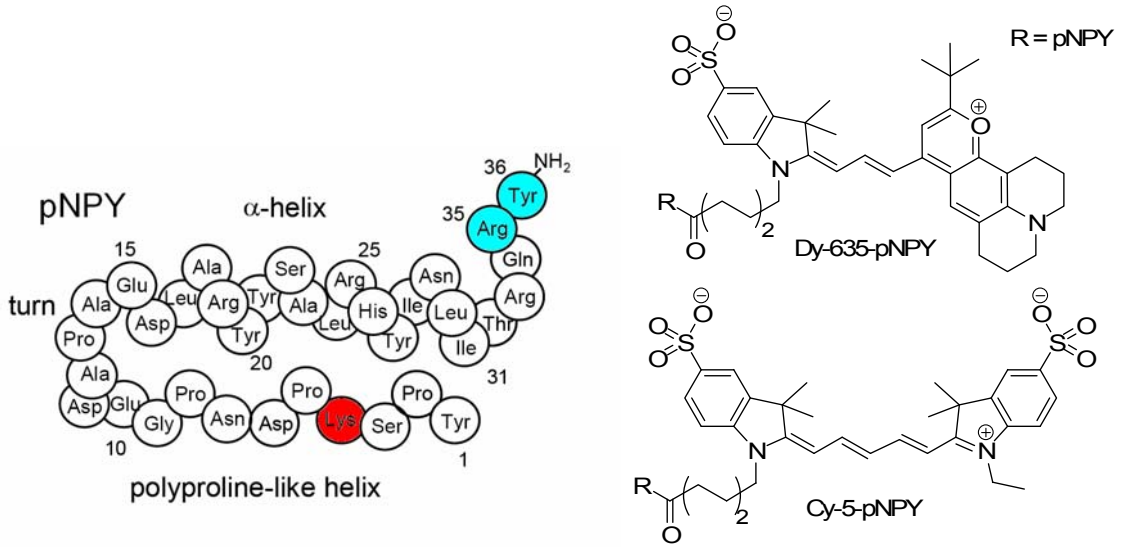

Fig. 1.2.1. *Structures of selected Y_1R agonists: porcine NPY and its far-red fluorescent derivatives. Dy-635-pNPY and Cy-5-pNPY were obtained by coupling of the ε-amino ogroup of Lys^4 of pNPY (shown in red) to the appropriate fluorescent dye by an amide bond (Schneider et al., 2006).*

However, the peptidic agonists have some drawbacks, as they may undergo both, proteolytic cleavage and adsorption (Ziemek, 2006). Moreover, long periods of incubation may implicate receptor internalization, making it difficult to interpret the binding data. Therefore, in order to avoid these limitations, small-molecule ligands have been developed for the Y_1R. The first non-peptidic Y_1R antagonist described in the literature was the arpromidine-type H_2R agonist BU-E-76, also referred to as HE 90481, with a pA_2 value of 4.43 in HEL cells (Buschauer, 1989; Michel and Motulsky, 1990). Significant increase in affinity and selectivity towards the NPY Y_1 receptor was reported for BIBP-3226 (Fig. 1.1.2) with K_i of 7 nM (Rudolf *et al.*, 1994). Noteworthy, BIBP-3226 shows structural similarity to the C-terminus of NPY, as it mimics the last two amino acid residues (Arg^{35} and Tyr^{36} shown in Fig. 1.2.1 in cyan).

Numerous analogs of this compound have been developed in our laboratory (Aiglstorfer *et al.*, 1998; Brennauer *et al.*, 2004) resulting in the synthesis and characterization of the first non-peptide fluorescent NPY Y_1 receptor ligands (Schneider and Keller *et al.*, 2007; Keller, 2008, Keller *et al.*, 2011) and the first selective Y_1R radioligand (Fig. 1.2.2).

In previous studies, the tritium-labelled N^G-propionylargininamide UR-MK114, structurally derived from the antagonist BIBP-3226, revealed excellent one-digit nanomolar affinity (K_d values: 2.9 ± 0.4 nM on MCF-7 cells; 1.2 ± 0.1 nM on SK-N-MC cells), achieving saturation of the receptors already at a concentration of approx. 4 nM (Keller, 2008; Keller *et al.*, 2008).

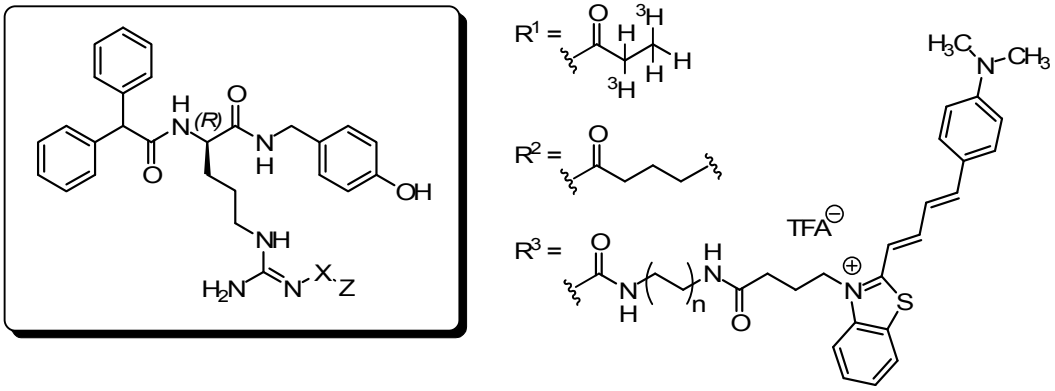

Compound	X	Z	n
BIBP-3226	H	-	0
[^{3}H]UR-MK114	R^1	-	0
UR-MK115	R^2	R^3	1
UR-MK131	-	R^3	2

Fig. 1.2.2. *The selective Y_1R antagonist BIBP-3226 and its derivatives: the radioligand [^{3}H]UR-MK114 (Keller et al., 2008) and the far-red fluorescent ligands UR-MK115 and UR-MK131 (cf. Keller, 2008; Keller et al., 2011).*

1.2.2 Histamine receptors

Histamine (2-(1*H*-imidazol-4-yl)ethanamine) is an important neurotransmitter and autacoid that exerts its function *via* four known receptor subtypes ($H_{1–4}$R), belonging to the aminergic class A GPCRs (de Esch *et al.*, 2005). The signal transduction pathways as well as the physiological role of histamine receptors are summarized in Table 1.2.1. More than 100 years of histamine research (discovery of histamine in 1910 by Barger and Dale) have resulted in the development of drugs, successfully applied in the therapy of allergy (H_1R) and gastric ulcer (H_2R). The recent discovery of new histamine receptor subtypes intensified the development of novel agents for the potential treatment of cognitive (H_3R) and inflammatory (H_4R) diseases (Hill *et al.*, 1997; Tiligada *et al.*, 2009). These receptors are also subjects of great interest in our department and appropriate pharmacological methods and tools, including selective radioligands and fluorescent ligands, have been already in our hands (Igel *et al.*, 2009; Erdmann, 2010).

Table 1.2.1. *Comparison of pharmacological profiles of the histamine receptor subtypes (cf. Hill et al., 1997; Tiligada et al., 2009).*

	Signaling	Distribution	Physiological role
H_1R	$G_{q/11}$, PLC (↑), Ca^{2+} (↑)	ubiquitous, blood vessels, ileum, lung, brain	contraction of smooth mucles
H_2R	G_s, cAMP (↑)	ubiquitous, stomach, heart, brain, monocytes	gastric acid secretion, increase in heart rate
H_3R	$G_{i/o}$, cAMP (↓), Ca^{2+} (↑), MAPK (↑)	central nervous system, presynaptic autoreceptor	memory processing, sleep, feeding behavior
H_4R	$G_{i/o}$, cAMP (↓), Ca^{2+} (↑), MAPK (↑)	hematopoietic cells, neurons	chemotaxis, control of pain and cell cycle

1.2.2.1 Pharmalogical tools for the histamine H_2 and H_4 receptors

The histamine H_2 receptor (H_2R) mediates numerous histamine-induced effects predominantly *via* coupling to G_s protein (cAMP-dependent signalling). The H_2R antagonists have been widely used for the treatment of peptic ulcer and gastroesophageal reflux disease, whereas the H_2R agonists are exclusively pharmacological tools (Fig. 1.2.3). N^G-Acylated hetarylpropylguanidines, developed in our research group, represent a new class of H_2R agonists with improved pharmacokinetic properties compared to the corresponding guanidines due to substantially reduced basicity (Ghorai *et al.*, 2008; Kraus *et al.*, 2009). Very recently, a tremendous increase in potency was achieved by applying the bivalent ligand approach to acylguanidine-type H_2R agonists (Fig. 1.2.4; Kraus, 2007; Birnkammer *et al.*, 2010).

In order to develop binding assays for flow cytometry and confocal microscopy, a series of green fluorescent ligands with the high affinity towards the H_2R (pA_2 up to 8.0 at the guinea-pig atrium) were previously developed in our research group (Li *et al.*, 2003). A new generation of pharmacological tools for the H_2R comprises far-red fluorescent ligands, which can be detected with 650 nm long-pass filters, as the autofluorescence of cells is marginal in this region of spectrum. These novel squaramide derivatives, synthetized by Dr. Daniela Erdmann, are labeled with the fluorescent dyes S-0536 (UR-DE54 and UR-DE56) or Dy-675 (UR-DE74), which have excitation maxima at approx. 670 nm, or with the pyrylium dye Py-5 (cf. UR-DE108) resulting in pyridinium fluorophores, which can be excited with the 488 nm line of an argon laser. Additionally, the new H_2R tritiated ligand [^{3}H]UR-DE257 has been recently developed for equilibrium and kinetic binding studies (Fig. 1.2.5, Erdmann, 2010).

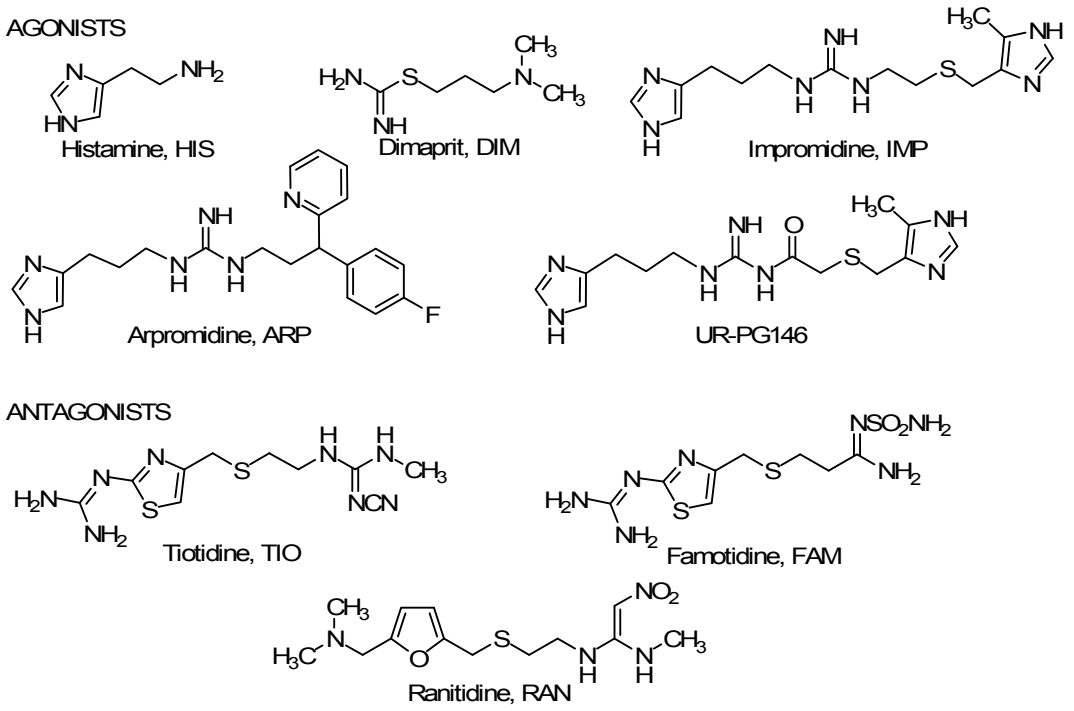

Fig. 1.2.3. *Selected H_2R agonists and antagonists (cf. Buschauer, 1989; Xie et al., 2006).*

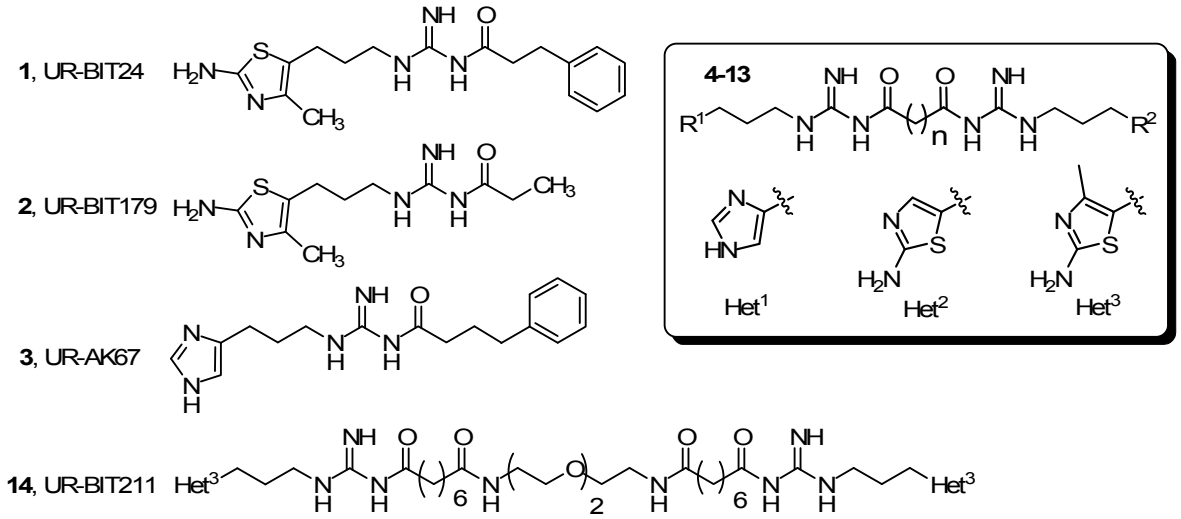

Compound	R^1	R^2	n	Compound	R^1	R^2	n
4, UR-AK480	Het^1	Het^1	8	**9**, UR-BIT271	Het^1	Het^1	14
5, UR-AK381	Het^3	Het^3	8	**10**, UR-BIT114	Het^2	Het^2	14
6, UR-BIT82	Het^1	Het^3	8	**11**, UR-BIT294	Het^1	Het^1	20
7, UR-BIT106	Het^2	Het^2	8	**12**, UR-BIT115	Het^2	Het^2	20
8, UR-BIT107	Het^2	Het^3	8	**13**, UR-AK428	Het^3	Het^3	20

Fig. 1.2.4. *Novel N^G-acylated monovalent (1–3) and bivalent (4–14) H_2R ligands.*

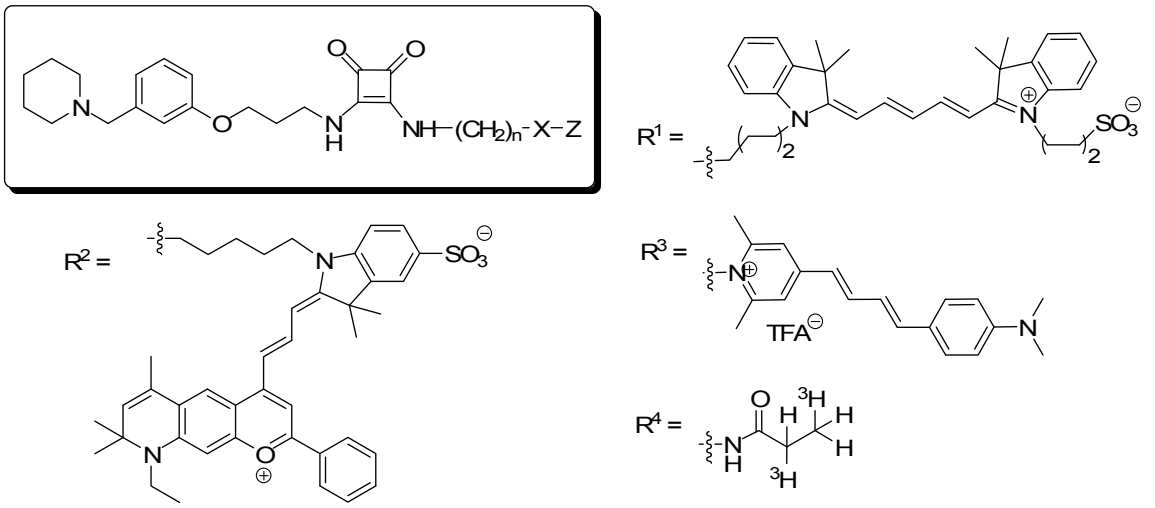

Compound	X	Z	n
UR-DE54	NHCO	R^1	4
UR-DE56	NHCO	R^1	6
UR-DE74	NHCO	R^2	4
UR-DE108	-	R^3	4
[^{3}H]UR-DE257	-	R^4	6

Fig. 1.2.5. *Pharmacological tools for the H_2R (cf. Erdmann, 2010).*

The discovery and cloning of the human histamine H_4 receptor in 2000 (Oda *et al.*, 2000) led to the revision of selectivity data of the ligands for other histamine receptor subtypes. For example, thioperamide (known so far as a H_3R ligand with pK_i of 7.2) showed high affinity towards the H_4R (pK_i of 7.4), being an inverse agonist (Fig. 1.2.6; cf. de Esch *et al.*, 2005; Tiligada *et al.*, 2009). It should be noted that the H_2R bivalent compounds of the imidazole series revealed one-digit nanomolar potency at the human H_4R (Kraus, 2007). The imidazolylpropylguanidine moiety turned out to be a privileged structure with respect to histamine receptors. Additionally, the H_4R antagonist JNJ7777120 (pK_i of 8.4) was reported to induce the recruitment of β-arrestins in a G-protein-independent manner, suggesting functional selectivity at this receptor (Rosethorne and Charlton, 2011; Seifert *et al.*, 2011).

Due to much higher affinity at the H_4R than at the H_2R, the natural ligand is routinely used as radioligand at the H_4R (cf. K_d value of [^{3}H]HIS: 11 ± 1 nM at the hH_4R expressed in SK-N-MC cells, Lim *et al.*, 2005; 9.8 ± 0.9 nM at Sf9 membranes expressing the hH_4R + $G_{i\alpha 2}$ + $G_{\beta 1\gamma 2}$ + GAIP, Schnell *et al.*, 2011). Very recently, tritium-labelled *N*^{1}-[3-(1*H*-imidazol-4-yl)propyl]-*N*^{2}-propionylguanidine ([^{3}H]UR-PI294) has been developed in our laboratory by Dr. Patrick Igel as a high-affinity H_3R and H_4R radioligand (Fig. 1.2.6; cf.

Igel *et al.*, 2009). In this context it is indispensable to mention that so far the only published results of kinetic studies on H_4R radioligands refer to [^{3}H]UR-PI294 (cf. chapter 5).

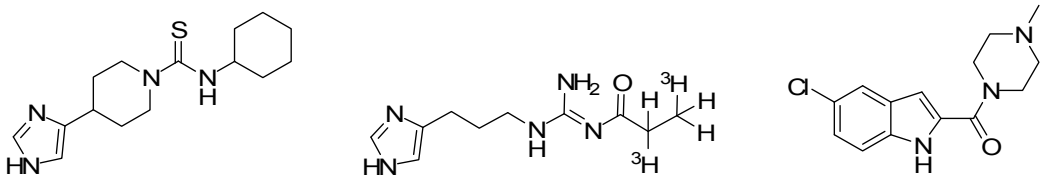

Fig. 1.2.6. *Selected H_4R ligands (cf. Igel et al., 2009; Tiligada et al., 2009).*

1.2.2.2 Selected testing systems for the histamine H_2 and H_4 receptors

The isolated guinea-pig right atrium is used in our institute (cooperation with Prof. Dr. Sigurd Elz, University of Regensburg) as a classical pharmacological test system for characterization of H_2R ligands (H_2R agonists induce a positive chronotropic response, Fig. 1.2.7 A). Nowadays, various readout systems using genetically engineered cells are standard, enabling the investigation of substance libraries at the human receptors of interest, at corresponding species orthologs and receptor mutants, e.g. cAMP and [^{3}H]cAMP accumulation assays, CRE (cAMP response element) gene transcription assays (Monczor *et al.*, 2006; Baker, 2008). In our laboratory, for instance, functional studies can be performed in GTPase assays at insect Sf9 (*Sporodoptera frugiperda*) membranes, expressing recombinant human (h) or guinea-pig (gp) H_2Rs (Schneider and Seifert, 2010). Additionally, the Sf9 cell/baculovirus system enables modifications of the receptor of interest including fusions with other proteins, for instance the expression of H_2Rs fused with the $G_{s\alpha S}$ protein (the short splice variant of the α subunit of G_s protein). The use of receptor-G_α fusion proteins provides a constant 1:1 coupling stoichiometry and stronger signals than in case of coexpressed receptors and G proteins (Seifert and Wieland, 2005). The H_4R can be fused, in turn, to GAIP (also referred to as the regulator of G-protein signaling RGS19) for more efficient signalling and can be coexpressed with the $G_{i\alpha 2}$ and $G_{\beta 1\gamma 2}$ subunits (Schneider and Seifert, 2009).

The access of ligands to the receptor of interest may strongly depend on the test system. For example, an exceptional latency period had been observed in experiments on the guinea-pig right atrium, where the positive inotropic effects of bivalent H_2R agonists at low concentrations (< 10 nM) reached a plateau not before 2.5 to 3 hours of incubation (Prof. Dr. Sigurd Elz, personal communication). These problems, resulting most probably from slow distribution of these ligands in the isolated organ, should be overcome at the

Sf9 membranes, due to simplicity of the system. A recent study by Saito *et al.* showed that Sf9 membrane preparations contain vesicles (Saito *et al.*, 2006). Moreover, scanning electron microscopy revealed that there were many pores formed in the Sf9 cell membranes 5 days after infection with baculoviruses. The imaging of membrane suspensions, prepared according to previously described procedures (Wenzel-Seifert *et al.*, 2001), confirmed that the investigated samples were composed of small, predominantly agregated vesicles (Fig. 1.2.7 B–G). Staining of the Sf9 membranes was performed with the fluorescent dye Cell Mask Deep Red (Invitrogen), Sudan Black (indication of lipids) and methylene blue according to Loeffler (indication of proteins). However, little is known about both, the orientation of the plasma membrane vesicles (inside-out or right-side-out) and the existence of the pores, as (according to the standard protocol) the membranes are harvested and prepared 48 hours after virus infection. Nevertheless, more detailed characterization of the morphology of the Sf9 membrane vesicles might be helpful for the elucidation of complex binding behavior of some ligands (e.g. slow dissociation of the radioligand [^{3}H]UR-DE257 as shown in Fig. 5.3.4; cf. Erdmann, 2010).

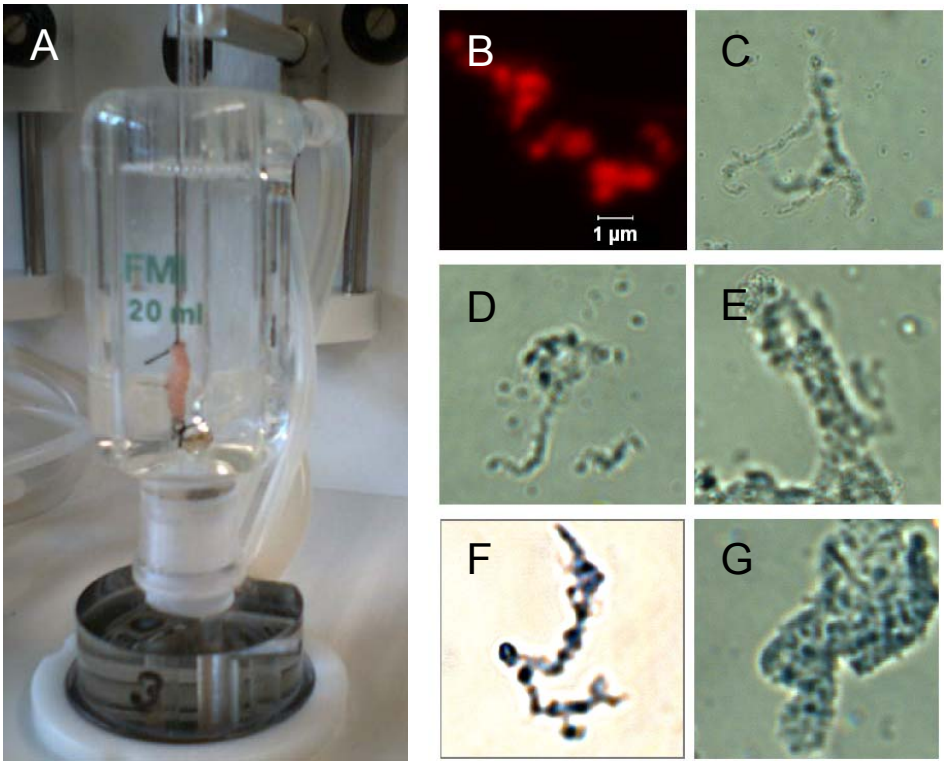

Fig. 1.2.7. *Testing systems for H_2R ligands: (A) spontaneously beating guinea-pig right atrium; (B–G) Sf9 membranes, expressing gpH_2R-$G_{s\alpha S}$ fusion proteins. The membranes were prepared as previously described (Wenzel-Seifert et al., 2001) and stained with: (B) Cell Mask Deep Red (microscope settings: Plan Apochromat 63x/1.4 Oil, HeNe 633, HFT UV/488/543/633, NFT 545, LP 650); (C–E) Sudan Black; (F–G) Loeffler's methylene blue. Images B–G were acquired with a Carl Zeiss Axiovert 200M inverted microscope coupled to a Zeiss LSM510 scanning device and an Axiocam digital camera.*

Experiments conducted on intact cells should provide closer similarity to physiological conditions than those performed on membranes, due to the higher complexity of the former. For example, high intracellular concentration of GTP in intact cells implicates that only the low-affinity binding site can be observed for agonists in radioligand binding studies, as it can be deduced from steep binding curves. By contrast, flat curves (resulting from the formation of the ternary complex) can be found for agonists in assays conducted with broken-cell preparations (Lazareno, 2001; Kenakin, 2006). Moreover, using the living cells allows for the investigations of agonist-induced receptor internalization. As reported previously, the endogenous hH_2R undergoes a rapid homologous desensitization upon the HIS stimulation both on the monocytic U-937 (Smit *et al.*, 1994) and the gastric carcinoma MKN-45 (Arima *et al.*, 1993) cell lines. Previous studies of guanidine-type H_2R agonists showed that human neutrophils are a valuable model for functional investigations on endogenously expressed H_2R, in particular by measuring superoxide (O_2^-) formation (Burde *et al.*, 1990). The additional expression of the hH_4R on the U-937 cells was recently the matter of a controversial discussion (Cao *et al.*, 2001; Damaj *et al.*, 2007).

1.3 Fluorescence- and radioactivity-based methods: selected aspects

Ligand binding studies and functional assays are indispensable to characterize receptor agonists and antagonists and are important methods to investigate the mechanisms of ligand-receptor interactions. Information on ligand affinities is often decisive for the development of new drug candidates and the optimization of lead structures. At the same time, binding experiments allow for the pharmacological characterization of drug targets (e.g. new receptor subtypes). The commonly approved strategies involve radioactive or fluorescent labelling of known ligands to obtain pharmacological tools, which are used for the investigation of novel chemical entities. Additionally, detailed analysis of both kinetic (time-course) and equilibrium binding data may provide a deeper insight into the assumed ligand binding mode, which in case of bivalent compounds may imply "bridging" of receptor dimers, the ternary complex model, allosteric interactions or multiple ligand-specific receptor conformations (Kenakin, 2006; Xie *et al.* 2006; Valant *et al.*, 2008, Shonberg *et al.*, 2011).

On the other hand, current progress in protein labelling techniques facilitates the elucidation of protein-protein interactions as well as the subcellular localization of the labelled structures. For example, fluorescent tagging of the GPCRs allows for the visualization of receptor dimerization and agonist-induced internalization (Milligan and Bouvier, 2005; Osawa *et al.*, 2005).

1.3.1 Requirements for ligand binding at equilibrium

In order to obtain information on binding parameters (K_d, B_{max}, Fig. 1.3.1), the system to-be-investigated has to attain *equilibrium* at the time point of the measurement.

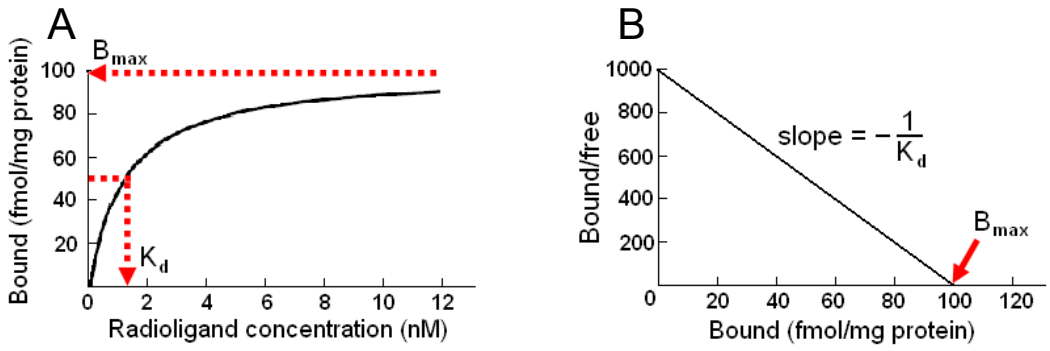

Fig. 1.3.1. *Saturation binding experiments at equilibrium allow measurements of both ligand affinity (K_d) and the number of receptors (B_{max}): (A) a saturation binding curve; (B) a Scatchard plot.*

For ligand binding at equilibrium, it is assumed that there is no ligand depletion. This requirement is fulfilled when the experimental settings are adjusted to ensure that the bound ligand fraction does not exceed 15% of the total amount of ligand (Lazareno, 2001). Another important assumption consists in a sufficiently long incubation period. A premature termination of incubation (pre-equilibrium) may lead to artefacts (Hulme, 1992).

According to the law of mass action (Motulsky and Christopoulos, 2004), binding of a ligand A to its receptor R is described by the following reaction, where k_1 (k_{on}) and k_2 (k_{off}) are association and dissociation rate constants, respectively (Eq. 1.3.1):

$$A + R \underset{k_2}{\overset{k_1}{\rightleftharpoons}} AR \qquad \text{(Eq. 1.3.1)}$$

$$\frac{d([AR])}{dt} = k_1[A]\cdot[R] - k_2[AR] \qquad \text{(Eq. 1.3.2)}$$

$$\frac{d([AR])}{dt} = 0 \Rightarrow [A]\cdot[R]\cdot k_1 = [AR]\cdot k_2 \qquad \text{(Eq. 1.3.3)}$$

$$\frac{[A]\cdot[R]}{[AR]} = \frac{k_2}{k_1} = K_d \qquad \text{(Eq. 1.3.4)}$$

The rate of forward binding is proportional to the concentrations of both the free ligand and the receptor, whereas the dissociation rate is proportional only to the concentration of the AR complex. Equilibrium is reached (steady state), when two reaction rates become equal (Eq. 1.3.2–3). Then the ratio of k_2 to k_1 defines the equilibrium dissociation constant K_d (Eq. 1.3.4).

The observed rate constant of radioligand association k_{obs} depends on the used ligand concentration [A], the equilibrium dissociation constant K_d and the dissociation rate constant k_2, as expressed by the Eq. 1.3.5–6 (cf. Lazareno, 2001):

$$\text{if } [A] = \text{const.} \Rightarrow k_{obs} = k_1[A] - k_2 \qquad \text{(Eq. 1.3.5)}$$

$$k_1 = \frac{k_2}{K_d} \Rightarrow k_{obs} = k_2 \cdot \left(\frac{[A]}{K_d} - 1\right) \qquad \text{(Eq. 1.3.6)}$$

A general rule defines the time needed for equilibration as a 5-fold half-life of the radioligand dissociation, if the used ligand concentration [A] is much less than K_d (Hulme, 1992). When higher concentrations are used, the equilibration becomes even faster (Eq. 1.3.5–6; cf. Lazareno, 2001):

$$\text{if} \quad [A] << K_d \;\Rightarrow\; k_{obs} \approx k_2 \qquad \text{(Eq. 1.3.7)}$$

$$\text{if} \quad [A] >> K_d \;\Rightarrow\; k_{obs} = k_2 \cdot \frac{[A]}{K_d} \qquad \text{(Eq. 1.3.8)}$$

1.3.2 Fluorescent proteins in confocal microscopy

Confocal laser scanning microscopy (CLSM) allows for real time visualization and even subcellular localization of fluorescently stained structures, due to significantly improved image resolution in comparison to the usual fluorescence microscopy. This methodology has been successfully applied also for the investigation of GPCRs in living cells, involving the parallel acquisition of multi-labelled specimen and colocalization studies, as well as imaging of receptor internalization and intracellular recycling (Leterrier *et al.*, 2004).

The discovery of the green fluorescent protein (GFP) and development of its numerous spectral variants (Fig. 1.3.2) by O. Shimomura, M. Chalfie and R. Y. Tsien revolutionized the studies on protein-protein interactions and was awarded with the Nobel Prize in Chemistry in 2008 (http://nobelprize.org/nobel_prizes/chemistry/laureates/2008/). The GFP-like proteins are very advantageous, due to quick chromophore formation, mostly enabling undisturbed folding and function of the tagged protein (Ormö *et al.*, 1996; Miyawaki *et al.*, 2003; Shaner *et al.*, 2005). Additionally, after successful transfection of the cells, no further chemical modifications are necessary (contrary to the BRET and FlAsH techniques; Hoffmann *et al.*, 2005; Milligan and Bouvier, 2005). Fig. 1.3.3 shows examples how fluorescent proteins have been applied to investigate the GPCR-mediated signal transduction.

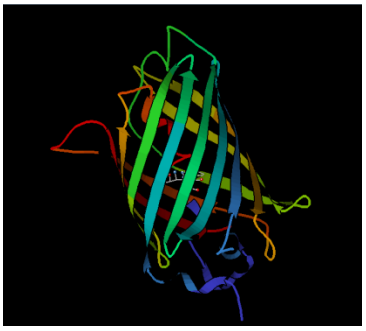

Fig. 1.3.2. *The enhanced cyan fluorescent protein (ECFP). The ECFP model was generated with the KiNG Viewer program (from the RCSB Protein Data Bank).*

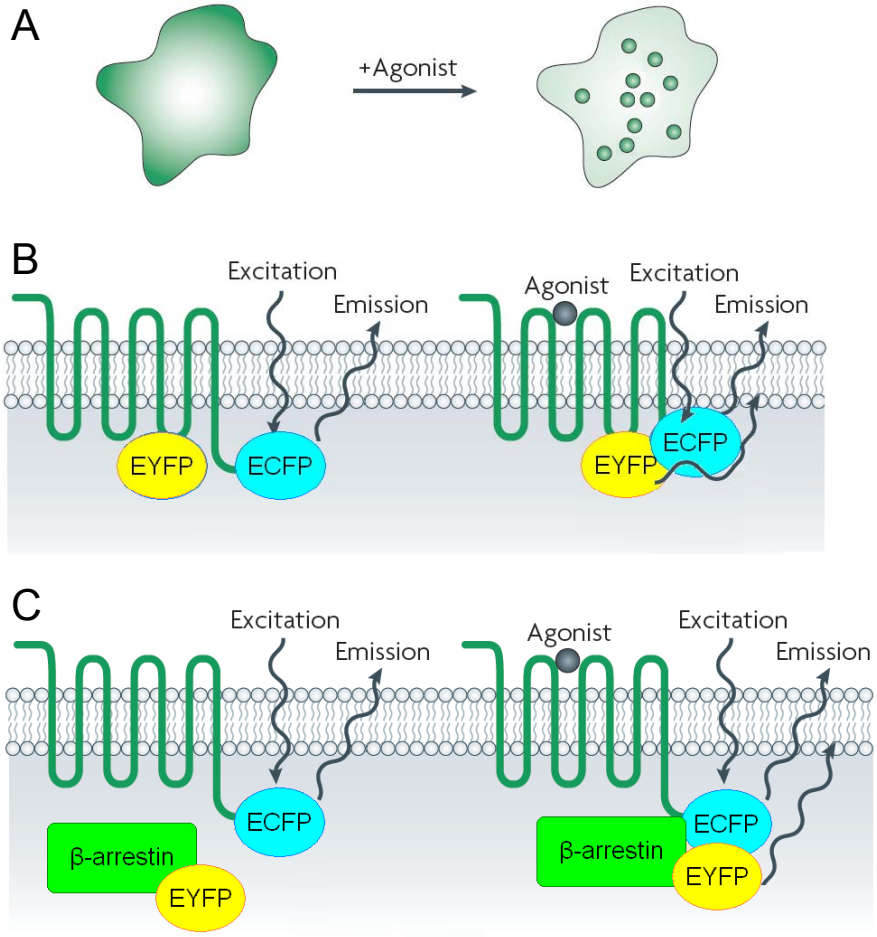

Fig. 1.3.3. *Selected applications of fluorescent proteins for the investigation of GPCR signalling: (A) redistribution (translocation) of GPCRs or β-arrestins, (B) conformational change of receptors, (C) proximity assays (recruitment of β-arrestins) upon agonist stimulation (adopted from Vilardaga et al., 2003; Rajagopal et al., 2010 with modifications).*

1.4 References

Aiglstorfer I *et al.*: NPY Y_1 antagonists: structure-activity relationships of arginine derivatives and hybrid compounds with arpromidine-like partial structures, *Regul Pept*, **1998**, *75-76*, 9-21.

Arima N *et al.*: Homologous desensitization of histamine H_2 receptors in the human gastric carcinoma cell line MKN-45, *Am J Physiol*, **1993**, *265*, G987-G992.

Baker JG: A study of antagonist affinities for the human histamine H_2 receptor, *Br J Pharmacol*, **2008**, *153*, 1011–1021.

Berglund MM *et al.*: Neuropeptide Y Y_4 receptor homodimers dissociate upon agonist stimulation, *J Pharmacol Exp Ther*, **2003**, *307*, 1120–1126.

Bhushan RG *et al.*: A bivalent ligand (KDN-21) reveals spinal *δ* and κ opioid receptors are organized as heterodimers that give rise to δ_1 and κ_2 phenotypes. Selective targeting of *δ*-κ heterodimers, *J Med Chem*, **2004**, *47,* 2969–2972.

Birnkammer T *et al.*: Structure-activity relationships of bivalent acylguanidine-type histamine H_2 receptor agonists, *5th Summer School "Medicinal Chemistry"*, University of Regensburg, **2010**, P4 (poster contribution).

Bjarnadóttir TK *et al.*: Comprehensive repertoire and phylogenetic analysis of the G protein-coupled receptors in human and mouse, *Genomics*, **2006**, *88*, 263–73.

Bokoch MP *et al.*: Ligand-specific regulation of the extracellular surface of a G-protein-coupled receptor, *Nature*, **2010**, *463*, 108–112.

Bonger KM *et al.*: Synthesis and evaluation of homo-bivalent GnRHR ligands, *Bioorg Med Chem*, **2007**, *15*, 4841–4856.

Bonger KM *et al.*: Synthesis and evaluation of homodimeric GnRHR antagonists having a rigid bis-propargylated benzene core, *Bioorg Med Chem*, **2008**, *16*, 3744–3758.

Brennauer A *et al.*: Structure-activity relationships of nonpeptide neuropeptide Y receptor antagonists. In: Michel MC (ed): Handbook of experimental pharmacology, *Springer-Verlag*, **2004**, *162*, 505–546.

Burde R *et al.*: Characterization of histamine H_2-receptors in human neutrophils with a series of guanidine analogues of impromidine. Are cell type-specific H_2-receptors involved in the regulation of NADPH oxidase? *Naunyn Schmiedebergs Arch Pharmacol*, **1990**, *341*, 455–461.

Buschauer A: Synthesis and in vitro pharmacology of arpromidine and related phenyl(pyridylalkyl)guanidines, a potential new class of positive inotropic drugs, *J Med Chem*, **1989**, *32*, 1963–1970.

Cao Y *et al.*: The fucosylated histo-blood group antigens H type 2 (blood group O, CD173) and Lewis Y (CD174) are expressed on CD34+ hematopoietic progenitors but absent on mature lymphocytes, *Glycobiology*, **2001**, *11*, 677–683.

Damaj BB *et al.*: Functional expression of H_4 histamine receptor in human natural killer cells, monocytes, and dendritic cells, *J Immunol*, **2007**, *179*, 7907–7915.

Daniels DJ *et al.*: Opioid-induced tolerance and dependence in mice is modulated by the distance between pharmacophores in a bivalent ligand series, Proc Natl Acad Sci U S A, **2005**, *102*, 19208–19213.

de Esch IJ *et al.*: The histamine H_4 receptor as a new therapeutic target for inflammation, *Trends Pharmacol Sci*, **2005**, *26*, 462–469.

DeWire SM *et al.*: β-Arrestin-mediated signaling regulates protein synthesis, *J Biol Chem*, **2008**, *283*, 10611–10620.

Dinger MC *et al.*: Homodimerization of neuropeptide Y receptors investigated by fluorescence resonance energy transfer in living cells, *J Biol Chem*, **2003**, *278*, 10562–10571.

Ehlert FJ: The relationship between muscarinic receptor occupancy and adenylate cyclase inhibition in the rabbit myocardium, *Mol Pharmacol*, **1985**, *28*, 410–421.

Erdmann D: Histamine H_2 and H_3 receptor antagonists: Synthesis and characterization of radiolabelled and fluorescent pharmacological tools: Doctoral thesis, University of Regensburg, **2010**.

Ferguson SSG: Evolving concepts in G protein-coupled receptor endocytosis: The role in receptor desensitization and signaling, *Pharmacol Rev*, **2001**, *53*, 1-24.

Ferré S *et al.*: Building a new conceptual framework for receptor heteromers (commentary), *Nat Chem Biol*, **2009**, *5*, 131–134.

Fotiadis D *et al.*: Structure of the rhodopsin dimer: a working model for G-protein-coupled receptors, *Curr Opin Struct Biol*, **2006**, *16*, 252-259.

Fukushima Y *et al.*: Oligomer formation of histamine H_2 receptors expressed in Sf9 and COS7 cells, *FEBS Lett*, **1997**, *409*, 283–286.

Gether U: Uncovering molecular mechanisms involved in activation of G protein-coupled receptors, *Endocr Rev*, **2000**, *21*, 90-113.

Ghorai P *et al.*: Acylguanidines as bioisosteres of guanidines: N^G-acylated imidazolylpropylguanidines, a new class of histamine H_2 receptor agonists, *J Med Chem*, **2008**, *51*, 7193–7204.

Gicquiaux H *et al.*: Rapid internalization and recycling of the human neuropeptide Y Y_1 receptor, *J Biol Chem*, **2002**, *277*, 6645–6655.

Gomes I *et al.*: G protein coupled receptor dimerization: implications in modulating receptor function, *J Mol Med*, **2001**, *79*, 226–242.

Gurevich VV and Gurevich EV: The structural basis of arrestin-mediated regulation of G-protein-coupled receptors, *Pharmacol Ther*, **2006**, *110*, 465–502.

Hill SJ *et al.*: International Union of Pharmacology. XIII. Classification of histamine receptors, *Pharmacol Rev*, **1997**, *49*, 253-78.

Hoffmann C *et al.*: A FlAsH-based FRET approach to determine G protein-coupled receptor activation in living cells, *Nat Methods*, **2005**, *2*, 171-176.

Hopkins AL and Groom CR: The druggable genome, *Nat Rev Drug Discov*, **2002**, *1*, 727-730.

Hulme EC (ed.): Receptor-ligand interactions: A practical approach, *IRL Press/Oxford University Press*, New York, **1992**.

Igel P *et al.*: Tritium-labeled N^1-[3-(1*H*-imidazol-4-yl)propyl]-N^2-propionylguanidine ([^{3}H]UR-PI294), a high-affinity histamine H_3 and H_4 receptor radioligand, *ChemMedChem*, **2009**, *4*, 225 – 231.

Keller M *et al.*: Bivalent argininamide-type neuropeptide Y Y_1 antagonists do not support the hypothesis of receptor dimerisation, *ChemMedChem*, **2009**, *4*, 1733–1745.

Keller M *et al.*: Guanidine-acylguanidine bioisosteric approach in the design of radioligands: synthesis of a tritium-labeled N^G-propionylargininamide ([^{3}H]-UR-MK114) as a highly potent and selective neuropeptide Y Y_1 receptor antagonist, *J Med Chem*, **2008**, *51,* 8168–8172.

Keller M *et al.*: Red-fluorescent argininamide-type NPY Y_1 receptor antagonists as pharmacological tools, *Bioorg Med Chem*, **2011**, *19*, 2859–2878.

Keller M: Guanidine-acylguanidine bioisosteric approach to address peptidergic receptors: pharmacological and diagnostic tools for the NPY Y_1 receptor and versatile building blocks based on arginine substitutes, Doctoral thesis, University of Regensburg, **2008**.

Kenakin T and Miller LJ: Seven transmembrane receptors as shapeshifting proteins: The impact of allosteric modulation and functional selectivity on new drug discovery, *Pharmacol Rev*, **2010**, *62*, 265–304.

Kenakin T: Differences between natural and recombinant G protein-coupled receptor systems with varying receptor/G protein stoichiometry, *Trends Pharmacol Sci*, **1997**, *18*, 456-464.

Kenakin TP: A pharmacology primer: Theory, application, and methods, *Academic Press – Elsevier*, Amsterdam – Tokyo, **2006**.

Kimura Y *et al.*: Surface of bacteriorhodopsin revealed by high-resolution electron crystallography, *Nature*, **1997**, *389*, 206–211.

Kraus A *et al.*: N^G-acylated aminothiazolylpropylguanidines as potent and selective histamine H_2 receptor agonists, *ChemMedChem*, **2009**, *4*, 232–240.

Kraus A: Highly potent, selective acylguanidine-type histamine H_2 receptor agonists: Synthesis and structure-activity relationships, Doctoral thesis, University of Regensburg, **2007**.

Kroeger KM *et al.*: G-protein coupled receptor oligomerization in neuroendocrine pathways, *Front Neuroendocrinol*, **2004**, *24*, 254–278.

Lazareno S: Quantification of receptor interactions using binding methods, *J Recept Signal Transduct*, **2001**, *21*, 139–165.

Leterrier C *et al.*: Constitutive endocytic cycle of the CB_1 cannabinoid receptor, *J Biol Chem*, **2004**, *279*, 36013–36021.

Lezoualc'h F *et al.*: Multivalent-based drug design applied to serotonin 5-HT_4 receptor oligomers, *Curr Pharm Des*, **2009**, *15*, 719 – 729.

Li L *et al.*: Synthesis and pharmacological activity of fluorescent histamine H_2 receptor antagonists related to potentidine, *Bioorg Med Chem Lett*, **2003**, *13*, 1717–1720.

Lim HD *et al.*: Evaluation of histamine H_1-, H_2-, and H_3-receptor ligands at the human histamine H_4 receptor: identification of 4-methylhistamine as the first potent and selective H_4 receptor agonist, *J Pharmacol Exp Ther*, **2005**, 314, 1310–1321.

Luttrell LM and Gesty-Palmer D: Beyond desensitization: physiological relevance of arrestin-dependent signaling, *Pharmacol Rev*, **2010**, *62*, 305–330.

MacNeil DJ: NPY Y_1 and Y_5 receptor selective antagonists as anti-obesity drugs, *Med. Chem.*, **2007**, *7*, 1721-1733.

Maguire ME *et al.*: An agonist-specific effect of guanine nucleotides on binding to the beta adrenergic receptor, *Mol Pharmacol*, **1976**, *12*, 335–339.

Marshall *et al.*: $GABA_B$ receptors function as heterodimers, *Biochem Soc Trans*, **1999**, *27*, 530–535.

May LT *et al.*: Allosteric modulation of G protein–coupled receptors, *Annu Rev Pharmacol Toxicol*, **2007**, *47*, 1–51.

Merten N and Beck-Sickinger AG: Molecular ligand-receptor interaction of the NPY/PP peptide family, *EXS*, **2006**, 35–62.

Michel MC and Motulsky HJ: HE 90481: A competitive nonpeptidergic antagonist at neuropeptide Y receptors, *Ann N Y Acad Sci*, **1990**, *611*, 392–394.

Michel MC *et al.*: XVI. International Union of Pharmacology recommendations for the nomenclature of neuropeptide Y, peptide YY, and pancreatic polypeptide receptors, *Pharmacol Rev*, **1998**, *50*, 143–50.

Milligan G and Bouvier M: Methods to monitor the quaternary structure of G protein-coupled receptors, *FEBS J*, **2005**, *272*, 2914–2925.

Miyawaki A *et al.*: Mechanisms of protein fluorophore formation and engineering, *Curr Opin Chem Biol*, **2003**, *7*, 557–562.

Monczor F *et al.*: Histamine H_2 receptor overexpression induces U937 cell differentiation despite triggered mechanisms to attenuate cAMP signalling, *Biochem Pharmacol*, **2006**, *71*, 1219–1228.

Motulsky HJ and Christopoulos A: Fitting models to biological data using linear and nonlinear regression: A practical guide to curve fitting*, GraphPad Software/Oxford University Press*, New York, **2004**.

Oda T *et al.*: Molecular cloning and characterization of a novel type of histamine receptor preferentially expressed in leukocytes, *J Biol Chem*, **2000**, *275*, 36781–36786.

Ormö M *et al.*: Crystal structure of the *Aequorea victoria* green fluorescent protein, *Science*, **1996**, *273*, 1392–1395.

Osawa S *et al.*: Alteration of intracellular histamine H_2 receptor cycling precedes antagonist-induced upregulation, *Am J Physiol Gastrointest Liver Physiol*, **2005**, *289*, G880-G889.

Palczewski K *et al.*: Crystal structure of rhodopsin: A G protein-coupled receptor, *Science*, **2000**, *289*, 739–745.

Perez M *et al.*: Dimerization of sumatriptan as an efficient way to design a potent, centrally and orally active 5-HT_{1B} agonist, *Bioorg Med Chem Lett*, **1998**, *8*, 675-80.

Preuss H *et al.*: Mutations of Cys-17 and Ala-271 in the human histamine H_2 receptor determine the species selectivity of guanidine-type agonists and increase constitutive activity, *J Pharmacol Exp Ther*, **2007**, *321*, 975–982.

Rajagopal S *et al.*: Teaching old receptors new tricks: biasing seven-transmembrane receptors, *Nat Rev Drug Discov*, 2010, 9, 373-386.

Rasmussen SG *et al.*: Crystal structure of the human β_2 adrenergic G-protein-coupled receptor, *Nature*, **2007**, *450*, 383–387.

Repke H and Liebmann C: Membranrezeptoren und ihre Effektorsysteme, *Akademie-Verlag*, Berlin, **1987**.

Rosenbaum DM *et al.*: GPCR engineering yields high-resolution structural insights into β_2-adrenergic receptor function, *Science*, **2007**, *318*, 1266–1273.

Rosethorne EM and Charlton SJ: Agonist-biased signalling at the histamine H_4 receptor: JNJ7777120 recruits beta-arrestin without activating G proteins, *Mol Pharmacol*, **2011**, *79*, 749-757.

Rudolf K *et al.*: The first highly potent and selective non-peptide neuropeptide Y Y_1 receptor antagonist: BIBP3226, *Eur J Pharmacol*, **1994**, *271*, R11-13.

Saito H *et al.*: A new strategy of high-speed screening and quantitative structure-activity relationship analysis to evaluate human ATP-binding cassette transporter ABCG2-drug interactions, *J Pharmacol Exp Ther*, **2006**, *317*, 1114–1124.

Schneider E, Keller M *et al.*: Synthesis and characterization of the first fluorescent non-peptide NPY Y_1 receptor antagonist, *ChemBioChem*, **2007**, *8*, 1981–1988.

Schneider E *et al.*: A simple and powerful flow cytometric method for the simultaneous determination of multiple parameters at G protein-coupled receptor subtypes, *ChemBioChem*, **2006**, *7*, 1400–1409.

Schneider E: Development of fluorescence-based methods for the determination of ligand affinity, selectivity and activity at G-protein coupled receptors, Doctoral thesis, University of Regensburg, **2005**.

Schneider EH and Seifert R: Histamine H_4 receptor–RGS fusion proteins expressed in Sf9 insect cells: A sensitive and reliable approach for the functional characterization of histamine H_4 receptor ligands, *Biochem Pharmacol*, **2009**, 78, 607–616.

Schneider EH and Seifert R: Sf9 cells: a versatile model system to investigate the pharmacological properties of G protein-coupled receptors, *Pharmacol Ther*, **2010**, *128*, 387–418.

Schnell D *et al.*: Expression and functional properties of canine, rat, and murine histamine H_4 receptors in Sf9 insect cells, *Naunyn Schmiedebergs Arch Pharmacol*, **2011**, *383*, 457-470.

Seifert R and Wieland Th: G protein-coupled receptors as drug targets: Methods and principles in medicinal chemistry, *Wiley-VCH*, Weinheim, **2005**.

Seifert R *et al.*: Paradoxical stimulatory effects of the “standard” histamine H_4-receptor antagonist JNJ7777120: The H_4-receptor joins the club of 7TM receptors exhibiting functional selectivity, *Mol Pharmacol*, **2011**, *79*, 631–638.

Shaner NC *et al.*: A guide to choosing fluorescent proteins, *Nat Methods*, **2005**, *2*, 905–909.

Shonberg J *et al.*: Design strategies for bivalent ligands targeting GPCRs, *ChemMedChem*, **2011**, *6*, 963–974.

Smit MJ *et al.*: Rapid desensitization of the histamine H_2 receptor on the human monocytic cell line U937, *Eur J Pharmacol*, **1994**, *288*, 17-25.

Tiligada E *et al.*: Histamine H_3 and H_4 receptors as novel drug targets, *Expert Opin Investig Drugs*, **2009**, *18*, 1519–1531.

Traiffort E *et al.*: Expression of a cloned rat histamine H_2 receptor mediating inhibition of arachidonate release and activation of cAMP accumulation, *Proc Natl Acad Sci USA*, **1992**, *89*, 2649-2653.

Valant C *et al.*: A novel mechanism of G protein-coupled receptor functional selectivity. Muscarinic partial agonist McN-A-343 as a bitopic orthosteric/allosteric ligand, *J Biol Chem*, **2008**, *283*, 29312-29321.

Venter JC *et al.*: The sequence of the human genome, *Science*, **2001**, *291*, 1304–1351. Erratum in: *Science*, **2001**, *292*, 1838.

Vilardaga J-P *et al.*: Measurement of the millisecond activation switch of G protein–coupled receptors in living cells, *Nat Biotechnol*, **2003**, *21*, 807-812.

Violin JD and Lefkowitz RJ: β-arrestin-biased ligands at seven-transmembrane receptors, *Trends Pharmacol Sci*, **2007**, *28*, 416–422.

Wenzel-Seifert K *et al.*: Similar apparent constitutive activity of human histamine H_2-receptor fused to long and short splice variants of $G_{s\alpha}$, *J Pharmacol Exp Ther*, **2001**, *299*, 1013–1020.

Xie SX *et al.*: Probing ligand-specific histamine H_1- and H_2-receptor conformations with N^G-acylated imidazolylpropylguanidines, *J Pharmacol Exp Ther*, **2006**, *317*, 139–146.

Ziemek R: Development of binding and functional assays for the neuropeptide Y Y_2 and Y_4 receptors, Doctoral thesis, University of Regensburg, **2006**.

Chapter 2

Scope and Objectives

2 Scope and Objectives

Membranal proteins as members of the family of G-protein-coupled receptors (GPCR) comprise a significant part of the druggable human genome. A well known and widely accepted pharmacological paradigm for this receptor class states that an elementary unit required for signal transduction in the cell involves a sole receptor molecule, interacting *via* its unique binding site with a single pharmacophoric moiety (Lazareno, 2001). However, in the last three decades, a plethora of experimental data (for example Förster resonance energy transfer (FRET) at fluorescently labelled receptors) supported the hypothesis of dimerization of the GPCRs, including neuropeptide Y (NPY Y_xR) and histamine (H_xR) receptors (Fukushima *et al.*, 1997; Kroeger *et al.*, 2004; Ferré *et al.*, 2009). Moreover, bivalent GPCR ligands, which might be capable of simultaneously binding to the orthosteric recognition sites of dimerizing protomers, have been reported (Bhushan *et al.*, 2004; Shonberg *et al.*, 2011). Thus, in addition to labelled receptors, ligand-based approaches might contribute to gain deeper insight into GPCR dimerisation. Additionally, targeting of GPCR dimers, although requiring the revision of the classical pharmacology, could be advantageous not only for understanding (patho)physiological processes, but also with respect to pharmacotherapy.

The aim of the present work was to explore the applicability of both approaches to the investigation of histamine and neuropeptide Y (NPY) receptor subtypes as examples of aminergic and peptidergic GPCRs. The aforementioned FRET measurements, enabling the non-radioactive investigation of receptor dimerization in living cells, involve tagging of receptors to fluorescent proteins, which constitute a donor and an acceptor of a FRET pair. At the beginning of this project it was known that the transiently expressed human NPY Y_1R, C-terminally tagged with enhanced cyan or yellow fluorescent proteins (ECFP and EYFP), were still able to bind the natural ligand and transduce the signal into the cell (Dinger *et al.*, 2003).Beyond that, doctoral projects pursued in parallel at our department, were aiming at the synthesis of bivalent ligands for the Y_1R (Keller *et al.*, 2009) and the histamine H_2R and H_4R, i. e. ligands fulfilling the structural requirements for binding to putative GPCR dimers were already available or are subject of ongoing work. For example, the application of the bivalent ligand approach to acylguanidine-type H_2R agonists resulted in the most potent agents known so far (up to 4000-fold more potent than histamine), both on the isolated guinea-pig right atrium and in steady-state GTPase assays on H_2R-$G_{s\alpha s}$ fusion proteins expressed in Sf9 cells. Surprisingly, the maximum of potency was obtained for compounds with relatively short octamethylene spacers (Kraus, 2007; Birnkammer *et al.*, 2010), theoretically insufficient to bridge the receptor dimers

(Bhushan *et al.*, 2004). As the reason for this tremendous gain in potency compared to monovalent analogues was unclear, this class of compounds was selected for more detailed analyses of the binding mode. The existence of an accessory (allosteric ?) binding site on the same receptor molecule should be taken into account. It is noteworthy that allosterically acting ligands have been reported for a few GPCR types (α_{2A}-adrenoreceptors, Leppik *et al.*, 1998; muscarinic receptors, Valant *et al.*, 2008), but only studies on the opioid receptors revealed advantages of compounds, which address receptor dimers (Daniels *et al.*, 2005).

Exploring the applicability of stably expressed fluorescently labelled NPY Y_1 receptors for prospective FRET-based investigations of receptor dimerization by means of confocal microscopy (van Rheenen *et al.*, 2004), was one subject of this work. As a first step, a cell line, stably expressing either Y_1R-ECFP or Y_1R-EYFP fusion proteins, should be established. The correct membranal localization of both, the receptor and the fluorescent protein, had to be examined by using a selective Y_1R radioligand (Keller *et al.*, 2008) and fluorescent ligands (Schneider *et al.*, 2006; Schneider, Keller *et al.*, 2007). If possible, a functional assay should be performed with the ratiometric calcium-chelating dye fura-2 (Kracht, 2001).

The second part of this doctoral project focused on the detailed analysis of H_2R binding in order to learn more about the differences between mono- and bivalent acylguanidines compared to the natural ligand. Radioligand competition binding studies with selected ligands should be performed at Sf9 cell membranes expressing the human or guinea pig H_2R alone, or as fusion proteins with $G_{s\alpha S}$ (Erdmann, 2010). Due to the recently revealed one-digit nanomolar affinity of these compounds at the human H_4R (Kraus, 2007), analogous experiments could be performed using this receptor as well (Igel *et al.*, 2009). As the Hill coefficients of both, saturation and competition curves, might be good indicators of cooperativity and ligand–receptor stoichiometry, binding isotherms of the mono- and bivalent ligands had to be carefully analyzed (Hill and Scatchard plots; Kenakin, 2006). In addition, the investigation of the sensitivity of ligand binding to guanine nucleotides and the screening of various cell lines for the expression of H_2R and H_4R were considered suitable for this project.

The assumed binding mode of bivalent acylganidines may imply, apart from receptor dimerization, the ternary complex model, allosteric interactions or functional selectivity. Simultaneous occupation of both, ortho- and allosteric binding sites, should lead to an altered dissociation of an orthosteric radioligand. Hence, potential allosterism could be verified by measuring radioligand off-rate at Sf9 cell membranes, expressing H_2Rs and

H_4Rs in the presence of different ligands, by analogy to the procedure described previously for muscarinic receptors (Kostenis and Mohr, 1996).

To further elucidate the intracellular fate of H_2Rs after exposure to the bivalent ligands, H_2R endocytosis (involving β-arrestins) had to be investigated in parallel with radioligand binding studies. It was planned to express the human H_2R, tagged with red fluorescent protein in CHO cells, in order to visualize agonist-induced receptor internalization by means of confocal microscopy (Osawa *et al.*, 2005; Shcherbo *et al.*, 2009). In combination with the results from the GTPase assays (receptor-dependent G-protein activation), previously obtained in our research group, this new approach was considered to be helpful to get a hint to functional selectivity at the human H_2R (Rajagopal *et al.*, 2010).

2.1 References

Bhushan RG *et al.*: A bivalent ligand (KDN-21) reveals spinal *δ* and κ opioid receptors are organized as heterodimers that give rise to δ_1 and κ_2 phenotypes. Selective targeting of *δ*-κ heterodimers, *J Med Chem*, **2004**, *47,* 2969–2972.

Birnkammer T *et al.*: Structure-activity relationships of bivalent acylguanidine-type histamine H_2 receptor agonists, *5th Summer School "Medicinal Chemistry"*, University of Regensburg, **2010**, P4 (poster contribution).

Daniels DJ *et al.*: Opioid-induced tolerance and dependence in mice is modulated by the distance between pharmacophores in a bivalent ligand series, *Proc Natl Acad Sci U S A*, **2005**, *102*, 19208–19213.

Dinger MC *et al.*: Homodimerization of neuropeptide Y receptors investigated by fluorescence resonance energy transfer in living cells, *J Biol Chem*, **2003**, *278*, 10562–10571.

Erdmann D: Histamine H_2 and H_3 receptor antagonists: Synthesis and characterization of radiolabelled and fluorescent pharmacological tools: Doctoral thesis, University of Regensburg, **2010**.

Ferré S *et al.*: Building a new conceptual framework for receptor heteromers (commentary), *Nat Chem Biol*, **2009**, *5*, 131–134.

Fukushima Y *et al.*: Oligomer formation of histamine H_2 receptors expressed in Sf9 and COS7 cells, *FEBS Lett*, **1997**, *409*, 283–286.

Igel P *et al.*: Tritium-labeled N^1-[3-(1*H*-imidazol-4-yl)propyl]-N^2-propionylguanidine ([^{3}H]UR-PI294), a high-affinity histamine H_3 and H_4 receptor radioligand, *ChemMedChem*, **2009**, *4*, 225 – 231.

Keller M *et al.*: Bivalent argininamide-type neuropeptide Y Y_1 antagonists do not support the hypothesis of receptor dimerisation, *ChemMedChem*, **2009**, *4*, 1733–1745.

Keller M *et al.*: Guanidine-acylguanidine bioisosteric approach in the design of radioligands: synthesis of a tritium-labeled N^G-propionylargininamide ([^{3}H]-UR-MK114) as a highly potent and selective neuropeptide Y Y_1 receptor antagonist, *J Med Chem*, **2008**, *51,* 8168–8172.

Kenakin TP: A pharmacology primer. Theory, application, and methods, *Academic Press – Elsevier*, Amsterdam – Tokyo, 2006.

Kostenis E and Mohr K: Two-point kinetic experiments to quantify allosteric effects on radioligand dissociation, *Trends Pharmacol Sci*, **1996**, *17*, 280–283.

Kracht J: Bestimmung der Affinität und Aktivität subtypselektiver Histamin- und Neuropeptid Y-Rezeptorliganden an konventionellen und neuen pharmakologischen *In-vitro*-Modellen, Doctoral thesis, University of Regensburg, **2001**.

Kraus A: Highly potent, selective acylguanidine-type histamine H_2 receptor agonists: Synthesis and structure-activity relationships, Doctoral thesis, University of Regensburg, **2007**.

Kroeger KM *et al.*: G-protein coupled receptor oligomerization in neuroendocrine pathways, *Front Neuroendocrinol*, **2004**, *24*, 254–278.

Lazareno S: Quantification of receptor interactions using binding methods, *J Recept Signal Transduct Res*, **2001**, *21*, 139–165.

Leppik RA *et al.*: Characterization of the allosteric interactions between antagonists and amiloride analogues at the human α_{2A}-adrenergic receptor, *Mol Pharmacol*, **1998**, *53*, 916-925.

Maurel D *et al.*: Cell-surface protein-protein interaction analysis with time-resolved FRET and snap-tag technologies: application to GPCR oligomerization, *Nat Methods*, **2008**, *6*, 561-567.

Osawa S *et al.*: Alteration of intracellular histamine H_2 receptor cycling precedes antagonist-induced upregulation, *Am J Physiol Gastrointest Liver Physiol*, **2005**, *289*, G880-G889.

Rajagopal S *et al.*: Teaching old receptors new tricks: biasing seven-transmembrane receptors, *Nat Rev Drug Discov*, **2010**, *9*, 373-386.

Schneider E, Keller M *et al.*, Synthesis and characterization of the first fluorescent non-peptide NPY Y1 receptor antagonist, *ChemBioChem*, **2007**, *8*, 1981–1988.

Schneider E *et al.*: A simple and powerful flow cytometric method for the simultaneous determination of multiple parameters at G protein-coupled receptor subtypes, *ChemBioChem*, **2006**, *7*, 1400–1409.

Shcherbo D *et al.*: Far-red fluorescent tags for protein imaging in living tissues, *Biochem J*, **2009**, *418*, 567–574.

Shonberg J *et al.*: Design strategies for bivalent ligands targeting GPCRs, *ChemMedChem*, **2011**, *6*, 963–974.

Valant C *et al.*: A novel mechanism of G protein-coupled receptor functional selectivity. Muscarinic partial agonist McN-A-343 as a bitopic orthosteric/allosteric ligand, *J Biol Chem*, **2008**, 283, 29312-29321.

van Rheenen J *et al.*: Correcting confocal acquisition to optimize imaging of fluorescence resonance energy transfer by sensitized emission, *Biophys J*, **2004**, *86*, 2517-2529.

Chapter 3

Stable expression of neuropeptide Y Y_1 receptors tagged with fluorescent proteins for the FRET-based investigation of receptor dimerization

3 Stable expression of neuropeptide Y Y_1 receptors tagged with fluorescent proteins for the FRET-based investigation of receptor dimerization

3.1 Introduction

Fluorescence-based techniques, especially fluorescence resonance energy transfer (FRET), have been used for the investigation of dimerization among numerous types of GPCRs, including NPY Y_1 receptors (Dinger *et al.*, 2003; Kroeger *et al.*, 2004; Hébert *et al.*, 2006; Ferré *et al.*, 2009). The hypothesis that receptor dimers can participate in trafficking, signal transduction and recycling (Smith and Milligan, 2010) has been gaining ever broader recognition for the last three decades, as an extremely challenging concept for both the molecular pharmacology and the drug design. The aforementioned FRET measurements require tagging of receptors to fluorescent proteins which constitute a donor and an acceptor of a FRET pair. When donor (ECFP) and acceptor (EYFP) molecules are in spatial proximity (most probably due to the interaction between two receptors; Fig. 3.1.1 A), the measurement of a FRET signal should be possible, enabling the non-radioactive investigation of receptor dimerization in living cells (Milligan and Bouvier, 2005). Moreover, transiently expressed NPY Y_1 receptors C-terminally tagged with enhanced cyan or yellow fluorescent proteins (ECFP and EYFP) have been previously reported to be able to bind the natural ligand and to remain functional (Dinger *et al.*, 2003). However, there is a very serious limitation of this method, namely that FRET signals come not exclusively from the cell membrane, but can also arise in cellular compartments (Maurel *et al.*, 2008) due to intracellular fluorophore interaction.

3.1.1 RET-based assays for the investigation of receptor dimerization

3.1.1.1 FRET between GPCRs tagged with fluorescent proteins

As mentioned in subsection 1.3.2, tagging with fluorescent proteins is a very attractive method for the detection of protein trafficking in living cells, as these fluorophores are genetically encoded and no additional chemical modification of the cells is needed. ECFP and EYFP are suited for the investigation of direct protein-protein interactions, involving FRET measurements, due to spectral overlap (Fig. 3.1.1 B). The experimental

setup requires an external source of light, proper for the excitation of the donor. In the absence of acceptor molecules, the excited donor fluoresces in the region of spectrum which is typical for the ECFP emission. However, when donor and acceptor molecules are in close spatial proximity (Förster radius, usually less than 10 nm), the energy of the ECFP can be transduced in a non-radiative manner onto the EYFP. As a result, the excited acceptor molecules emit the light of the wavelength, characteristic for EYFP emission (Milligan and Bouvier, 2005). Fluorescence signals can be detected by means of fluorimetry or confocal microscopy and converted into FRET signals. Other combinations of fluorophores for FRET are also possible (Pfleger and Eidne, 2005), including green or yellow fluorescing donors (e.g. GFP or fluorescein isothiocyanate FITC) and red fluorescing acceptors (e.g. RFP/DsRed or rhodamine derivatives like Texas Red).

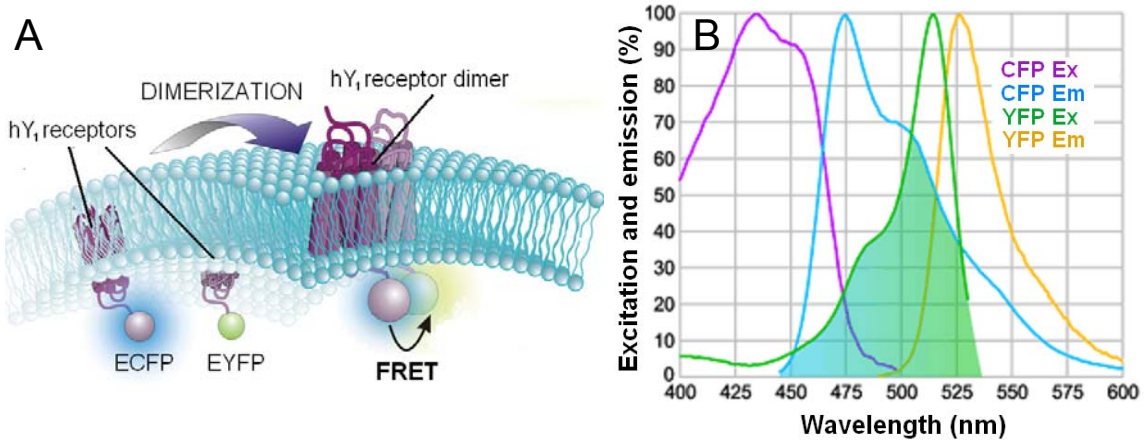

Fig. 3.1.1. *ECFP and EYFP as a donor-acceptor FRET pair in receptor dimerization studies: (A) FRET signal resulting from receptor dimerization (adopted from Pfleger and Eidne, 2005 with modifications), (B) the excitation and emission spectra of ECFP and EYFP – the overlapping part of the ECFP emission and the EYFP excitation is shown in green (adopted from http://www.semrock.com/fret.aspx with modifications).*

3.1.1.2 BRET-based experiments

Another method for investigation of GPCR dimerization, utilizing fluorescent proteins as acceptors, is bioluminescence resonance energy transfer (BRET). In contrast to FRET, an external light source is not required in this technique, because the excitation is provided by photochemical reactions catalyzed by *Renilla* luciferase-coupled donors. Thus, BRET is characterized by a relatively simple experimental setup and the lack of photobleaching, which is a common problem for FRET. As a consequence of the negligible autofluorescence, BRET measurements provide a higher signal-to-noise ratio than those based on FRET (Milligan, 2004), but the addition of a substrate for the photochemical reaction is mandatory.

3.2 Materials and methods

3.2.1 Materials

The hY_1R-pECFP-N1 and hY_1R-pEYFP-N1 plasmids (Dinger *et al.*, 2003) were kind gifts from Prof. Dr. Annette G. Beck-Sickinger (University of Leipzig, Germany), whereas the pECFP-Mito, pQCXIP/ECFP-Mem and pEYFP-N1 plasmids were from Dr. Dietmar Gross (University of Regensburg).

RNase A (100 µg/mL), Mass Ruler DNA Ladder mix, *EcoR*I (10 U/µL), *Not*I (10 U/µL), 6x Loading Dye, 10x "O" (orange) buffer and 10x Tango buffer were purchased from MBI Fermentas (St. Leon-Rot, Germany) and 10x BSA (0.1%) solution was from Amersham Pharmacia Biotech (Piscataway, NJ, USA). Gel chambers of the PerfectBlue Mini S gel system and agarose were from Peqlab (Erlangen, Germany). Ethidium bromide solution was obtained from Janssen Chimica (Beerse, Belgium). Tris·HCl was from Serva (Heidelberg, Germany), whereas tris base was from USB (Cleveland, OH, USA). NaOH, KAc, glacial acetic acid and EDTA (obtained as Titriplex III) were from Merck (Darmstadt, Germany). Phenol-chloroform-isoamylalcohol (25:24:1) was from Carl Roth (Karlsruhe, Germany). Ethanol was from Mallinckrodt Baker (Griesheim, Germany). SDS and kanamycin was from Sigma-Aldrich (Steinheim, Germany). QIAquick Gel Extraction and QIAGEN Plasmid Maxi kits were from QIAGEN (Hilden, Germany).

CHO cells were from the DSMZ (Deutsche Sammlung für Mikroorganismen und Zellkulturen, Braunschweig, Germany), whereas A-431, MCF-7, U-118 MG and U-373 MG cells were purchased from the ATCC (American Type Culture Collection; Manassas, VA, USA). MCF-7-Y_1 cells (a MCF-7 subclone with higher Y_1 receptor expression) were recently established in our laboratory (Keller, 2008; Memminger, 2009). FuGENE 6 and HD transfection reagents were from Roche Diagnostics (Mannheim, Germany), whereas Lipofectamine 2000 was from Invitrogen (Karlsruhe, Germany). Ham's nutrient mixture F12, Eagle's minimum essential medium (EMEM), Dulbecco´s minimum essential medium (DMEM) and stabilized penicillin−streptomycin−neomycin solution were purchased from Sigma-Aldrich. Fetal calf serum (FCS) and geneticin (G418) were from Biochrom (Berlin, Germany). Trypsin-EDTA (10x) was from PAA Laboratories (Pasching, Austria).

The NPY Y_1R selective ligands: BIBP 3226, the fluorescent ligands UR-MK115 and UR-MK131 as well as the radioligand N^{ω}-([2,3-^{3}H]propionyl)-BIBP 3226 ([^{3}H]UR-MK114; 1.9 TBq/mmol) were synthesized by Dr. Max Keller as described previously (Fig. 1.2.2; Keller, 2008; Keller *et al.*, 2008). The fluorescent ligands Dy-635-pNPY and Cy5-pNPY

were synthesized by Dr. Erich Schneider (Fig. 1.2.1; Schneider, 2005; Schneider *et al.*, 2006). The pNPY was kindly provided by Prof. Dr. Chiara Cabrele (Ruhruniversität Bochum). HEPES was from Serva (Heidelberg, Germany). NaCl, KCl, $CaCl_2 \cdot 2H_2O$, KH_2PO_4, $MgCl_2 \cdot 6H_2O$, $MgSO_4 \cdot 7H_2O$, $NaHCO_3$, urea, glacial acetic acid and 1 N NaOH were from Merck. BSA, bacitracin and Triton-X-100 were from Sigma (Deisenhofen, Germany). The 8-well Lab-Tek chambers were from Nunc (Wiesbaden, Germany). Leibovitz's L-15 medium without phenol red and fura-2/AM were from Invitrogen. LysoTracker Green DND-26 was purchased from Invitrogen (Molecular Probes; Eugene, OR, USA) and DRAQ5 was from Biostatus Limited (Leicestershire, UK). Microscopic images were taken with a Carl Zeiss Axiovert 200M LSM510 confocal laser-scanning microscope (Oberkochen, Germany).

3.2.2 Transformation of bacteria and preparation of plasmids

3.2.2.1 Transformation of bacteria

The transformation of competent *E. coli* bacteria (TOP10 strain) was conducted as in subsection 6.2.3 with minor modifications. Briefly, 25 ng (10 µL) of either the hY_1R-pECFP-N1 or hY_1R-pEYFP-N1 plasmid (Fig. 3.2.1) were added to 100 µL of bacterial suspension and incubated with SOC medium at 37 °C for 1 hour under shaking at 150 rpm. The transformed bacteria were plated on an agar plate containing kanamycin (30 µg/mL) for selection, as both vectors enclose a *kanamycin/neomycin resistance* gene. Subsequently, the agar plates were incubated overnight at 37 °C.

3.2.2.2 Mini-Prep

For each plasmid used for transfection, one colony was picked from the bacteria grown on the selective agar plate to inoculate 5 mL of LB medium, containing 30 µg/mL kanamycin. After overnight incubation at 37 °C under shaking at 250 rpm, the suspensions were centrifuged for 1 min at 13,000 rpm. To purify the DNA samples, small-scale alkaline lysis (Mini-Prep) was performed in parallel (3 x 1.5 mL of each bacterial suspension) as described before by Dr. Nathalie Pop (Pop, 2010). DNA concentration was measured by UV spectroscopy: the concentration of aqueous solution of double-stranded DNA in µg/mL was calculated from absorbance at 260 nm A_{260} and dilution factor F, according to Eq. 3.2.1.

$$c_{DNA}\left[\frac{\mu g}{mL}\right] = A_{260} \cdot F \cdot 50 \qquad \text{(Eq. 3.2.1)}$$

The purity was considered sufficient if the ratio of absorbances measured at 260 nm and 280 nm A_{260}/A_{280} was higher than 1.5. The purified plasmids were stored at -20 °C until use for transformation.

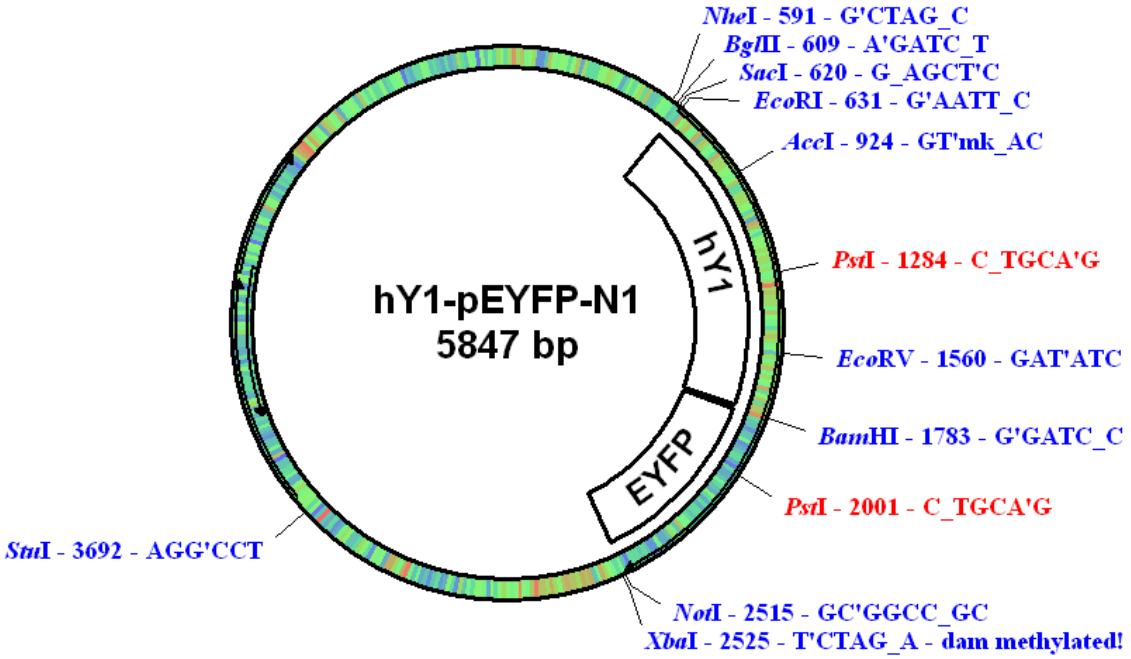

Fig. 3.2.1. *Map of the unique restriction sites for enzymatic digest of the hY_1R-pEYFP-N1 plasmid (as generated by the pDRAW32 programm). The hY_1R-pECFP-N1 plasmid contains the sequence of ECFP instead of EYFP.*

3.2.2.3 Restriction analysis and agarose gel electrophoresis

Double digestion of both plasmids was performed in a final volume of 15 µL under following conditions: 1 µL of either the hY_1R-pECFP-N1 or hY_1R-pEYFP-N1 plasmid was added to 10.5 µL of Millipore water. The mixture was supplied with 1.5 µL of 10x "O" (orange) buffer, 1 µL of *EcoR*I (10 U/µL) and 1 µL of *Not*I (10 U/µL). The samples were mixed, shortly centrifuged and incubated for 1 hour at 37 °C. Thereafter, 3 µL of 6x loading dye were added and the samples were mixed.

Agarose gel electrophoresis was performed as described in subsection 6.2.2.2. Briefly, 18 µL of each DNA sample as well as 10 µL of ready-to-use MassRuler DNA Ladder Mix (for reference) were pipetted to separate pockets of the 1.5% agarose gel. The voltage (90 V) was supplied and the gel was running for approx. 50 min. The separated DNA bands were visualized by transillumination at 254 nm while using the Quantity One soft-

ware (Gel Doc 2000; Bio-Rad Laboratories, Munich, Germany). The illumination of the analytic gel revealed the expected lengths (cf. Fig. 3.2.1) of the digested *EcoR*I-hY$_1$R-ECFP(EYFP)-*Not*I fragment (1900 bp) as shown in Fig. 3.2.2.

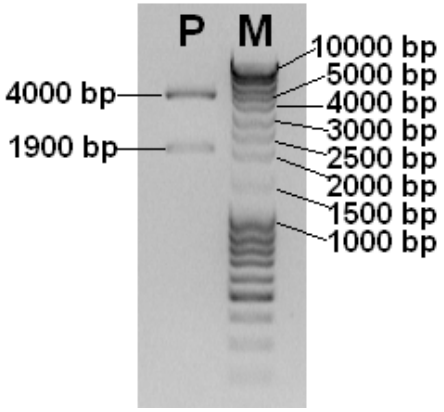

Fig. 3.2.2. *The digested Mini-Prep product (P) contained EcoRI-hY$_1$R-ECFP-NotI fragment (1900 bp) and the rest of the vector (4000 bp). The MassRuler DNA Ladder Mix was used as a DNA marker (M).*

Additionally, the fragments of the purified plasmids encoding the hY$_1$R, ECFP and EYFP were inspected by sequencing, performed by Entelechon (Regensburg, Germany), using the following primers:

- for hY$_1$R-pECFP:
  - pEGFP-N1-fwd (forward: annealing upstream of the hY$_1$R gene),
  - pEGFP-N1-rwd (reverse: annealing at the beginning of the ECFP gene),
  - pECFP-C1-rev (reverse: annealing downstream of the ECFP gene);
- for hY$_1$R-pEYFP:
  - pECFP-N1-fwd (forward: annealing upstream of the hY$_1$R gene),
  - pECFP-N1-rwd (reverse: annealing at the beginning of the EYFP gene),
  - pECFP-C1-rev (reverse: annealing downstream of the EYFP gene).

In both plasmids, the sequences of the hY$_1$R and the fluorescent protein were identically equal to those from Prof. Dr. A. Beck-Sickinger (University of Leipzig, Germany).

3.2.3 Cell culture and transfection

3.2.3.1 Cell culture

To prepare 1 L of trypsin, 100 mL of 10-fold trypsin-EDTA solution were diluted in 900 mL PBS, sterile filtered and stored at -20 °C in 50-mL or 100-mL aliquots.

Cells were maintained in the culture media listed in Table 3.2.1 at 37 °C in the humidified atmosphere containing 5% CO_2. Every 4–7 days, cells were trypsinized and passaged (1:10) to a fresh 25-cm^2 culture flask.

Table 3.2.1. *Cell culture conditions.*

Cell line	Cell culture conditions
A-431	EMEM + 5% FCS (Guiswé, 2000)
A-431 hY_1R-EYFP	EMEM + 5% FCS + 400 or 750 µg/mL G418
CHO-K1	Ham's F12 + 10% FCS
U-118 MG	DMEM + 5% FCS (Müller, 2007)
U-118 hY_1R-ECFP	DMEM + 5% FCS + 400 µg/mL G418
U-373 MG	EMEM + 5% FCS (Müller, 2007)
U-373 hY_1R-ECFP	EMEM + 5% FCS + 400 or 750 µg/mL G418
U-373 hY_1R-EYFP	EMEM + 5% FCS + 400 or 750 µg/mL G418

3.2.3.2 Stable transfection

Two days prior to transfection, the glioblastoma/astrocytoma U-373 MG cells were seeded in a 24-well plate. The confluent cells were transfected with the mammalian expression vectors hY_1R-pECFP-N1 or hY_1R-pEYFP-N1 using the FuGENE 6, the FuGENE HD or the Lipofectamine 2000 transfection reagent in different reagent-to-plasmid DNA ratios according to manufacturer's instructions. Lipofectamine revealed to be not suitable for transfection as it was toxic. The obtained stable transfectant clones of U-373 cells were selected as described in subsection 6.2.5, using 400 or 750 µg/mL G418, and subsequently tested in fluorimetric calcium assays as well as in radioligand and flow cytometric binding studies. Also the glioblastoma/astrocytoma U-118 MG and the skin epidermoid carcinoma A-431 cells were used for the transfection with the hY_1R-pECFP-N1 or hY_1R-pEYFP-N1 plasmid, respectively. The resulting transfectant clones were tested in preliminary radioligand binding studies (not shown) and illuminated by means of CLSM, but they were not suitable for further cultivation (A-431 cells were resistant to trypsin, whereas U-118 MG cells did not grow in monolayers).

3.2.3.3 Transient transfection

CHO-K1 and U-373 MG cells were transfected with the localization vector pECFP-Mito and/or the retroviral expression vector pQCXIP/ECFP-Mem (Gross, 2006) as positive controls for mitochondrial and membranal expression of ECFP, respectively. U-373 MG cells were transfected with pEYFP-N1 plasmid for the cytosolic expression of EYFP (control for microscope settings). Two days prior to transfection, the cells were seeded in 8-well Lab-Tek chambers (approx. 65,000 cells per well) and cultivated without antibiotics. Transfection was performed with 1 µL of FuGENE 6 and 250 ng of the appropriate plasmid per well. The cells were imaged (CLSM) on the next day.

3.2.4 Radioligand binding on intact cells

Binding buffer was prepared as described before (cf. buffer I, Kracht, 2001) by dissolving 2.38 g of HEPES (10 mM), 8.77 g of NaCl (150 mM), 373 mg of KCl (5 mM), 368 mg of $CaCl_2 \cdot 2H_2O$ (2.5 mM $CaCl_2$), 163 mg of KH_2PO_4 (1.2 mM), 296 mg of $MgSO_4 \cdot 7H_2O$ (1.2 mM $MgSO_4$) and 2.1 g of $NaHCO_3$ (25 mM) in 1 L of Millipore water. After pH was adjusted to 7.4, using 1 N NaOH, the solution was sterile filtered and stored at 4 °C until use. For the preparation of 500 mL of lysis solution (Keller, 2008), 240.2 g of urea (8 M), 85.8 mL of acetic acid (3 M) and 6 mL of Triton-X-100 (1% m/m) were dissolved in Millipore water.

Radioligand binding assays were performed in triplicate according to the protocol used in our research group (Aiglstorfer *et al.*, 1998; Keller *et al.*, 2009) with minor modifications. Two days prior to the binding assay, cells were seeded in 24-well plates. On the day of experiment, confluent cells were carefully washed (2 x 300 µL) with binding buffer and covered with 200 µL of binding buffer containing 1% BSA and 0.01% (m/v) bacitracin (added in order to prevent the peptide ligand pNPY from adsorption and protease-mediated degradation, respectively). Then 25 µL of binding buffer (for total binding) or 25 µL of pNPY (1.8 µM final, for unspecific binding) were added to each well. After 3 min of preincubation, the samples were completed by addition of 25 µL of N^{ω}-([2,3-^{3}H]propionyl)-BIBP 3226 ([^{3}H]UR-MK114) to yield a final concentration of 6 nM and incubated for 12 min at room temperature (20–23 ºC). The binding buffer was removed by aspiration and the cells were gently washed (2 x 500 µL) with ice-cold binding buffer (approx. 20 s). Finally, 200 µL of lysis solution were added to each well and the plates were incubated for at least 30 min under gentle shaking. The lysates were transferred into scintillation vials (filled with 3 mL of scintillator). The wells were washed with 100 µL

of lysis solution and the lysates were transferred into the vials. Samples were measured for 5 min in a LS 6500 Liquid Scintillation Counter from Beckman Coulter (Krefeld, Germany). The hY_1R number/cell was calculated by using the specific radioactivity of radioligand (cf. Eq. 4.2.2).

3.2.5 Flow cytometric binding and cell sorting

3.2.5.1 Binding assays

Binding buffer for flow cytometry was prepared as described before (Sheikh and Williams, 1990; cf. buffer II, Kracht, 2001; Ziemek, 2006) by dissolving 5.95 g of HEPES (25 mM), 368 mg of $CaCl_2 \cdot 2H_2O$ (2.5 mM $CaCl_2$) and 203 mg of $MgCl_2 \cdot 6H_2O$ (1 mM $MgCl_2$) in 1 L of Millipore water. After pH was adjusted to 7.4 using 1 N NaOH, the solution was sterile filtered and stored at 4 °C until use.

Flow cytometric binding assays were performed as described previously by Dr. Ralf Ziemek (Ziemek, 2006) with minor modifications. Briefly, 4–6 days prior to the experiment, the stably transfected cells were seeded in 1–3 fresh 175-cm^2 culture flasks in medium without antibiotics. On the day of the experiment, the cells were trypsinized and centrifuged for 5 min at 1000 rpm (300 g) with a Minifuge RF from Heraeus Sepatech (Osterode, Germany). The pelleted cells were washed with binding buffer and centrifuged again. Subsequently, the cells were resuspended in fresh binding buffer containing 1% BSA and 0.01% (m/v) bacitracin (cf. subsection 3.2.4) to obtain the required density of 1 million cells per mL. For unspecific binding, 5 µL of the porcine NPY (800 nM final) or BIBP 3226 solution (1 µM or 10 µM final) were pipetted to siliconized 1.5-mL reaction vessels, whereas 5 µL of the appropriate solvent were used for total binding. Thereafter, 490 µL of the cell suspension were added and incubated for 2 hours with 5 µL of Dy-635-pNPY (8 nM final) under gentle shaking (light protected). Samples were measured in a FACSCalibur flow cytometer from Becton Dickinson (Heidelberg, Germany). The acquired data (fluorescence from Fl-4 channel) were processed with WinMDI2.9 software (Phoenix, AZ, USA).

3.2.5.2 Cell sorting (FACS)

The U-373 hY_1R-ECFP cells were sorted by Dr. Louay Jouma (Institute of Immunology, University Regensburg) using a BD FACSAria cell sorter, equipped with a 407 nm violet laser and 450/40 nm BP filter (Pacific blue filter sets, cf. the excitation and emission spectra of ECFP in Fig. 3.1.1 B). Four days prior to sorting, the wild-type and the transfected U-373 cells (in presence of G418) were seeded in a 75-cm^2 and a 25-cm^2 culture flask, respectively. On the day of the experiment, the cells were trypsinized, centrifuged at 300 g for 7 min (at 4 °C) and suspended in PBS (phosphate buffered saline) with 2% FCS to obtain the density of 2–3 million cells per mL. A FSC/SSC gate was set for the wild-type U-373 MG cells, and the U-373 hY_1R-ECFP cells were sorted into 1 mL of FCS (100%) according to the fluorescence signal of ECFP. The sorted cells (15,000 events) were put on ice, centrifuged and suspended in culture medium with 5% FCS and 400 µg/mL G418. Finally, the cells were seeded in one well of a 96-well plate.

The U-373 hY_1R-EYFP cells were sorted with a Becton Dickinson FACSCalibur flow cytometer according to the manufacturer's instructions, using the FACSComp software. Briefly, 5 days prior to sorting, the cells were seeded in a 75-cm^2 culture flask in presence of G418. Additionally, 5 L of PBS were prepared and sterile filtered. One day before sorting, four 50-mL tubes were filled with sterile 4% BSA and stored at 4 °C. On the day of the sorting, 4% BSA was replaced with EMEM containing 25% FCS (5 mL in each tube). The flow cytometer was sterilized with 70% ethanol and washed with sterile PBS. The freshly trypsinized cells were centrifuged for 5 min at 1000 rpm (300 g) and suspended in sterile PBS to obtain the density of 1 million cells per mL (17 million cells). The cells were sorted in the 'single cell' mode (approx. 120,000 events) into the prepared 50-mL tubes with EMEM and 25% FCS, using fluorescence from Fl-1 channel (488 nm argon laser, 530/30 BP filter; cf. the excitation and emission spectra of EYFP in Fig. 3.1.1 B). The wild-type U-373 cells were used to set up a FSC/SSC gate. After successful sorting, the tubes with the hY_1R-EYFP cells were put on ice and centrifuged at 300 g for 10 min. The resulting cell pellets were suspended in culture medium with 20% FCS and seeded in a 12.5-cm^2 flask. After reaching confluence, the cells were passaged into a 25-cm^2 culture flask. To prevent contaminations, a mixture of penicillin (100 U/mL), streptomycin (100 µg/mL) and neomycin (200 µg/mL) was added to culture medium for approx. 3 weeks after sorting (Lindl, 2000).

3.2.6 Fluorescence-based ratiometric calcium assays

The stably transfected cells were loaded with fura-2/AM as described by Dr. Erich Schneider (Schneider, 2005). Samples were excited alternately at 340 and 380 nm and fluorescence was detected at 510 nm using a LS 50 B Luminescence Spectrometer from Perkin Elmer (Überlingen, Germany). Fluorescence intensity ratios R were counted as F_{340}/F_{380} and the intracellular Ca^{2+} concentration was calculated according to the Grynkiewicz equation (Eq. 3.2.2; Grynkiewicz *et al.*, 1985):

$$\left[Ca^{2+}\right] = K_d \cdot \frac{(R - R_{min})}{(R_{max} - R)} \cdot SFB \qquad \text{(Eq. 3.2.2)}$$

where K_d (dissociation constant of fura-2-Ca^{2+} complex; 224 nM) is the concentration of calcium at which 50% of fura-2 molecules bind calcium ions and R, R_{min} as well as R_{max} are ratios measured at different Ca^{2+} concentrations (at a Ca^{2+} concentration to be determined, in absence of Ca^{2+} and in presence of a saturating Ca^{2+} concentration, respectively). The SFB value, determined while calibration, is the ratio of fluorescence intensities of calcium-free and calcium-bound fura-2 at 380 nm.

3.2.7 Confocal microscopy experiments

3.2.7.1 Preparation of specimens

Cells were seeded in 8-well Lab-Tek chambers 2 days before imaging (Gross, 2006) and cultivated without antibiotics at 37 °C in the humidified atmosphere with 5% CO_2 (cf. subsection 6.2.6.1). For experiments with MCF-7-Y_1 cells, 1 nM estrogen (1:000 dilution of 1 µM solution in ethanol) was added to culture medium (Keller, 2008; Memminger, 2009). Shortly before imaging, culture medium was carefully changed to Leibowitz's L-15 medium. For better orientation, the cell nuclei were stained with the red nuclear dye DRAQ5 at a final concentration of 5 µM (1:1000 dilutions in L-15). The nuclei were visible already 5 min after staining; no washing was required. Appropriate controls (unstained cells) were performed to exclude the possibility of cross-talk and bleed-through between fluorophores. For binding studies with fluorescent Y_1R ligands, cells were covered with 240 µL of L-15 medium. Than 80 µL of either BIBP 3226 (for unspecific binding, final 5 µM) or Millipore water (for total binding) were used. Finally, the samples were completed by addition of 80 µL of a 5-fold concentrated solution of an appropriate fluorescent ligand in L-15 medium and incubated at room temperature (20 °C) in the dark. Non-

peptide fluorescent Y_1R antagonists were solved in 100% DMSO and stored at -80 °C (1 or 2 mM stock solutions; cf. Keller, 2008). Therefore, for microscopic binding studies, 5-fold concentrated solutions of those ligands in L-15 were prepared freshly from 10 µM auxiliary solutions in 20% DMSO. Specimens were investigated with a Carl Zeiss Axiovert 200M LSM510 microscope.

3.2.7.2 Microscope settings

For imaging of ECFP, the excitation line of an argon ion laser (Ar) of 458 nm (transmission >86%), a 458 nm main dichroic beam splitter (HauptFarbTeiler, HFT) and a 475 nm long-pass (LP) or a 475–525 nm band-pass (BP) filter were used. If not otherwise stated, EYFP was detected with FITC filter sets: a 488 nm excitation line of an Ar laser (transmission of 3-12%), a 488 nm HFT, a 515 nm secondary dichroic beam splitter (NebenFarbTeiler, NFT) and a 505–550 nm BP filter (cf. the excitation and emission spectra of ECFP and EYFP in Fig. 3.1.1 B). For the fluorescent proteins in combination with the red nuclear counterstain DRAQ5, a helium ion laser of 543 nm (transmission of 37%), a 458/543 nm HFT, a 545 nm NFT and a 650 nm LP filter were additionally used, using the multi-track facility of the CLSM (with switching of Ar and HeNe lasers after each frame). Fluorescence of the fluorescent ligand UR-MK115 was detected using the 488 nm excitation line of an Ar laser (5% transmission), a 488 nm HFT, a 515 nm or a 545 nm NFT and a 650 LP filter, whereas for binding studies with the non-peptide UR-MK131 and the peptide Cy5-pNPY fluorescent ligands a 633 nm excitation line of HeNe laser (14% transmission), a UV/488/543/633 nm HFT and a 650 nm LP filter were used (multi-track acquisition mode).

3.3 Results and discussion

The FRET-based investigations of receptor dimerization require comparable expression levels of the receptors fluorescently labelled with donor (e.g. ECFP) and acceptor (e.g. EYFP) molecules simultaneously in the same cell (Dinger *et al.*, 2003; Carrillo *et al.*, 2004). However, in order to prove proper expression and functionality of the fusion proteins, the U-373 MG (HTB-17) glioblastoma/astrocytoma cells were transfected exclusively with either the hY_1R-pECFP-N1 or the hY_1R-pEYFP-N1 plasmid (single labelling, controls). To quantify the expression level of the hY_1R tagged with either ECFP or EYFP, stably transfected U-373 cells were investigated with a selective hY_1R radioligand (Keller *et al.*, 2008) and fluorescent ligands by means of flow cytometry (Schneider, Keller *et al.*, 2007). As the wild-type U-373 MG cells utilize calcium ions as a second messenger (Kracht, 2001), it was also possible to perform a functional assay, using the calcium-chelating dye fura-2 (Schneider, 2005). Finally, confocal microscopy imaging (CLSM) enabled the detection of the subcellular localization of the hY_1R-ECFP and the hY_1R-EYFP fusion proteins in the transfected U-373 and in other cell lines (A-431, U-118 and CHO).

3.3.1 Stable expression of the functionally active NPY Y_1R tagged with ECFP and EYFP

3.3.1.1 Radioligand binding

The quantification of hY_1R binding sites on the cells expressing the fusion proteins was performed with a selective neuropeptide Y Y_1 receptor radioligand synthesized in our research group by Dr. Max Keller (Keller, 2008). In previous studies, the tritium-labeled N^G-propionylargininamide UR-MK114, structurally derived from the selective NPY Y_1 receptor antagonist BIBP 3226 (Aiglstorfer *et al.*, 1998), revealed excellent one-digit nanomolar affinity (K_d values: 2.9 ± 0.4 nM on MCF-7 cells; 1.2 ± 0.1 nM on SK-N-MC cells), achieving saturation of the receptors already at a concentration of approx. 4 nM (Keller *et al.*, 2008). Therefore, a radioligand concentration of 6 nM was chosen for the estimation of hY_1R expression to saturate the binding sites. Significant specific binding of the radioligand was found in both the transfected U-373 hY_1R-ECFP and U-373 hY_1R-EYFP cells. The measured values of bound radioactivity per cell were converted into receptor number per cell, using the specific activity of the radioligand (cf. Eq. 4.2.2). Among the cells expressing hY_1R-ECFP fusion proteins, the highest receptor density

was obtained for the transfectant clones 1 and 4, corresponding to 35,000 and 90,000 receptors per cell, respectively (Table 3.3.1 and Fig. 3.3.1). Similarly, radioligand binding confirmed the presence of Y_1R binding sites on the U-373 hY_1R-EYFP cells, with the highest density of 30,000 and 40,000 receptors per cell for the clones 7 and 10, respectively (Table 3.3.2 and Fig. 3.3.2).

Table 3.3.1. *Different U-373 hY_1R-ECFP cell clones and conditions for their stable selection. The transfectant clones were used for binding experiments as shown in Fig. 3.3.1.*

U-373 hY_1R-ECFP transfectant clone	Transfectant reagent	FuGENE:DNA ratio [µL:µg]	Concentration of G418 [µg/mL]
1	**FuGENE 6**	**6:2**	**750**
2	FuGENE 6	8:2	750
3	FuGENE HD	8:2	400
4	**FuGENE 6**	**10:2**	**400**

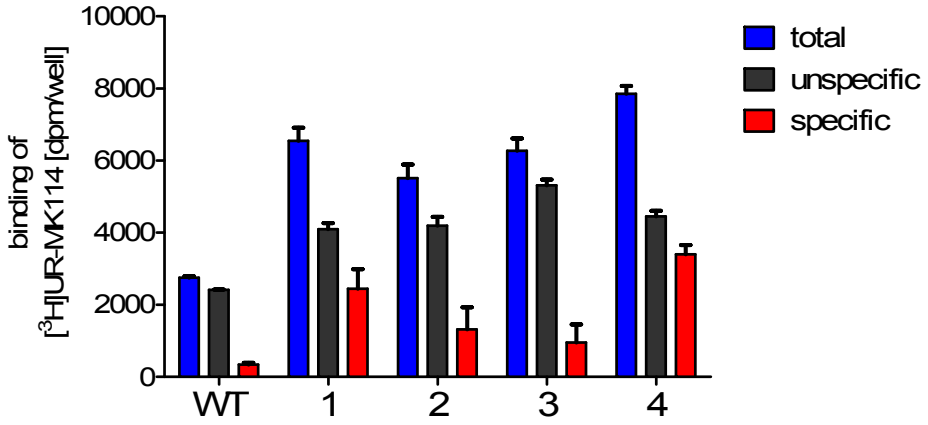

Fig. 3.3.1. *Binding of 6 nM [^{3}H]UR-MK114 on wild-type (WT) and transfected U-373 cells expressing hY_1R-ECFP (different transfectant clones 1–4, see Table 3.3.1). Data are mean values ± SEM of an experiment performed in 3–6 replicates for each clone.*

Table 3.3.2. *Different U-373 hY$_1$R-EYFP cell clones and conditions for their stable selection. The transfectant clones were used for binding experiments shown in Fig. 3.3.2.*

U-373 hY$_1$R-EYFP transfectant clone	Transfectant reagent	FuGENE:DNA ratio [µL:µg]	Concentration of G418 [µg/mL]
5	FuGENE HD	6:4	750
6	FuGENE HD	8:4	750
7	**FuGENE 6**	**6:4**	**750**
8	FuGENE 6	8:4	750
9	FuGENE 6	8:4	400
10	**FuGENE 6**	**6:4**	**400**

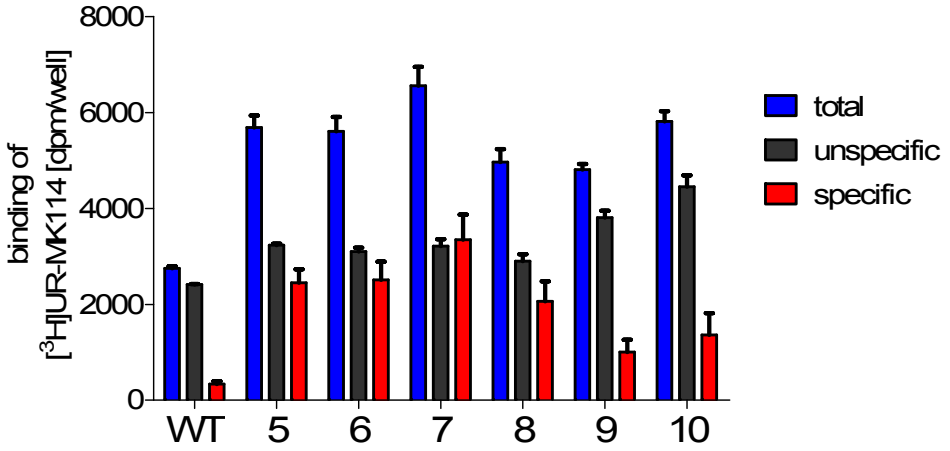

Fig. 3.3.2. *Binding of 6 nM [^{3}H]UR-MK114 on wild-type (WT) and transfected U-373 cells expressing hY$_1$R-EYFP (different transfectant clones 5–10, see Table 3.3.2). Data are mean values ± SEM of an experiment performed for each clone in triplicate (wild-type cells) or sextuplicate (clones 5–10).*

Table 3.3.3 and Fig 3.3.3 show the expression levels of the hY$_1$R-ECFP and hY$_1$R-EYFP fusion proteins for the best transfectant clones. After sorting of the U-373 hY$_1$R-EYFP cells according to the fluorescence signal of EYFP (as described under 3.2.5), the number of the radioligand binding sites increased. This result correlated with the data from flow cytometric binding assays (cf. Fig. 3.3.6).

Table 3.3.3. *Estimation of hY_1R number per cell for the best transfectant clones (calculated according to Eq. 4.2.2, using the binding data from Fig. 3.3.3).*

	U-373 cell clone (n=6)	Cells/well	Receptors/well
A	**hY_1R-ECFP**	192,000	90,000
B1	**hY_1R-EYFP before FACS**	287,000	30,000
B2	**hY_1R-EYFP after FACS**	189,000	70,000

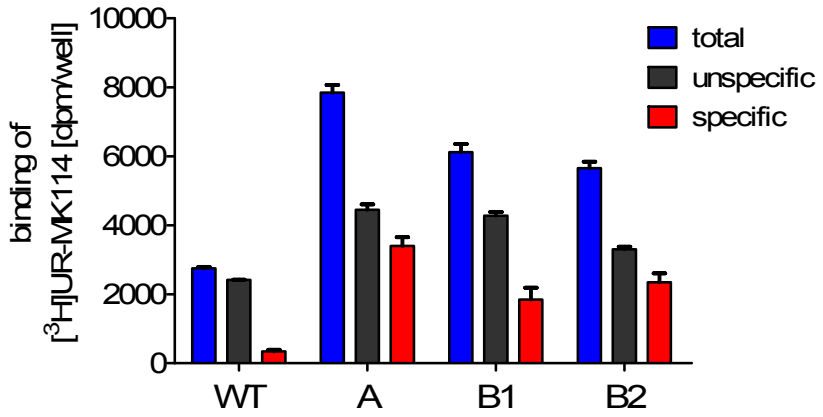

Fig. 3.3.3. *Binding of 6 nM [^{3}H]UR-MK114 to wild-type (WT) and transfected U-373 cells: hY_1R-ECFP, clone 4 (A); hY_1R-EYFP, clone 7 (B1 – before and B2 – after sorting). These cells revealed high specific binding, allowing the estimation of receptor number, as shown in Table 3.3.3.*

High specific binding of [^{3}H]UR-MK114 confirmed the presence of hY_1R binding sites on the surface of the stably transfected U-373 cells. This is in accordance with previous studies (Keller *et al.*, 2008). As reported earlier by Prof. Dr. A. Beck-Sickinger and colleagues, the transiently transfected BHK or CHO cells expressed functionally active hY_1R-ECFP and hY_1R-EYFP fusion proteins, as shown by binding of [^{3}H]propionyl-NPY and inhibition of adenylyl cyclase (Dinger *et al.*, 2003).

3.3.1.2 Flow cytometry

Like in the radioligand binding assay, the U-373 hY_1R-ECFP cells showed significant specific binding of a fluorescent pNPY derivative, Dy-635-pNPY (Fig. 3.3.4 A). However, in case of the U-373 cells expressing the hY_1R-EYFP, no specific binding of the fluorescent ligand could be measured (data not shown).

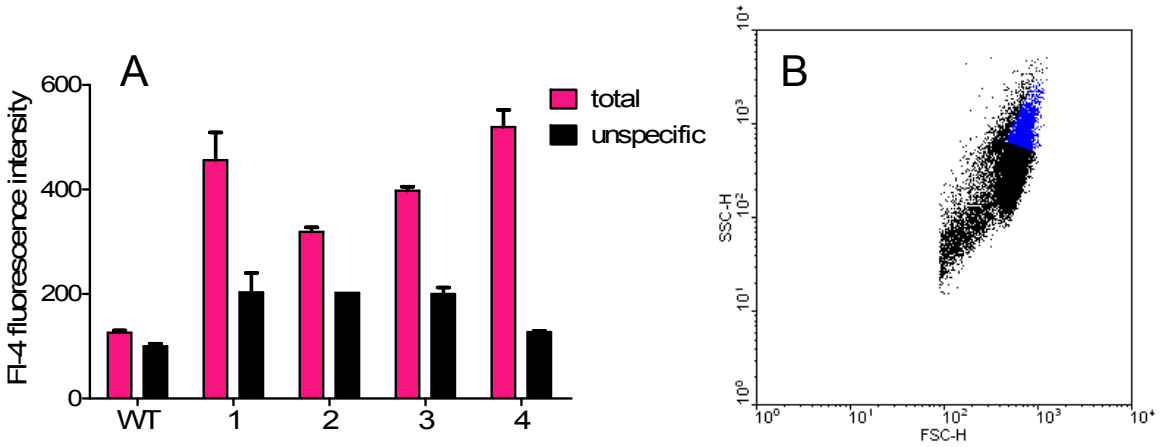

Fig. 3.3.4. *Binding of 8 nM Dy-635-pNPY on wild-type (WT) and transfected U-373 cells expressing hY_1R-ECFP (different transfectant clones 1–4). (A) Data are mean values ± SEM of an experiment performed for each cell clone in 2–6 replicates. Unspecific binding was determined in the presence of 800 nM pNPY. (B) Only the events from the selected blue gate (on the shown FSC/SSC dot plot) were used for counting the binding data (about 10-20% of all acquired events).*

Therefore, the cells were sorted in a FACSCalibur flow cytometer according to the fluorescence signal of EYFP from the Fl-1 channel (488 nm excitation line of an argon laser; 530 ± 15 nm band pass filter), as depicted in Fig. 3.3.5 (cf. Materials and methods, subsection 3.2.5.2). After sorting, the difference between total and unspecific binding was measurable but still not as pronounced as for the U-373 hY_1R-ECFP cells, indicating the lower hY_1 receptor density (Fig. 3.3.6). Nevertheless, the concentrations of unlabelled pNPY and BIBP 3226, needed for the displacement of Dy-635-pNPY, were much higher than those determined at native hY_1Rs in HEL cells (cf. K_i of pNPY: 1.3 ± 0.2 nM; K_d of BIBP 3226: 2.7 ± 0.5 nM; Schneider, 2005; Schneider *et al.*, 2006).

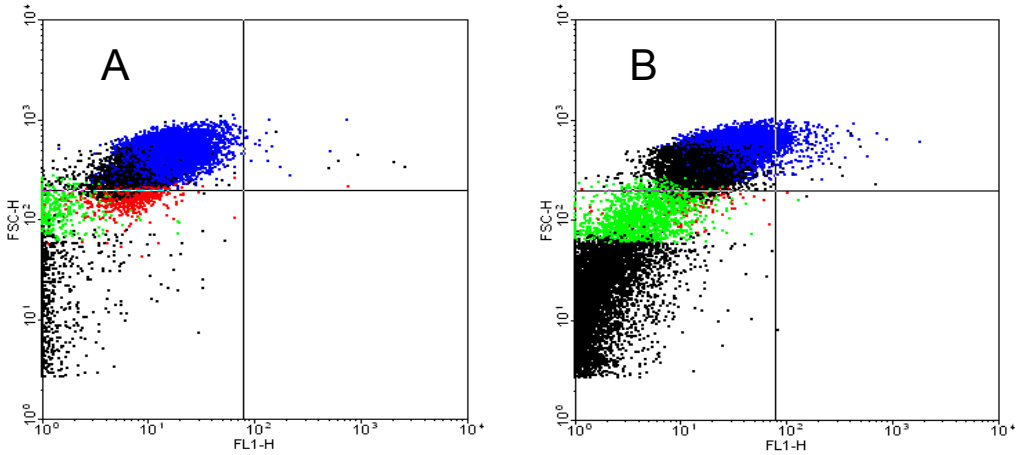

Fig. 3.3.5. *Forward scatter light (FSC, depending on the size of particles) plotted against fluorescence signal of EYFP from Fl-1 channel: (A) U-373 MG cells, (B) U-373 hY_1R-EYFP cells. Only the U-373 hY_1R-EYFP cells in the right upper quadrant were sorted in a FACSCalibur flow cytometer.*

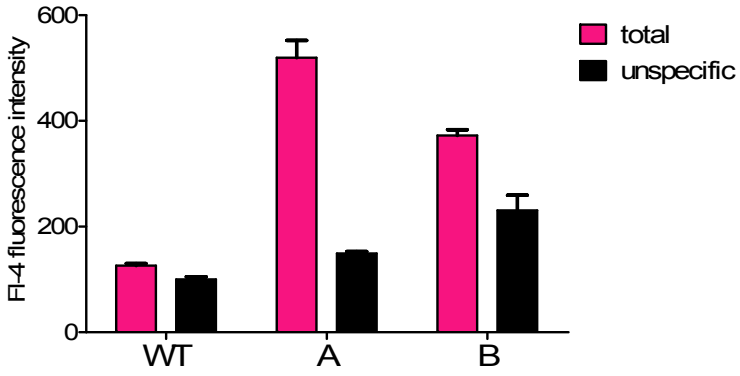

Fig. 3.3.6. *Flow cytometric binding assays on wild-type (WT) and stably transfected U-373 cells, expressing either the hY_1R-ECFP (A) or the hY_1R-EYFP (B) – the latter after sorting (see text). The data (total and unspecific binding of 8 nM Dy-635-pNPY) are mean values ± SEM of an experiment performed for each cell clone in 2–6 replicates. Unspecific binding was measured in the presence of 1 µM (A) or 10 µM (B) of BIBP 3226.*

3.3.1.3 Ratiometric calcium assays

The U-373 MG cells utilize Ca^{2+} ions as a second messenger (Kracht, 2001). Therefore it was possible to perform a functional assay with the ratiometric Ca^{2+}-chelating dye fura-2 (cf. subsection 3.2.6). In the cells stably expressing hY_1R-ECFP or hY_1R-EYFP fusion proteins a minor mobilization of intracellular Ca^{2+} was observed in response to 100 nM NPY (Fig. 3.3.7 A), while there was no effect of 100 nM NPY on the wild-type U-373 MG cells (data not shown). This indicated the presence of functionally active hY_1Rs at the transfected cells, but the number of receptors was rather low. As shown in Fig. 3.3.7 B for the hY_1R-EYFP, the response to NPY was blocked when the cells were preincubated with BIBP 3226. As positive control, the U-373 hY_1R-ECFP were stimulated with 30 µM histamine, as the histamine H_1 receptor is constitutively expressed by the U-373 MG cells (Kracht, 2001). As expected, the effect of histamine was suppressed when the cells were preincubated for 15 min with the H_1R antagonist mepyramine (Fig. 3.3.7 A).

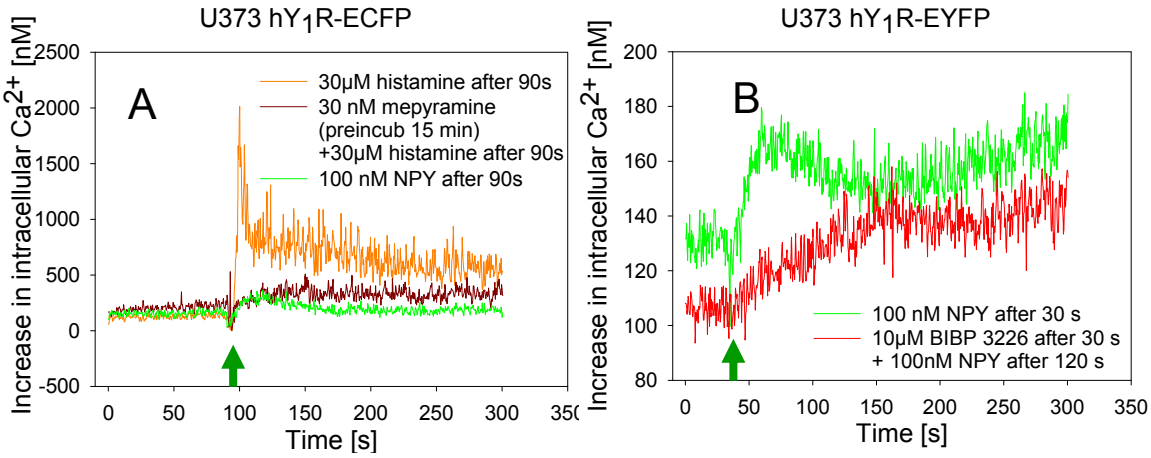

Fig. 3.3.7. *Fluorimetric calcium assays in U-373 hY_1R-ECFP (A) and U-373 hY_1R-EYFP cells (B). Both fusion proteins hY_1R-ECFP and hY_1R-EYFP transduced the signal (addition of NPY indicated by a green arrow) into cells that led to intracellular Ca^{2+} mobilization. The intracellular calcium concentration was counted from fluorescence intensities ratios according to the Grynkiewicz equation (cf. Eq. 3.2.2). For reference, 30 µM histamine (in the presence or absence of 30 nM mepyramine) was used, as wild-type U-373 MG cells express the histamine H_1 receptor (panel A).*

The stably transfected U-373 MG cells expressed functional hY_1R-ECFP or hY_1R-EYFP fusion proteins, as revealed in binding studies with the specific Y_1R radioligand UR-MK114 (Fig. 3.3.1 and 3.3.2) and the fluorescent agonist Dy-635-pNPY (Fig. 3.3.4 and 3.3.6) as well as in ratiometric calcium assays with fura-2 (Fig. 3.3.7 A and B). The sorting of the U-373 hY_1R-EYFP cells increased the mean number of binding sites, as confirmed in radioligand (Table 3.3.3) and flow cytometric binding studies (cf. Fig. 3.3.6).

3.3.2 Confocal microscopy imaging of fluorescently labelled NPY Y_1Rs

3.3.2.1 Subcellular localization of the hY_1R-ECFP

In order to obtain positive controls of membranally expressed ECFP (ECFP-Mem), both CHO and U-373 MG cells were transiently transfected with the retroviral expression vector pQCXIP/ECFP-Mem, as described in subsection 3.2.3.3. For the visualization of nuclei in confocal microscopy, specimens were stained with DRAQ5 (cf. Gross, 2006) and prepared as stated in subsection 3.2.7.1. Both CHO and U-373 cells expressed the ECFP-Mem in the cell membrane as well as in the intracellular compartments (Fig. 3.3.8). However, most probably due to the low transfection efficiency, there was no expression of the ECFP-Mem in many cells. As expected, there was no cross-talk (spectral interference) between the ECFP and the DRAQ5 channels (negative control: cells with the stained cell nuclei, but without ECFP-Mem in Fig. 3.3.8).

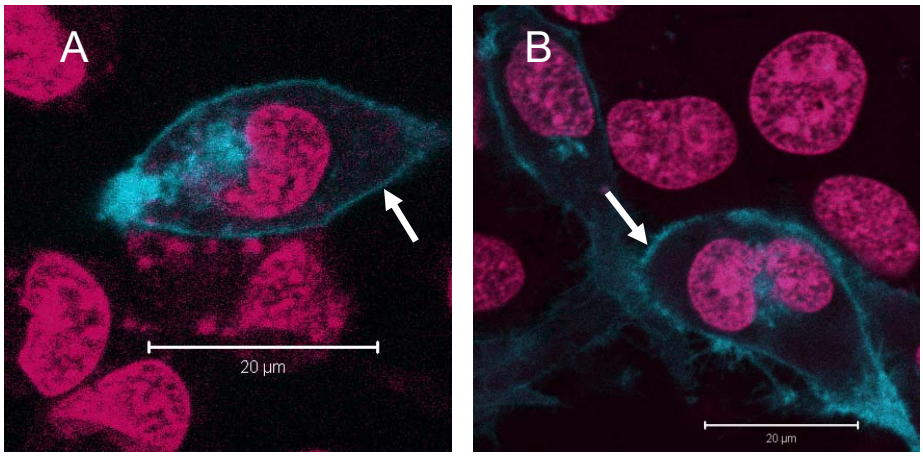

Fig. 3.3.8. *Expression of ECFP-Mem in transiently transfected CHO (A) and U-373 MG cells (B) found in the cell membrane (indicated by arrows) as well as in the intracellular compartments. Plan-Apochromat 63x/1.4 oil; ECFP (cyan): Ar 458, HFT 458, LP 475; nuclear dye DRAQ5 (magenta): HeNe 543, HFT 458/543, LP 650.*

Confocal imaging demonstrated that only approx. 5% of the transfected U-373 hY_1R-ECFP cells expressed the fluorescently tagged Y_1 receptors. Moreover, the fluorescence signal of ECFP was very weak (Fig. 3.3.9 A) and did not exclusively arise in the cell membrane, but – for the most part – in the intracellular compartments (Fig. 3.3.9 B). Therefore, although there was no detectable cross-talk with the filter settings for EYFP (Fig. 3.3.9 C), the found distribution pattern of hY_1R-ECFP fusion proteins disqualifies their usage as donors in the prospective FRET-based investigations of receptor dimerization in the cell membranes.

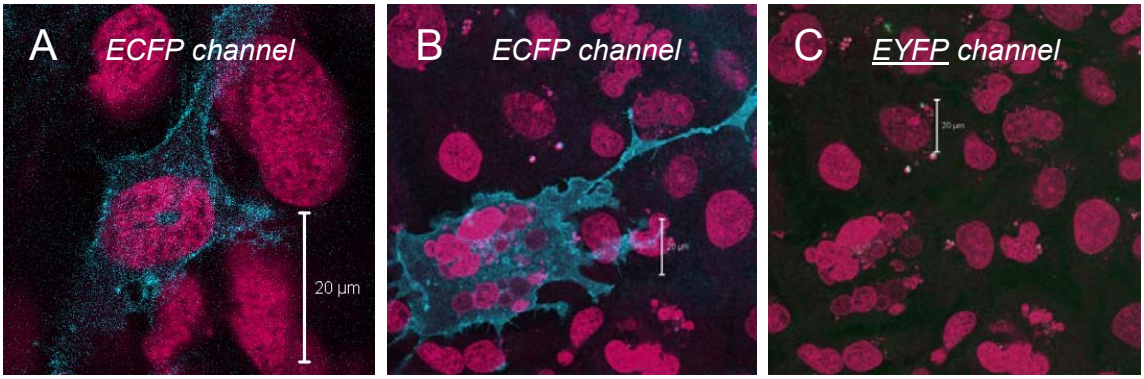

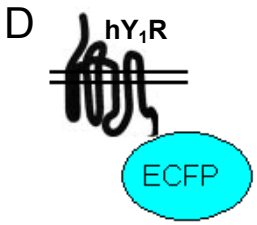

Fig. 3.3.9. *Expression of hY_1R-ECFP fusion proteins by U-373 MG cells: (A) clone 4 (Ar 458, HFT 458, LP 475) and (B) clone 1 (Ar 458, HFT 458, BP 475–525). (C) There was no detectable cross-talk with the EYFP channel (the same specimen as in B; EYFP: Ar 488, HFT 488, BP 505-550; DRAQ5: HeNe 543, HFT 458/543, LP 650). Plan-Apochromat 63x/1.4 oil. (D) The schematic drawing represents the hY_1R-ECFP in the cell membrane.*

Also the glioblastoma/astrocytoma U-118 MG cells were stably transfected with the hY_1R-pECFP-N1 plasmid, as described in subsection 3.2.3.2. However, due to the relatively high autofluorescence and the lacking emission signal in the cell membrane (Fig. 3.3.10), no further experiments were performed with these cells.

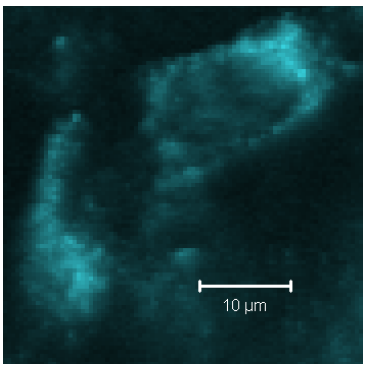

Fig. 3.3.10. *The U-118 MG cells stably transfected with the hY_1R-pECFP-N1 plasmid. Plan-Apochromat 63x/1.4 oil, Ar 458, HFT 458, LP 475.*

3.3.2.2 Subcellular localization of the hY_1R-EYFP

The U-373 MG cells transiently transfected with pEYFP-N1 plasmid (for the cytosolic expression of EYFP) revealed a strong fluorescence signal in the EYFP channel and were used as positive control (Fig. 3.3.11 A). The detected EYFP fluorescence of the stably transfected U-373 hY_1R-EYFP cells was much lower than that of the control cells (Fig. 3.3.11 B and 3.3.12). Thus, increased laser transmission was required (6% instead of 2%) to detect the fluorescence signal of the fusion protein.

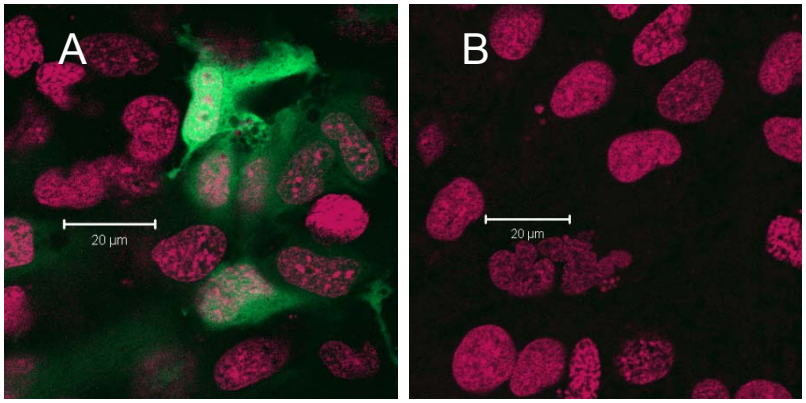

Fig. 3.3.11. *Filter settings for EYFP emission: (A) U-373 cells expressing cytosolic EYFP; (B) no detection of the EYFP signal in the U-373 hY$_1$-EYFP cells (with the same settings as in panel A). Plan-Apochromat 63x/1.4 oil; EYFP (pale green): Ar 488 (2%), HFT 488, BP 505-550; DRAQ5 (magenta): HeNe 543 (37%), HFT 458/543, LP650).*

Similarly to U-373 hY$_1$R-ECFP cells, extremely high heterogeneity of the U-373 MG cells expressing hY$_1$R-EYFP fusion proteins was found, concerning both the amount and the localization of the EYFP-tagged Y$_1$ receptors (Fig. 3.3.12 A–C). Although sorting of the cells increased the mean number of binding sites (cf. Table 3.3.3 and Fig. 3.3.6), the expression pattern of the hY$_1$R-EYFP was not improved. Cells, which either did not fluoresce or with improper intracellular localization of the fusion proteins were still present (Fig. 3.3.12 D)

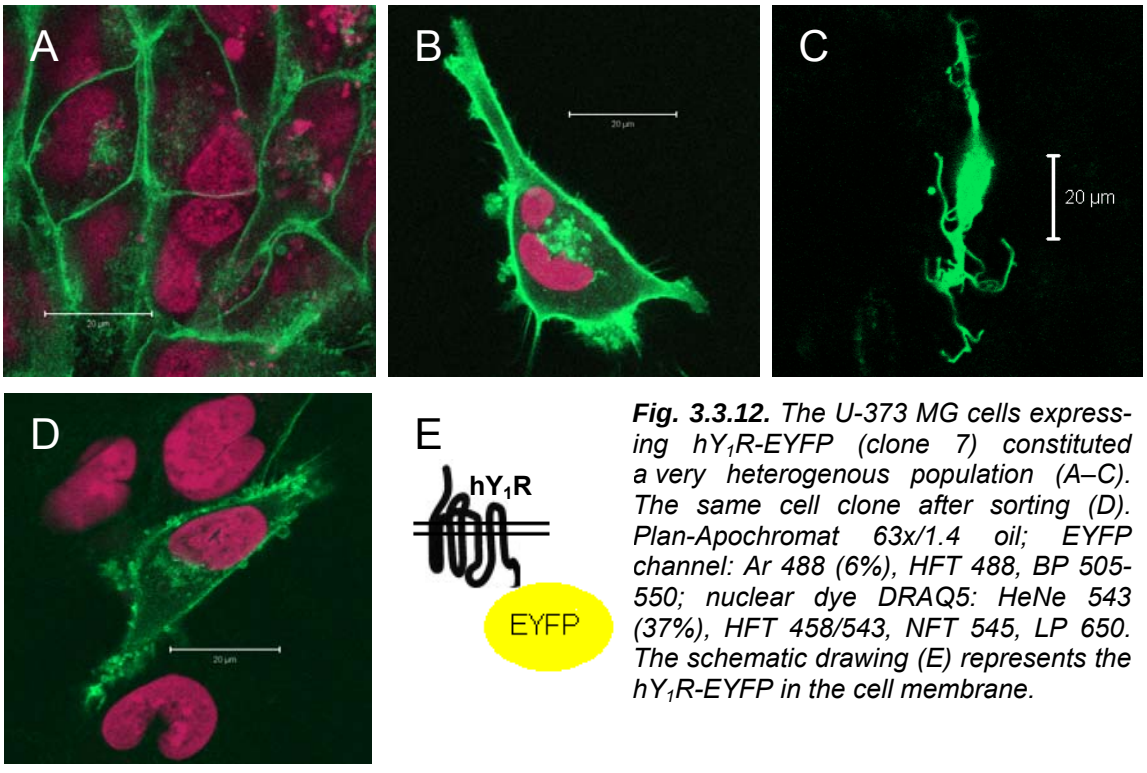

Fig. 3.3.12. *The U-373 MG cells expressing hY$_1$R-EYFP (clone 7) constituted a very heterogenous population (A–C). The same cell clone after sorting (D). Plan-Apochromat 63x/1.4 oil; EYFP channel: Ar 488 (6%), HFT 488, BP 505-550; nuclear dye DRAQ5: HeNe 543 (37%), HFT 458/543, NFT 545, LP 650. The schematic drawing (E) represents the hY$_1$R-EYFP in the cell membrane.*

Additionally, epidermoid skin carcinoma A-431 cells were stably transfected with the hY_1R-pEYFP-N1 plasmid (subsection 3.2.3.2). Nevertheless, the fluorescence signal of these transfected cells was similar to the autofluorescence of the wild-type cells (Fig. 3.3.13 A), excluding the A-431 cell line from further studies. At the same time, confocal imaging of the transiently transfected CHO cells revealed a similar hY_1R-EYFP expression pattern to that in U-373 MG cells – EYFP fluorescence was found in both the cell membrane and intracellular compartments (Fig. 3.3.13 B).

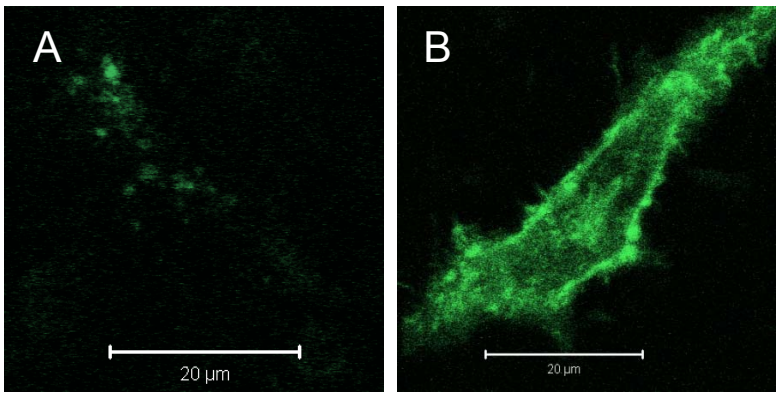

Fig. 3.3.13. *Other cell lines transfected with the hY_1R-pEYFP-N1 plasmid: (A) stably transfected A-431 cells (C-Apochromat 40x/1.2 W corr, Ar 514 (2%), HFT 458/514 nm, BP 530-600); (B) transiently transfected CHO cells (Plan-Apochromat 63x/1.4 oil, Ar 488 (4%), HFT 488, NFT 490, BP 505-550).*

Limitations of the fluorescent protein-based RET techniques. Despite the fact that the tagging of receptors with GFP-like proteins is a very useful method, it has also some drawbacks. Typically, FRET- or BRET-based proximity assays for the identification of GPCR dimerization are performed on systems with *overexpressed* receptors, although the efficiency of resonance energy transfer depends strongly on the expression level of the interacting partners (Table 3.3.4; cf. James *et al.*, 2006).

Table 3.3.4. *The expected BRET efficiency ($BRET_{eff}$) in systems coexpressing BRET partners (donors D and acceptors A) in case of random or dimeric interactions between A and D (cf. James et al., 2006). The variable parameters are the total expression level of acceptor and donor molecules (A+D) as well as the acceptor-to-donor ratio (A/D).*

Expected BRET efficiency depending on the expression of D and A	**The nature of interactions between BRET partners**	
	Random interactions	**Oligomeric interactions**
constant A+D; increasing A/D (above threshold)	**constant** (the same distance between D and A)	**increasing hyperbolic** (depending on stoichiometry; self-associating D decreases $BRET_{eff}$)
increasing A+D; constant A/D	**pseudo-linear** falling to 0 at low A+D	**expression level dependent**, but not falling to 0 at low A+D in case of non-constitutive dimers (**independent of expression level** in case of constitutive dimers)

The second major disadvantage of the usage of GFP-like proteins for FRET is the fluorescent signal occurring in the intracellular compartments, where the FP-tagged receptor proteins are synthesized and post-translationally modified prior to being transported to the cell membrane (Fig. 3.3.14, cf. Dinger *et al.*, 2003). According to Pin and colleagues, in such a case, FRET signals do not refer exclusively to the protein-protein interaction at the cell surface, disabling the unequivocal confirmation or rejection of receptor oligomerization in the cell membrane (Maurel *et al.*, 2008). Therefore, it is crucial to prove the subcellular localization of fluorescent proteins and confirm the membranal expression of the FP-tagged GPCRs, using selective radioactive tracers or fluorescent ligands by means of flow cytometry and confocal microscopy.

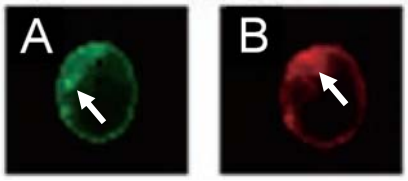

Fig. 3.3.14. *The confocal images of the BHK cells cotransfected with hY_1R-GFP and hY_1R-DSRed fusion proteins: (A) in the GFP channel and (B) in the DSRed channel (adopted from Dinger et al., 2003 with modifications). The arrows indicate the fluorescently tagged Y_1 receptors in the intracellular compartments.*

3.3.2.3 Alternative methods for labelling of receptor dimers

In order to avoid the artefacts due to intracellular aggregation of FP-tagged receptors, alternative FRET-based techniques have been developed for the investigation of the quaternary structure of GPCRs at the surface of living cells. These included the application either of well-established fluorescently labelled antibodies or of small-sized genetically encoded tags for receptor labelling (e.g. *snap* or *tetracysteine tags*). The latter

might be very advantageous as biosynthesis, folding and trafficking of the tagged receptors remain almost unchanged (Maurel *et al.*, 2008). Furthermore, the low-molecular-weight tags should allow virtually undisturbed protein-protein interactions of the tagged GPCRs, including their putative dimerization.

Receptor proteins might be tagged with a *tetracysteine* sequence, which enables labelling with a fluorescein derivative containing two arsen-(III) substituents (*fluorescein arsenical hairpin binder* = *FlAsH*). The membrane-permeant FlAsH, being non-fluorescent in a free form, reveals high fluorescence, when bound to a specific amino acid sequence at the C-terminus of a receptor (Hoffmann *et al.*, 2005). Such FlAsH-labelled receptors can function as FRET partners (acceptors) for receptors tagged with CFP (donors). However, the main drawbacks of this method are a certain level of unspecific binding of FlAsH to other proteins in the cell membrane as well as toxicity.

Another labeling method utilizes so called “snap tags”, which are genetically fused to receptors (N-terminally) and encode O6-guanine nucleotide alkyltransferase. The enzyme reacts with fluorescently labelled benzyl guanine (BG), catalyzing covalent labelling of receptors with fluorophores carried by the benzyl group of BG. By using non-permeant fluorescent BG derivatives, only snap-tagged receptors on the cell surface should be labelled, as shown in Fig. 3.3.15 B (cf. Maurel *et al.*, 2008).

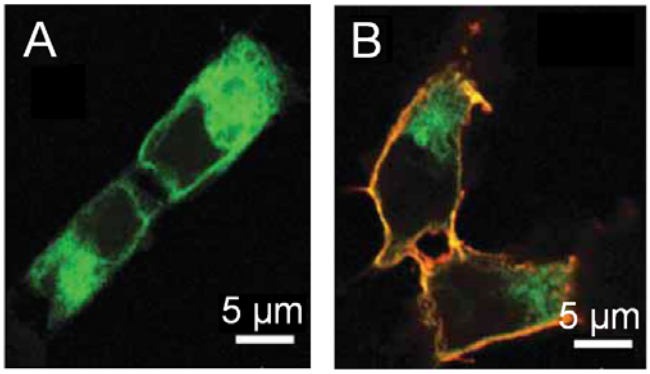

Fig. 3.3.15. *The confocal images of the $GABA_{B1}$-receptors fused to snap tags and GFP (green, FRET donor), expressed alone (A). The same receptors coexpressed with $GABA_{B2}$ receptors and labelled with the BG-d2 fluorescent dye (orange) as FRET acceptor (B). Noteworthy, only the cell-surface receptors were labelled with the d2 (adopted from Maurel et al., 2008, with modifications).*

3.3.2.4 Binding studies with the fluorescent Y_1R ligands

In order to examine the prevalence of human Y_1 receptor binding sites on the stably transfected U-373 MG cells expressing hY_1R-ECFP and hY_1R-EYFP fusion proteins, the samples were incubated with a specific Y_1R fluorescent ligand, UR-MK131, synthesized in our research group by Dr. Max Keller (Keller, 2008, Keller *et al.*, 2011).

The fluorescent Y_1R ligand UR-MK131 was bound to the membranes of the U-373 cells stably expressing hY_1R-ECFP fusion proteins (Fig. 3.3.16 A). This interaction could be blocked in the presence of the unlabelled Y_1R antagonist BIBP 3226 (Fig. 3.3.16 D). A strong colocalized signal (overlapping fluorescence of ECFP and UR-MK131) detected for total binding (Fig. 3.3.16 C) disappeared in the presence of excessive BIBP 3226 (Fig. 3.3.16 F), confirming the expression of Y_1R binding sites on the cell surface. Similar results were obtained for the U-373 cells stably expressing the hY_1R-EYFP fusion proteins (Fig. 3.3.17 A and C).

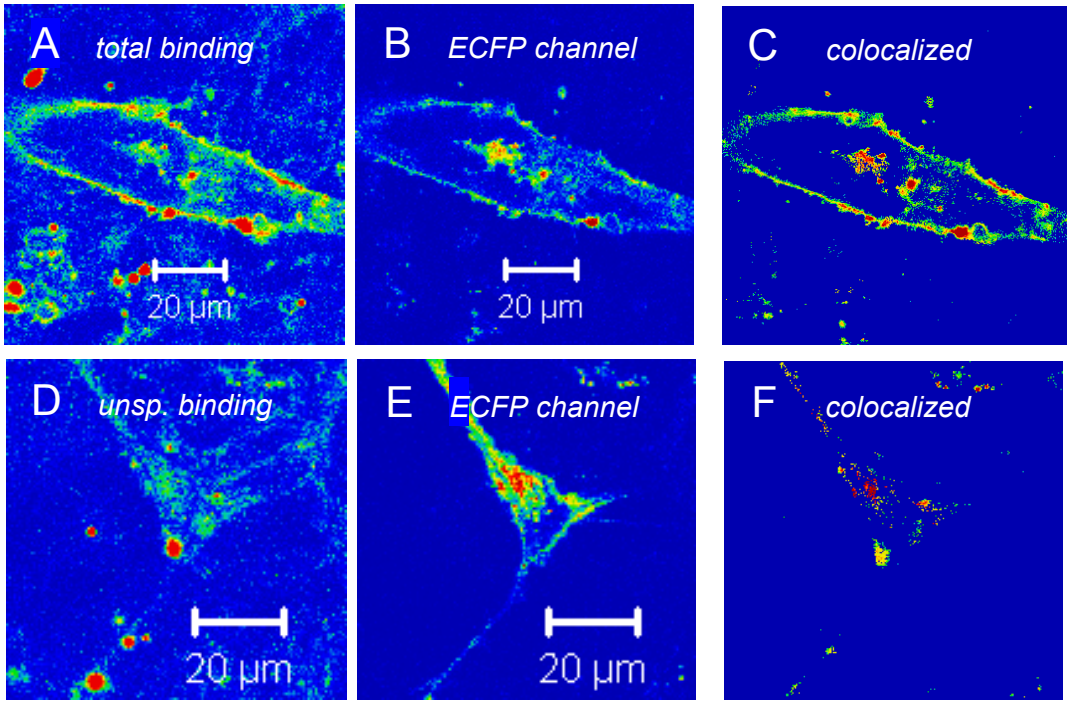

Fig. 3.3.16. *Binding of 70 nM UR-MK131 to the hY_1R-ECFP cells after 25 min of incubation: (A) total and (D) unspecific binding (after 1 min of preincubation with 10 µM BIBP 3226). Additionally, the images with the corresponding ECFP signals (B and E) and the colocalized pictures (C and F) are shown. Plan-Apochromat 63x/1.4 oil; EYFP channel: Ar 458 (86%), HFT 458, BP 475-525; UR-MK131 channel: HeNe 543 (38%), HFT 458/543, NFT 545, LP 650.*

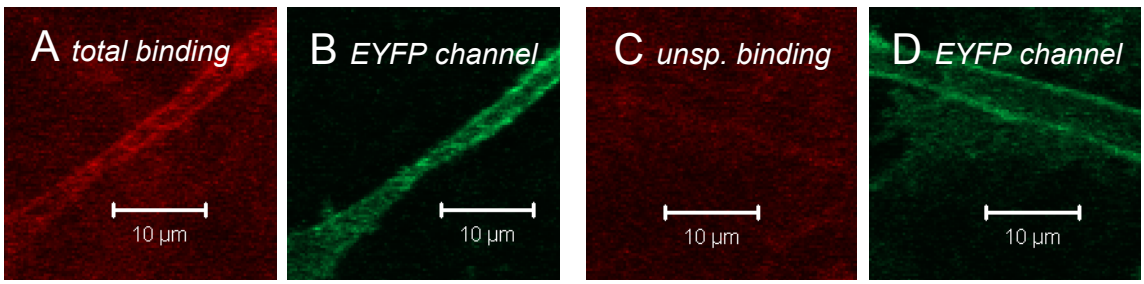

Fig. 3.3.17. *Binding of 70 nM UR-MK131 to the hY_1R-EYFP cells (shown are cell protrusions) after 15 min of incubation: (A) total and (C) unspecific binding (after 5 min of preincubation with 5 µM BIBP 3226). The images B and D show the corresponding fluorescence of EYFP. Plan-Apochromat 63x/1.4 oil; EYFP channel: Ar 488 (12%), HFT 488, BP 505-550; UR-MK131 channel: HeNe 633 (14%), HFT UV/488/543/633, LP 650.*

Binding studies on the U-373 hY$_1$R-EYFP cells were also performed with another far-red fluorescent ligand, UR-MK115 (Keller, 2008), which can be excited at 488 nm. Unexpectedly, confocal imaging of the cells treated with this fluorescent ligand (incubation period: 8–50 min) revealed the far-red emission signal arising in the perinuclear region instead of the cell membrane (Fig. 3.3.18 A and B). Moreover, the binding of UR-MK115 could not be displaced by an excess of the Y$_1$R antagonist (Fig. 3.3.18 C).

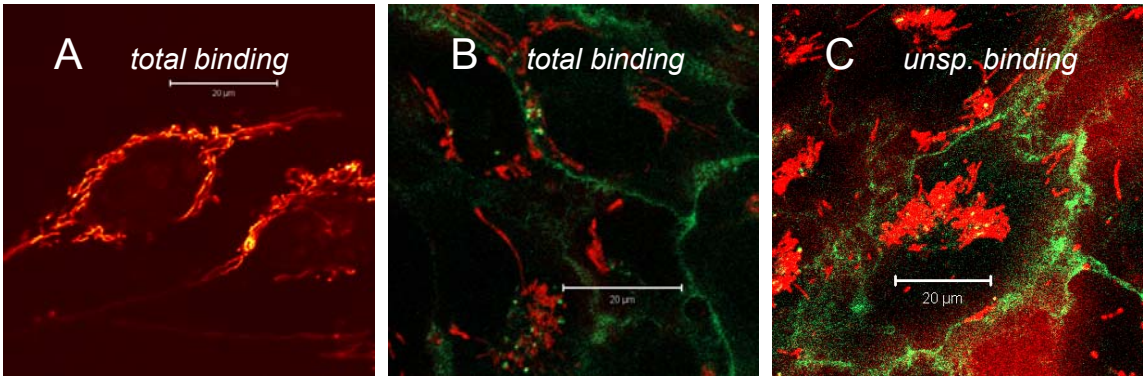

Fig. 3.3.18. *Binding of 70 nM UR-MK115 to the U-373 hY$_1$R-EYFP cells: (A) total binding after 35 min of incubation (far-red channel: Ar 488 (5%) HFT 488, LP 650); (B) total binding after 8 min of incubation (EYFP channel: Ar 488 (9%), HFT 488, BP 505-550; far-red channel as in panel A); (C) unspecific binding after 28 min of incubation in the presence of 5 µM BIBP 3226 (1 min of pre-incubation; filter settings as in panel B). Plan-Apochromat 63x/1.4 oil.*

Any spectral interference with the EYFP should be excluded, as no far-red fluorescence could be detected for the untreated hY$_1$R-EYFP cells (Fig. 3.3.19 B). Interestingly, staining of the wild-type U-373 cells with UR-MK115 revealed filamentous structures similar to the mitochondria (Fig. 3.3.20). To reject or confirm this hypothesis, further experiments were performed with the U-373 cells transiently transfected with the localization vector pECFP-Mito (cf. subsection 3.2.3.3) for mitochondrial expression of the ECFP (Fig. 3.3.21). The comparison of the confocal images allowed the definite identification of the structures labelled by UR-MK115 as the mitochondria.

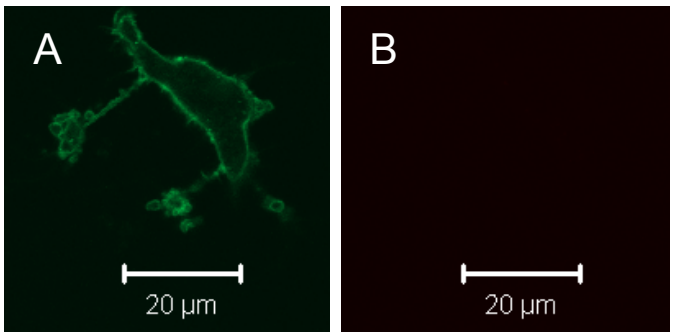

Fig. 3.3.19. *The untreated U-373 hY$_1$R-EYFP cells in the EYFP (A) and the far-red (B) channels. No signal could be detected in the far-red channel, excluding the possibility of cross-talk with the fluorescent ligand UR-MK115. Plan-Apochromat 63x/1.4 oil; EYFP channel: Ar 488 (9%), HFT 488, BP 505-550; far-red channel for UR-MK115: Ar 488 (5%), HFT 488, LP650.*

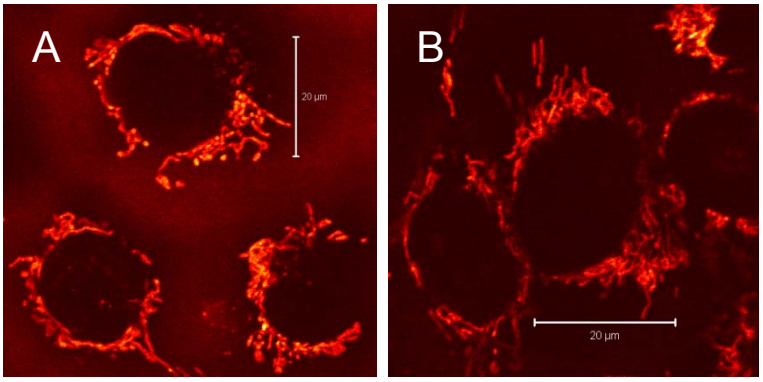

Fig. 3.3.20. *Binding of 70 nM UR-MK115 to the wild-type U-373 cells after 28 min of incubation: (A) total and (B) unspecific binding (after 1 min of preincubation with 5 µM BIBP 3226). Plan-Apochromat 63x/1.4 oil, Ar 488, HFT 488, LP650.*

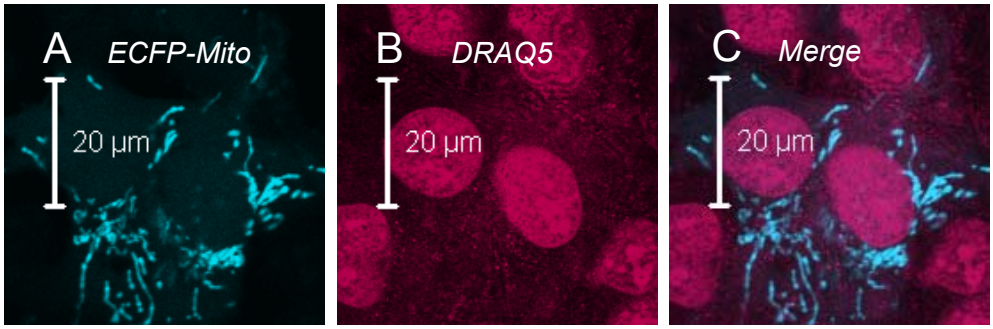

Fig. 3.3.21. *Mitochondrial ECFP in the transiently transfected U-373 cells: (A) fluorescence of ECFP (Ar 458, HFT 458, LP 475); (B) fluorescence of the nuclear dye DRAQ5 (HeNe 543, HFT UV/488/543/633, LP650); (C) merged images. Plan-Apochromat 63x/1.4 oil.*

In contrast, UR-MK115 revealed a clear difference between total and unspecific binding to the membranes of breast cancer MCF-7-Y_1 cells, as shown in Fig. 3.3.22. In order to additionally increase the expression of Y_1 receptors, the ER positive MCF-7-Y_1 cells were cultured in the presence of 1 nM estradiol 2 days prior to experiments. Cross-talk activation pathways between estrogen and NPY Y_1 receptors have been namely reported before (Memminger, 2009). Moreover, in MCF-7 breast cancer cells the Y_1R mRNA was shown to be up-regulated by estrogen (Amlal *et al.*, 2006). Therefore, the observed binding of the fluorescent ligand UR-MK115 might depend not only on the used cell line, but also on the Y_1 receptor density.

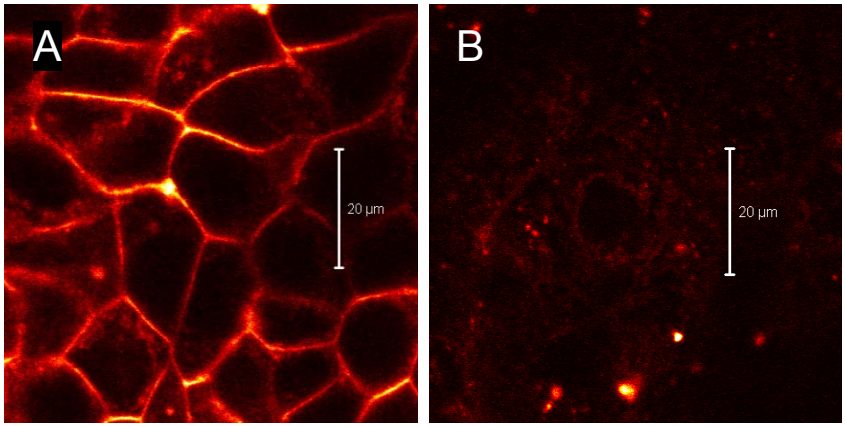

Fig. 3.3.22. *Binding of 70 nM UR-MK115 to the MCF-7-Y_1 cells after 10 min of incubation: (A) total and (B) unspecific binding (after 1 min of preincubation with 5 µM BIBP 3226). Plan-Apochromat 63x/1.4 oil, Ar 488 (5%), HFT 488, NFT 545, LP 650.*

3.3.2.5 Internalization of the NPY hY_1R

The breast cancer MCF-7- Y_1 cells were used again as a control system for the investigation of the Y_1 receptor internalization, showing high binding of the fluorescently labelled endogenous agonist, Cy-5-pNPY (Fig. 3.3.23 A and B). However, under the same conditions, there was only weak binding of Cy-5-pNPY on the stably transfected U-373 hY_1R-EYFP cells (Fig. 3.3.23 C), perhaps due to low receptor density equalling to approx. 30,000 receptors per cell (cf. Table 3.3.3 – B1). For comparison, MCF-7-Y_1 cells showed approx. 300,000 sites per cell (determined by radioligand binding studies), when cultured with 1 nM estrogen (Keller, 2008; Memminger, 2009). Thus, the MCF-7-Y_1 cells revealed to be the more suitable cell line for imaging of the Y_1 receptor endocytosis induced by the far-red fluorescent agonist.

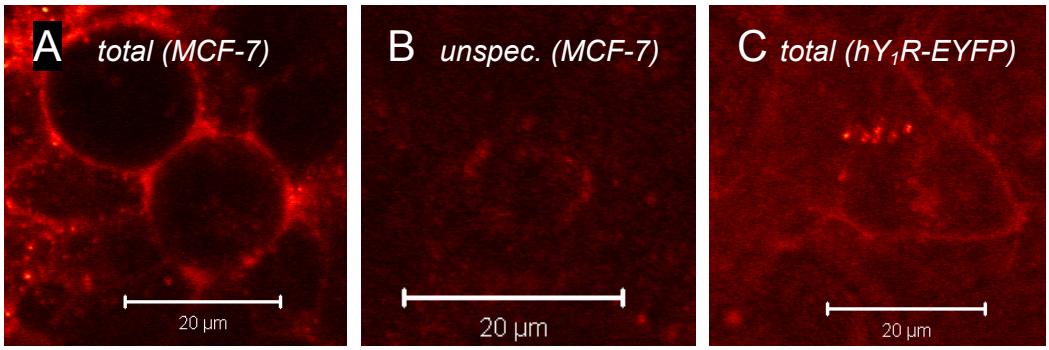

Fig. 3.3.23. *Binding of 10 nM Cy-5-pNPY after 7 min of incubation with the MCF-7-Y_1 cells: (A) total binding, (B) unspecific binding (after 1 min of preincubation with 10 µM BIBP 3226) as well as with the U-373 hY_1R-EYFP cells (C). C-Apochromat 40x/1.4 W corr, HeNe 633 (10%), HFT 514/633, NFT 545, LP 650.*

Incubation with Cy-5-pNPY for a longer period of time led to the internalization of Y_1 receptors in the MCF-7-Y_1 cells (Fig. 3.3.24 A). Similar effect was observed after prolonged incubation with the unlabelled pNPY on the transfected U-373 cells, as the fluorescence of the hY_1R-EYFP fusion proteins was detected mainly in vesicles (Fig. 3.3.24 B).

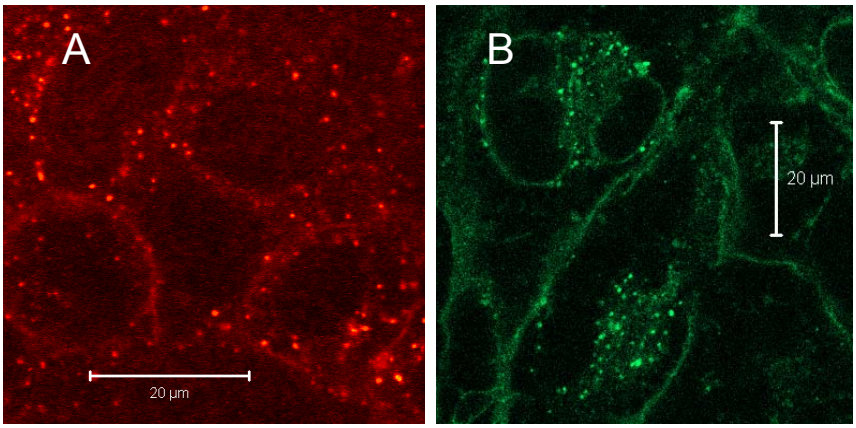

Fig. 3.3.24. *Agonist-induced internalization (A) in the MCF-7-Y_1 cells after 15 min of incubation with 10 nM Cy-5-pNPY (C-Apochromat 40x/1.2 W: HeNe 633 (10%), HFT 514/633, LP650) and (B) in the U-373 hY1R-EYFP cells after 3 hours of incubation with 500 nM of pNPY (Plan-Apochromat 63x/1.4 oil, Ar 488 (6%), HFT 488, BP 505-550).*

In later studies, the MCF-7- Y_1 cells were labeled with the LysoTracker Green, a fluorescent dye staining preferably the lysosomes, as described in subsection 6.2.6. After 4 hours of incubation with 10 nM Cy-5-pNPY, the far-red fluorescent ligand was localized exclusively in vesicles, but no colocalization with lysosomes (green) could be detected (Fig. 3.3.25). Thus, it can be concluded that human Y_1 receptors undergo an NPY-induced internalization, but are not the trafficked to lysosomes for enzymatic degradation within a few hours of exposure to the endogenous agonist (cf. Fig. 1.1.7 and agonist-induced internalization of human H_2Rs, Fig. 6.3.23).

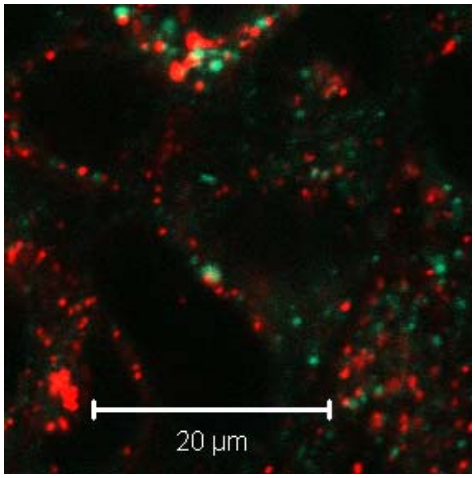

Fig. 3.3.25. *Agonist-induced Y_1R internalization in the MCF-7-Y_1 cells. No colocalization of the internalized hY_1Rs (red) and lysosomes (green) could be detected after 230 min of incubation with 10 nM Cy-5-pNPY. The cells were stained for 2 hours with 50 nM LysoTracker Green. Plan-Apochromat 63x/1.4 oil; LysoTracker Green: Ar 488 (5%), HFT 488, BP 505-530; Cy-5-pNPY: HeNe 633 (10%), HFT 514/633, NFT 545, LP 650.*

3.4 Summary and conclusion

In order to obtain single-labelled receptors (controls) for FRET-based measurements of receptor dimerization, human U-373 brain tumor cells were stably transfected with either hY_1R-pECFP-N1 or hY_1R-pEYFP-N1 plasmids (Dinger *et al.*, 2003). The results of binding and functional studies on living cells expressing human Y_1 receptors tagged with ECFP or EYFP indicate that:

1) The membranal localisation of the hY_1R-ECFP and hY_1R-EYFP fusion proteins was confirmed in radiochemical binding studies by using the selective radioligand Y_1R N^{ω}-([2,3-^{3}H]propionyl)-BIBP 3226 (Fig. 3.3.3; [^{3}H]UR-MK114; cf. Keller *et al.*, 2008) as well as in flow cytometric binding assays with the fluorescent ligand Dy-635-pNPY (Fig. 3.3.6; Schneider, 2005; Schneider *et al.*, 2006); however, the second method was applicable for the hY_1R-EYFP only after cell sorting.
2) As the U-373 MG cells involve calcium ions as a second messenger (Kracht, 2001), it was possible to perform a functional assay using the calcium-chelating dye fura-2 (Schneider, 2005). Weak calcium signal detected in the transfected cells confirmed at least functionality of the fusion proteins (Fig. 3.3.7).
3) Nevertheless, confocal microscopy imaging of U-373 hY_1R-ECFP and U-373 hY_1R-EYFP cells revealed that the Y_1 receptors fluorescently tagged with ECFP or EYFP were located mostly in the intracellular compartments (Fig. 3.3.9 B and 3.3.12). The membranal expression of Y_1 binding sites (detected by colocalization studies with the far-red fluorescent ligand UR-MK131, Fig. 3.3.16–17; cf. Keller, 2008, Keller *et al.*, 2011) could not be improved by cell sorting (FACS).
4) Similarly, the hY_1R-EYFP fusion proteins were found in both the cell membrane and intracellular compartments of the transiently transfected CHO cells (Fig. 3.3.13 B). However, neither the U-118 (Fig. 3.3.10) nor the A-431 cells (Fig. 3.3.13 A), transfected with hY_1R-pECFP-N1 or hY_1R-pEYFP-N1 plasmids, respectively, revealed the membranal expression of the fluorescently tagged Y_1 receptors.
5) The hY_1R-EYFP fusion proteins underwent agonist-induced internalisation in the transfected U-373 cells (Fig.. 3.3.24 B), but low receptor density disabled further imaging of the internalization with the far-red fluorescent agonist Cy-5-pNPY (Fig. 3.3.23 C; cf. Schneider, 2005; Schneider *et al.*, 2006).

The human Y_1 receptors tagged with either ECFP or EYFP were distributed not exclusively in the cell membrane, but also in the intracellular compartments of the stably transfected U-373 cells (Fig. 3.3.9 B and 3.3.12, respectively). The same expression pattern of the hY_1R-EYFP fusion proteins was found in the transiently transfected CHO cells (Fig. 3.3.13 B), showing serious limitations on the use of GFP-like proteins in the FRET-based investigation of receptor dimerization in the cell membranes. On account of that, the present data confirm reports on possible drawbacks of this approach (Maurel *et al.*, 2008).

3.5 References

Aiglstorfer I *et al.*: NPY Y_1 antagonists: structure-activity relationships of arginine derivatives and hybrid compounds with arpromidine-like partial structures, *Regul Pept*, **1998**, *75-76*, 9-21.

Amlal H *et al.*: Estrogen up-regulates neuropeptide Y Y_1 receptor expression in a human breast cancer cell line, *Cancer Res*, **2006,** *66*, 3706–3714.

Carrillo JJ *et al.*: Multiple interactions between transmembrane helices generate the oligomeric α_{1b}-adrenoceptor, *Mol Pharmacol*, **2004**, *66*, 1123–1137.

Dinger MC *et al.*: Homodimerization of neuropeptide Y receptors investigated by fluorescence resonance energy transfer in living cells, *J Biol Chem*, **2003**, *278*, 10562–10571.

Ferré S *et al.*: Building a new conceptual framework for receptor heteromers, *Nat Chem Biol*, **2009**, 5, 131–134.

Gross D: New approaches to the chemotherapy of glioblastoma: investigations on doxorubicin nanoparticles, inhibition of PDGF receptors and kinesin Eg5, with emphasis on confocal laser-scanning microscopy, Doctoral thesis, University of Regensburg, **2006**.

Grynkiewicz G *et al.*: A new generation of Ca^{2+} indicators with greatly improved fluorescence properties, *J Biol Chem*, **1985**, *260*, 3440-3450.

Guiswé P: Biomimetische Synthese mariner Alkaloide vom Bis-1-oxachinolizidintyp und deren biologische Wirkung, Doctoral thesis, University of Regensburg, **2000**.

Hébert TE *et al.*: Detecting and imaging protein-protein interactions during G protein-mediated signal transduction in vivo and in situ by using fluorescence-based techniques, *Cell Biochem Biophys*, **2006**, *45*, 85-109.

Hoffmann C *et al.*: A FlAsH-based FRET approach to determine G protein-coupled receptor activation in living cells, *Nat Methods*, **2005**, *2*, 171-176.

James JR *et al.*: A rigorous experimental framework for detecting protein oligomerization using bioluminescence resonance energy transfer, *Nat Methods*, **2006**, *3*, 1001-1006.

Keller M *et al.*: Bivalent argininamide-type neuropeptide Y Y_1 antagonists do not support the hypothesis of receptor dimerisation, *ChemMedChem*, **2009**, *4*, 1733–1745.

Keller M *et al.*: Guanidine-acylguanidine bioisosteric approach in the design of radioligands: synthesis of a tritium-labeled N^G-propionylargininamide ([^{3}H]-UR-MK114) as a highly potent and selective neuropeptide Y Y_1 receptor antagonist, *J Med Chem*, **2008**, *51,* 8168–8172.

Keller M *et al.*: Red-fluorescent argininamide-type NPY Y_1 receptor antagonists as pharmacological tools, *Bioorg Med Chem*, **2011**, *19*, 2859–2878.

Keller M: Guanidine-acylguanidine bioisosteric approach to address peptidergic receptors: pharmacological and diagnostic tools for the NPY Y_1 receptor and versatile building blocks based on arginine substitutes, Doctoral thesis, University of Regensburg, **2008**.

Kracht J: Bestimmung der Affinität und Aktivität subtypselektiver Histamin- und Neuropeptid Y-Rezeptorliganden an konventionellen und neuen pharmakologischen *In-vitro*-Modellen, Doctoral thesis, University of Regensburg, **2001**.

Kroeger KM *et al.*: G-protein coupled receptor oligomerization in neuroendocrine pathways, *Front Neuroendocrinol*, **2004**, *24*, 254–278.

Lindl T: Zell- und Gewebekultur: Einführung in die Grundlagen sowie ausgewählte Methoden und Anwendungen, *Spektrum Akademischer Verlag*, Heidelberg – Berlin, **2000**.

Maurel D *et al.*: Cell-surface protein-protein interaction analysis with time-resolved FRET and snap-tag technologies: application to GPCR oligomerization, *Nat Methods*, **2008**, *5*, 561-567.

Memminger M: Synthesis and characterization of subtype-selective estrogen receptor ligands and their application as pharmacological tools - Cross-talk between estrogen and NPY Y_1 receptors in human breast cancer cells, Doctoral thesis, University of Regensburg, **2009**.

Milligan G and Bouvier M: Methods to monitor the quaternary structure of G protein-coupled receptors, *FEBS J*, **2005**, *272*, 2914–2925.

Milligan G: Applications of bioluminescence- and fluorescence resonance energy transfer to drug discovery at G protein-coupled receptors, *Eur J Pharm Sci*, **2004**, *21*, 397-405.

Müller Ch: New approaches to the therapy of glioblastoma: investigations on RNA interference, kinesin Eg5 and ABCB1/ABCG2 inhibition, Doctoral thesis, University of Regensburg, **2007**.

Pfleger KD and Eidne KA: Monitoring the formation of dynamic G-protein-coupled receptor-protein complexes in living cells, *Biochem J*, **2005**, *385*, 625–637.

Pop N: Development of functional assays for human neuropeptide Y ($Y_{1,2,4,5}$) receptors exploiting GTPase activity and (bio)luminescence as readout, Doctoral thesis, University of Regensburg, **2010**.

Schneider E *et al.*: A simple and powerful flow cytometric method for the simultaneous determination of multiple parameters at G protein-coupled receptor subtypes, *ChemBioChem*, **2006**, *7*, 1400–1409.

Schneider E, Keller M *et al.*: Synthesis and characterization of the first fluorescent non-peptide NPY Y_1 receptor antagonist, *ChemBioChem*, **2007**, *8*, 1981 – 1988.

Schneider E: Development of fluorescence-based methods for the determination of ligand affinity, selectivity and activity at G-protein coupled receptors, Doctoral thesis, University of Regensburg, **2005**.

Sheikh SP and Williams JA: Structural characterization of Y_1 and Y_2 receptors for neuropeptide Y and peptide YY by affinity cross-linking, *J Biol Chem*, **1990**, *265*, 8304–8310.

Smith NJ and Milligan G: Allostery at G protein-coupled receptor homo- and heteromers: uncharted pharmacological landscapes, *Pharmacol Rev*, **2010**, *62*, 701–725.

Ziemek R: Development of binding and functional assays for the neuropeptide Y Y_2 and Y_4 receptors, Doctoral thesis, University of Regensburg, **2006**.

Chapter 4

Radioligand binding studies of bivalent histamine H_2 and H_4 receptor ligands at (pre)equilibrium conditions

4 Radioligand binding studies of bivalent histamine H_2 and H_4 receptor ligands at (pre)equilibrium conditions

4.1 Introduction

N^G-Acylated hetarylpropylguanidines represent a new class of H_2R agonists with improved pharmacokinetic properties compared to the corresponding guanidines due to substantially reduced basicity (Ghorai *et al.*, 2008; Kraus *et al.*, 2009). Very recently, a tremendous increase in potency was achieved by applying the bivalent ligand approach to acylguanidine-type H_2R agonists (Birnkammer *et al.*, 2008). These compounds, composed of two sets of pharmacophoric groups joined with an alkanedioic linker, are up to 4000-fold more potent than HIS (Kraus, 2007; Birnkammer *et al.*, 2010), both, on the isolated guinea-pig right atrium (cf. Fig. 1.2.7 A) and in steady-state GTPase assays on hH_2R- and gpH_2R-$G_{s\alpha S}$ fusion proteins expressed in Sf9 cells (cf. Fig. 1.2.7, panels B–G; Wenzel-Seifert *et al.*, 2001). Initially, such "twin compounds" were designed as potential tools to study putative H_2R dimers. However, as shown in Fig. 4.1.1 B, in the most potent bivalent H_2R ligands the linkers, connecting the carbonyl functions, comprise only 6–8 methylene groups. Hence, those compounds cannot bridge H_2R dimers in a manner proposed by Portoghese and colleagues (Fig. 4.1.1 A; cf. Bhushan *et al.*, 2004; Daniels, 2005 a; Shonberg *et al.*, 2011).

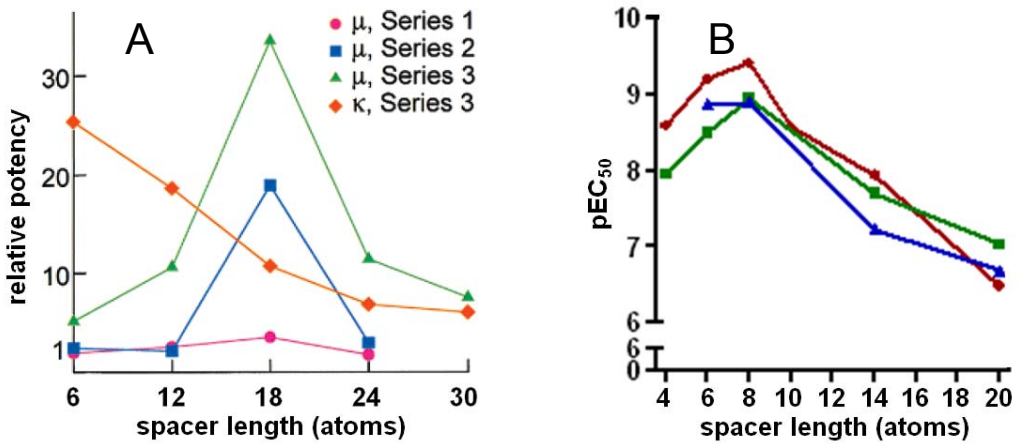

Fig. 4.1.1. *Relationship between spacer length and potency of symmetric bivalent ligands. (A) Relative agonist and antagonist potencies of of different series of bivalent ligandsat opioid receptors. The potencies of bivalent compounds (normalized to morphine) were related to the potencies of monovalent counterparts of intermediate-length spacers (normalized to morphine); adopted from Portoghese et al., 1986 and Portoghese, 2001, with modifications. (B) Agonist potencies at the gpH_2R-$G_{s\alpha S}$ (in red – ligands containing 2-amino-4-methylthiazole, in blue – 2-aminothiazole and in green – imidazole rings, adopted from Birnkammer et al., 2010, with modifications). Similar results were obtained at the hH_2R-$G_{s\alpha S}$.*

The present investigation was focused on a more detailed analysis of the binding of mono- and bivalent ligands at the H_2R. Since the imidazolylpropylguanidine moiety turned out to be a privileged structure with respect to histamine receptors, the investigations were extended to the H_4R (Kraus, 2007).

4.1.1 Explanatory power of the Hill slope in radioligand saturation and competition binding assays at equilibrium

4.1.1.1 Indicators of cooperativity and ligand–receptor stoichiometry

Estimation of the inflection points of semilogarithmic binding curves provides information on ligand affinities (Fig. 4.1.2 A). It is assumed that binding has reached equilibrium, thereby obeying the law of mass action and that ligand-receptor interactions occur according to a 1:1 stoichiometry. Therefore, the Hill slope (n_H) is usually adjusted to unity and the competition curve between 10% and 90% displacement covers approx. a hundredfold range of ligand concentrations (between 0.1- and 10-fold·IC_{50}; cf. Lazareno, 2001), as depicted in Fig. 4.1.2 B ("normal" curve is linear between approx. 20 and 80% displacement). However, algorithms for fitting experimental data by a four-parameter logistic curve with a variable slope often yield a slope different from unity (Prinz and Schönichen, 2008). In such cases, curves do not cover 10–90% occupancy over a range of 2 log units (Lazareno, 2001; cf. shallow and steep curves in Fig. 4.1.2 B).

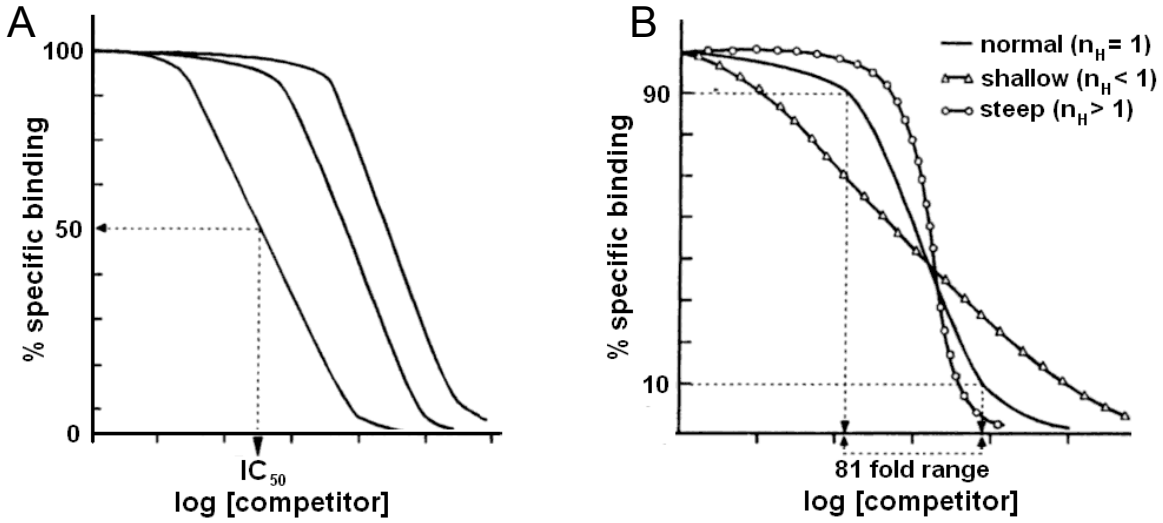

Fig. 4.1.2. *Pharmacologic parameters derived from the analysis of competition binding curves: (A) the inflection point (IC_{50}) and (B) Hill slope n_H (adopted from Limbird, 2004 with modifications).*

Table 4.1.1. *Various possible explanations for $n_H \neq 1$ (cf. Repke and Liebmann, 1987).*

The value of n_H	Possible explanations
0.5	Heterogenic ligand binding sites Negative cooperativity
1	Homogenic population of ligand binding sites
2	Positive cooperativity

Derived from the Hill equation, the Hill slope corresponds to the number of ligand molecules interacting with a receptor in an "all or none" reaction, and therefore it might reflect the actual ligand-receptor stoichiometry (cf. Eq. 4.1.1–2).

$$nA + R \leftrightarrow A_nR \qquad \text{(Eq. 4.1.1)}$$

$$\frac{B}{B_{max}} = \frac{[A]^{nH}}{[A]^{nH} + K^{nH}} \qquad \text{(Eq. 4.1.2)}$$

Depending on the position of the binding pockets for the two pharmacophoric moieties of a twin compound on a single receptor molecule, two independent receptors or a receptor dimer, the value of n_H could vary between 0.5 and 2, as shown in Fig. 4.1.3. Nevertheless, apart from the ligand-receptor stoichiometry, other important factors should be considered as well, for example cooperativity (Table 4.1.1; cf. Repke and Liebmann, 1987).

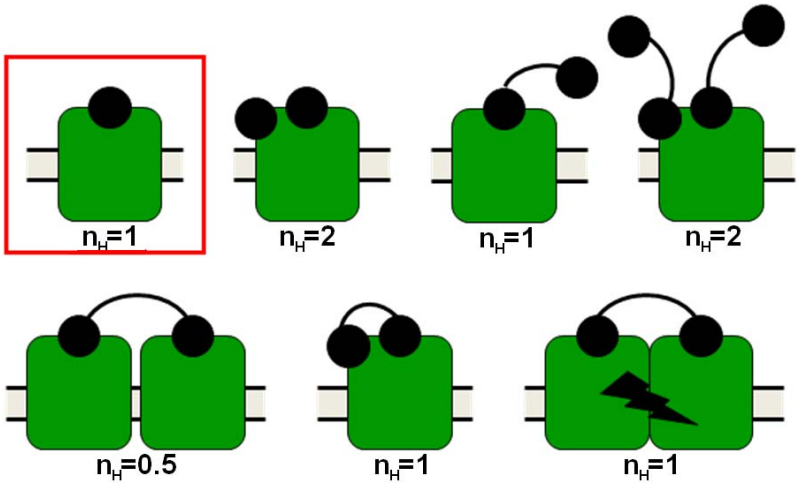

Fig. 4.1.3. *Possible spatial arrangements of ligands (mono- or bivalent) and receptors (a single receptor, two non-linked receptors or a conformationally linked receptor dimer). The values of Hill slopes correspond to the number of ligand molecules interacting with a receptor in an "all or none" reaction (Eq. 4.1.1). The classical situation with the 1:1 ligand-receptor stoichiometry is highlighted by a red box.*

4.1.1.2 Biphasic Scatchard plots

The analysis of saturation binding curves might also elucidate the binding mode of a radioligand. According to Scatchard, in case of a competitive ligand-receptor interaction with 1:1 stoichiometry, the classical linearizing transformation of the radioligand saturation curve gives a single straight line, as shown in Fig. 1.3.1 B, where the dissociation constant K_d equals the negative inverse of the slope (Lazareno, 2001). However, a previous study by Monczor et colleagues on U-937 cells, using [^{3}H]TIO as the radioligand, revealed a convex (biphasic) shape of the Scatchard plot (Fig. 4.1.4 A). This phenomenon might be explained either by incorrectly determined unspecific binding (competitor concentration too low) or by the existence of binding sites with different affinity for the radioligand (Repke and Liebmann, 1987). Indeed, low and high affinity binding sites were found for [^{3}H]TIO, with the high-affinity binding site disappearing in the presence of 10 µM GTPγS. Thus, binding of TIO to H_2Rs present in the free and in the G-protein-coupled form is a plausible explanation of these results. The obvious preference of TIO for G-protein-bound receptors indicates an inverse agonism of TIO, as predicted by the extended ternary complex model (cf. Fig. 1.1.6), assuming the existence of two classes of interconverting binding sites (Fig. 4.1.4 B; cf. Monczor *et al.*, 2003).

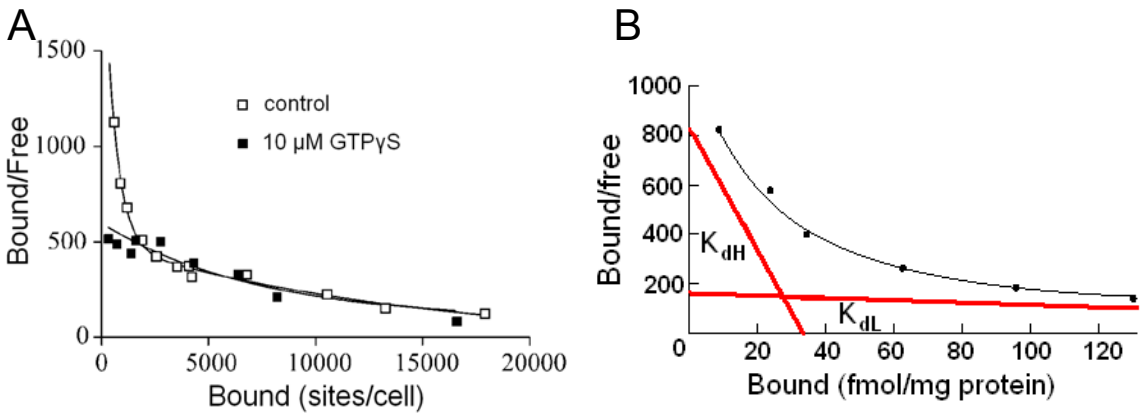

Fig. 4.1.4. *Biphasic Scatchard plots: (A) saturation binding of [^{3}H]TIO at the H_2R in U-937 cells. Purified fractions of U-937 membranes were incubated for 2 hours (adopted from Monczor et al., 2003 with modifications). (B) Two-site model of ligand-receptor interactions. The slopes of the red lines equal the negative inverses of the affinity constants of high-affinity (K_{dH}) and low-affinity (K_{dL}) binding sites (adopted from http://www.chemistry.emory.edu/justice/test/receptor_measurement.htm with modifications).*

N.B. Hill slopes of competition curves smaller than unity can also result from the existence of two non-interconverting (ortho- and allosteric) binding sites on the same receptor molecule. The hypothesis of allosterism will be addressed in chapter 5.

4.2 Materials and methods

4.2.1 Materials

Sf9 cells and high-titer baculovirus stocks, encoding H_2Rs, $G_{s\alpha S}$, $G_{i\alpha 2}$, $G_{\beta 1\gamma 2}$ proteins as well as H_2R-$G_{s\alpha S}$ and hH_4R-GAIP fusion proteins, were kindly provided by Prof. Dr. Roland Seifert (Institute of Pharmacology, Medical School of Hannover, Germany). The generation of the baculoviruses encoding the hH_2R-$G_{s\alpha S}$ and the gpH_2R-$G_{s\alpha S}$ has been described elsewhere (Kelley *et al.*, 2001).

The mono- and bivalent H_2R ligands (Fig. 1.2.4) were synthesized and provided by Dr. Anja Kraus (Kraus, 2007; Kraus *et al.*, 2009) and Mr. Tobias Birnkammer (cf. prospective doctoral thesis of T. Birnkammer). HIS was from Acros Organics (Geel, Belgium). RAN and FAM were obtained from Sigma (St. Louis, MO, USA). TIO was donated by Prof. Dr. Sigurd Elz (Institute of Pharmacy, University of Regensburg, Germany). GTPγS (Fig.1.1.4) was from Roche Diagnostics (Mannheim, Germany). Radioactive tracers [^{35}S]GTPγS (1100 Ci/mmol), [^{3}H]HIS (14.2 Ci/mmol) and [^{3}H]TIO (77.2 and 82.2 Ci/mmol) were from PerkinElmer Health Sciences (Boston, MA, USA) and [^{3}H]TIO (82.2 Ci/mmol) was from American Radiolabeled Chemicals (St. Louis, MO, USA). [^{3}H]UR-DE257 (69.3 Ci/mmol) and the red fluorescent H_2R ligands were synthesized by Dr. Daniela Erdmann in our laboratory as described previously (Fig. 1.2.5; Erdmann, 2010).

Insect-Xpress medium for Sf9 cells was from Lonza (Verviers, Belgium). BSA was from Behringwerke (Marburg, Germany). FCS was obtained from Biochrom (Berlin, Germany). Gentamicin was from Lonza (Walkersville, MD, USA). Tris was purchased from USB (Cleveland, OH, USA). $MgCl_2$ and EDTA were from Merck (Darmstadt, Germany). Polyethylenimine (PEI) and phenylmethylsulfonyl fluoride (PMSF) were from Sigma-Aldrich (Steinheim, Germany). Benzamidine was from Acros Organics (Geel, Belgium). Leupeptin was obtained from Gerbu Biotechnik (Gaiberg, Germany). DC protein assay kit was purchased from Bio-Rad Laboratories (Munich, Germany) Round-bottom polypropylene test tubes (4 mL) were from Kabe Labortechnik (Nümbrecht, Germany). Needles Neolus were from VWR International (Ismaning, Germany). GF/B glass-fibre filters were purchased from Brandel (Gaithersburg, MD, USA). The 6-mL scintillation counting vials were obtained from Sarstedt (Nümbrecht, Germany). Scintillation cocktail Rotiszint eco plus was from Carl Roth (Karlsruhe, Germany). High purity water, used in all assays, was prepared with Milli-Q Reagent Water System from Millipore (Molsheim, France).

The human promonocytic U-937 cell line was a kindly provided by Prof. Dr. Roland Seifert. CHO-rH_2R-A_2 cells (Traiffort *et al.*, 1992) were a gift by Dr. Jean-Michel Arrang (Institut National de la Santé et de la Recherche Médicale, Paris, France). The generation of CHO-hH_2R-$G_{\alpha 16}$ cells was described before (Schneider, 2005). CHO cells were from the DSMZ (Deutsche Sammlung für Mikroorganismen und Zellkulturen, Braunschweig, Germany). The pcDNA3.1(+)-Neo-hH_4R plasmid was from the Guthrie cDNA Resource Center (Sayre, USA; cf. Mosandl, 2009). The jetPEI transfection reagent, from Polyplus-transfection (Illkirch, France), was donated by Peqlab Biotechnologie (Erlangen, Germany). DMEM and Ham's F12 nutrient mixtures were purchased from Sigma-Aldrich. FCS and geneticin (G418) were from Biochrom (Berlin, Germany). Hygromycin B was obtained from Mobitec (Göttingen, Germany). Trypsin-EDTA (10x) was from PAA Laboratories (Pasching, Austria). Leibovitz' L-15 medium, without phenol red, was from Invitrogen (Karlsruhe, Germany). Transparent 6-well and 96-well plates were purchased from Greiner (Frickenhausen, Germany), whereas transparent 24-well plates were from Becton Dickinson (Heidelberg, Germany). Safety-Multifly needles (21G) and 4-mL S-Monovettes (for blood collection by venous puncture) were from Sarstedt. Lymphoprep solution was from Axis-Shield PoC (Oslo, Norway).

All experimental data were analyzed with the Prism 5 program (GraphPad Software, San Diego, CA, USA).

4.2.2 Membrane Preparation

Sf9 cells were seeded in Insect-Xpress medium supplemented with 5% (v/v) FCS and 0.1 mg/ml gentamicin in 250- or 500-mL Erlenmeyer flasks at the density of 3 million cells/mL and infected with a 1:100 dilution of high-titer baculovirus stocks, encoding the H_2R (hH_2Rs or gpH_2Rs either alone, as -$G_{s\alpha S}$ fusion proteins or coexpressed with $G_{s\alpha S}$) or the H_4R (hH_4R-GAIP fusion proteins coexpressed with $G_{i\alpha 2}$ and $G_{\beta 1\gamma 2}$).

After 48 hours of incubation at 28 ºC under rotation at 150 rpm in an Excella E24R incubator shaker from New Brunswick Scientific (Edison, NJ, USA), Sf9 membranes were prepared from the transfected cells as described previously (Seifert *et al.*, 1998), using 1 mM EDTA as well as protease inhibitors: 0.2 mM PMSF, 10 µg/ml benzamidine and 10 µg/ml leupeptin. Membranes were suspended in binding buffer (12.5 mM $MgCl_2$, 1 mM EDTA and 75 mM Tris/HCl, pH 7.4) and stored at -80 °C in 1-mL aliquots until use.

Protein concentration of each membrane preparation was determined in triplicate by Lowry's protein assay (Lowry *et al.*, 1951), using a Bio-Rad DC protein assay kit according

to the manufacturer's protocol (http://wolfson.huji.ac.il/). Absorbance was measured at 750 nm. Each time the assay was performed, a calibration curve with different concentrations of BSA (150-2000 µg/mL) was prepared to assign absorbance values to protein concentrations.

4.2.3 Radioligand binding assays with Sf9 membranes

If not otherwise stated, binding assays were carried out at room temperature (20–23 ºC) in 4-mL polypropylene tubes in triplicate and set up to fit the format of an M-48 harvester from Brandel (Gaithersburg, MD, USA). Each tube (total volume of 250 µL) contained 50-200 µg of protein in case of the H_2R and 30–100 µg of protein in case of the H_4R.

4.2.3.1 Competition binding assay

Firstly, 25 µL of a feed solution of an unlabeled ligand, 10-fold concentrated compared to the final concentration, were pipetted into tubes. For the determination of unspecific binding, the highest concentration of an unlabeled ligand or final concentrations of 100 µM FAM (in case of the H_2R) or 10–20 µM THIO (in case of the H_4R) was chosen. In order to determine total binding of the radioactive tracer, 25 µL of water were used instead of an unlabeled competitor. Secondly, an appropriate volume of BSA dissolved in binding buffer was added to each tube to give a BSA final concentration of 0.2% (m/v). Addition of BSA prevents adsorption of membranes and lipophilic compounds, especially at low concentrations, to the tube material (Seifert and Wieland, 2005). To determine the effect of exogenous guanine nucleotides in competition binding assays at the H_2R, 25 µL of GTPγS (final concentration: 10 µM) or water were pipetted into the tubes.

Thereafter, 25 µL of the radioactive tracer dissolved in binding buffer were added to each tube. In case of the H_2R, the radioligands were diluted with the respective unlabelled ligand (reduction of specific activity to save radiotracers: [^{3}H]TIO plus unlabeled TIO were used to obtain a final ligand concentration of 10–30 nM, [^{3}H]HIS plus HIS yielding a final agonist concentration of 1 µM, and [^{3}H]UR-DE257 plus unlabeled UR-DE257 to yield a final concentration of 25 nM. In assays at the H_4R, [^{3}H]HIS was added as obtained from the manufacturer to get final concentrations from 10 to 100 nM. Parallel to the dilution of the radioligand, Sf9 membranes were allowed to thaw, put on ice and gently suspended (using a 1-mL syringe: 4 times with a 0.7-mm needle and 4 times with a 0.4-mm needle). Then membranes were centrifuged at 4 ºC and 15000 g (13000 rpm)

and resuspended in an appropriate volume of the ice-cold binding buffer. This washing step was performed in order to remove residual endogenous guanine nucleotides, which could disturb the the effect of exogenous GTP or GTPγS on the binding of an agonist or an inverse agonist (Seifert and Wieland, 2005). To obtain homogenous suspensions, membranes were resuspended 30 times with the same syringe (0.4-mm needle) shortly before incubation. The incubation for 90–450 min (at 20–23 ºC under shaking at 250 rpm) was started by addition of 50 µL of the membrane suspension to each tube.

The reaction was stopped by addition of approx. 2 mL of ice-cold binding buffer. The bound radioligand was separated from the free radioligand by rapid filtration through a GF/B glass-fibre filter followed by two washes with approx. 2 mL of ice-cold binding buffer. The filter was pretreated with ice-cold 0.3% (v/v) polyethyleneimine (PEI) to reduce unspecific binding of positively charged radioligands to negatively charged silanol ($-SiO^-$) groups of the filter material. Although [^{3}H]TIO was found to bind to the pretreated filters to the same extent as to untreated filters (data not shown), PEI pretreatment was always done as a standard procedure.

Thereafter, filter discs were allowed to equilibrate overnight with 3 mL of Rotiszint eco plus in 6-mL mini-vials. Filter-bound radioactivity was measured in a LS 6500 Liquid Scintillation Counter from Beckman Coulter (Krefeld, Germany) for 5 min. To avoid radioligand depletion, the experimental settings were adjusted to ensure that no more than 5% of the total radioligand added to test tubes were bound to the filter.

4.2.3.2 Saturation binding of [^{3}H]tiotidine

Experiments were essentially performed as described for competition binding assays. For the determination of total binding, the tubes contained: 25 µL of water, 150 µL of BSA in binding buffer, 25 µL of the radioligand (0.3 to 40 nM [^{3}H]TIO plus unlabeled TIO to yielding final ligand concentrations $\leq$ 200 nM) and 50 µL of an appropriate membrane suspension. Unspecific binding was examined in the presence of 100 µM FAM (final). Samples were incubated for 90 min. Specific binding of the radioligand to the H_2R was obtained by subtracting unspecific binding from total binding for each given [^{3}H]TIO concentration.

4.2.4 [^{35}S]GTPγS binding assay with Sf9 membranes

Experiments were performed as described previously (Schnell *et al.*, 2010) with a few modifications: 25 µL of water or HIS (final 100 µM) as well as 150 µL of binding buffer, containing BSA (final 0.05%) and GDP (final 1µM), were added into each tube. For unspecific binding, 25 µL of unlabeled GTPγS in binding buffer were used (10 µM final). The samples were completed by addition of 25 µL of an appropriate membrane suspension (3–4 µg of protein), prepared as described for [^{3}H]TIO binding, and incubation was started by addition of 25 µL of [^{35}S]GTPγS (1 nM final) diluted with unlabeled GTPγS (9 nM final). Incubation was performed in quadruplicate for 120 min at room temperature (20–23 ºC) under shaking at 250 rpm. Subsequently, the reaction was terminated, and the bound radioactivity was measured as described for [^{3}H]TIO binding assays.

4.2.5 Cell culture and transfection

Cells were maintained in the culture media (listed in Table 4.2.1) at 37 °C in the humidified atmosphere containing 5% CO_2. Every 4–7 days, cells were trypsinized and passaged (1:10) to a fresh 25-cm^2 culture flask, except for U-937 cells, growing in suspension, which were passaged to a fresh 75-cm^2 culture flask.

Table 4.2.1. *Cell culture conditions of the used cell lines.*

Cell line	Cell culture conditions
U-937	RPMI + 5% FCS
CHO-rH_2R-A_2	DMEM / Ham's F12 (1:1) + 10% FCS
CHO-hH_2R-$G_{\alpha16}$	Ham's F12 + 10% FCS +400 µg/mL G418 +400 µg/mL hygromycin B
CHO-K1	Ham's F12 + 10% FCS
CHO-hH_4R	Ham's F12 + 10% FCS+ 400 µg/mL G418

CHO-K1 cells were transfected using the jetPEI transfection reagent according to the manufacturer's protocol. The cells were seeded one day prior to transfection in a 24-well plate in Ham's F12 medium containing 10% FCS. On the day of transfection, 4 µL of the pcDNA3.1(+)-Neo-hH_4R plasmid (1 µg/µL) were mixed with 200 µL of 150 mM NaCl solution and 8 µL of the jetPEI reagent (7.5 mM solution of nitrogen residues) were added to 200 µL of 150 mM NaCl solution. The amounts of DNA and jetPEI were adjusted to provide ionic balance between the nitrogen residues of jetPEI (one third of N atoms are cations) and the phosphate anions of the DNA backbone. Optimal transfection efficiency

was obtained at the N/phosphate ratio of 5. Then, both solutions were combined and incubated for 30 min. Afterwards, 50 µL (in duplicate), 100 µL (in duplicate) or 0 µL (control in unicate) of the mixture were added per well onto the confluent cells (for optimal transfection with jetPEI, 50-60% confluent cells are recommended).

The selection of the stably transfected CHO-hH_4R cells was done with the aminoglycoside antibiotic geneticin (G418), as described in subsection 6.2.5. Briefly, on the next day the transfected cells were passaged into a new 6-well plate, and two days later each of the 5 transfectant clones was passaged into a fresh 25-cm^2 culture flask. On two subsequent days, the culture medium was changed against medium containing G418 (400 µg/mL). Six days after transfection, all non-transfected cells (the control) were killed. Only a few cells transfected with 50 µL of the mixture survived, but among the cells transfected with 100 µL of the mixture groups of living cells were found. These cells, bearing the genes for the hH_4R and the resistance against antibiotic geneticin (G418), were passaged into a fresh 75-cm^2 culture flask (always in the culture medium with 400 µg/mL G418).

Due to the limited stability of antibiotics in culture media (e.g. 5 days for the aminoglycosides kanamycin and neomycin at 37 °C; Lindl, 2000) and to avoid underdosing of the antibiotic, the respective selection media, listed in Table 4.2.1, were always prepared immediately before passaging of the cells.

4.2.6 Radioligand binding assays with whole cells

Radioligand binding on whole cells was determined as described by Dr. Johannes Mosandl (Mosandl, 2009). 4–6 days prior to an experiment, appropriate cells were passaged to 1–3 fresh 175-cm^2 culture flasks and cultivated in the absence of antibiotics. On the day of experiment, cells were trypsinized, centrifuged for 5 min at 1000 rpm (300 g), washed with L-15 medium and centrifuged again. Subsequently, the cells were resuspended in fresh L-15 medium to obtain the required density. 20 µL of either a 10-fold concentrated FAM solution (in PBS or L-15, for unspecific binding) or the corresponding solvent (for total binding) as well as 160 µL of the cell suspension and 20 µL of a 10-fold concentrated radioligand solution (cf. subsection 4.2.3) were added per well of a 96-well plate. Incubation was conducted for 90 min at room temperature (20–23 ºC) under shaking at approx 100 rpm. The reaction was terminated with a cell harvester by rapid filtration through a GF/B glass-fibre filter, pretreated with the ice-cold 0.3% (v/v) PEI. The harvested cells were immediately washed with ice-cold PBS for approx. 10 s. The filter-bound radioactivity was estimated by means of liquid scintillation, as described for Sf9

membrane preparations in subsection 4.2.3. The corresponding receptor number per cell (RN) was calculated by using the total amount of radioactivity added to the tubes (TA) (Eq. 4.2.1) or, more accurately, by involving the specific radioactivity of the radioligand (Eq. 4.2.2):

$$RN = \frac{\text{spec. binding}[\text{dpm}] \cdot TA\,[\text{nM}] \cdot V\,[\text{L}] \cdot N_A}{TA\,[\text{dpm}] \cdot 10^9 \cdot \text{cells}[1/\text{well}]} \qquad \text{(Eq. 4.2.1)}$$

$$RN = \frac{\text{spec.binding}[\text{dpm}] \cdot N_A}{\text{spec.activity}[\text{Bq}/\text{nmol}] \cdot 60 \cdot 10^9 \cdot \text{cells}[1/\text{well}]} \qquad \text{(Eq. 4.2.2)}$$

where V is the volume of the incubation mixture ($2 \cdot 10^{-4}$ L) and N_A the Avogadro constant ($6.022 \cdot 10^{23}$ mol^{-1}). The calculations always considered the reduction of the specific activity of the radioligand (cf. subsection 4.2.3).

4.2.7 Isolation of human neutrophilic granulocytes from whole blood

Neutrophils were isolated from venous blood as described (Seifert *et al.*, 1989) with minor modifications. At 9 a.m. (after having breakfast) 20 mL of blood were obtained from the medial cubital vein of a healthy male volunteer (age of 28; without medication for at least one month), by using a Safety-Multifly needle (21G) and 4-mL S-Monovettes (containing EDTA as an anticoagulant). All following isolation steps were carried out at room temperature (approx. 20 ºC). Each 10 mL of blood were diluted with 25 mL of PBS (1x) and then carefully layered on top of 15 mL of Lymphoprep solution (density of 1.077 g/mL, osmolality of 290 mOsm) in a 50-mL centrifuge tube. This centrifugation step was performed at 400 g for 30 min in a swing-out rotor. After centrifugation, a distinct lymphocyte layer had formed at the interface between the plasma and the Lymphoprep phase, whereas granulocytes and erythrocytes were in the pellet as shown in Fig. 4.2.1.

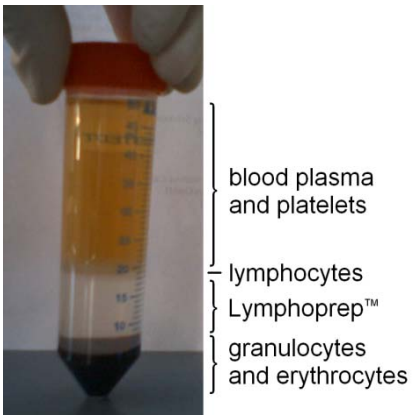

Fig. 4.2.1. *Distribution of blood components after centrifugation with Lymphoprep separation fluid. Neutrophilic granulocytes and red blood cells were in the pellet.*

Then, the three upper layers were completely removed with an electronic dispenser (first, the lymphocytes, by moving the dispenser in a sweeping motion; next, the plasma; and finally, the Lymphoprep solution) and the granulocyte-erythrocyte pellet was suspended in 20 mL of Millipore water. After 60 s of haemolysis (longer incubation could lead to the lysis of granulocytes), 2 mL of 10x PBS were added for equilibration and the mixture was centrifuged for 5 min at 300 g. The supernatant was discarded and the erythrocytes, remaining in the diffuse pellet, were lysed by addition of 10 mL of Millipore water. After 30 s of gentle agitation, 1 mL of 10x PBS was added for equilibration, and the mixture was centrifuged for 5 min at 300 g. The supernatant was carefully discarded and the granulocytes were washed with 5 mL of PBS. After centrifugation (5 min at 300 g) the upper part of the supernatant was carefully discarded with the dispenser and the rest of the supernatant (and some hemoglobin over the pellet) was removed with a 1-mL Eppendorf pipette. Finally, the granulocytes were resuspended in 1 mL of PBS and counted with a Casy 1 TTC cell counter from Schärfe System (Reutlingen, Germany), yielding approx. 33 million cells/mL.

4.3 Results and discussion

4.3.1 Saturation binding assays on H_2Rs

The investigation of agonists and antagonists on H_2R-$G_{s\alpha S}$ fusion proteins expressed by means of the *Sporodoptera frugiperda* cell/baculovirus system is a very useful alternative to the classical testing on isolated animal organs. It provides defined receptor-to-G-protein stoichiometry and very efficient coupling, which can be measured by GTP hydrolysis (Wenzel-Seifert *et al.*, 2001). The presence of G proteins is essential for functional studies, such as steady-state GTPase assays, but should be dispensable for binding studies. Nevertheless, the receptor-to-G-protein stoichiometry may affect the shape of binding curves (Kenakin, 1997 and 2006; Lazareno, 2001). Therefore, saturation binding studies were performed at gpH_2R-$G_{s\alpha S}$ fusion proteins and at gpH_2Rs coexpressed with $G_{s\alpha S}$ proteins. This could be useful to elucidate the competition experiments conducted in the presence of GTPγS on Sf9 membranes expressing gpH_2R-$G_{s\alpha S}$ fusion proteins, gpH_2Rs alone or coexpressing gpH_2Rs and $G_{s\alpha S}$ proteins (cf. subsection 4.3.2). As the pretreatment of glass-fibre filters with PEI has become a standard procedure, the estimated radioligand affinities might slightly differ from the values from literature, which were determined without PEI treatment (Kelley *et al.*, 2001). This improvement should be considered, when analyzing binding data from competition assays.

4.3.1.1 Saturation binding of [^{3}H]tiotidine

The gpH_2R-$G_{s\alpha S}$ fusion protein, expressed in Sf9 membranes, bound [^{3}H]TIO with a K_d of 40.0 ± 6.3 nM and a B_{max} of 0.66 ± 0.04 pmol/mg of membrane protein (Fig. 4.3.1). This was in line with data from the literature (reported: K_d 34.4 ± 8.4 nM, B_{max} 0.72 ± 0.02 pmol/mg; Kelley *et al.*, 2001).

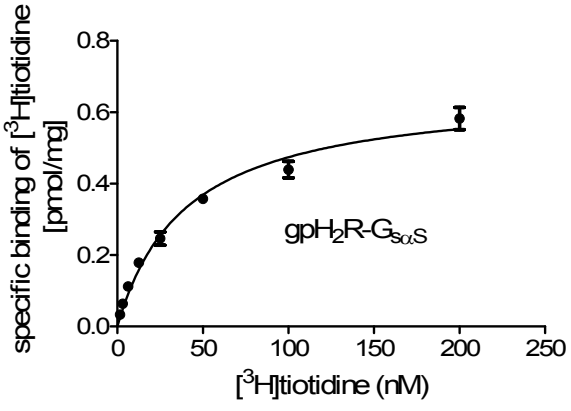

Fig. 4.3.1. *Saturation binding of [^{3}H]TIO. Sf9 membranes expressing the gpH_2R-$G_{s\alpha S}$ were incubated with [^{3}H]TIO for 90 min. Unspecific binding was determined in the presence of 100 µM FAM. Data were analyzed by nonlinear regression (one-site model) and are mean values ± SEM of an experiment performed in triplicate.*

Similarly, the analysis of the saturation binding data of [^{3}H]TIO at the hH_2R-$G_{s\alpha S}$ revealed a K_d of 43.3 ± 17.9 nM and a B_{max} of 0.54 ± 0.09 pmol/mg of membrane protein (raw data kindly provided by Dr. Heidrun Appl, Institute of Pharmacy, University of Regensburg; cf. Appl, 2010), which is in agreement with data reported previously (K_d: 32.0 ± 4.6 nM, B_{max}: 0.43 ± 0.02 pmol/mg; Wenzel-Seifert *et al.*, 2001). Therefore, in competition binding assays at gpH_2R-$G_{s\alpha S}$ and hH_2R-$G_{s\alpha S}$, the K_d values of [^{3}H]TIO of 40 and 43 nM, respectively, were used for calculation of K_i values from IC_{50} values of unlabeled test compounds according to the Cheng-Prusoff equation (Cheng and Prusoff, 1973).

In order to investigate whether the $G_{s\alpha S}$ protein C-terminally fused to receptor could alter the binding of [^{3}H]TIO, saturation binding of the radioligand was performed in Sf9 membranes coexpressing gpH_2Rs and $G_{s\alpha S}$ proteins. The radioligand was bound with a K_d of 40.1 ± 6.4 nM and a B_{max} of 0.37 ± 0.02 pmol/mg of membrane protein (Fig. 4.3.2).

The gpH_2R-$G_{s\alpha S}$ bound [^{3}H]TIO with the same affinity as the gpH_2R coexpressed with the G protein (K_d = 40 nM), but the expression level of the fusion protein was increased, compared to the coexpressed receptors. ***N.B.*** similar effects were observed previously in case of hH_4R-RGS4 and hH_4R-GAIP fusion proteins, when compared to the hH_4R in the standard co-expression system (Schneider and Seifert, 2009).

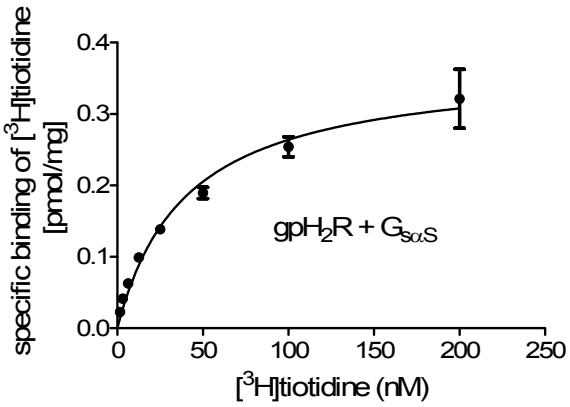

Fig. 4.3.2. *Saturation binding of [^{3}H]TIO. Sf9 membranes coexpressing gpH_2Rs and $G_{s\alpha S}$ proteins were incubated with [^{3}H]TIO for 90 min. Unspecific binding was determined in the presence of 100 µM FAM. Data were analyzed by nonlinear regression (one-site model) and are mean values ± SEM of two independent experiments performed in triplicate.*

Scatchard representations of the binding of [^{3}H]TIO to both the gpH_2R-$G_{s\alpha S}$ and the gpH_2R (coexpressed with $G_{s\alpha S}$ proteins) revealed convex curves, transformed as described before (Motulsky and Christopoulos, 2004). For classical competitive binding (single-site model), straight lines are expected. Therefore, the data points were refitted according to Graphpad Prism's built-in two-site binding equation (Eq. 4.3.1):

$$Y = \frac{B_{max1} \cdot X}{K_{d1} + X} + \frac{B_{max2} \cdot X}{K_{d2} + X} \qquad \text{(Eq. 4.3.1)}$$

Two different binding sites were obtained for [^{3}H]TIO at the gpH$_2$R coexpressed with the G$_{s\alpha S}$ protein (Fig. 4.3.3 B): a high-affinity (K_d 7.5 ± 1.1 nM, B_{max} 0.11 ± 0.01 pmol/mg) and a low-affinity binding site (K_d 146.8 ± 21.1 nM, B_{max} 0.38 ± 0.01 pmol/mg). The fitting failed in case of data from gpH$_2$R-G$_{s\alpha S}$; thus only a single line, corresponding to the non-linear regression fit (single-site), was graphed on the Scatchard plot (Fig. 4.3.3 A).

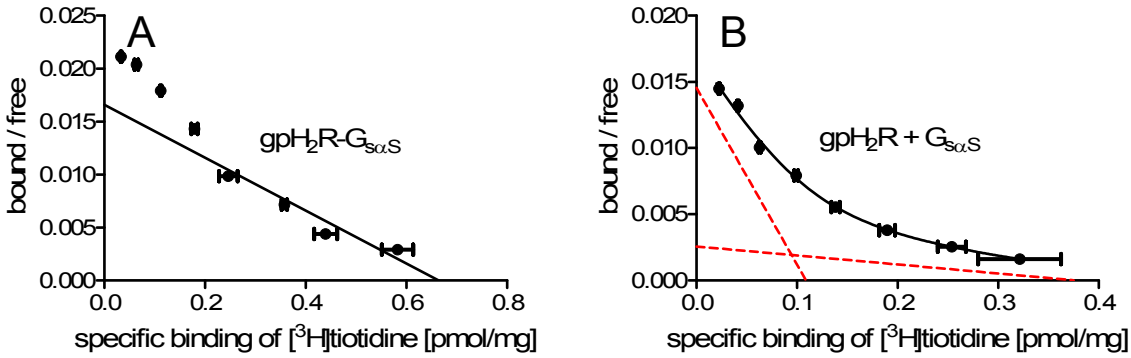

Fig. 4.3.3. *Binding data from Fig. 4.3.1 (A) and Fig. 4.3.2 (B) analyzed according to Scatchard. For the gpH$_2$R coexpressed with G$_{s\alpha S}$, two binding sites were found (red dashed lines).*

Scatchard plots for binding of [^{3}H]TIO on gpH$_2$R-G$_{s\alpha S}$ fusion proteins and gpH$_2$R + G$_{s\alpha S}$ coexpressed in Sf9 cells revealed a convex (biphasic) shape of the lines. Biphasic Scatchard representation was also found for [^{3}H]TIO on hH$_2$R-G$_{s\alpha S}$ fusion proteins (raw binding data kindly provided by Dr. Heidrun Appl, University of Regensburg). The shape of the Scatchard plots could result either from the incorrectly determined unspecific binding (too low competitor concentration) or from the existence of multiple binding sites for the radioligand (Repke and Liebmann, 1987).

The first possible explanation could be rejected, as the unspecific binding of [^{3}H]TIO was determined using 100 µM FAM (a concentration approx. 2000-fold higher than the K_i) after 90 min of incubation. The concentration of the unlabeled competitor was in the same range as that used in the previously reported studies on H$_2$R-G$_{s\alpha S}$ fusion proteins (100 µM of unlabeled TIO, equalling to a 3000-fold K_d, 90 min incubation; Kelley *et al.*, 2001) and by far exceeded the competitor concentration used at whole cells expressing H$_2$Rs (1 µM of unlabeled TIO referring to a 50-fold K_d, 40 min incubation at 4 ºC; Legnazzi *et al.*, 2000). In this context it is indispensable to mention that, after 3 hours of incubation with 10 nM [^{3}H]TIO in Sf9 membranes expressing gpH$_2$R-G$_{s\alpha S}$, FAM behaved different than expected from a competitive antagonist, revealing a slope of the competition curve smaller than unity (-0.71 ± 0.06, cf. Fig. 4.3.10) and stabilizing the ternary complex (Fig. 4.3.11 B). However, the determined K_i value for FAM of 17 ± 3 nM was in the same range as the functional (K_b 38 ± 3 nM; Table 4.3.3; cf. Kelley *et al.*, 2001) and

the binding data published before (K_i of 6 nM in membranes of the guinea-pig brain cortex after 60 min incubation at 37 ºC, Krielaart *et al.*, 1990).

As [^{3}H]TIO reveals a more complex binding behavior than described by the law of mass action, the existence of two distinct binding sites for the radioligand is proposed (cf. Fig. 4.3.3). This finding is in agreement with recently published results for [^{3}H]TIO at whole promonocytic U-937 cells, bearing the endogenous hH_2R (K_d of 2.2 ± 0.8 nM for the high-affinity binding site and 20 ± 3 nM for the low-affinity binding site, Monczor *et al.*, 2006). Previous studies indicate that the high-affinity binding site for [^{3}H]TIO at U-937 cell membranes disappeared after addition of 10 µM GTPγS, indicating a typical agonist binding profile. Moreover, TIO was able to reduce the increased basal cAMP levels in both the forskolin-stimulated U-937 cells and in the mammalian COS-7 cells, expressing heterologous H_2Rs (Monczor *et al.*, 2003) in a dose-dependent manner. TIO also reduced basal GTPase activity on hH_2R-$G_{s\alpha S}$ and gpH_2R-$G_{s\alpha S}$ fusion proteins (Kelley *et al.*, 2001). Taken together, TIO behaves as an inverse H_2R agonist. This contributes to the complexity of the H_2R signal transduction pathway and should be taken into account, when interpreting radioligand binding data.

4.3.1.2 (Functional) H_2R/G-protein stoichiometry: coexpressed and fused proteins

The receptor-to-G-protein ratio can influence the shapes of saturation and competition curves. In systems with limited capability of G-protein coupling, binding isoterms of a ligand that produces a ternary complex will not be monophasic (Kenakin, 1997 and 2006; Lazareno, 2001).

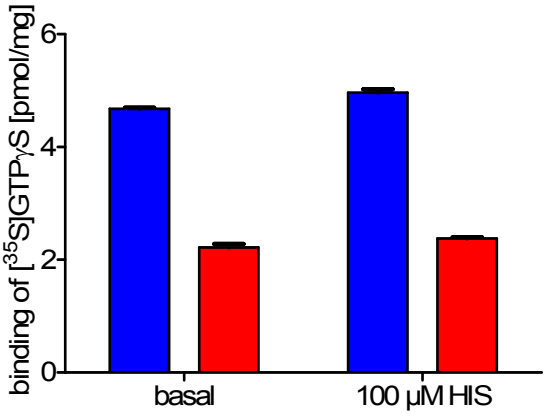

Fig. 4.3.4. *Total (blue) and unspecific (red) binding of [^{35}S]GTPγS to membranes co-expressing gpH_2Rs and $G_{s\alpha S}$ proteins. Specific binding in the absence of HIS amounted to 2.46 ± 0.07 pmol/mg and increased to 2.59 ± 0.06 pmol/mg after stimulation with 100 µM HIS. Data shown are mean values of an experiment performed in quadruplicate. The same membrane preparations were used as in [^{3}H]TIO binding assays.*

Therefore, apart from quantifying the number of receptors *via* the [^{3}H]TIO binding, the total content of functional G proteins was estimated, using a saturating concentration of [^{35}S]GTPγS/GTPγS (final 10 nM). Unspecific binding was determined in the presence of

10 µM of unlabeled GTPγS. Noticeably, in membranes coexpressing gpH_2R and $G_{s\alpha S}$, only a minor difference (0.13 ± 0.09 pmol/mg) was found between the HIS-stimulated and ligand-independent [^{35}S]GTPγS binding to $G_{s\alpha S}$ (Fig. 4.3.4). For this reason, in similar experiments on the gpH_2R-$G_{s\alpha S}$, the addition of HIS was resigned.

The number of specific [^{35}S]GTPγS binding sites, detected in the absence of agonists, was 1.76 ± 0.09 pmol/mg for gpH_2R-$G_{s\alpha S}$ fusion proteins and 2.46 ± 0.07 pmol/mg in membranes coexpressing gpH_2Rs and $G_{s\alpha S}$ proteins (Fig. 4.3.4). These results, disproving the hypothesis of limited G-protein coupling, showed that there are more functional G proteins than functional gpH_2Rs, determined by [^{3}H]TIO saturation binding: B_{max} of 0.66 ± 0.04 pmol/mg (Fig. 4.3.1) and 0.37 ± 0.02 pmol/mg (Fig. 4.3.2), respectively. Surprisingly, in preliminary experiments the ratio of gpH_2Rs to (functional) G proteins was about 1:3 for the fusion protein, whereas it amounted to about 1:7 for the coexpression. The last finding was in good agreement with the data reported previously for other histamine receptor subtypes coexpressed with appropriate G proteins (hH_3R, Schnell *et al.*, 2010; hH_4R, Schneider *et al.*, 2009).

4.3.2 Competition binding assays on the H_2R non-fused and fused to the $G_{s\alpha S}$

4.3.2.1 GTPγS-dependent shift of [^{3}H]tiotidine competition curves

Because acylguanidines are generally more potent at gpH_2R-$G_{s\alpha S}$ than hH_2R-$G_{s\alpha S}$ fusion protein (Xie *et al.*, 2006; Kraus, 2007), the investigations with guanine nucleotides (cf. Fig. 1.1.4) were done preferably on gpH_2Rs. It is also noteworthy that in the binding experiments the incubation period was set to 90 min, considered sufficient to reach the equilibrium (Lazareno, 2001) as it exceeded a five-fold dissociation half-value period for [^{3}H]TIO, which was found to be not longer than 11 min (Fig. 5.3.1; cf. Foreman *et al.*, 1985).

The detailed analysis of the binding curves of HIS and the symmetric bivalent imidazole-type compound **4** at hH_2R-$G_{s\alpha S}$ and gpH_2R-$G_{s\alpha S}$ fusion proteins revealed Hill coefficients smaller than unity (n_H of HIS: 0.5; n_H of agonist **4**: 0.6–0.8; Fig. 4.3.5 A–D). In the presence of 10 µM GTPγS the binding curves of HIS at hH_2R-$G_{s\alpha S}$ and gpH_2R-$G_{s\alpha S}$ fusion proteins were, however, shifted to the right, and the Hill coefficients increased approximating unity (cf. Fig. 4.3.5 B: pIC_{50} of HIS at the gpH_2R-$G_{s\alpha S}$: 6.17 ± 0.09, Hill slope: -0.49 ± 0.05; in the presence of 10 µM GTPγS: pIC_{50} 5.03 ± 0.05, Hill slope -1.15 ± 0.16). As expected for an antagonist, the competition curve of TIO was not affected by

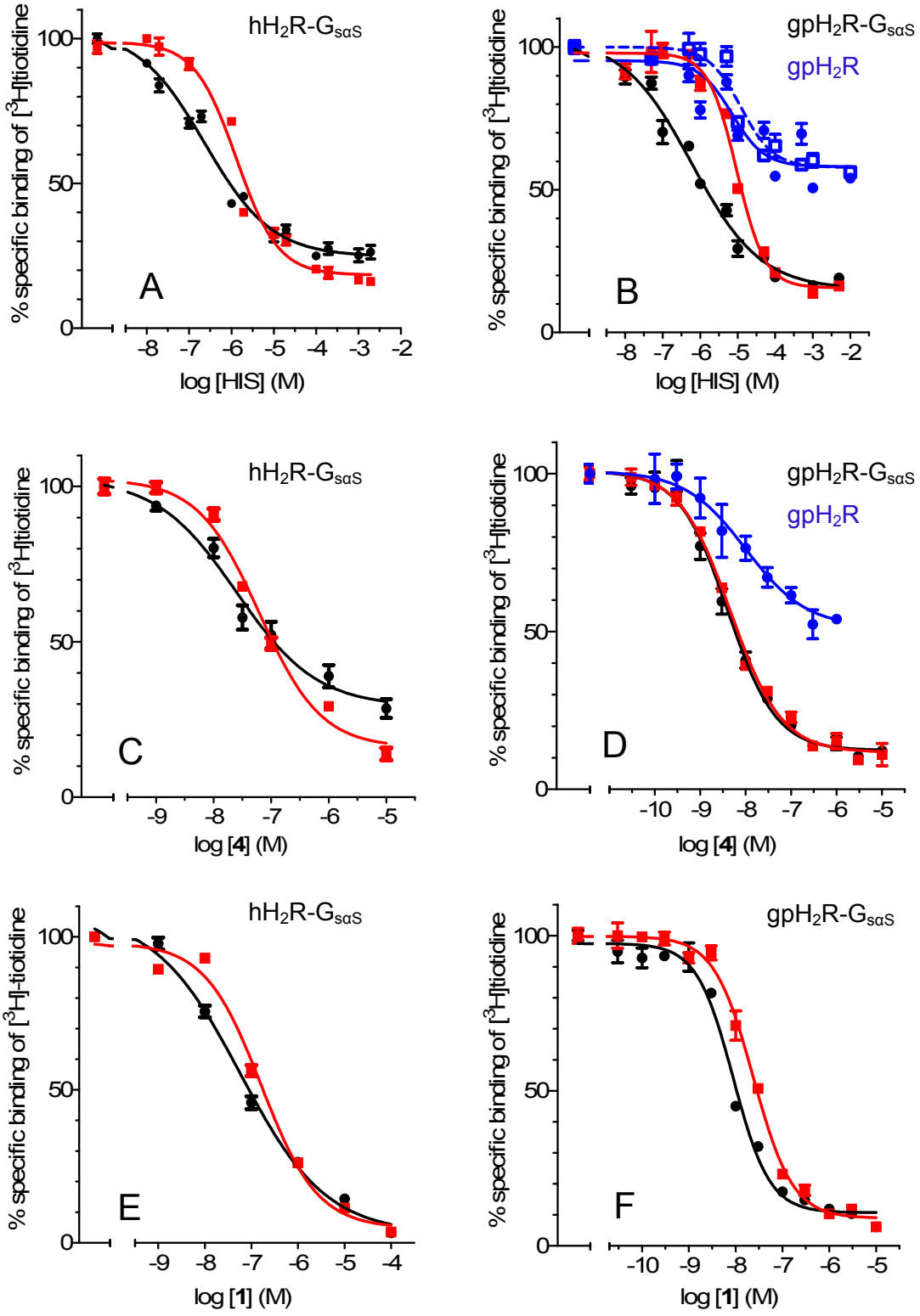

Fig. 4.3.5. *Effect of HIS (A, B), the bivalent agonist **4** (C, D) and the monovalent agonist **1** (E, F) on the displacement of [^{3}H]TIO (10 nM) from hH_2R-$G_{s\alpha S}$ or gpH_2R-$G_{s\alpha S}$ fusion proteins as well as from the gpH_2R alone (panels B and D, in blue) in the absence (circles) or presence (squares) of 10 μM GTPγS. Data shown are mean values ± SEM of two independent experiments performed in triplicate (panel C and E – one experiment, respectively). Best fit with a variable slope.*

guanine nucleotides and the Hill slope equalled 1, Fig. 4.3.6 A). In case of the monovalent agonist 1, the curves at both hH_2R-$G_{s\alpha S}$ and gpH_2R-$G_{s\alpha S}$ fusion proteins were shifted to the right (Fig. 4.3.5 E and F) as for HIS. Nevertheless, the binding curve of the bivalent agonist **4** at the gpH_2R-$G_{s\alpha S}$ was not affected by GTPγS at all, indicating rather antagonistic properties (cf. Fig. 4.3.5 D: pIC_{50} of **4** at gpH_2R-$G_{s\alpha S}$: 8.39 ± 0.07, Hill slope: -0.81 ± 0.09; in the presence of 10 µM GTPγS: pIC_{50} 8.34 ± 0.04, Hill slope -0.77 ± 0.05). In contrast, addition of 10 µM GTPγS led to a small rightward shift and a steepening of the curve for ligand **4** at the hH_2R-$G_{s\alpha S}$ (Fig. 4.3.5 C). Such species differences in sensitivity to GTPγS were reported previously for N^G-acylated guanidines (Xie *et al.*, 2006). The affinities of HIS and the bivalent compound **4** were similar at the gpH_2R expressed alone (Fig. 4.3.5 B and D, in blue) and at the gpH_2R-$G_{s\alpha S}$ in the presence of 10 µM GTPγS (Fig. 4.3.5 B and D, in red). Moreover, no GTPγS-dependent rightward shift was observed for HIS at the gpH_2R in the absence of $G_{s\alpha S}$ protein (Fig. 4.3.5 B, in blue).

Similar results were found in another experiment at the gpH_2R-$G_{s\alpha S}$. As depicted in Fig. 4.3.6 B, HIS and the monovalent agonist **1** showed the highest sensitivity to GTPγS at concentrations close to their K_i values, whereas binding of the bivalent agonist **4** and FAM remained unchanged in the presence of GTPγS at concentration up to 10 µM, confirming the insensitivity towards guanine nucleotides. The results are summarized in Table 4.3.1.

Similar differences in sensitivity to GTPγS were reported previously for arpromidine, impromidine and monovalent N^G-acylguanidines at the hH_2R-$G_{s\alpha S}$ and the gpH_2R-$G_{s\alpha S}$, as some of the tested agonists revealed no GTPγS-dependent shift, indicating rather antagonistic properties (Fig. 4.3.7, cf. Kelley *et al.*, 2001; Xie *et al.*, 2006). It may be speculated that the effect of G protein on ligand binding might be too low to be detectable, due to the relatively short third intracellular loop (IL3) of the H_2R (Prof. Dr. Stefan Dove, University of Regensburg, personal communication). Another possible explanation could be that bivalent H_2R agonists are able to stabilize distinct ligand-specific H_2R conformations (cf. chapter 6).

Table 4.3.1. *The rightward shift of the competition curves of H_2R ligands at the gpH_2R-$G_{s\alpha S}$ fusion proteins in the presence of 10 μM GTPγS.*

	HIS	1, monovalent agonist	4, bivalent agonist	FAM
GTPγS-dependent shift	**yes**[§]	**yes**	**no**	**no**

[§] *the same effect observed also at the hH_2R-$G_{s\alpha S}$ and the gpH_2R coexpressed with the $G_{s\alpha S}$*

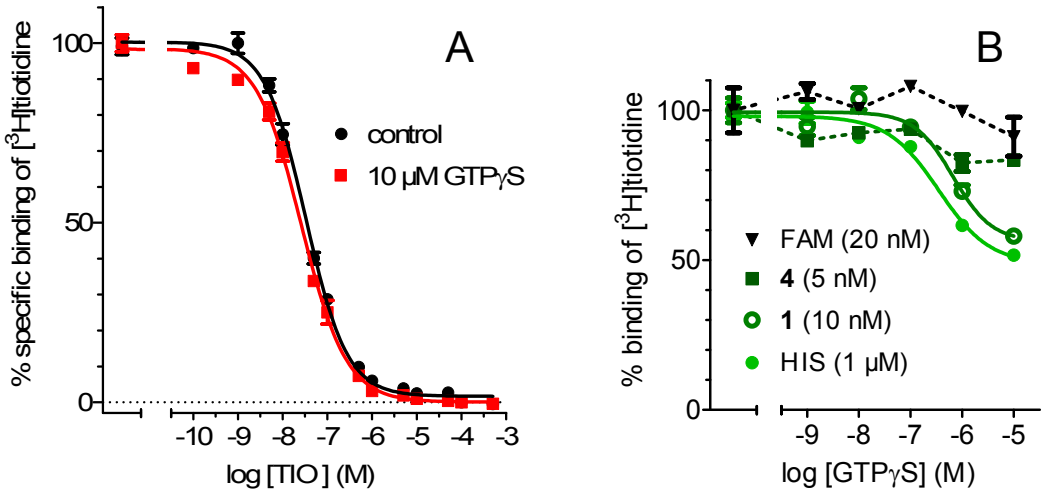

Fig. 4.3.6. *The effect of GTPγS on the displacement of [^{3}H]TIO (10 nM) from the gpH_2R-$G_{s\alpha S}$ after addition of (A) TIO and (B) representative H_2R ligands at the concentrations indicated in parentheses (close to their K_i values). Data shown are mean values ± SEM of an experiment performed in triplicate (A) or duplicate (B). Binding isotherms in the presence of TIO, HIS and compound **1** were analyzed by nonlinear regression with a variable slope.*

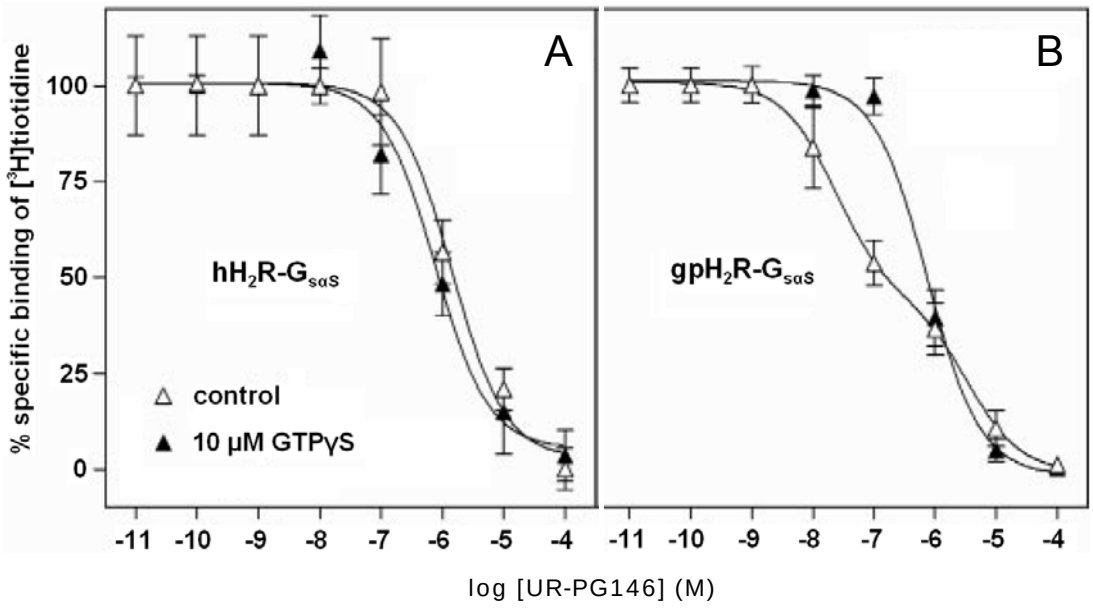

Fig. 4.3.7. *Effect of the N^G-acylated guanidine UR-PG146 (H_2R agonist, carbonyl derivate of IMP) on the binding of 10 nM [^{3}H]TIO in the presence or absence of 10 μM GTPγS at hH_2R-$G_{s\alpha S}$ (A) and gpH_2R-$G_{s\alpha S}$ (B) fusion proteins expressed in Sf9 cells (adopted from Xie et al., 2006 with modifications).*

4.3.2.2 Impact of (functional) receptor/G-protein stoichiometry on the Hill slope

In theory, the shape of a curve in the absence of guanine nucleotides depends on the ratio of receptors to G proteins. In systems with limited G proteins (or with over-expressed receptors), usually a non-radioactive agonist displaces an antagonist radioligand with a Hill slope less than unity (Fig. 1.1.5; Kenakin, 1997 and 2006; Lazareno, 2001). The assumption that the presented flat competition curves of HIS could result from insufficient amounts of functional G proteins would, however, contradict the previous findings. As shown in subsection 4.3.1, no limited coupling of G proteins to receptors was found on Sf9 membranes expressing both the gpH_2R-$G_{s\alpha S}$ fusion proteins and the gpH_2Rs coexpressed with the $G_{s\alpha S}$ proteins.

Therefore, it was necessary to compare the Hill slopes of the endogenous ligand and bivalent H_2R agonists at receptors fused to G proteins and in standard coexpression systems. Like at gpH_2R-$G_{s\alpha S}$ fusion proteins, the competition curve of HIS at Sf9 membranes *coexpressing* gpH_2Rs and $G_{s\alpha S}$ proteins revealed a Hill slope significantly smaller than unity (95% CI: 0.32–0.65). Similarly, in the presence of 10 µM GTPγS, the binding curve of the natural ligand at the coexpressed receptors was significantly shifted to the right and the Hill coefficient increased approximating unity (cf. Fig. 4.3.8: pIC_{50} of HIS at gpH_2R + $G_{s\alpha S}$: 6.12 ± 0.15, Hill slope: -0.49 ± 0.08; in the presence of 10 µM GTPγS: pIC_{50} 4.67 ± 0.17, Hill slope -0.98 ± 0.31). This again confirms the aforementioned behaviour of the radioligand, independent of the expression pattern (cf. subsection 4.3.1).

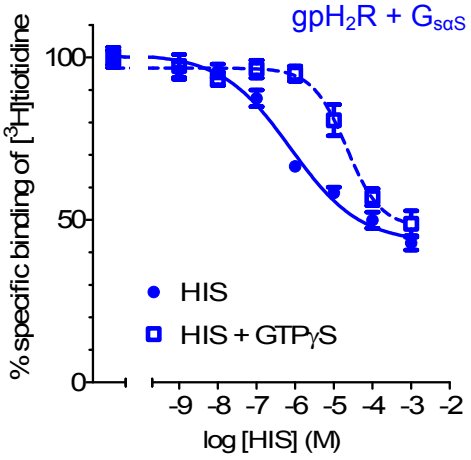

Fig. 4.3.8. *Effect of HIS on the displacement of [^{3}H]TIO (10 nM) from Sf9 membranes coexpressing gpH_2Rs and $G_{s\alpha S}$ proteins in the absence (circles, solid line) or presence (open squares, dashed line) of 10 µM GTPγS. Data shown are mean values ± SEM performed in three independent experiments. Binding curves were analyzed by nonlinear regression with a variable slope.*

The endogenous ligand displaced 10 nM [^{3}H]TIO in the same manner (IC_{50} of approx. 0.2–0.7 μM; Hill slope of about 0.5) at the hH_2R-$G_{s\alpha S}$ (Fig. 4.3.5 A), the gpH_2R-$G_{s\alpha S}$ (Fig. 4.3.5 B) and the gpH_2R coexpressed with the $G_{s\alpha S}$ protein in Sf9 membranes (Fig. 4.3.8). Also the effect of 10 μM GTPγS – rightward shift and steepening of HIS binding curves – was the same at these membranes. Surprisingly, the binding of the bivalent agonist **4**, at the gpH_2R-$G_{s\alpha S}$ was not affected by GTPγS at all, suggesting rather antagonistic than agonistic properties (cf. Fig. 4.3.5 D). Contrary to that, in the presence of GTPγS, the competition curve for ligand **4** at the hH_2R-$G_{s\alpha S}$ was slightly shifted to the right and steepened (Fig. 4.3.5 C). Similar discrepancies were reported previously for some monovalent N^G-acylguanidines at the hH_2R-$G_{s\alpha S}$ and the gpH_2R-$G_{s\alpha S}$ (Xie *et al.*, 2006).

Given that the relative G protein concentration is low anyway, there should be a discrepancy in the displacing potency of an unlabelled agonist, when using an agonist *vs*. antagonist radioligand (Kenakin, 1997). Both unlabelled and radioactively labelled agonists would preferentially bind to the small part of receptors coupled to G protein. As a result, a monophasic competition curve should be observed. Contrary to that, an antagonistic radioligand should bind to all forms of receptors, not discriminating between the G-protein coupled and the free receptor fraction.

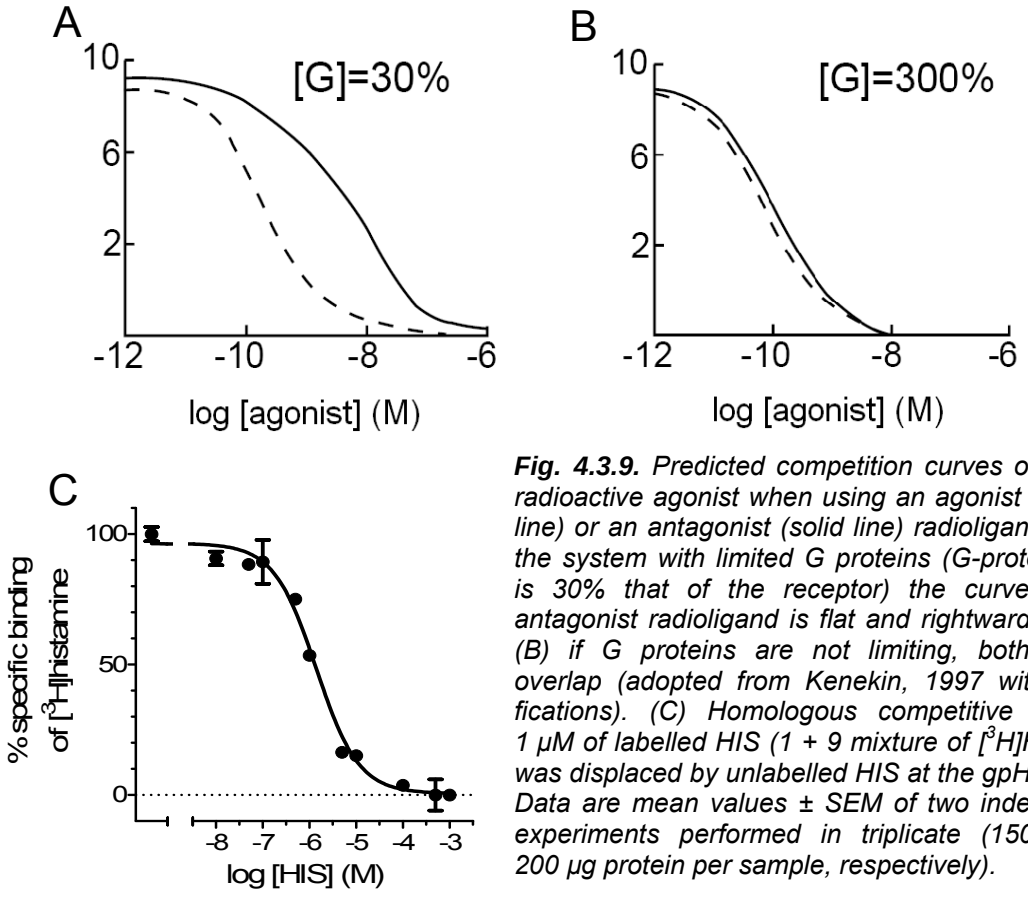

Fig. 4.3.9. *Predicted competition curves of a non-radioactive agonist when using an agonist (dashed line) or an antagonist (solid line) radioligand: (A) in the system with limited G proteins (G-protein level is 30% that of the receptor) the curve for an antagonist radioligand is flat and rightward shifted; (B) if G proteins are not limiting, both curves overlap (adopted from Kenekin, 1997 with modifications). (C) Homologous competitive binding. 1 μM of labelled HIS (1 + 9 mixture of [^{3}H]HIS/HIS) was displaced by unlabelled HIS at the gpH_2R-$G_{s\alpha S}$. Data are mean values ± SEM of two independent experiments performed in triplicate (150 μg or 200 μg protein per sample, respectively).*

As already mentioned, a non-radioactive agonist would displace the radioligand preferably from G-protein-complexed receptors. In systems provided with unlimited amounts of G proteins, full agonists could stabilize all receptors in the G-protein-coupled form (as ternary complexes). However, if there were a shortage of G proteins, only a small portion of receptors would exist in complexes with G proteins. Therefore, much higher concentrations of an agonist competitor would be required to displace the radioligand from the rest of its binding sites. This should in turn result in a flattening and a rightward shift of the agonist competition curve (Fig 4.3.9 A). Assuming that there were enough G proteins for all receptors, competition curves for agonist and antagonist radioligands should overlap (Fig. 4.3.9 B).

The homologous displacement of [^{3}H]HIS by non-radioactive HIS at the gpH_2R-$G_{s\alpha S}$ revealed a monophasic curve (n_H = 1), as shown in Fig. 4.3.9 C. Under the assumptions that both the tritiated and the unlabelled ligands had the same affinity to the receptor (K_d = K_i) and that there was no cooperativity, the K_d value of HIS could be calculated according to the simplified Cheng-Prusoff equation (Eq. 4.3.2; cf. Motulsky and Christopoulos, 2004):

$$K_d = IC_{50} - [\text{radioligand}] \qquad \text{(Eq. 4.3.2)}$$

The determined K_d value of 0.40 ± 0.13 µM was not significantly different from the K_i value, obtained for HIS at the gpH_2R-$G_{s\alpha S}$ using [^{3}H]TIO (K_i of 0.63 ± 0.26 µM, cf. Table 4.3.3). This again contradicts the aforementioned hypothesis of an insufficient supply of G proteins. A plausible explanation of the flat [^{3}H]TIO competition curves for HIS (Fig. 4.3.5 A, B and Fig. 4.3.8) could be the inverse agonism of TIO rather than the receptor/G-protein ratio. This would be in line with the biphasic Scachard plots in the saturation studies (cf. Fig. 4.3.3) and with results from the literature (Kelley *et al.*, 2001; Monczor *et al.*, 2003).

4.3.2.3 Ternary complex model for the H_2R

The presented binding curves of HIS in the absence of GTPγS revealed Hill slopes significantly smaller than unity upon incubation with 10 nM [^{3}H]TIO for 90 min (Fig. 4.3.5 A, B and Fig. 4.3.8). As mentioned above, this might reflect a more complex binding mechanism than described by the simple law of mass action (Lazareno, 2001) and could be taken as a hint to negative cooperativity between two non-interconverting binding sites at the same receptor molecule (Repke and Liebmann, 1987). However, the GTPγS-dependent shift and the steepening of the shallow binding curve of HIS, might be better

explained by the ternary complex model, proposing two independent non-interacting binding sites with different affinities for the natural ligand (cf. Fig. 1.1.3). According to this two-site model, agonists should bind to those receptors, which are coupled to G proteins, with much higher affinity than to the free receptors. Therefore, the formation of ternary agonist-receptor-G-protein complexes is promoted and two maxima of the biphasic curve, corresponding to the two classes of binding sites, can be observed. However, in the presence of exogenous GTPγS, a non-hydrolyzable analogue of GTP, receptors cannot couple to G proteins and ternary complexes are disrupted (Lazareno, 2001). The high-affinity binding site, corresponding to the subset of gpH_2Rs coupled to G proteins, disappears (Monczor *et al.*, 2003) and only the low-affinity binding site can be detected (Kenakin, 2006). As a result, a steep and rightward-shifted curve can be seen as in Fig. 4.3.5 A–B.

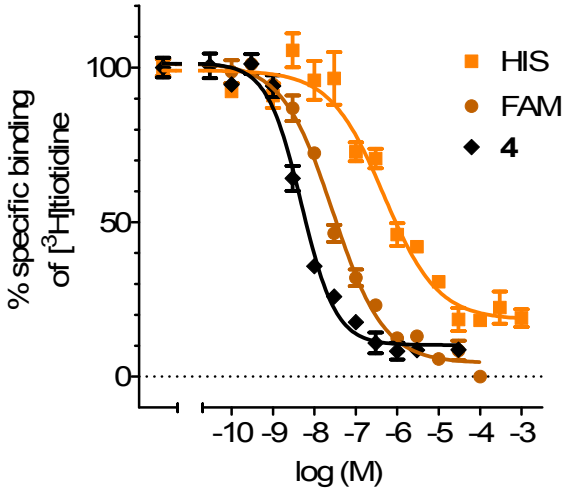

Fig. 4.3.10. *Competition of test compounds with 30 nM [^{3}H]TIO for binding at the gpH_2R-$G_{s\alpha S}$ after 3 hours of incubation. Data shown are mean values ± SEM of two independent experiments for each ligand (using different membrane preparations). Binding curves were analyzed by nonlinear regression with a variable slope.*

To exclude any artefacts resulting from the premature termination of the incubation, three representative compounds were incubated for 3 hours. Additionally, the final concentration of the radioactive tracer was increased to 30 nM, to expedite equilibration of the system. Fitting of the data according to the logistic curve with a variable slope revealed for HIS a slight increase in both the affinity and the Hill slope, with the latter, however, still remaining significantly smaller than unity. For FAM, no significant change was observed, but for the bivalent compound **4** the Hill coefficient of the binding curve increased, approximating to unity, whereas its affinity remained unchanged (cf. Fig. 4.3.10: pIC_{50} of HIS: 6.33 ± 0.11, K_i: 270 nM, Hill slope: -0.67 ± 0.10; pIC_{50} of FAM: 7.55 ± 0.06, K_i: 17 nM, Hill slope: -0.71 ± 0.06; pIC_{50} of compound **4**: 8.31 ± 0.06, K_i: 3 nM, Hill slope: -1.05 ± 0.13). This indicates a very slow equilibration of the bivalent ligand. Interestingly, a latency period had also been observed in experiments on the guinea-pig right atrium, where at low concentrations the positive inotropic effects of bivalent H_2R agonists reached a plateau not before 2.5 to 3 hours of incubation (Prof. Dr. Sigurd Elz, University

of Regensburg, personal communication). However, with respect to an interpretation of the impact of prolonged periods of incubation, additional investigations with other bivalent H_2R agonists should be done (cf. subsection 4.3.3).

A prolonged incubation period (from 90 min to 3 hours) had a minor effect on HIS binding. Only a small increase in the proportion of high-affinity binding sites for HIS from 48% to 67% was observed (cf. Table 4.3.2). The prevalence of high-affinity sites for the bivalent N^G-acylated guanidine **4** changed slightly from 82% to 94%, suggesting a stronger stabilizing effect on the ternary complex than in the case of HIS. This was in line with the previous studies, in which some monovalent N^G-acylguanidines were found to stabilize the ternary complex on hH_2R-$G_{s\alpha S}$ and/or gpH_2R-$G_{s\alpha S}$ fusion proteins expressed in Sf9 cells, as indicated by the biphasic shapes and the GTPγS-dependent rightward shifts of their competition curves (cf. Fig. 4.3.7 B; Xie *et al.*, 2006).

Table 4.3.2. *The distribution of high- and low-affinity binding sites for HIS as well as the corresponding IC_{50} values ± SEM in the absence of GTPγS (calculated separately for the experiments, shown in Fig. 4.3.11 A and B, and then averaged).*

Competition curves of HIS	**90 min incubation (cf. Fig. 4.3.11 A)**	**180 min incubation (cf. Fig. 4.3.11 B)**
Fraction of high-affinity sites	48%	67%
high-affinity IC_{50}	104 ± 83 nM	69 ± 11 nM
low-affinity IC_{50}	9.7 ± 7.1 µM	3.3 ± 0.3 µM

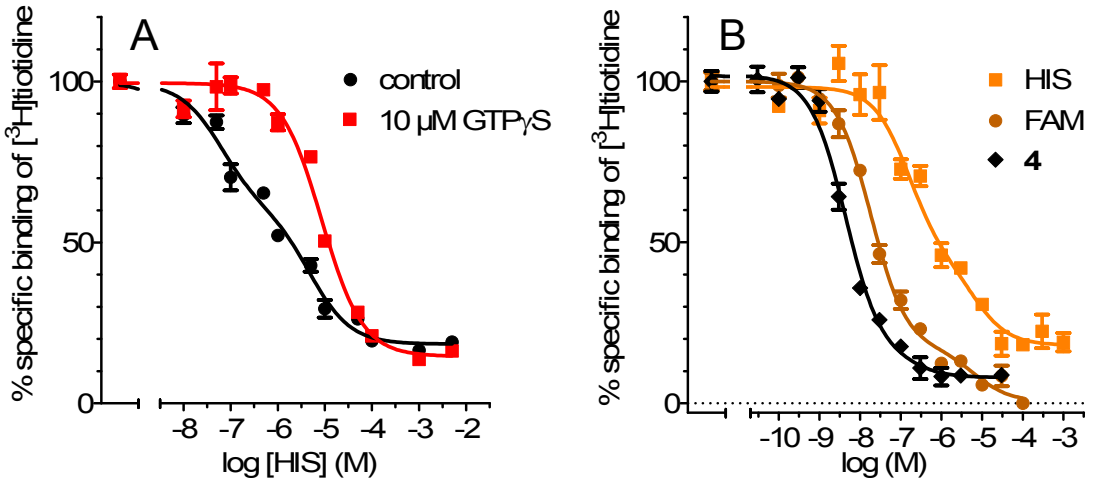

Fig. 4.3.11. *Competitive binding with [^{3}H]TIO after 90 min (A) and 180 min (B) of incubation. The data from Fig. 4.3.5 B and Fig. 4.3.10, fitted according to the two-site model.*

Fitting of the binding data from Fig. 4.3.5 B (90 min of incubation) and Fig. 4.3.10 (180 min of incubation) with biphasic curves (Graph Prism: "Two sites – Fit logIC_{50}") revealed the existence of two binding sites for both HIS and the bivalent agonist **4** at the gpH_2R-$G_{s\alpha S}$ in the absence of GTPγS (Fig. 4.3.11 A and B, respectively). After a prolonged incubation period the Hill slope of HIS remained smaller than unity, whereas that of the bivalent agonist **4** increased, approximating unity. Additionally, the bivalent H_2R agonist **4** was found to be an efficient stabilizer of the ternary complex (Fig. 4.3.11 B).

The H_2R agonists, tested at the hH_2R-$G_{s\alpha S}$, the gpH_2R-$G_{s\alpha S}$, the gpH_2R expressed alone and the gpH_2R coexpressed with $G_{s\alpha S}$, showed similar binding behaviour, consistent with the ternary complex model. The calculated high and low affinity values of the bivalent compound **4** were similar at the gpH_2R expressed alone and at the gpH_2R-$G_{s\alpha S}$ fusion protein (cf. Fig. 4.3.5 D). Only the percentage of the high-affinity binding sites was reduced at the gpH_2R (54%), when compared with the fusion proteins (83%). Additionally, a minor rightward shift of the binding curve of the monovalent agonist 1, observed at both hH_2R-$G_{s\alpha S}$ and gpH_2R-$G_{s\alpha S}$ fusion proteins in the presence of GTPγS, indicated less efficient stabilization of the ternary complex than in the case of HIS (Fig. 4.3.5 E and F). Moreover, a pronounced rightward shift and steepening of the competition curve for HIS, observed in case of coexpressed gpH_2R + $G_{s\alpha S}$ after addition of unlabeled GTPγS (cf. Fig. 4.3.8), was similar to that at the gpH_2R-$G_{s\alpha S}$ fusion protein. Contrary to that, the affinity of HIS at the gpH_2R expressed alone was decreased (approx. 8 µM, cf. Fig. 4.3.5 B, in blue) – when compared with both fusion proteins and the gpH_2R coexpressed with the $G_{s\alpha S}$ – and was almost not affected by addition of 10 µM GTPγS. In the latter case the high-affinity binding site, predicted for agonists by the ternary complex model, was not detectable. Probably, due to the lack of G protein, the formation of the ternary complex was impossible in the respective test system. However, the relatively high dispersion of data points precludes a detailed analysis.

The ternary complex model seems to be a valuable concept for the interpretation of the binding behaviour of various H_2R ligands. For example, the prototypical imidazolylpropylguanidine ARP was previously reported to be a partial agonist at gpH_2R-$G_{s\alpha S}$ fusion proteins expressed in Sf9 cells, efficiently stabilizing the ternary complex (76% high-affinity binding sites). However, there was no characteristic rightward shift of the agonist binding curve after addition of GTPγS (Xie *et al.*, 2006). The apparently flat competition curve of ARP, found at hH_2R-$G_{s\alpha S}$ fusion proteins, expressed in Sf9 membranes (Mosandl, 2009), revealed two distinct binding sites, when the experimental data were fitted as a biphasic competition curve (Fig. 4.3.12). The calculated K_i values were 140 nM (95% CI:

40-495 nM) for the high-affinity binding site and 6.6 µM (95% CI: 0.4 – 103.7 µM) for the low-affinity binding site. In theory, the latter value should be the "true" ligand affinity (Lazareno, 2001). Indeed, ARP bound to hH_2Rs with K_i of 5.4 ± 1.3 µM, when the experiment was performed on the intact cells (Mosandl, 2009). In such a case, the relatively high intracellular concentration of GTP leads to the disruption of the ternary complex and, therefore, only the low-affinity binding site can be detected. Contrary to that, when a membrane preparation is used, G-protein coupling and the resulting two independent non-interacting binding sites can be observed (Kenakin, 2006).

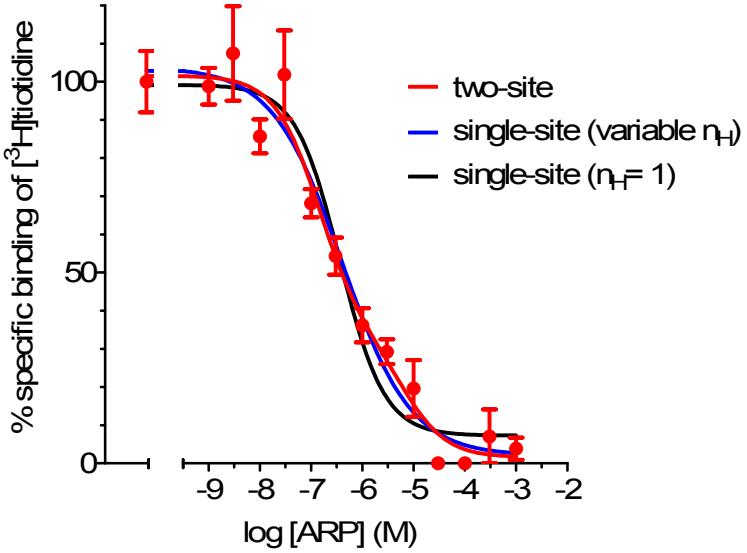

Fig. 4.3.12. *Displacement of 10 nM [^{3}H]TIO by ARP on hH_2R-$G_{s\alpha S}$ fusion proteins expressed in Sf9 membranes (Mosandl, 2009); as indicated, binding data were fitted according to different models.*

4.3.3 Detailed analysis of Hill slopes in case of the bivalent H_2R ligands

4.3.3.1 Affinities and Hill slopes of monovalent and bivalent H_2R ligands

Bivalent ligands are considered pharmacological tools for investigation of hypothetical GPCR dimers. Applying this approach to N^G-acylated gunanidines yielded compounds which are up to 4000-fold more potent than HIS at the isolated guinea-pig right atrium as well as at hH_2R-$G_{s\alpha S}$ and gpH_2R-$G_{s\alpha S}$ fusion proteins expressed in Sf9 cells (Kraus, 2007; Birnkammer *et al.*, 2008). However, this behaviour could not be explained by simultaneous interaction with neighbouring GPCRs. As shown for opioid receptors, only bivalent compounds possessing a linker of about 21 carbon atoms in length between both sets of pharmacophoric groups, are capable of bridging the binding pockets of δ-κ opioid receptor heterodimers (Daniels *et al.*, 2005 b). Among the bivalent N^G-acylated guanidines, possessing 4 to 20 methylene groups as linkers between the carbonyl func-

tions, the highest potency at both, the hH_2R-$G_{s\alpha S}$ and the gpH_2R-$G_{s\alpha S}$, has been found for ligands with octamethylene spacers, which are too short to allow the bridging of the two adjacent receptor molecules (Fig. 4.1.1 B; cf. Kraus, 2007; Birnkammer *et al.*, 2010).

As shown before, one of the most potent bivalent agonists, compound **4**, revealed a Hill slope smaller than 1 after 90 min of incubation at gpH_2R-$G_{s\alpha S}$. The interpretation of such a finding, rarely described in the literature (Prinz and Schönichen, 2008), is not simple. If only the artefacts (e.g. incomplete equilibration, cf. Fig. 4.3.23) could be excluded, this result might hint at divergences from the standard model of receptor binding, allowing exclusively monophasic curves (Lazareno, 2001). The Hill coefficient approximated unity only after 3 hours of incubation (cf. Fig. 4.3.10). Additionally, the binding of the bivalent agonist **4** was insensitive towards GTPγS and there was a detectable alteration of the [^{3}H]TIO dissociation rate in the presence of the ligand **4** (cf. Fig. 5.3.2 B). In order to elucidate these findings, also other bivalent H_2R agonists with octamethylene linkers, their monovalent counterparts and standard H_2R ligands were investigated by way of example for their affinity and n_H on the Sf9 membranes expressing hH_2R-$G_{s\alpha S}$ and gpH_2R-$G_{s\alpha S}$ fusion proteins.

In competition binding assays with [^{3}H]TIO (after 90 min of incubation), the affinities of the investigated H_2R ligands were approximately in the same range as the functional data from GTPase assays (two-digit nanomolar at the hH_2R-$G_{s\alpha S}$ and one-digit nanomolar at the gpH_2R-$G_{s\alpha S}$, cf. Table 4.3.3 and Fig. 4.3.13). Most of the tested agonists revealed Hill slopes significantly smaller than 1 (Table 4.3.3–4 and Fig. 4.3.14).

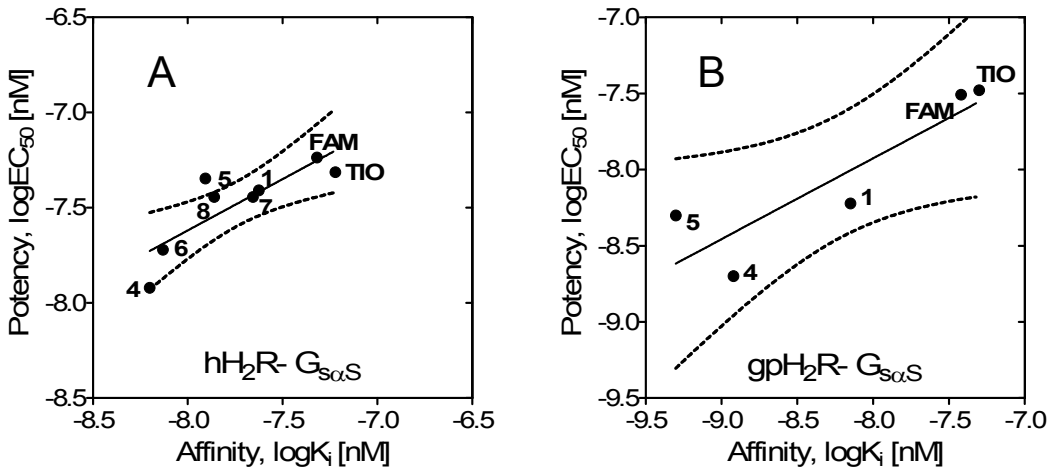

Fig. 4.3.13. *Correlation between the potencies (FAM and TIO – antagonistic activities) and the affinities of representative ligands from Table 4.3.3: (A) at the hH_2R-$G_{s\alpha S}$ (slope: 0.53; r^2: 0.77) and (B) at the gpH_2R-$G_{s\alpha S}$ (slope: 0.54; r^2: 0.69); 95% CI of the regression lines (dashed).*

Table 4.3.3. *Potencies (EC_{50}), efficacies, antagonistic activities (K_b), affinities (K_i) and slopes of displacement curves of representative ligands determined at the hH_2R-$G_{s\alpha S}$ and the gpH_2R-$G_{s\alpha S}$ fusion proteins expressed in Sf9 cell membranes. Efficacy in GTPase assays: the maximum stimulatory effect of HIS was set to 1.00 and the stimulatory effects of other agonists were referred to this value (Kelley et al., 2001; Birnkammer et al., 2008; Kraus et al., 2009). Binding assays: the hH_2R-$G_{s\alpha S}$ and the gpH_2R-$G_{s\alpha S}$ fusion proteins bound [^{3}H]TIO with a K_d of 43 nM and 40 nM respectively; incubation time 90 min; binding data are mean values ± SEM from at least two independent experiments performed in triplicate (*compound **2** – one experiment). Binding curves were analyzed by nonlinear regression with a variable slope.*

hH_2R-$G_{s\alpha S}$				
Compound	**EC_{50} / K_b [nM]**	**Efficacy**	**K_i [nM]**	**Slope**
TIO	60 (30–130)	inv. -0.04 ± 0.09	48.5 ± 0.2	-1.08 ± 0.14
HIS	990 ± 92	1.00	283 ± 92	-0.59 ± 0.07
1	22.2 ± 5.1	0.79 ± 0.02	39 ± 5	-0.44 ± 0.03
4	6.3 ± 0.9	0.82 ± 0.04	12 ± 3	-0.53 ± 0.07
5	12.4 ± 6.4	0.53 ± 0.04	45 ± 12	-0.79 ± 0.11
6	7.4 ± 0.6	0.79 ±0.06	19 ± 8	-0.57 ± 0.05
7	22.1 ± 3.4	0.76 ± 0.03	36 ± 1	-0.71 ± 0.03
8	13.8 ± 3.5	0.77 ± 0.03	36 ± 2	-0.66 ± 0.02
FAM	48 ± 10	inv. -0.10 ± 0.02	58 ± 5	-0.51 ± 0.01
gpH_2R-$G_{s\alpha S}$				
Compound	**EC_{50} / K_b [nM]**	**Efficacy**	**K_i [nM]**	**Slope**
TIO	50 (30–90)	inv. -0.12 ± 0.08	27 ± 1	-0.95 ± 0.04
HIS	850 ± 340	1.00	628 ± 260	-0.47 ± 0.02
1	7.5 ± 0.9	0.76 ± 0.02	6 ± 1	-0.94 ± 0.13
4	1.2 ± 0.4	0.98 ± 0.05	2 ± 1	-0.58 ± 0.09
5	0.5 ± 0.1	0.79 ± 0.07	5*	-0.60 ± 0.09
6	0.9 ± 1.1	1.01 ± 0.03	*n.d.*	*n.d.*
7	6.2 ± 2.3	0.94 ± 0.01	*n.d.*	*n.d.*
8	5.5 ± 3.7	0.89 ± 0.04	*n.d.*	*n.d.*
FAM	38 ± 3	inv. -0.10 ± 0.01	39 ± 23	-0.73 ± 0.08

The affinity of the monovalent acylguanidine-type ligand **7**, containing a small propionyl moiety, at the hH_2R-$G_{s\alpha S}$ fusion protein was comparable to that of the natural ligand. Surprisingly, in case of monovalent agonist **1**, the presence of an aromatic ring in the acyl portion led to a 10-fold increase in affinity, which was almost comparable to that of

the bivalent H_2R ligands. Interestingly, the presence of the second set of pharmacophoric groups (as in compound **5**) did not result in any significant further increase in affinity (Fig. 4.3.14).

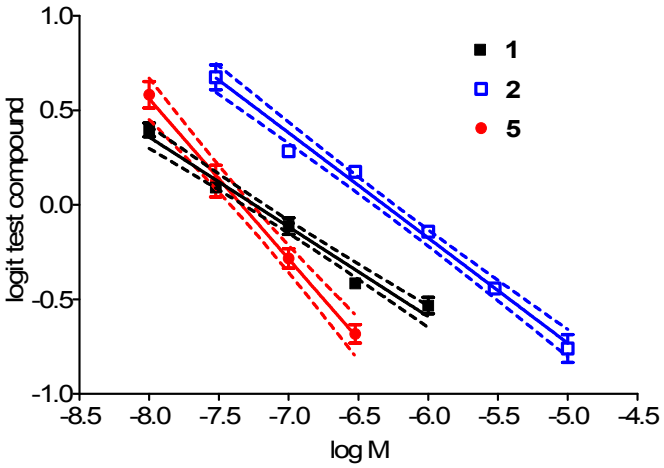

Fig. 4.3.14. *Hill plots of binding data corresponding to 16-84% displacement of 10 nM [^{3}H]TIO at the hH_2R-$G_{s\alpha S}$ by the monovalent agonists **1**, (6 experiments) and **2** (1 experiment) as well as their bivalent counterpart **5**, (4 experiments). Data are mean values ± SEM; 95% CI of the regression lines (dashed). Hill coefficients are negative, because the linearized competition curves go downhill (cf. Table 4.3.3–4, Fig. 4.3.20 A and B as well as Fig. 4.3.22 B).*

Table 4.3.4. *Affinities (K_i), Hill slopes and coefficients of determination (r^2, goodness of fit) of the binding data transformed according to Hill, as shown in Fig. 4.3.14.*

Parameters	1	2	5
K_i	46 nM	388 nM	37 nM
Hill slope **95% CI of Hill slope**	**-0.47 ± 0.02** **-0.52 to -0.43**	**-0.56 ± 0.02** **-0.61 to -0.51**	**-0.85 ± 0.06** **-0.97 to -0.73**
r^2	0.831	0.975	0.824

4.3.3.2 Impact of the linker length on affinities and Hill slopes of bivalent H_2R ligands

Due to the inverse agonism of [^{3}H]TIO, complicating the interpretation of pharmacological data (cf. subsection 4.3.1), its high costs and frequent shortages, the usage of other H_2R radioligands, such as tritiated HIS, was considered. However, [^{3}H]HIS has a weak micromolar affinity to the H_2R, which makes its utilization very expensive. Additionally, as an agonist, it binds preferably to the subpopulation of receptors coupled to G proteins. This results in a complete loss of affinity in the presence of guanine nucleotides and precludes the observation of GTPγS-dependent rightward shifts of the competition curves (Fig. 4.3.15).

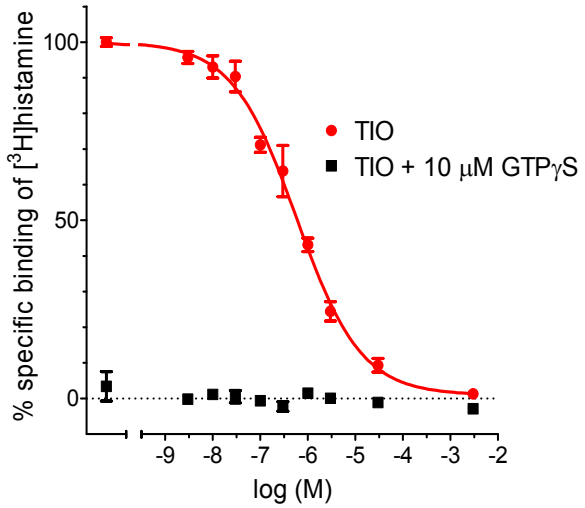

Fig. 4.3.15. *Influence of TIO on the binding of 100 nM [^{3}H]HIS (added as obtained from the manufacturer) at the gpH$_2$R-G$_{s\alpha S}$ in the presence or absence of GTPγS. Data are mean values ± SEM of two independent experiments (100 µg protein per sample) performed in triplicate.*

Therefore, further binding experiments were performed with the new tritiated H$_2$R antagonist [^{3}H]UR-DE257, which was recently developed in our research group by Dr. Daniela Erdmann (cf. Fig. 1.2.5; Erdmann, 2010). Competition binding studies with 10 nM [^{3}H]TIO at the hH$_2$R-G$_{s\alpha S}$ revealed a K_i value of 12.7 ± 0.2 nM (Fig. 4.3.16), whereas saturation experiments at the hH$_2$R-G$_{s\alpha S}$ afforded a K_d value of 27 nM (Erdmann, 2010). Thus, for competition binding assays [^{3}H]UR-DE257 was used at a concentration of 25 nM.

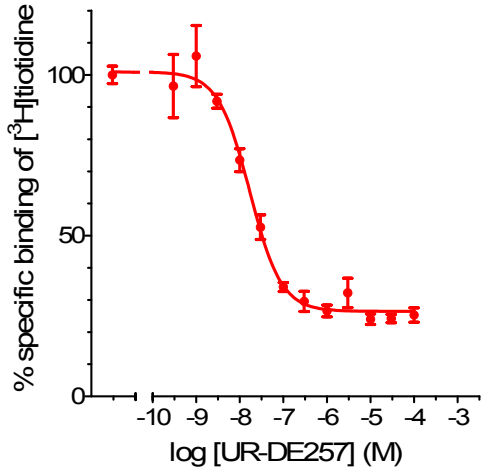

Fig. 4.3.16. *Displacement of 10 nM [^{3}H]TIO by non-radioactive UR-DE257 at the hH$_2$R-G$_{s\alpha S}$ in the presence of 1% DMSO. Data are mean values ± SEM of two independent experiments (100 µg protein per sample) performed in triplicate.*

In theory, bivalent ligands containing a 20-membered spacer between the carbonyl groups, like compound **11**, could bridge the binding pockets of two neighbouring receptor molecules (Daniels *et al.*, 2005 b). Surprisingly, the displacement curve of **11** at the gpH$_2$R-G$_{s\alpha S}$ was extremely steep (n_H of 2.26; 95% CI: 1.86 to 2.67), indicating positive cooperativity. Additionally, there was no rightward shift in the presence of 10 µM GTPγS (Fig. 4.3.17). In this context, it is indispensable to mention that this compound showed partial agonistic activity (EC_{50} of 46 nM; efficacy 22%) at the gpH$_2$R-G$_{s\alpha S}$ in GTPase as-

says, whereas at the hH_2R-$G_{s\alpha S}$ it behaved as an antagonist (K_b of 371 nM; cf. Birnkammer *et al.*, 2010).

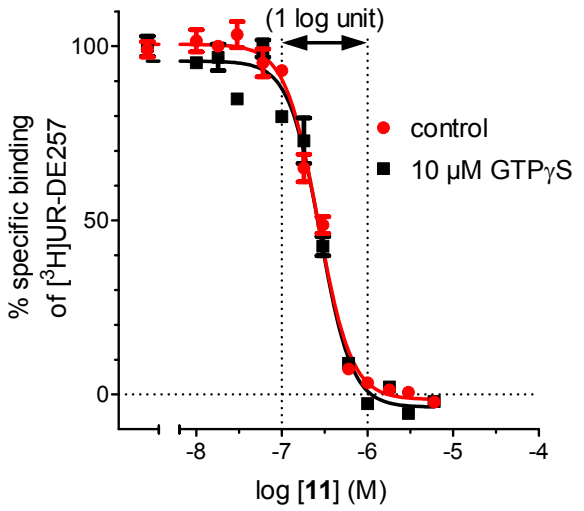

Fig. 4.3.17. *Displacement of 25 nM [^{3}H]UR-DE257 by the bivalent ligand **11** at the gpH_2R-$G_{s\alpha S}$ in the presence or absence (control) of 10 µM GTPγS. Data are mean values ± SEM of two independent experiments performed in triplicate.*

A steep competition curve was also obtained for the bivalent H_2R agonist **9**, containing a tetradecamethylene spacer between the C=O groups (n_H of 1.72; 95% CI: 1.15 to 2.28), but not for the bivalent agonist **4** which has an octamethylene linker (n_H not statistically different from 1). Moreover, the longer the alkanediyl spacer, the lower was the affinity of the bivalent competitor. On one hand, these data confirmed previous observations from GTPase assays (Birnkammer *et al.*, 2010). On the other hand, the results raised doubts whether the model proposed by Portoghese is suitable for the bivalent H_2R ligands, as the highest affinity at the gpH_2R-$G_{s\alpha S}$ has been found for ligands with octamethylene spacers, which are too short to allow the bridging of the two adjacent receptor molecules. The corresponding curves of the symmetric bivalent ligands containing an imidazole moiety are shown in Fig. 4.3.18.

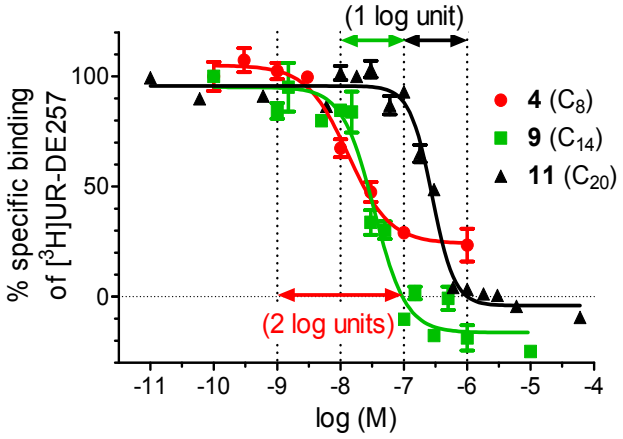

Fig. 4.3.18. *Relationship between the spacer length of the bivalent ligand and the Hill coefficient at the gpH_2R-$G_{s\alpha S}$. Data are mean values ± SEM of one (compound **4**), two (compound **9**) and three (compound **11**) independent experiments performed in triplicate.*

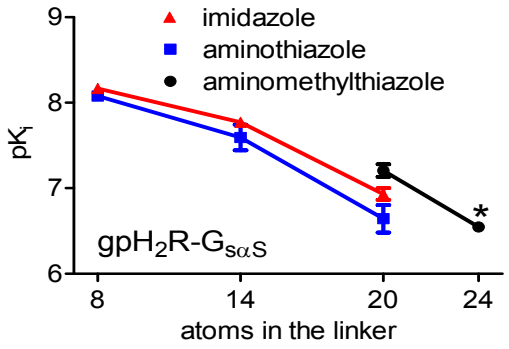

Fig. 4.3.19. *Relationship between spacer lengths and affinities of the symmetric bivalent ligands, containing different heterocycles, measured at the gpH$_2$R-G$_{s\alpha S}$ fusion protein. The pK$_i$ values are mean values ± SEM of 1-3 displacement experiments for each compound. Asterisk (*) corresponds to the bivalent ligand* ***14****, containing a hydrophilic 24-atom linker between the carbonyl groups, instead of an alkanediyl spacer.*

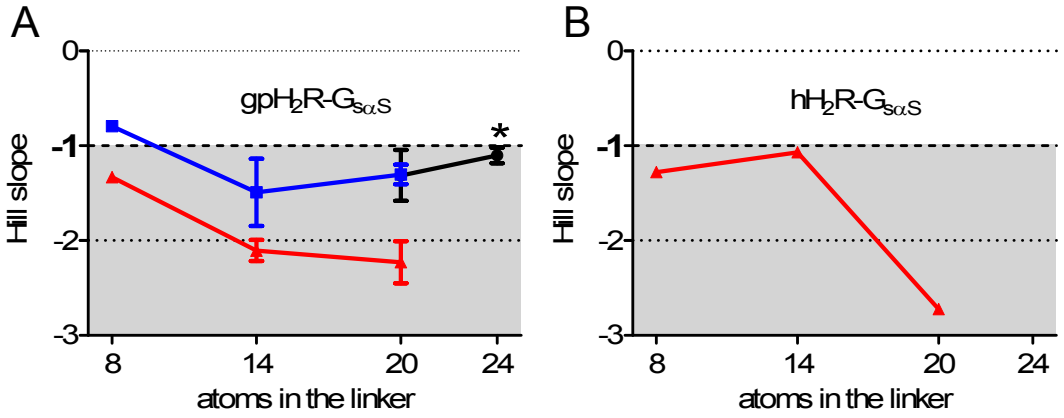

Fig. 4.3.20. *Relationship between spacer lengths and Hill slopes of the symmetric bivalent ligands, containing different heterocycles (cf. Fig. 4.3.19), measured at the gpH$_2$R-G$_{s\alpha S}$ (A) and the hH$_2$R-G$_{s\alpha S}$ (B). The Hill slopes are mean values ± SEM of 1-3 displacement experiments for each compound. Asterisk (*) in panel A corresponds to the bivalent ligand* ***14****, containing a hydrophilic 24-atom linker between the carbonyl groups, instead of an alkanediyl spacer.*

After a 90-min incubation with gpH$_2$R-G$_{s\alpha S}$, the bivalent ligands of the imidazole series, compounds **9** and **11**, possessing a 14- and a 20-atom linker, respectively, revealed a n_H value significantly higher than 1 (Fig. 4.3.17 and Fig. 4.3.18). Further studies at the hH$_2$R-G$_{s\alpha S}$ as well as at the gpH$_2$R-G$_{s\alpha S}$ with other homobivalent ligands, belonging to the aminothiazole and the aminomethylthiazole series, were in line with the results, already observed at the gpH$_2$R-G$_{s\alpha S}$ fusion protein for the ligands of the imidazole series (Fig. 4.3.19). Some of the ligands with longer linkers revealed apparent positive cooperativity, as their Hill slopes were greater than unity (Fig. 4.3.20).

4.3.4 Competition binding assays at the H_4R

4.3.4.1 Impact of incubation time on affinities and Hill slopes of bivalent H_4R ligands

The imidazolylpropylguanidine moiety is a priviliged structure in terms of histamine receptor binding. N^G-acylated imidazolylpropylguanidines turned out to be highly potent ligands also at the H_4R (Igel *et al.*, 2009). For example, the bivalent compound **4** with an octamethylene linker, known for its high affinity towards H_2Rs (cf. Table 4.3.3), revealed a one-digit nanomolar potency at the hH_4R (EC_{50} of 3 nM, efficacy: 0.36; Kraus, 2007). Therefore, to expand the pharmacological characterisation of our bivalent ligands, two compounds (one with a shorter and one with a longer spacer) were investigated for their affinities and Hill slopes at the hH_4R, C-terminally fused to the GAIP (RGS19) and coexpressed with $G_{i\alpha2}$ and $G_{\beta1\gamma2}$ proteins in Sf9 membranes, as described before (Schneider and Seifert, 2009). Competition experiments were performed with 10 nM [^{3}H]HIS as radioligand (cf. K_d of 9.8 ± 0.9 nM at the hH_4R + $G_{i\alpha2}$ + $G_{\beta1\gamma2}$ + GAIP; cf. Schnell *et al.*, 2011) with varying time periods of incubation. ***N.B.*** the kinetics of [^{3}H]HIS at the hH_4R-GAIP+ $G_{i\alpha2}$ + $G_{\beta1\gamma2}$ (e.g. dissociation half-value period) is described in subsection 5.3.1.

After 90 min of incubation in the presence of hH_4R-GAIP + $G_{i\alpha2}$ + $G_{\beta1\gamma2}$, the bivalent ligand **4** showed a K_i value of 7 nM (similar to EC_{50}) and a Hill slope of 1.44 (95% CI: 1.21–1.67), whereas the bivalent compound **11** revealed a K_i value of 57 nM and a Hill slope of 2.22 (95% CI: 1.69–2.74). Thus, in both cases an apparent positive cooperativity was observed, as shown in Fig. 4.3.21 and Fig. 4.3.22. However, a prolonged incubation period (3 to 7.5 hours) led to the alteration of the Hill slopes, approximating unity (Fig. 4.3.22 B). At the same time, the affinity remained almost unchanged (Fig. 4.3.22 A).

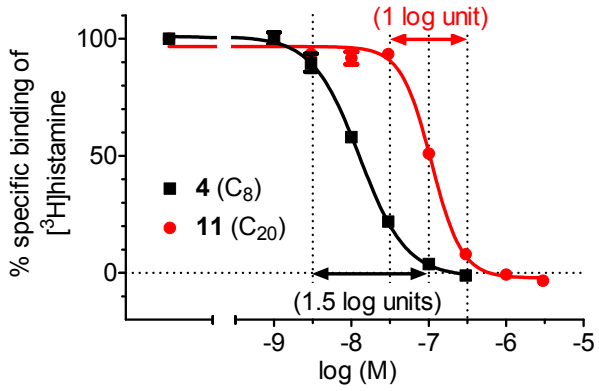

Fig. 4.3.21. *Displacement of 10 nM [^{3}H]HIS by the imidazole-type bivalent ligands **4** and **11** (with a different length of a linker) at Sf9 membranes expressing the hH_4R-GAIP + $G_{i\alpha2}$ + $G_{\beta1\gamma2}$ after 90 min of incubation. Each curve is representative of two independent experiments performed in triplicate. Data shown are mean values ± SEM.*

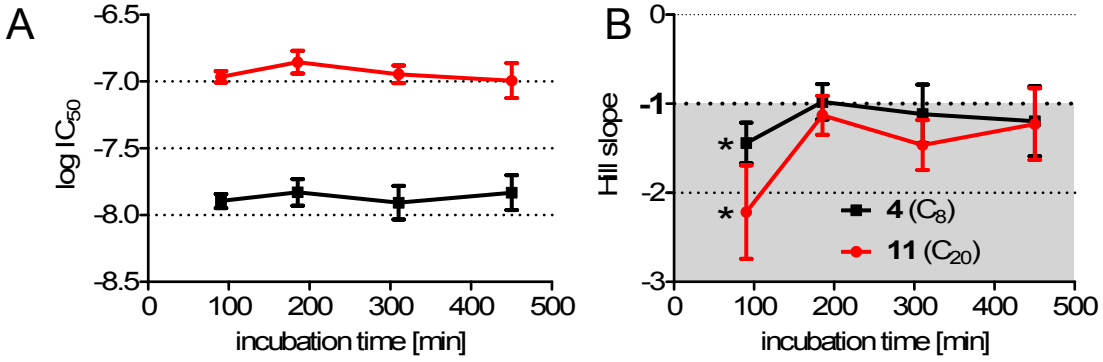

Fig. 4.3.22. *Effect of a prolonged incubation period of representative bivalent ligands on their affinity (A) and the Hill slope (B) in the presence of hH_4R-GAIP + $G_{i\alpha 2}$ +$G_{\beta 1\gamma 2}$. Competition assays with 10 nM [^{3}H]HIS. The data are mean values ± 95% CI of two experiments for each incubation time; performed in triplicate (only the data at 90 and 450 min were from single experiments). Asterisks (*) in panel B indicate the Hill slopes significantly different from the unity (details in the text).*

4.3.4.2 Artefacts at pre-equilibrium

As already mentioned, a prerequisite for competition and saturation studies is the assumption that the system is at equilibrium at the time point of the measurement. Only then, the observed Hill slope can be correctly interpreted, as suggested in Table 4.1.1. The period of time, required for equilibration can be estimated by multiplying the known half-life of the dissociation of the radioligand by 5 (cf. subsection 1.3.1). However, the presence of additional competitors prolongs the time required for equilibration, as the apparent value of K_d of the radioligand increases, in turn leading to a decrease in k_{obs} (limited by the value of k_2), which corresponds to slower association (cf. Eq. 1.3.6). Addition of a compound with a k_2 smaller than that of the radioligand initially leads to a relative increase in radioligand binding, before it decreases at equilibrium to the correct value (Lazareno, 2001). The accompanying changes of the n_H value are shown in Fig. 4.3.23 A. Thus, the binding experiments at pre-equilibrium lead to an underestimation of the competitor´s affinity (rightward shift) and in a steepening of the competition binding curve (artefactual positive cooperativity). Contrary to that, in the presence of a faster component (higher k_2 indicative of a faster dissociation compared to the radioligand), the initially low rate of radioligand binding increases, when the radioligand slowly equilibrates. Therefore, at pre-equilibrium the apparent affinity of the competitor is higher, leading to a leftward shift and a steepening of the inhibition curve, which can be misinterpreted as positive cooperativity (Fig. 4.3.23 B).

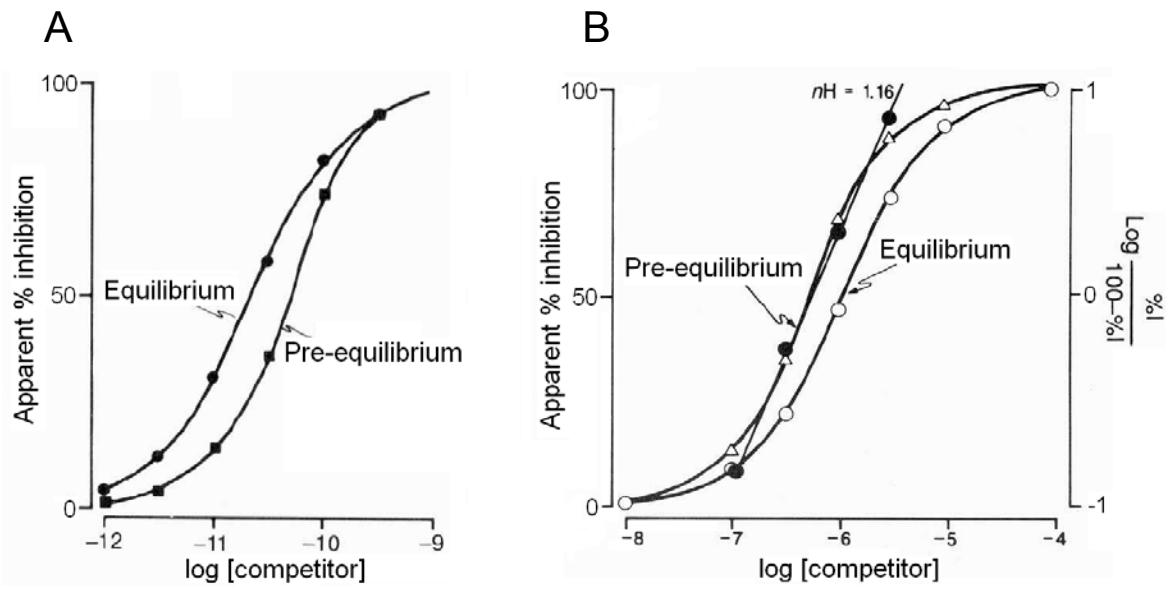

Fig. 4.3.23. *The presence of slower (A) and faster (B) components leads at pre-equilibrium to the artefactual changes in the competitor affinity (under- and overestimation, respectively) and to apparent positive cooperativity (adopted from Hulme, 1992).*

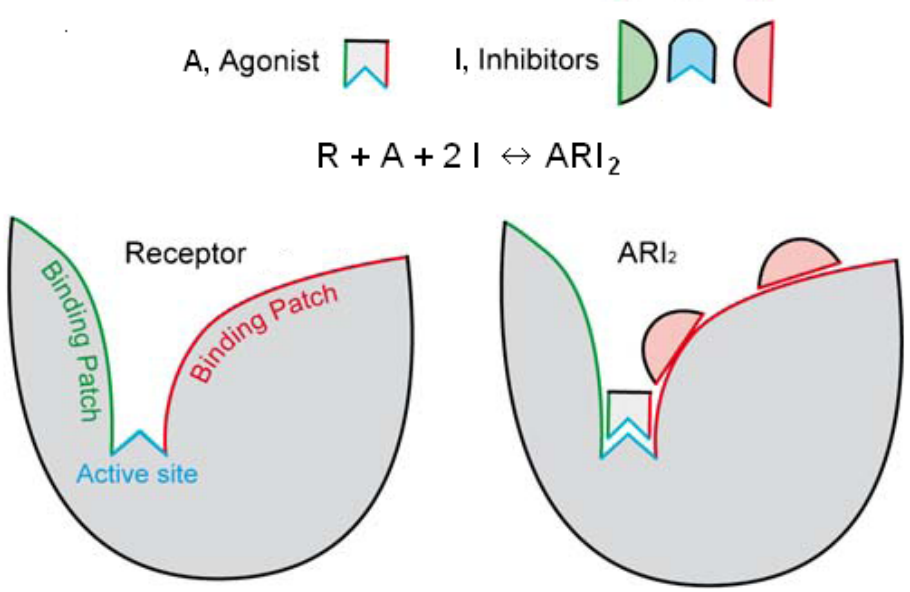

Fig. 4.3.24. *Simplified molecular model of R (receptor or enzyme) with one active site (blue) and two different binding patches (green and red). Before the agonist A reaches the active site (blue), it binds with its corresponding 'side' (green or red) to one binding patch. Different inhibitors I (green, blue, or red) are specific for the active site (blue) but also for a corresponding binding patch (green or red). Binding of agonist A and one type of inhibitors I to the receptor R is illustrated for one possible complex ARI_2. Although a classical model for 1:1 competition predicts a similar endpoint, it does not consider different binding patches as drug targets (adopted from Prinz and Schönichen, 2008 with modifications).*

The slowly altering Hill slopes of the competition binding curves, observed for the bivalent ligands at the H_2R and the H_4R, indicate the failure to obtain equilibrium and might be a sign of delayed changes of receptor conformation. These, in turn, might be a consequence of allosterism (chapter 5), existence of ligand-specific conformations (chapter 6) or simply toxicity. Namely, the amphiphilic character of the bivalent ligands might account for changes in the receptor protein structure, especially as a cytotoxic potential was confirmed for some of the bivalent ligands depending on their physicochemical properties (Ms. Melanie Kaske and Mr. Tobias Birnkammer, University of Regensburg, personal communication). Nevertheless, considering the size of the twin compounds, the additional temporary interactions with the extracellular domains of GPCRs seem to be inevitable (Fig. 4.3.24). Such interactions and ligand-receptor binding dynamics have been recently considered to be crucial for ligand efficacy and subtype selectivity (Bokoch *et al.*, 2010).

4.3.5 Screening of various cell lines for the expression of H_2R and H_4R

As already mentioned in section 1.3, experiments performed on whole cells and broken-cell membrane preparation can result in different results. Intact cells – due to their higher complexity – reveal closer similarity to physiological conditions (Kenakin, 2006). Therefore, characterization of cells expressing the receptor of interest as surrogate systems for the H_2R and the H_4R was performed by means of radioligand and flow cytometric binding studies (cf. subsection 4.2.6).

4.3.5.1 CHO-hH_2R-G$_{\alpha16}$ cells

Binding experiments on the CHO cells, stably expressing the hH_2R and the promiscuous $G_{\alpha16}$ protein (clone 4; Schneider, 2005), yielded 15,000 receptors per cell (Fig. 4.3.25). The difference between the total and the unspecific binding, encountered for 20 nM [^{3}H]TIO (cf. Fig. 4.3.25 B), should enable the analysis of competition binding data. An example is a monophasic competition curve of FAM, depicted in Fig. 4.3.26 (n_H of 0.91 ± 0.13; K_i of 15 nM, counted according to the Cheng-Prusoff equation, where the IC_{50} was 31 nM, 95% CI: 22-43 nM, and the K_d for TIO was set to 20 nM; cf. Monczor, 2006). However, the determined binding constant for FAM was lower than the K_b values found previously on CHO-hH_2R-G$_{\alpha16}$ expressing cells (where FAM suppressed an ARP-induced Ca^{2+} mobilization with a K_b of 143 nM; Schneider, 2005) and at the gpH_2R-G$_{s\alpha S}$ fusion protein (K_b of 48 ± 10 nM; Preuss *et al.*, 2007).

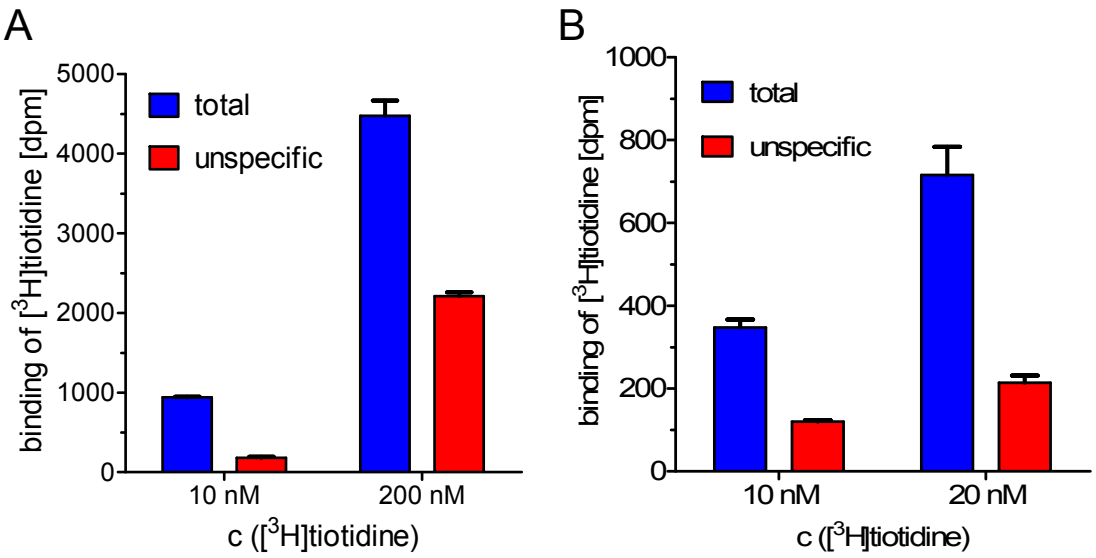

Fig. 4.3.25. *Binding assays on the CHO-hH_2R-$G_{\alpha 16}$ cells, clone 4. The radioligand was used at a saturating concentration for the estimation of the number of H_2Rs per cell (A) as well as at concentrations used in competition assays (B). The binding of [^{3}H]TIO (added as obtained from the manufacturer; specific activity: 82.2 Ci/mmol = 3041.4 kBq/nmol) was measured in the presence of PBS (total) or 1 mM FAM (unspecific). Data from each panel are mean values ± SEM of a single experiment performed in triplicate (500,000 cells in 200 µL).*

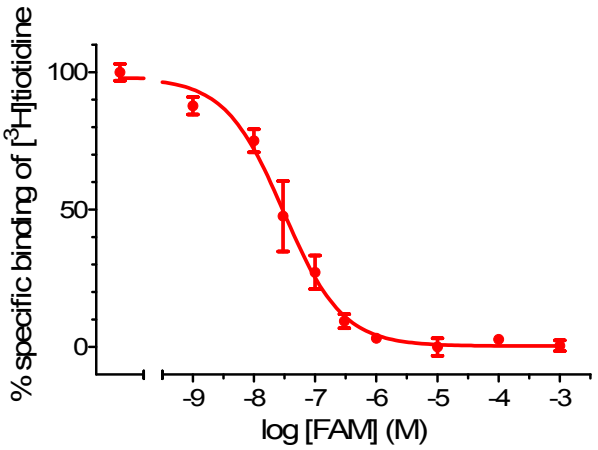

Fig. 4.3.26. *Effect of famotidine (FAM) on the displacement of 20 nM [^{3}H]TIO from the CHO-hH_2R-$G_{\alpha 16}$ cells clone 4. Data are mean values ± SEM of an experiment performed in duplicate (500,000 cells in 200 µL).*

4.3.5.2 CHO-rH_2R-A_2 cells

CHO cells, stably expressing the rH_2R (Traiffort *et al.*, 1992,) were previously used in our research group for the functional characterisation of H_2R ligands in cAMP assays (Kracht, 2001). The binding of the specific H_2R radioligand [^{3}H]UR-DE257 on these cells revealed the density of 30,000 binding sites per cell (Fig. 4.3.27).

Earlier studies on the transfected CHO cells revealed that 100 µM CIM and 10 µM RAN concentration-dependently increased the number of the constitutively active rH_2Rs, whereas 100 µM HIS reduced the receptor density (cf. Fig. 6.3.11; Smit *et al.*, 1996 a). Moreover, the maximal effect was observed, when the ligands were preincubated for periods longer than 16 hours (Smit *et al.*, 1996 b). Therefore, 1.2 µM of the bivalent H_2R

antagonist **11** (cf. K_b of 371 nM; Birnkammer *et al.*, 2010), 60 µM FAM and 60 µM HIS (cf. Table 4.3.3) were incubated with the cells for 24 hours, before the binding of [^{3}H]UR-DE257 was measured, as shown in Fig. 4.3.28.

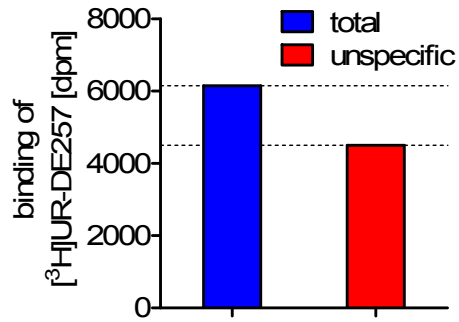

Fig. 4.3.27. *Estimation of the rH$_2$R number per cell at CHO-rH$_2$R-A$_2$ cells. Binding of 100 nM [^{3}H]UR-DE257/UR-DE257 (1 + 1 dilution, undiluted specific activity: 69.3 Ci/mmol = 2564.1 kBq/nmol) was tested in the presence of PBS (total) or 100 µM FAM (unspecific). Data are mean values ± SEM of an experiment performed in sextuplicate (500,000 cells in 200 µL).*

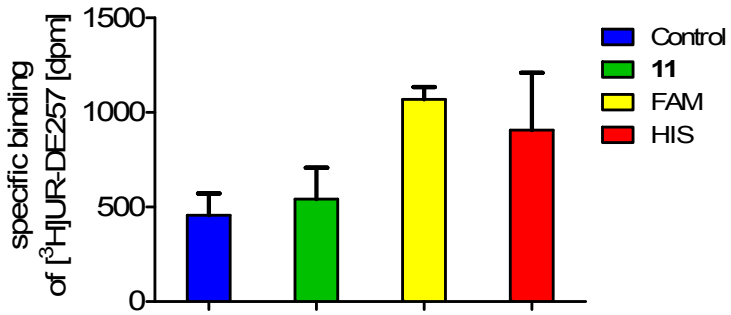

Fig. 4.3.28. *Influence of incubation of CHO-rH$_2$R-A$_2$ cells for 24 hours with different H$_2$R ligands on the receptor density. The binding of 100 nM of the tracer [^{3}H]UR-DE257/UR-DE257 was determined in the presence of PBS (total) or 100 µM FAM (unspecific). Data are mean values ± SEM of an experiment performed in triplicate (250,000 cells in 200 µL).*

After incubation with different ligands for 24 hours, rH$_2$Rs were still available on the cell surface. However, the presented results barely confirmed the ligand-dependent mechanism of the rH$_2$R redistribution, as also HIS increased the specific binding of [^{3}H]UR-DE257. This might at least partially result from the ligand-independent H$_2$R internalization (cf. Fig. 6.3.4-5). On the other hand, the relatively high errors precluded a detailed analysis. Further investigations of the H$_2$R endocytic cycle are described in subsection 6.3.2.

4.3.5.3 U-937 cells (endogenously expressing the H$_2$R)

As the human monocytic U-937 cells endogenously express functional hH$_2$Rs (cf. subsection 1.2.2.2), the question was raised, whether these cells can be used as a model for the investigation of H$_2$R ligands. Possible advantages over recombinant systems, such as transfected CHO cells, might result from the natural regulation of receptor biosynthesis, trafficking, signal transduction, up- and down-regulation. Fig. 4.3.29 illustrates the binding experiments with [^{3}H]TIO, which revealed approx. 10,000 receptors per cell. This result is comparable with the reported number of low-affinity binding sites on U-937 cells

(B_{max} of 23,000 ± 3000 sites per cell; K_d of 20 ± 3 nM; Monczor *et al.*, 2006). Nevertheless, the determined receptor density is considered too low for the performance of standard competition assays, utilizing 10-20 nM [^{3}H]TIO.

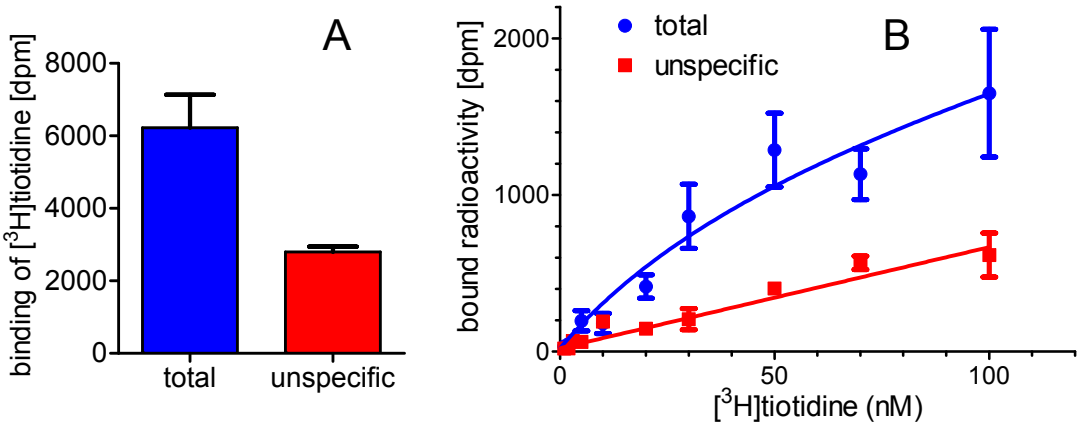

Fig. 4.3.29. *[^{3}H]Tiotidine ([^{3}H]TIO) binding experiments on U-937 cells. (A) Estimation of the number of H_2Rs per U-937 cell. Binding of 200 nM [^{3}H]TIO (added as obtained from the manufacturer, specific activity: 77.2 Ci/mmol = 2856.4 kBq/nmol) was tested in the presence of PBS (total) or 1 mM FAM (unspecific). Data are mean values ± SEM of an experiment performed in triplicate (1.5 million cells in 200 µL). (B) The saturation binding (the same radioligand batch as in Fig. 4.3.25; K_d value of 61 ± 48 nM). Data are mean values ± SEM of two independent experiments performed in triplicate (750,000 cells in 200 µL).*

The application of the red fluorescent H_2R ligands, developed in our research group by Dr. Daniela Erdmann (cf. Fig. 1.2.5; Erdmann, 2010), allowed a nonradioactive investigation of H_2R binding e.g. by means of flow cytometry or confocal microscopy (cf. subsection 6.3.1). Thus, flow cytometric binding assays were performed, as described under Materials and methods (section 3.2), with the fluorescent squaramide derivatives UR-DE56 and UR-DE108 (K_d of approx. 170 nM and 180 nM, respectively; Mosandl, 2009; Erdmann, 2010). Unfortunately, the U-937 cells showed only poor specific binding as illustrated by Fig. 4.3.30 and Fig. 4.3.31.

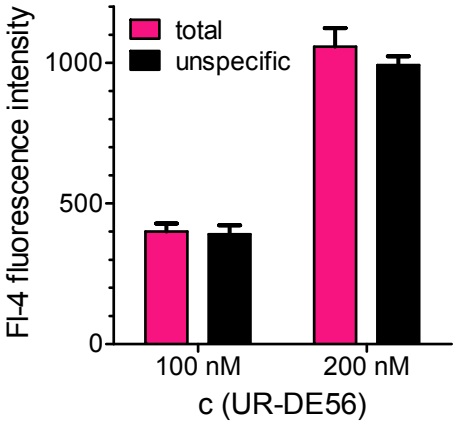

Fig. 4.3.30. *Binding of UR-DE56 determined by flow cytometry on U-937 cells. The binding of UR-DE56 was estimated after 40 min of incubation in the absence (total) or presence of 100 µM FAM (unspecific). Data are mean values ± SEM of an experiment performed in quadruplicate.*

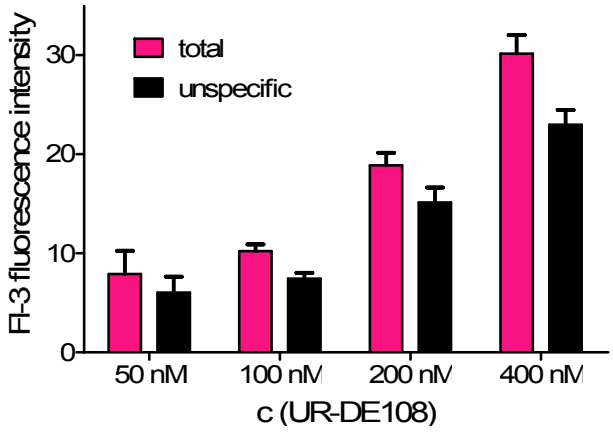

Fig. 4.3.31. *Binding of UR-DE108 determined by flow cytometry on U-937 cells. The binding of UR-DE108 was estimated after 30 min of incubation in the absence (total) or presence of 500 µM FAM (unspecific). Data are mean values ± SEM of an experiment performed in duplicate.*

4.3.5.4 Human neutrophils

Previous studies of guanidine-type H_2R agonists showed that human neutrophils are a valuable model for functional investigations on endogenously expressed H_2R, in particular by measuring superoxide (O_2^-) formation (Burde *et al.*, 1990). In the current study, an attempt was made towards the estimation of the hH_2R number by using the above-mentioned red fluorescent H_2R ligands (cf. Erdmann, 2010), similarly to the experiments on U-937 cells. The isolation of neutrophils from whole blood was performed in cooperation with Ms. Irena Brunskole (Institute of Pharmacy, University of Regensburg), as described in subsection 4.2.7. The flow cytometric binding experiment was conducted within 3.5 hours after the isolation. Unfortunately, almost no difference between total and unspecific binding of the three red fluorescent ligandes could be detected on neutrophils after 37 min of incubation as shown in Fig. 4.3.32 A (cf. 37 min of incubation; Mosandl, 2009).

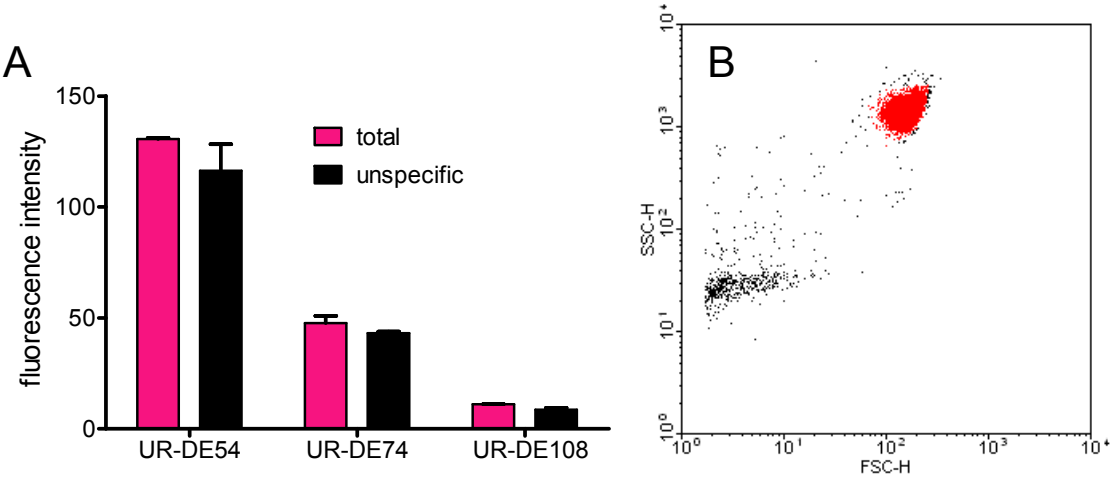

Fig. 4.3.32. *Flow cytometric binding assay on human neutrophils. (A) The binding of 500 nM of the red fluorescent H_2R ligands: UR-DE54 (Fl-4), UR-DE74 (Fl-4) and UR-DE108 (Fl-3) was estimated after 37 min of incubation in the absence (total) or presence of 30 µM FAM (unspecific). Data were calculated for the cell population shown in the red gate (B) and are mean values ± SEM of an experiment performed in duplicate.*

In order to find out the reason for the merely detectable specific binding of the fluorescent H_2R ligands, neutrophils were imaged by means of confocal microscopy, as described in subsection 3.2.7. Surprisingly, red autofluorescence of granula was almost as high as fluorescence of the cells labeled with 200 nM UR-DE74 (Fig. 4.3.33). These observations correlated well with the results from flow cytometric binding assays, shown in Fig. 4.3.34 A. Further experiments revealed also time-dependent penetration of the fluorescent ligands into the cells, disabling competitive binding (Fig. 4.3.34 B).

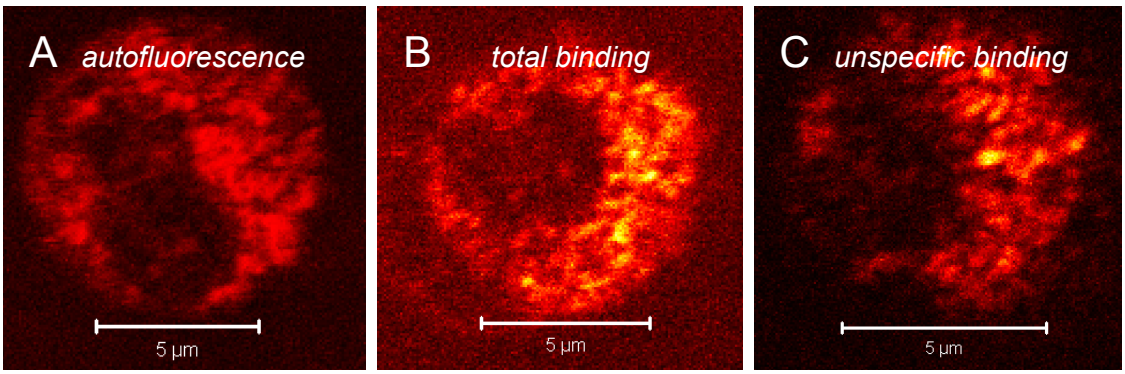

Fig. 4.3.33. *Confocal imaging of human neutrophils: autofluorescence (A) as well as the cells labelled with 200 nM UR-DE74 after 3 min of incubation (total binding, B) or after 38 min of incubation in the presence of 100 µM FAM (unspecific binding, C). Plan-Apochromat 63x/1.4 oil, HeNe 633 (15–18%), HFT UV/488/543/633, NFT 545, LP 650, pinhole = 1 a.u.*

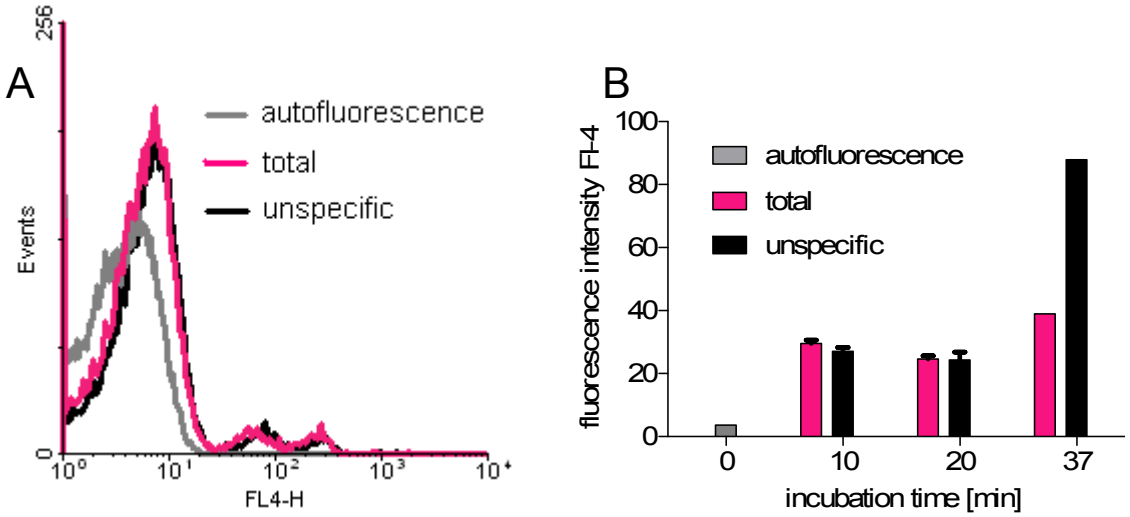

Fig. 4.3.34. *Flow cytometric binding assay on human neutrophils. (A) Histograms for neutrophils: unlabelled (autofluorescence) or labelled with 150 nM UR-DE74 after 10 min of incubation in the absence (total) or presence of 30 µM FAM (unspecific). (B) Binding of 200 nM UR-DE54 after different incubation periods in the absence (total) or presence of 30 µM FAM (unspecific). Data are mean values ± SEM of an experiment performed in 1–3 replicates. Fluorescence intensity FI-4 was calculated for the cell population shown in the red gate in Fig. 4.3.32 B.*

4.3.5.5 CHO-hH$_4$R cells

As described in section 4.3.4, the imidazole-type bivalent N^G-acylated hetarylpropylguanidines proved to be also active as a hH$_4$R agonists at nanomolar concentrations. Therefore, an attempt was made to obtain a cellular system for the testing of the H$_4$R ligands. CHO cells were stably transfected with the pcDNA3.1(+)-Neo-hH$_4$R plasmid as described under Materials and methods (subsection 4.2.5). Unfortunately, the CHO-hH$_4$R cells revealed only approx. 2000 receptors per cell (measured as [^{3}H]HIS binding sites, Fig. 4.3.35). This number might be underestimated, as the used agonistic radioligand preferably binds to the subpopulation of receptors coupled to G protein (Kenakin, 1997). However, the results are in accordance with a low expression of functional H$_4$R by transfected cells reported by Dr. Johannes Mosandl (Mosandl, 2009). As specific binding of 10 nM [^{3}H]HIS was not detectable (Fig. 4.3.36), competition binding studies were discontinued.

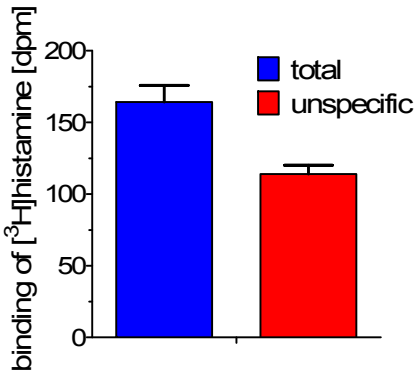

Fig. 4.3.35. *Saturation binding on CHO-hH$_4$R cells. The binding of 100 nM [^{3}H]HIS (added as obtained from the manufacturer, specific activity: 14.1 Ci/mmol = 521.7 kBq/nmol) was estimated in the presence of PBS (total) or 50 µM of the H$_3$/H$_4$ antagonist THIO (unspecific). Data are mean values ± SEM of an experiment performed in sextuplicate (500,000 cells in 200 µL).*

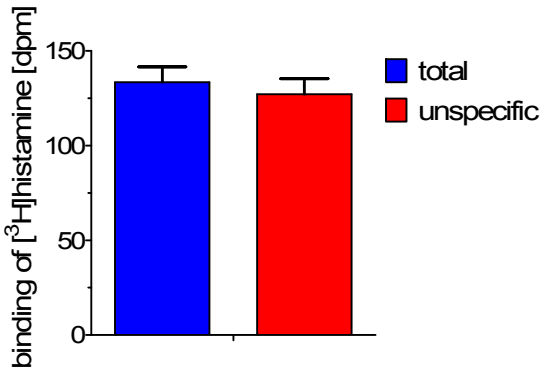

Fig. 4.3.36. *Binding of 10 nM [^{3}H]HIS on the CHO-hH$_4$R cells (added as obtained from the manufacturer, specific activity: 14.1 Ci/mmol = 521.7 kBq/nmol). The unspecific binding was estimated in the presence of 10 µM THIO. Data are mean values ± SEM of an experiment performed in sextuplicate (170,000 cells per sample).*

The genetically engineered cells CHO-hH_2R-$G_{\alpha16}$ and CHO-rH_2R-A_2 revealed hH_2R densities of approx. 15,000 and 30,000 receptors per cell, respectively, sufficient to perform binding studies with [^{3}H]TIO and [^{3}H]UR-DE257 (cf. Fig. 4.3.25 and 4.3.27). In contrast, the amount of approx. 10,000 H_2Rs per cell, endogenously expressed by the human monocytic U-937 cell line, was too low for the characterization of ligands, as shown in radioligand and flow cytometric binding assays (cf. Fig. 4.3.29–31). Due to the high autofluorescence of human neutrophils and the time-dependent penetration of the fluorescent ligands (cf. Fig. 4.3.32–34), no binding studies could be performed on these cells. Unfortunately, an attempt to establish a cell line stably expressing the hH_4R was not successful (cf. Fig. 4.3.35–36), similar to findings reported previously in terms of functional H_4Rs (Mosandl, 2009).

4.4 Summary and conclusion

The Hill slope, obtained from radioligand saturation and competition binding assays at equilibrium, is a very useful pharmacological parameter, with respect to the explanation of a more complicated binding behaviour than predicted by the law of mass action (cf. Table 4.1.1; Repke and Liebmann, 1987; Lazareno, 2001; Motulsky and Christopoulos, 2004; Kenakin, 2006). However, for the correct interpretation of the experimental binding data, it is essential to provide that there is no radioligand depletion and that incubation time is sufficient to reach equilibrium at the time point of the measurement (Hulme, 1992; cf. Fig. 4.3.23).

A) If ligands bind to receptors in a competitive manner (without any cooperativity), the competition curve is monophasic with the n_H equalling 1 and the Scatchard representation of binding data is linear (Fig. 4.4.1 A).

B) However, if n_H is smaller than 1, a curvilinear saturation curve and a biphasic (convex) Scatchard plot are expected (Fig. 4.4.1 B). Additionally, a competition curve might reveal a more or less clear biphasic course, when fitted to two-site model instead of logistic function. This could be due to negative cooperativity (allosterism), but other possible reasons for the acquisition of flat competition curves have to be considered too, such as the existence of various receptor subtypes or different conformations of the same receptor, characterized by different affinities to the G protein (ternary complex model).

C) Finally, if $n_H > 1$, a concave Scatchard plot and a bell-shaped competition curve are common (Fig. 4.4.1 C). These findings could be consistent with the positive cooperativity. However, also the premature termination of incubation may lead to apparently similar results.

Moreover, the phenomenon of cooperativity might occur not only when ligands bind to the distinct binding sites at the same receptor (Repke and Liebmann, 1987), but also if they interact with different protomers within receptor dimers or even dimeric receptors (Albizu *et al.*, 2006).

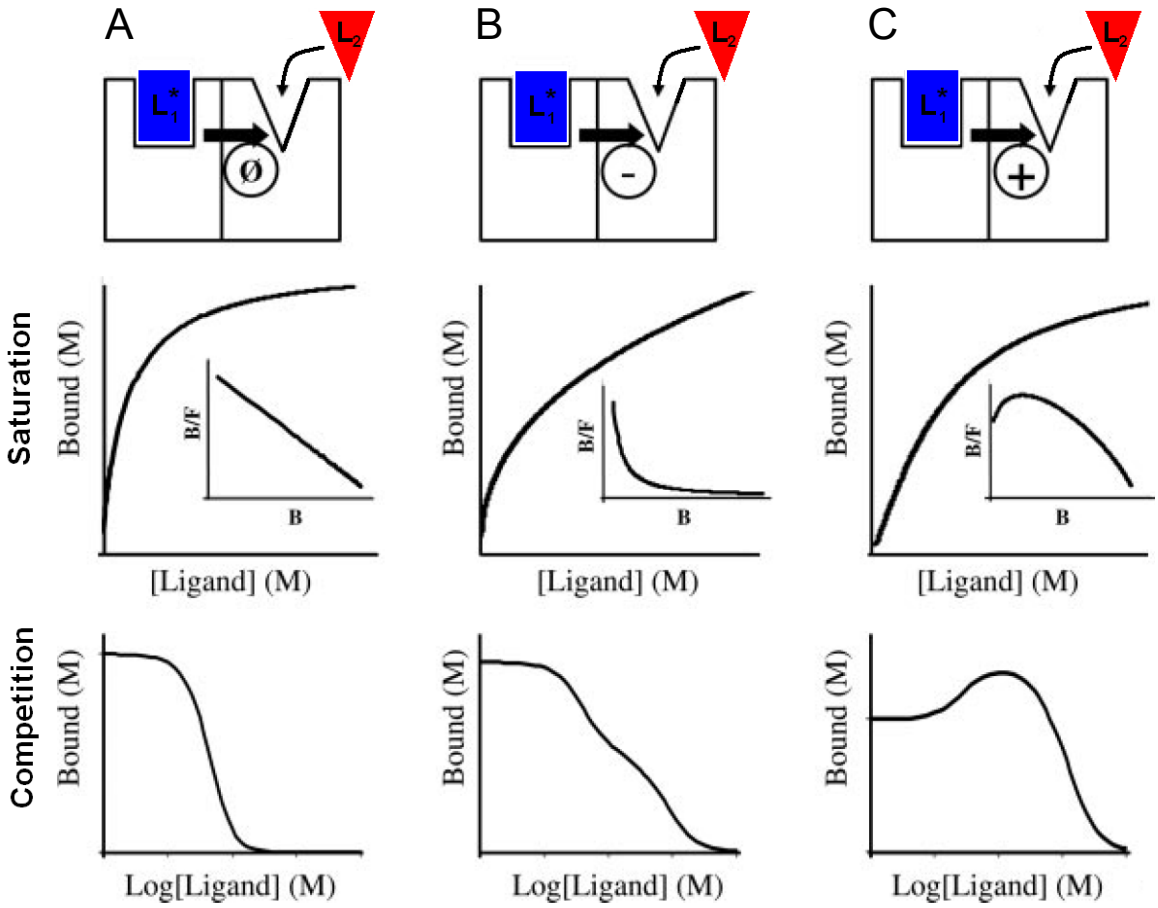

Fig. 4.4.1. *Predicted binding behaviour of radioligand (L_1*) and unlabelled ligand (L_2) in saturation (middle, Scatchard plots as inset) and competition assays (bottom) in the case of (A) lacking, (B) negative or (C) positive cooperativity (adopted from Albizu et al., 2006 with modifications).*

Addressing dimers of G-protein-coupled receptors has been suggested as a very promising concept in drug discovery (Daniels *et al.*, 2005 a; Shonberg *et al.*, 2011). Thus, bivalent N^G-acylated guanidines were developed in our research group as pharmacological tools for exploration of the putative H_2R dimerization (Fukushima, 1997). However, the most potent bivalent ligands had only 6- to 8-membered linkers connecting the two sets of pharmacophoric groups, i. e. the acylguanidine moieties. This is considered insufficient for the bridging the receptor molecules of a H_2R dimer (Fig. 4.1.1 B and Fig. 4.3.19; cf. Kraus, 2007). The presented radioligand binding studies provided new insights into the mode of action of the bivalent ligands at the H_2R and the H_4R. The investigation of the latter became possible with imidazole-type bivalent acylguanidines which, in addition to H_2R agonistic properties, turned out to possess rather high H_4R potency in functional assays:

1) All of the tested bivalent agonists with octamethylene linkers as well as HIS showed flat competition curves on Sf9 membranes, expressing hH_2R-$G_{s\alpha S}$ or gpH_2R-$G_{s\alpha S}$ fusion proteins, after 90 min of incubation with [^{3}H]TIO (Table 4.3.3). From a theoretical point of view, one could argue against a simple model of competitive binding, as equilibrium should have been already reached at this incubation time ($t_{0.5}$ of [^{3}H]TIO dissociation of approx. 10 min; Fig. 5.3.1; cf. Foreman *et al.*, 1985). However, after prolonged (up to 3 hours) incubation period with [^{3}H]TIO, the Hill slope of HIS remained smaller than 1, whereas that of the bivalent agonist **3** increased, approximating unity (Fig. 4.3.10).

2) This phenomenon cannot be explained by the peculiarities of the fusion proteins:

   a. Saturation binding of [^{3}H]TIO and [^{35}S]GTPγS revealed the resemblance between the gpH_2R-$G_{s\alpha S}$ fusion protein and the gpH_2R coexpressed with $G_{s\alpha S}$ in Sf9 membranes, as [^{3}H]TIO bound to both receptor forms with a K_d of 40 nM (Fig. 4.3.1-2). This is in agreement with previous studies (K_d value of 34.4 ± 8.4 nM reported by Kelley *et al.*, 2001). The estimated H_2R-to-(functional)G-protein ratios for the fusion protein (unexpectedly 1:3, single experiment only) and for the coexpressed proteins (about 1:7; Fig.4.3.4) contradicted the hypothesis that flat competition curves resulted from the limited G proteins. Moreover, the coupling factor for the coexpressed gpH_2R was in line with the literature (cf. other coexpressed histamine receptor subtypes: hH_3R, Schnell *et al.*, 2010; hH_4R, Schneider *et al.*, 2009).

   b. The competition binding curves of HIS were shallow at both fused (Fig. 4.3.5 A and B) and coexpressed H_2Rs (Fig. 4.3.8). Fitting the data to the two-site binding equation revealed two independent non-interacting binding sites for HIS in the absence of GTPγS. Additionally, GTPγS-dependent shift and steepening of the binding curve of the natural ligand were observed, as predicted by the ternary complex model (Fig. 4.3.11 A). The bivalent H_2R agonist **4** with an octamethylene linker was found to be an efficient stabilizer of the ternary complex at the gpH_2R-$G_{s\alpha S}$ (Fig. 4.3.11 B), but its binding was insensitive towards 10 µM GTPγS, indicating antagonism rather than agonism (Fig. 4.3.5 D). By contrast, in the presence of GTPγS, the competition curve for ligand **4** at the hH_2R-$G_{s\alpha S}$ was slightly shifted to the right and steepened (Fig. 4.3.5 C). Such species-dependent differences in sensitivity to GTPγS were reported previously for some monovalent N^G-acylguanidines at the hH_2R-$G_{s\alpha S}$ and the gpH_2R-$G_{s\alpha S}$ (Xie *et al.*, 2006).

c. The biphasic Scatchard representations of [^{3}H]TIO binding to the gpH_2R-$G_{s\alpha S}$ fusion proteins and the gpH_2R coexpressed with $G_{s\alpha S}$ (Fig. 4.3.3), consistent with the ternary complex model, were in line with previous studies reporting the inverse agonism of TIO (Monczor *et al.*, 2003).

3) The bivalent compound **11** with a 20-membered alkanediyl linker, which is supposed to be sufficiently long to bridge the binding pockets of two dimerised receptor molecules (Bhushan *et al.*, 2004), revealed apparent positive cooperativity after 90 min of incubation at the hH_2R-$G_{s\alpha S}$, the gpH_2R-$G_{s\alpha S}$ and the hH_4R-GAIP + $G_{i\alpha 2}$ + $G_{\beta 1\gamma 2}$ fusion proteins (Hill slopes of the binding curves greater than 2, cf. Fig. 4.3.17–21). However, the extension of the incubation period at the hH_4R to 3-7.5 hours resulted in classical monophasic competition curves (Fig. 4.3.22 B).

Binding studies of mono- and bivalent ligands support the ternary complex model (two non-interacting binding sites at the H_2R), but not the hypothetical “bridging” of H_2R dimers. Ligand affinity dropped with increasing the number of methylene groups in the linker up to 20 (Fig. 4.3.19), which is the expected the optimum length to enable simultaneous occupation of the binding sites in two neighbouring protomers by twin compounds (Bhushan *et al.*, 2004). The analysis of the slopes of competition binding curves (after 90 min of incubation) indicated the apparent negative cooperativity for the shorter bivalent ligands at the H_2R (Table 4.3.3). However, this effect depended on the used radioligand ($n_H < 1$ for [^{3}H]TIO in Fig. 4.3.5 C and D; $n_H > 1$ for [^{3}H]UR-DE257 in Fig. 4.3.20). By contrast, apparent positive cooperativity was observed for the higher homologues among the bivalent ligands at the H_2R and the H_4R (Fig. 4.3.17–21). Nevertheless, after extended incubation periods, the Hill slopes changed in both cases, approximating unity (Fig. 4.3.10 and Fig. 4.3.22 B, respectively), whereas the affinity of the bivalent ligands did not significantly alter, suggesting unexpectedly slow equilibration.

4.5 References

Albizu L *et al.*: Probing the existence of G protein-coupled receptor dimers by positive and negative ligand-dependent cooperative binding, *Mol Pharmacol*, **2006**, *70*, 1783-1791.

Appl H: Molecular analysis of the interaction of the four histamine receptor subtypes with antidepressant and antipsychotic drugs, Doctoral thesis, University of Regensburg, **2010**.

Bhushan RG *et al.*: A bivalent ligand (KDN-21) reveals spinal *δ* and κ opioid receptors are organized as heterodimers that give rise to δ_1 and κ_2 phenotypes: Selective targeting of *δ*-κ heterodimers, *J Med Chem*, **2004**, *47,* 2969–2972.

Birnkammer T *et al.*: Bivalent acylguanidine-type ligands as potent and selective histamine H_2 receptor agonists, *Drugs Fut*, **2008**, *33* (Suppl. A), 127-128 (P205).

Birnkammer T *et al.*: Structure-activity relationships of bivalent acylguanidine-type histamine H_2 receptor agonists, *5th Summer School "Medicinal Chemistry"*, University of Regensburg, **2010**, P4 (poster contribution).

Bokoch MP *et al.*: Ligand-specific regulation of the extracellular surface of a G-protein-coupled receptor, *Nature*, **2010**, *463*, 108-112.

Burde R *et al.*: Characterization of histamine H_2-receptors in human neutrophils with a series of guanidine analogues of impromidine: Are cell type-specific H_2-receptors involved in the regulation of NADPH oxidase? *Naunyn Schmiedebergs Arch Pharmacol*, **1990**, *341*, 455–461.

Cao Y *et al.*: The fucosylated histo-blood group antigens H type 2 (blood group O, CD173) and Lewis Y (CD174) are expressed on CD34+ hematopoietic progenitors but absent on mature lymphocytes, *Glycobiology*, **2001**, *11*, 677–683.

Cheng Y-C and Prusoff WH: Relationship between the inhibition constant (K_i) and the concentration of inhibitor which causes 50 per cent inhibition (IC_{50}) of an enzymatic reaction, *Biochem Pharmacol*, **1973**, *22*, 3099–3108.

Damaj BB *et al.*: Functional expression of H_4 histamine receptor in human natural killer cells, monocytes, and dendritic cells, *J Immunol*, **2007**, *179*, 7907–7915.

Daniels DJ *et al.* (a): Opioid-induced tolerance and dependence in mice is modulated by the distance between pharmacophores in a bivalent ligand series, *Proc Natl Acad Sci USA*, **2005**, *102*, 19208–19213.

Daniels DJ *et al.* (b): A bivalent ligand (KDAN-18) containing δ-antagonist and κ-agonist pharmacophores bridges δ_2 and κ_1 opioid receptor phenotypes, *J Med Chem*, **2005**, *48*, 1713-1716.

Erdmann D: Histamine H_2 and H_3 receptor antagonists: Synthesis and characterization of radiolabelled and fluorescent pharmacological tools, Doctoral thesis, University of Regensburg, **2010**.

Foreman JC *et al.*: The binding of [^{3}H]-tiotidine to homogenates of guinea-pig lung parenchyma, *Br J Pharmacol*, **1985**, *86*, 475–482.

Fukushima Y *et al.*: Oligomer formation of histamine H_2 receptors expressed in Sf9 and COS7 cells, *FEBS Lett*, **1997**, *409*, 283–286.

Ghorai P *et al.*: Acylguanidines as bioisosteres of guanidines: N^G-acylated imidazolylpropylguanidines, a new class of histamine H_2 receptor agonists, *J Med Chem*, **2008**, *51*, 7193-7204.

http://wolfson.huji.ac.il/purification/PDF/Protein_Quantification/BIORAD_DC_Instr_Protein_Assay.pdf

Hulme EC (ed.): Receptor-ligand interactions: A practical approach, *IRL Press/Oxford University Press*, New York, **1992**.

Igel P *et al.*: N^G-acylated imidazolylpropylguanidines as potent histamine H_4 receptor agonists: selectivity by variation of the N^G-substituent, *J Med Chem*, **2009**, *52*, 2623–2627.

Kelley MT *et al.*: Distinct interaction of human and guinea pig histamine H_2-receptor with guanidine-type agonists, *Mol Pharmacol*, **2001**, *60*, 1210–1225.

Kenakin T: Differences between natural and recombinant G protein-coupled receptor systems with varying receptor/G protein stoichiometry, *Trends Pharmacol Sci*, **1997**, *18*, 456-464.

Kenakin TP: A pharmacology primer: Theory, application, and methods, *Academic Press – Elsevier*, Amsterdam – Tokyo, **2006**.

Kracht J: Bestimmung der Affinität und Aktivität subtypselektiver Histamin- und Neuropeptid Y-Rezeptorliganden an konventionellen und neuen pharmakologischen In-vitro-Modellen, Doctoral thesis, University of Regensburg, **2001**.

Kraus A *et al.*: N^G-acylated aminothiazolylpropylguanidines as potent and selective histamine H_2 receptor agonists, *ChemMedChem*, **2009**, *4*, 232-240.

Kraus A: Highly potent, selective acylguanidine-type histamine H_2 receptor agonists: Synthesis and structure-activity relationships, Doctoral thesis, University of Regensburg, **2007**.

Krielaart MJ *et al.*: Mechanism of action of H_2-antagonists on histamine- or dimaprit-stimulated H_2-receptors of spontaneously beating guinea-pig atrium, *Agents Actions*, **1990**, *31*, 23-35.

Kroeger KM *et al.*: G-protein coupled receptor oligomerization in neuroendocrine pathways, *Front Neuroendocrinol*, **2004**, *24*, 254–278.

Lazareno S: Quantification of receptor interactions using binding methods, *J Recept Signal Transduct*, **2001**, *21*, 139–165.

Legnazzi BL *et al.*: Rapid desensitization and slow recovery of the cyclic AMP response mediated by histamine H_2 receptors in the U937 cell line, *Biochem Pharmacol*, **2000**, *60*, 159–166.

Lezoualc'h F *et al.*: Multivalent-based drug design applied to serotonin 5-HT_4 receptor oligomers, *Curr Pharm Des*, **2009**, *15*, 719 – 729.

Limbird LE: Cell surface receptors: a short course on theory and methods, *Springer*, New York, **2004**.

Lindl T: Zell- und Gewebekultur: Einführung in die Grundlagen sowie ausgewählte Methoden und Anwendungen, *Spektrum Akademischer Verlag*, Heidelberg – Berlin, **2000**.

Lowry OH *et al.*: Protein measurement with the Folin phenol reagent, *J Biol Chem,* **1951**, *193*, 265–275.

May LT *et al.*: Allosteric modulation of G protein–coupled receptors, *Annu Rev Pharmacol Toxicol*, **2007**, *47*, 1–51.

Monczor F *et al.*: Histamine H_2 receptor overexpression induces U937 cell differentiation despite triggered mechanisms to attenuate cAMP signalling, *Biochem Pharmacol*, **2006**, *71*, 1219–1228.

Monczor F *et al.*: Tiotidine, a histamine H_2 receptor inverse agonist that binds with high affinity to an inactive G-protein–coupled form of the receptor: Experimental support for the cubic ternary complex model, *Mol Pharmacol,* **2003,** *64*, 512–520.

Mosandl J: Radiochemical and luminescence-based binding and functional assays for human histamine receptors using genetically engineered cells, Doctoral thesis, University of Regensburg, **2009**.

Motulsky HJ and Christopoulos A: Fitting models to biological data using linear and nonlinear regression: A practical guide to curve fitting, *GraphPad Software/Oxford University Press*, New York, **2004**.

Portoghese PS *et al.*: Opioid agonist and antagonist bivalent ligands. The relationship between spacer length and selectivity at multiple opioid receptors, *J Med Chem*, **1986**, *29*, 1855-1861.

Portoghese PS: From models to molecules: opioid receptor dimers, bivalent ligands, and selective opioid receptor probes, *J Med Chem*, **2001**, *44*, 2259-69.

Preuss H *et al.*: Mutations of Cys-17 and Ala-271 in the human histamine H_2 receptor determine the species selectivity of guanidine-type agonists and increase constitutive activity, *J Pharmacol Exp Ther*, **2007**, *321*, 975–982.

Prinz H and Schönichen A: Transient binding patches: a plausible concept for drug binding, *J Chem Biol*, **2008**, *1*, 95–104.

Repke H and Liebmann C: Membranrezeptoren und ihre Effektorsysteme, *Akademie-Verlag*, Berlin, **1987**.

Schneider E: Development of fluorescence-based methods for the determination of ligand affinity, selectivity and activity at G-protein coupled receptors, Doctoral thesis, University of Regensburg, **2005**.

Schneider EH and Seifert R: Histamine H_4 receptor–RGS fusion proteins expressed in Sf9 insect cells: A sensitive and reliable approach for the functional characterization of histamine H_4 receptor ligands, *Biochem Pharmacol*, **2009**, 78, 607–616.

Schneider EH *et al.*: High constitutive activity and a G-protein-independent high-affinity state of the human histamine H_4-receptor, *Biochemistry*, **2009**, *48*, 1424–1438.

Schnell D *et al.*: Expression and functional properties of canine, rat, and murine histamine H_4 receptors in Sf9 insect cells, *Naunyn Schmiedebergs Arch Pharmacol*, **2011**, *383*, 457-470.

Schnell D *et al.*: No evidence for functional selectivity of proxyfan at the human histamine H_3 receptor coupled to defined G_i/G_o protein heterotrimers, *J Pharmacol Exp Ther*, **2010**, *332*, 996–1005.

Seifert R and Wenzel-Seifert K: Constitutive activity of G-protein-coupled receptors: cause of disease and common property of wild-type receptors, *Naunyn Schmiedebergs Arch Pharmacol*, **2002**, *366*, 381–416.

Seifert R and Wieland Th: G protein-coupled receptors as drug targets: Methods and principles in medicinal chemistry, *Wiley-VCH*, Weinheim, **2005**.

Seifert R *et al.*: Lack of effect of opioid peptides, morphine and naloxone on superoxide formation in human neutrophils and HL-60 leukemic cells, *Naunyn Schmiedebergs Arch Pharmacol*, **1989**, *340*, 101–106.

Seifert R *et al.*: Reconstitution of β_2-adrenoceptor-GTP-binding-protein interaction in Sf9 cells: High coupling efficiency in a β_2-adrenoceptor-$G_{s\alpha}$ fusion protein. *Eur J Biochem,* **1998**, *255*, 369–382.

Shonberg J *et al.*: Design strategies for bivalent ligands targeting GPCRs, *ChemMedChem*, **2011**, *6*, 963–974.

Smit MJ *et al.* (a): Inverse agonism of histamine H_2 antagonists accounts for upregulation of spontaneously active histamine H_2 receptors, *Proc Natl Acad Sci USA*, **1996**, *93*, 6802-6807.

Smit MJ *et al.* (b): Two distinct pathways for histamine H_2 receptor down-regulation: H_2 $Leu^{124} \rightarrow$ Ala receptor mutant provides evidence for a cAMP-independent action of H_2 agonists, *J Biol Chem*, **1996**, *271*, 7574-7582.

Traiffort E *et al.*: Expression of a cloned rat histamine H_2 receptor mediating inhibition of arachidonate release and activation of cAMP accumulation, *Proc Natl Acad Sci USA*, **1992**, *89*, 2649-2653.

Valant C *et al.*: A novel mechanism of G protein-coupled receptor functional selectivity: Muscarinic partial agonist McN-A-343 as a bitopic orthosteric/allosteric ligand, *J Biol Chem*, **2008**, *283* (43), 29312-29321.

Wenzel-Seifert K *et al.*: Similar apparent constitutive activity of human histamine H_2-receptor fused to long and short splice variants of $G_{s\alpha}$. *J Pharmacol Exp Ther*, **2001**, *299*, 1013-1020.

Xie SX *et al.*: Probing ligand-specific histamine H_1- and H_2-receptor conformations with N^G-acylated imidazolylpropylguanidines, *J Pharmacol Exp Ther*, **2006**, *317*, 139–146.

Chapter 5

Radioligand binding kinetics at histamine H_2 and H_4 receptors

5 Radioligand binding kinetics at histamine H_2 and H_4 receptors

5.1 Introduction

The spacers of the most potent bivalent N^G-acylated guanidines comprised only 6–8 methylene groups (cf. Fig. 4.1.1 B; Kraus, 2007; Birnkammer *et al.*, 2010) and thus cannot bridge H_2R dimers in a manner proposed by Portoghese and colleagues (Bhushan *et al.*, 2004). Therefore, the shallow binding curves of the most potent bivalent H_2R ligands (cf. Table 4.3.3) could not be explained by the interaction of a single bivalent ligand with two adjacent receptor molecules at the same time (cf. Fig. 4.1.3). Other possible binding modes of bivalent ligands are illustrated in Fig. 1.1.2 and include allosteric and univalent binding. As already mentioned in subsections 4.1.1 and 4.3.2, an explanation of Hill slopes < 1 (with [^{3}H]TIO as radioligand) may be provided either by the ternary complex model or by allosteric interactions.

Allosterism might result from negative cooperativity between two non-overlapping and non-interconverting binding sites on the same receptor molecule. Indeed, this was postulated previously at the α_{2A}-adrenoreceptor (Leppik *et al.*, 1998) and the dopamine D_2 receptor (Hoare and Strange, 1996). Moreover, simultaneous interactions of both pharmacophoric moieties of bivalent compounds with ortho- and allosteric binding sites have been recently reported for the muscarinic M_2 receptor (Valant *et al.*, 2008; Antony *et al.*, 2009). The allosteric sites of the rhodopsin-like subfamily of GPCRs are believed to be located at the extracellular loops, as well as at the top of transmembrane domain 7 (May *et al.*, 2007). Due to the relatively low sequence conservation among receptor subtypes, an allosteric binding site seems to be a very promising target for the discovery of new therapeutics with improved selectivity, when compared with the orthosteric binding site (Avlani *et al.*, 2004; Smith and Milligan, 2010).

5.1.1 Radioligand dissociation kinetics

Whereas binding to the orthosteric site can be easily followed by the competitive displacement of a radioactive tracer, the interaction with an allosteric site is sometimes camouflaged by neutral equilibrium binding cooperativity, as shown in Fig. 5.1.1. Therefore,

the putative allosteric behaviour should rather be investigated by the radioligand dissociation kinetics (Kostenis and Mohr, 1996).

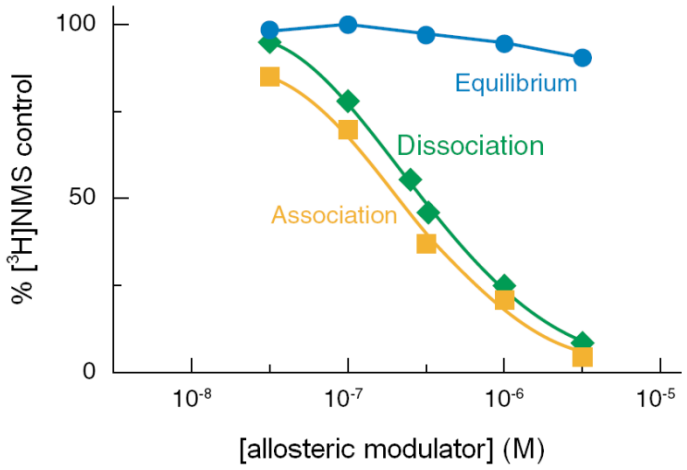

Fig. 5.1.1. *Binding of an allosteric modulator, at M_2 muscarinic receptors. The neutral equilibrium binding cooperativity with [^{3}H]N-methylscopolamine ([^{3}H]NMS) masked its allosteric properties, which could be revealed only by association or dissociation kinetics of [^{3}H]NMS (adopted from May et al., 2007 with modifications).*

Given that ligands bind only to a single class of receptor binding sites in a classical competitive manner, there should be no change of the radioligand dissociation rate (k_2, k_{off}), when the respective receptors are incubated with unlabelled competitors (Kostenis and Mohr, 1996; Valant *et al.*, 2008). In such cases, monophasic dissociation curves of the orthosteric radioligand should be expected (Lazareno, 2001).

5.1.1.1 Pharmacological implications of changes in the radioligand dissociation rate

In the presence of an allosteric modulator, the radioligand off-rate might be changed in a concentration-dependent manner (Kenakin, 2006). The quantification of these changes is usually a cumbersome procedure. Nevertheless, it can be simplified by extrapolation on condition that the dissociation curves (specific binding *vs*. time), acquired in the absence and in the presence of putative allosteric modulators, fulfill the requirement of monophasicity (Fig. 5.1.2 A). As shown in Fig. 5.1.2 B, these monophasic curves can be easily linearized by logarithmization (Eq. 5.1.1, where B_0 and B_t refer to specific binding observed at times 0 and t, respectively). The half-life time of radioligand dissociation ($t_{0.5}$) is given by Eq. 5.1.2 (Lazareno, 2001):

$$B_t = B_0 \cdot e^{-k_2 \cdot t} \Rightarrow \ln\frac{B_t}{B_0} = -k_2 \cdot t \qquad \text{(Eq. 5.1.1)}$$

$$t_{0.5} = \frac{\ln 2}{k_2} \qquad \text{(Eq. 5.1.2)}$$

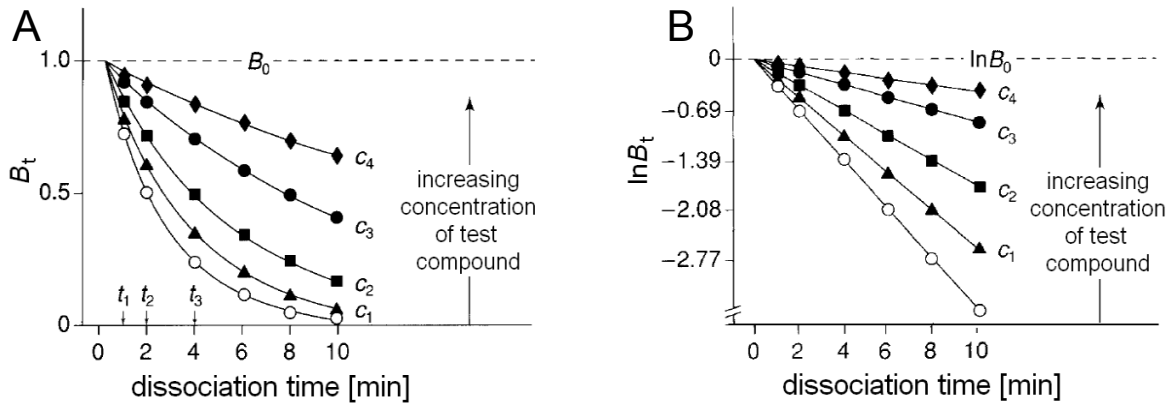

Fig. 5.1.2. *Radioligand dissociation kinetics represented by (A) monophasic curves and (B) their linearizing transforms (cf. Eq. 5.1.1; adopted from Kostenis and Mohr, 1996 with modifications).*

As in geometry any straight line is defined by 2 points, the laborious experimental procedure can be reduced to a minimum by performing so called “two-point kinetics”. The experimentator has to obey the following procedure (detailed protocol in subsection 5.2.2):

1) Acquisition of initial binding data (before dissociation) and after a defined period of dissociation (as shown in Table 5.2.2) corrected for unspecific binding.
2) Transformation of the data according to Eq. 5.1.1 yielding k_2 values (Fig. 5.1.3 A).
3) Plotting the relative k_2 values (as percentage of control) against the logarithmized modulator concentration (Fig. 5.1.3 B) and fitting the data by non-linear regression.

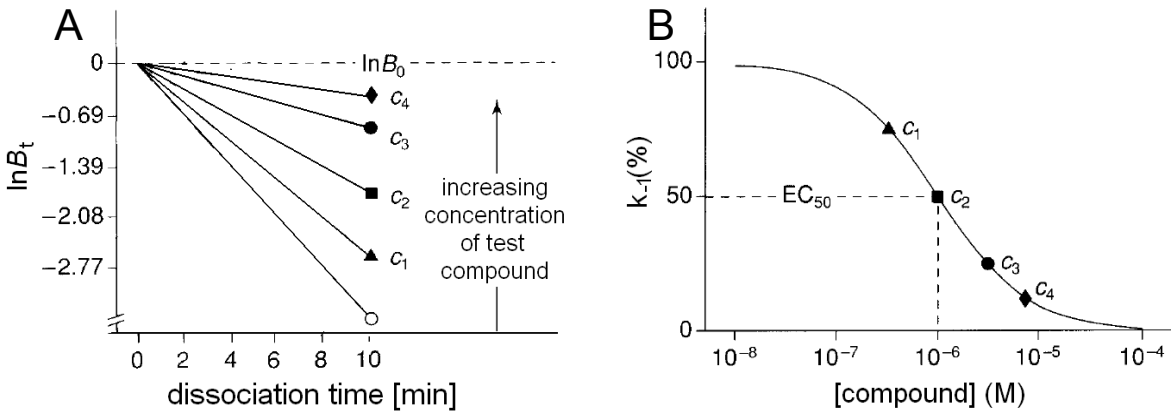

Fig. 5.1.3. *Two-point kinetics of radioligand dissociation: (A) logarithmized binding data for the calculation of k_2 (k_{off}) values, (B) the effect of the modulator concentration on the rate constant of radioligand dissociation k_2 (adopted from Kostenis and Mohr, 1996, with modifications).*

5.1.2 Association kinetics

In addition to radioligand dissociation, association kinetics allows the verification of the pharmacological model chosen for the interpretation of binding data (cf. subsection 1.4.2). Assuming the competitive binding to a single class of binding sites, the rate constant of radioligand association k_1 (k_{on}) could be counted from association experiments performed with at least two different concentrations of a radioligand (Fig. 5.1.4). The observed rate constant (k_{obs}) should namely increase linearly with the concentration of radioligand, thus allowing the quantification of k_1 and k_2 (cf. Eq. 1.3.5). Otherwise, the k_1 value has to be calculated by using the k_2 (k_{off}) value obtained from dissociation experiments. Additionally, if ligand-receptor interactions follow the law of mass action, the radioligand affinity constant K_d determined by saturation binding should match the K_d value assessed by kinetic experiments (cf. Eq. 1.3.4; Motulsky and Christopoulos, 2004).

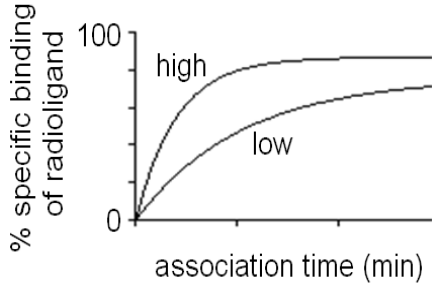

Fig. 5.1.4. *Radioligand association kinetics performed with high and low concentrations of radioligand. The k_1 and k_2 values can be calculated from the exponential association curves (cf. Eq. 1.3.5).*

5.1.2.1 Kinetics of competitive binding

Competition studies with bivalent acylguanidines revealed a complex binding behaviour of these ligands. The found Hill slopes were significantly greater than one after a standard incubation period of 90 min at both the H_2R and the H_4R (with [^{3}H]UR-DE257 and [^{3}H]HIS as radioligands, respectively; cf. subsections 4.3.3 and 4.3.4), but approximating unity when extending the incubation time longer than 3 hours (cf. Fig. 4.3.22 B). These changes of the Hill coefficients may suggest that competitors dissociate more rapidly or slowly than the radioligand.

In order to determine the kinetics of an unlabelled ligand, radioligand association experiments have to be conducted in the presence of a constant concentration of a radioligand and at least two different concentrations of a “cold” compound (Motulsky and Mahan, 1984; Motulsky and Christopoulos, 2004). Given that binding follows the law of mass action, the on- and off-rates of an unlabelled ligand (k_3 and k_4) as well as its affinity constant (K_i) could be calculated from kinetics of competitive binding according to the

following equations (Eq. 5.1.3–6; under assumption that the concentrations of a radioligand A and an unlabelled ligand B are constant):

$$A+B+R \underset{k_2,\ k_4}{\overset{k_1,\ k_3}{\rightleftharpoons}} AR+BR \qquad \text{(Eq. 5.1.3)}$$

$$\frac{d([AR])}{dt} = k_1[A]\cdot(R_0 - [AR] - [BR]) - k_2[AR] \qquad \text{(Eq. 5.1.4)}$$

$$\frac{d([BR])}{dt} = k_3[B]\cdot(R_0 - [AR] - [BR]) - k_4[BR] \qquad \text{(Eq. 5.1.5)}$$

$$K_i = \frac{k_4}{k_3} \qquad \text{(Eq. 5.1.6)}$$

As shown in Fig. 5.1.5, in the presence of both slowly and rapidly dissociating competitors, time required for equilibration with a radioligand would be increased. This could be the reason for the underestimated affinity of a “slow competitor” as well as the overestimated affinity of a “fast competitor”, measured in competition experiments after the premature termination of incubation (Hulme, 1992). Moreover, the failure to obtain equilibrium might result in the steepening of displacement curves, also referred to as the apparent positive cooperativity (cf. Fig. 4.3.23).

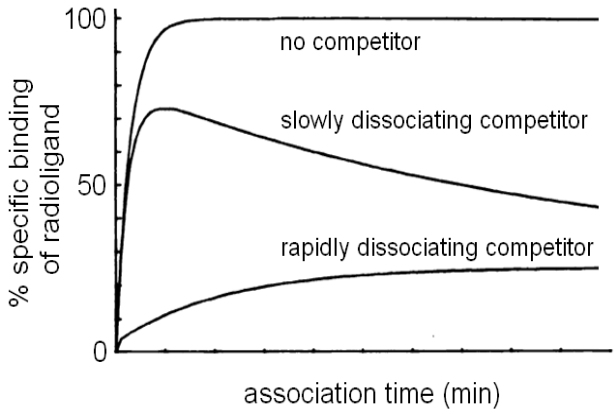

Fig. 5.1.5. *The kinetics of competitive radioligand binding as predicted by the law of mass action (adopted from Motulsky and Mahan, 1984 with modifications).*

5.2 Materials and methods

5.2.1 Materials

All dissociation and association binding experiments at the hH_4R-GAIP + $G_{i\alpha 2}$ + $G_{\beta 1\gamma 2}$, expressed in the insect Sf9 membranes, were performed using the same chemicals as described in subsection 4.2.1. Assays were carried out at room temperature (20–23 ºC) in a total volume of 250 µL and set up to fit the 48 wells of a M-48 harvester from Brandel (Gaithersburg, MD, USA).

5.2.2 Kinetics of radioligand dissociation at the gpH_2R and the hH_4R

To study the kinetics of radioligand dissociation, assays were carried out, according to the protocols kindly provided by Ms. Dorina Kaufel (Institute of Pharmacy, University of Bonn, Germany) with following modifications.

5.2.2.1 Radioligand dissociation from the gpH_2R-$G_{s\alpha S}$ and the hH_4R

For experiments with [^{3}H]TIO, 150 µL of 0.33% BSA in binding buffer (0.2% BSA final) and 50 µL of Sf9 membrane suspension (gpH_2R-$G_{s\alpha S}$; cf. subsection 4.2.3) were pipetted into 4-mL polypropylene tubes. Then, at different periods of time (0–30 min), 25 µL of the radioactive tracer ([^{3}H]TIO with unlabeled TIO in binding buffer to obtain a final ligand concentration of 10 nM) were added to each tube. Addition of the radioligand was performed in reverse chronological order (first for the samples with longer association times, then for those with shorter association times). Equilibration with the radioligand was performed in duplicate at room temperature (20–23 ºC) under shaking at 250 rpm within 30 min for each sample. Dissociation started by addition of 25 µL of a 10-fold concentrated feed solution of FAM (100 µM final) in the presence or absence of HIS (100 µM final) or the bivalent compound **4** (1 µM final). The reaction was terminated simultaneously for all samples by addition of ice-cold binding buffer and rapid filtration with a M-48 harvester, providing appropriate dissociation times, as indicated on abscissa. Filter-bound radioactivity was measured in a LS 6500 Liquid Scintillation Counter from Beckman Coulter as described in subsection 4.2.3.

Dissociation kinetics of [^{3}H]UR-DE257 (K_d value of 27 nM; Erdmann, 2010) was performed similar to [^{3}H]TIO with minor modifications: the radioligand at the final concentration of 25 nM (7–10 nM of radioactive + 15–18 nM of non-radioactive tracer) was added to gpH_2R-$G_{s\alpha S}$ membranes at different time points between 0 and 90 min. As the radioligand association and dissociation kinetics were quite slow (association half-life of 64 min and dissociation half-life of 122 min; cf. Erdmann, 2010), membranes were equilibrated with the radioligand for 100 min, prior to the addition of unlabelled competitors.
Kinetics of [^{3}H]HIS dissociation was carried out by analogy with the procedure for the investigation of [^{3}H]UR-DE257 (cf. Table 5.2.1). Unspecific binding at the hH_4R was determined in the presence of 10–20 µM THIO.

Table 5.2.1. *Experimental setup for the radioligand dissociation kinetics.*

Radioligand	Final conc.	Cold tracer added	Preincub. time	Sf9 membrane (protein content)	
[^{3}H]TIO	10 nM	no	30 min	gpH_2R-$G_{s\alpha S}$	100 µg/sample
[^{3}H]UR-DE257	25 nM	yes	100 min	gpH_2R-$G_{s\alpha S}$	100 µg/sample
[^{3}H]HIS	10 nM	no	60–90 min	hH_4R[a]	33–40 µg/sample

[a] *hH_4R-GAIP+ $G_{i\alpha 2}$ + $G_{\beta 1\gamma 2}$*

5.2.2.2 Simplified measurement of [^{3}H]HIS dissociation ("two-point kinetics")

In order to investigate the influence of competitor concentration on the dissociation of [^{3}H]HIS at the hH_4R, "two-point kinetic experiments" were carried out (Kostenis and Mohr, 1996) according to the time schedule presented in Table 5.2.2. Each sample contained 150 µL of 0.3% BSA in binding buffer (0.2% BSA final), 25 µL of [^{3}H]HIS solution in binding buffer (without reduction of specific activity, 10 nM final), 25 µL of the hH_4R-GAIP + $G_{i\alpha 2}$ + $G_{\beta 1\gamma 2}$ membrane (35–40 µg protein per sample, freshly resuspended before addition; cf. subsection 4.2.3), 25 µL of either THIO solution (20 µM final) or Millipore water (for total binding) and 25 µL of either a 10-fold concentrated feed solution of an unlabelled competitor in 10% DMSO (1% DMSO final) or 10% DMSO only (1% DMSO final for total and unspecific binding). The addition of DMSO improved the solubility of the tested bivalent compounds. The equilibration of the membrane with the radioligand was conducted at 20-23 ºC with shaking at 250 rpm either in test tubes (for control samples: total and unspecific binding) or together in a separate vessel (for other samples). Dissociation was started by addition of the radioligand-receptor complexes to the competitor-THIO mixtures in triplicate and terminated by rapid filtration after the next

28 min (the most significant changes of the filter-bound radioactivity were observed in kinetic experiments at approx. 28–30 min of [^{3}H]HIS dissociation). The filtration of samples and the determination of the specific [^{3}H]HIS binding (at 0 and 28 min of dissociation) were performed as described for the complete kinetic experiments. The value of radioligand off-rate measured under control conditions (20 µM THIO in the absence of modulators) was set to 100%.

Table 5.2.2. *Time schedule for the "two-point kinetics" of radioligand dissociation.*

min	Procedures
0	Equilibrate 2700 µL of 0.3% BSA and 450 µL of membrane in a separate 15-mL vessel with 450 µL of radioligand for 90 min (Master-Mix)
30	Add radioligand (25 µL per sample) and membrane (25 µL per sample) to the prepared tubes with mixtures for total (0.3% BSA, water) and unspecific binding (0.3% BSA, water, THIO) and incubate for 90 min
92	Add 200 µL of Master-Mix (per sample) to the prepared tubes with competitor-THIO mixtures to start the dissociation
120	Filtration

5.2.3 Radioligand association at the hH_4R

5.2.3.1 Association kinetics

First, 175 µL of BSA solution in binding buffer (0.2% BSA final) and 50 µL of the hH_4R-GAIP + $G_{i\alpha 2}$ + $G_{\beta 1\gamma 2}$ membrane suspension (cf. subsection 4.2.3) were added to each 4-mL polypropylene tube. Immediately afterwards the tubes were shaken at 250 rpm for 15 min, while the Sf9 membranes were allowed to adsorb at the sides of tubes until addition of the radioligand. This initial shaking provided the constant amounts of receptor protein during the subsequent incubation with the radioligand. Concomitantly, 100 µL of an auxiliary radioligand feed solution were prepared in a 1.5-mL reaction vessel by dilution of the stock solution of [^{3}H]HIS in binding buffer. To receive 750 µL of the [^{3}H]HIS-binding buffer mixtures for both total and unspecific binding, 550 µL of binding buffer and 150 µL of either Millipore water (for total binding) or 1 mM THIO (for unspecific binding, 20 µM THIO final) were added to two separate 2-mL reaction vessels and supplied by 50 µL of the (previously prepared) auxiliary radioligand feed solution. The obtained mixtures contained a 10-fold concentrated solution of the radioligand (the final concentration of [^{3}H]HIS was 10, 30 or 100 nM, depending on the experiment). At the defined time

points between 0 min and 230 min, 25 µL of the appropriate mixture were added in triplicate to the membrane suspensions with BSA (in reverse chronological order: first for the samples with longer association times, then for those with shorter association times) and the samples were shaken at 250 rpm. The termination of [^{3}H]HIS association and the measurement of the filter-bound radioactivity were performed as described in subsection 4.2.3. The experimental settings (amount of membrane protein, [^{3}H]HIS concentration) were chosen to ensure that no more than 5% of the radioactivity added to test tubes were bound to filters.

5.2.3.2 Kinetics of competitive binding

Kinetic measurements of competitive binding of [^{3}H]HIS in the presence of the bivalent H_2R ligand **11** were performed as described above for [^{3}H]HIS association kinetics, with minor modifications. The appropriate volume of binding buffer in the mixtures for both total and unspecific binding was replaced by 10 µM or 100 µM solution of ligand **11**, to obtain a 10-fold concentrated feed solution of compound **11**. Association was started at the defined time points between 0 min and 230 min by addition of 25 µL of the mixtures for both total and unspecific binding to the membrane suspensions with BSA. The final concentration of compound **11** was – depending on the experiment – 50, 150 or 500 nM.

5.3 Results and discussion

5.3.1 Kinetics of radioligand dissociation at the gpH_2R and the hH_4R

5.3.1.1 Kinetics of [^{3}H]tiotidine dissociation at the gpH_2R-$G_{s\alpha S}$

With respect to an explanation of the peculiarities of the bivalent acylguanidine-type H_2R agonists, the dissociation kinetics at the gpH_2R-$G_{s\alpha S}$ was determined to distinguish between ortho- and allosteric ligands (Valant, 2008). As expected, [^{3}H]TIO dissociated according to the one-phase exponential decay after addition of 100 µM FAM (approx. 2000-fold K_i). The rate constant of radioligand dissociation amounted to 0.076 ± 0.003 min^{-1} (95% CI of k_2: 0.068–0.084 min^{-1}, dissociation half-life time of 9 min; results from six independent experiments performed with 100 µM FAM in the presence or absence of 100 µM HIS), which was in good agreement with data from the literature (k_2 of [^{3}H]TIO of 0.063 ± 0.005 min^{-1} for guinea pig lung parenchyma; Foreman *et al.*, 1985). No significant difference in k_2 was observed when a mixture of 100 µM FAM and 100 µM HIS (approx. 250-fold K_d; cf. Fig. 4.3.9) was added instead of 100 µM FAM only, confirming the classical competitive behaviour of HIS (Fig. 5.3.1 A and Fig. 5.3.2 A; k_2 with 100 µM FAM: 0.080 ± 0.002 min^{-1}; k_2 with 100 µM FAM and 100 µM HIS: 0.080 ± 0.002 min^{-1}).

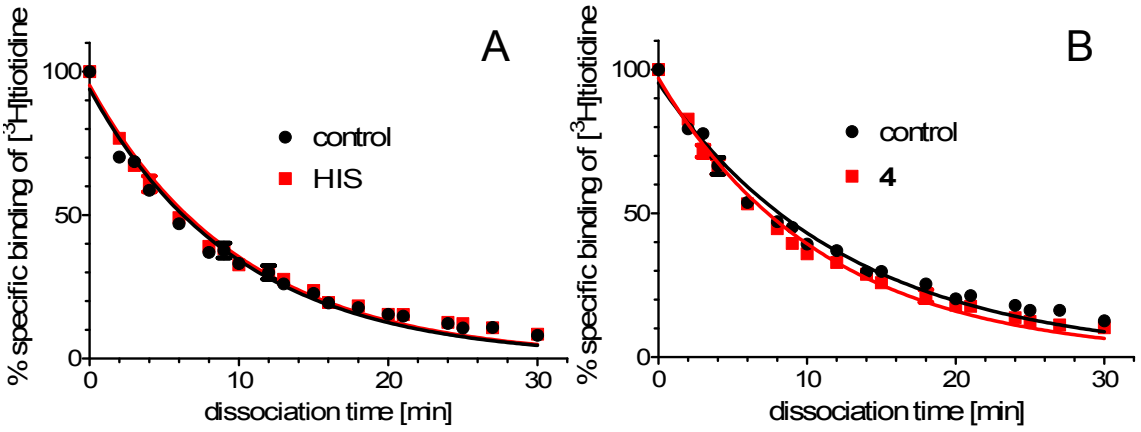

Fig. 5.3.1. *Dissociation of [^{3}H]TIO from the gpH_2R-$G_{s\alpha S}$ after addition of 100 µM FAM in the absence (control) or presence of either (A) 100 µM HIS or (B) 1 µM of the bivalent* ***4****. Data are means ± SEM of two experiments performed in duplicate.*

Statistically different dissociation rates were found when, apart from FAM, 1 µM of the bivalent compound **4** (approx. 500-fold K_i) was added (k_2 with 100 µM FAM: 0.066 ± 0.002 min^{-1}; k_2 with 100 µM FAM and 1 µM of the ligand **4**: 0.076 ± 0.002 min^{-1}; P<0.0001), giving a hint to a weak allosteric interaction (Fig. 5.3.1 B and Fig. 5.3.2 B).

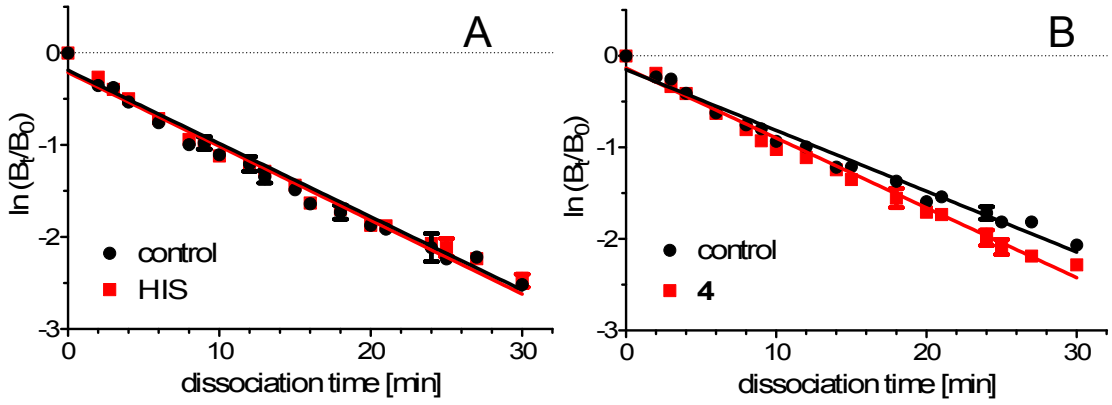

Fig. 5.3.2. *The linearized data from Fig. 5.3.1, transformed according to Eq. 5.1.1. B_0 was uninhibited specific binding of [^{3}H]TIO shortly before addition of the unlabeled competitor(s) (t=0 min); B_t was specific binding of [^{3}H]TIO remaining at time t after addition of 100 µM FAM in the absence (control) or presence of either (A) 100 µM HIS or (B) 1 µM of the bivalent **4**. Results are means ± SEM. The rate constants of [^{3}H]TIO dissociation (slopes) in panel B are statistically different (P<0.0001).*

5.3.1.2 Kinetics of [^{3}H]UR-DE257 dissociation from the gpH$_2$R-G$_{s\alpha S}$

Unspecific binding, determined after addition of unlabelled compounds (5-100 µM FAM alone or in combination with other ligands) prior to the preincubation with [^{3}H]UR-DE257 (cf. subsection 5.2.2), yielded approx. 10–30% of the uninhibited total binding. However, kinetic experiments revealed a relatively high amount of residual binding after 90 min of radioligand dissociation, equalling to approx. 50% of the uninhibited total binding (cf. control, HIS and RAN in Fig. 5.3.4). This observation was in close agreement with the findings from previous studies, suggesting *apparent insurmountable antagonism* of [^{3}H]UR-DE257, probably due to its slow kinetics (Erdmann, 2010). Nevertheless, interpretation of these results was possible, as k_2 values obtained in the presence of modulators were always compared with control off-rates (in the absence of modulators) within the same experiment. This comparison helped also to avoid artefacts, resulting from the inter-experimental fluctuations of the radioligand dissociation rate. In some experiments, the value of uninhibited binding (residual binding at the time point 0 min of dissociation) deviated strongly from other data points. In such cases, unhibited binding was excluded and the maximal binding was set to the next data point (e.g. residual binding at 2 min), to avoid the analysis of data sets including outliers.

The dissociation rate of [^{3}H]UR-DE257 at the gpH$_2$R-G$_{s\alpha S}$, measured after addition of 5 µM FAM (approx. 100-fold K_i; cf. Table 4.3.3), was the same as in the presence of 250 µM HIS (approx. 600 K_d, achieving saturation of the receptors; cf. Fig. 4.3.9). Thus,

a concentration of 5 µM was chosen as the minimal concentration of FAM (unlabelled competitor) for the estimation of the [^{3}H]UR-DE257 control off-rate at the gpH_2R-$G_{s\alpha S}$.

As shown in Fig. 5.3.3 A, no change of the radioligand dissociation rate could be observed also in the presence of 3 µM of the monovalent agonist **1** (500-fold Ki, cf. Table 4.3.3). As expected for competitive binding, radioligand off-rates were not significantly different (k_2 for FAM alone: 0.0103 ± 0.0010 min^{-1}; k_2 for FAM with compound **1**: 0.0106 ± 0.0008 min^{-1}; P = 0.8394) and corresponded to 67 min and 66 min of the dissociation half-life time ($t_{0.5}$ counted according to Eq. 5.1.2).

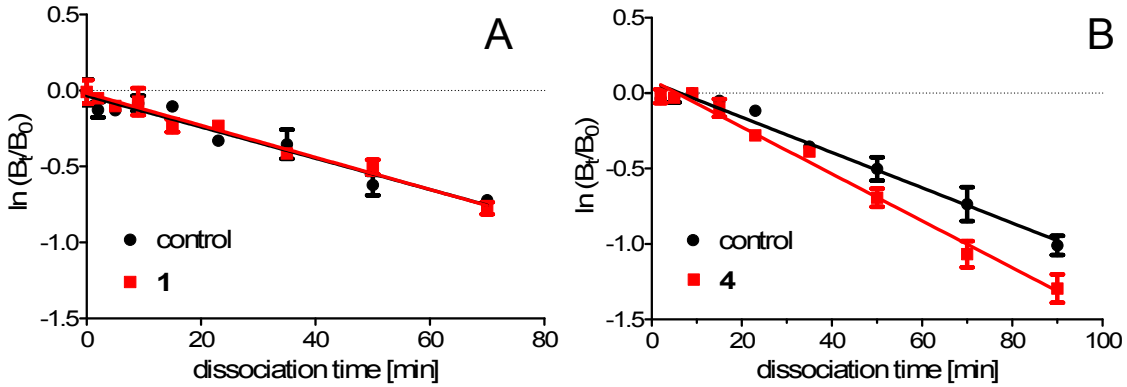

Fig. 5.3.3. *Dissociation of [^{3}H]UR-DE257 from gpH_2R-$G_{s\alpha S}$ after addition of 5 µM FAM in the absence (control) or presence of (A) 3 µM of monovalent agonist **1** and (B) 1 µM of bivalent agonist **4**. Results in both panels are means ± SEM of an experiment performed in duplicate, respectively. Linearization was performed as in Fig. 5.3.2.*

By contrast, significantly different off-rates values of the radioligand were obtained at 1 µM (approx. 500-fold K_i; cf. Table 4.3.3) of the bivalent agonist **4** (k_2 for FAM alone: 0.0117 ± 0.0006 min^{-1}; k_2 for FAM with compound **4**: 0.0156 ± 0.0006 min^{-1}; P = 0.00014), corresponding to 59 min and 45 min of half-life time of radioligand dissociation (Fig. 5.3.3 B). This confirmed the results obtained with [^{3}H]TIO after addition of ligand **4** (cf. Fig. 5.3.2 B).

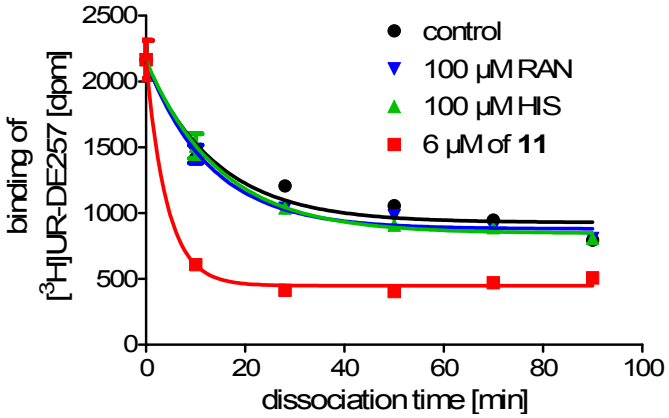

Fig. 5.3.4. *Dissociation of [^{3}H]UR-DE257 from gpH_2R-$G_{s\alpha S}$ after addition of 5 µM FAM in the absence (control) or presence of different ligands. The values of residual binding are means ± SEM of an experiment performed in duplicate. Best fit with the one-phase exponential decay.*

As shown in Fig. 5.3.4, the radioligand dissociation, commenced by addition of 5 µM FAM, was mostly not affected in the presence of an excess of HIS and RAN, as expected for competitive binding. By contrast, 6 µM (16-fold K_b; Birnkammer *et al.*, 2010) of the bivalent compound **11**, which has a 20-membered linker, accelerated dissociation of [^{3}H]UR-DE257 and replaced the radioligand more efficiently than the standard H_2R ligands.

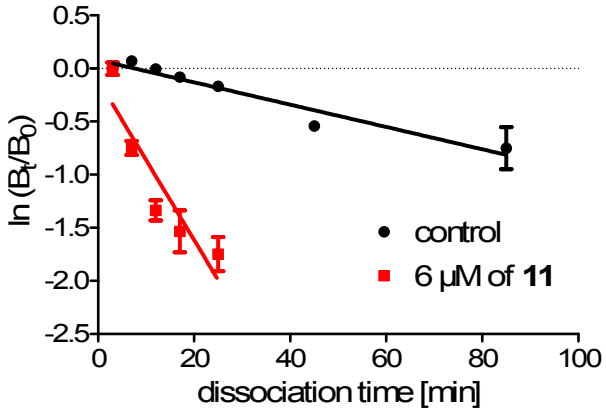

Fig. 5.3.5. *Dissociation of [^{3}H]UR-DE257 from gpH_2R-G_{saS} after addition of 100 µM FAM in the absence (control) or presence of 6 µM of the bivalent compound **11**. Data are means ± SEM of an experiment performed in duplicate.*

Dissociation kinetics of [^{3}H]UR-DE257, performed with 100 µM FAM and 6 µM of the bivalent compound **11** (16-fold K_b; Birnkammer *et al.*, 2010) was accelerated by up to 7 times, when compared with control (k_2 for FAM alone: 0.0105 ± 0.0012 min^{-1}; k_2 for FAM with compound **11**: 0.0753 ± 0.0128 min^{-1}; $P < 0.0001$). The half-life time of radioligand dissociation was reduced from 66 min to only 9 min, respectively (Fig. 5.3.5). Similar results were obtained also for 5 µM of the bivalent ligand **9** with a 14-membered linker (data not shown).

It is also noteworthy that concentration-dependent changes of the radioligand off-rate in the presence of two unlabelled ligands were previously reported at the muscarinic M_2 receptor (Kostenis *et al.*, 1996). The dissociation of [^{3}H]NMS, commenced by addition of the competitive antagonist atropine, was considerably slowed down by ring-substituted bispyridinium compounds (Fig. 5.3.6).

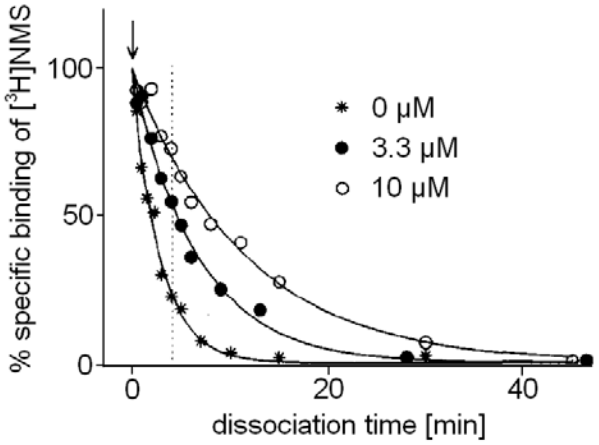

Fig. 5.3.6. *Dissociation of 0.2 nM [^{3}H]NMS from porcine cardiac membranes, expressing M_2 muscarinic receptors, in the presence of 1 µM atropine and the indicated concentrations of a ring-substituted bispyridinium compound. The addition of atropine is indicated by an arrow (adopted from Kostenis et al., 1996 with modifications).*

Similarly, concentration-dependent changes of the radioligand off-rate were observed at the α_{2A}-adrenoreceptor (Leppik *et al.*, 1998; Kenakin, 2006). However, in the latter case, the dissociation rate constant of [^{3}H]yohimbine, determined after addition of an excess of the α-adrenoreceptor antagonist phentolamine, was increased in the presence of amiloride and its analogues (Fig. 5.3.7). Interestingly, amiloride also increased the dissociation rate of [^{3}H]spiperone at the dopamine D_2 receptor (Hoare and Strange, 1996). Further examples of GPCR ligands, showing such a non-competitive behaviour in kinetic binding studies, have been reviewed elsewhere (May *et al.*, 2007).

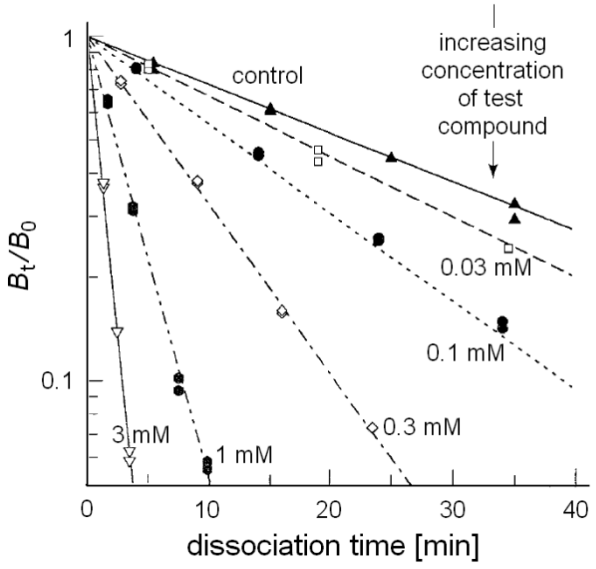

Fig. 5.3.7. *The dissociation of [^{3}H]yohimbine in the presence of 20 µM phentolamine (control) and the indicated concentrations of the amiloride analogue EPA. Membranes expressing the α_{2A}-adrenoreceptor were first pre-equilibrated with the radioligand. Dissociation started by addition of phentolamine and EPA (adopted from Leppik et al., 1998 with modifications).*

5.3.1.3 Kinetics of [^{3}H]histamine dissociation from the hH_4R

The imidazole-type acylguanidines contain imidazolylpropylguanidine, a privileged structure with respect to histamine receptor binding. The ligands **3**, **4**, **9** and **11** are highly potent ligands also at the H_4R (cf. subsection 4.3.4). As shown in Fig. 5.3.8 A, tritiated HIS revealed monophasic dissociation curves at the hH_4R-GAIP+ $G_{i\alpha 2}$ + $G_{\beta 1\gamma 2}$, but the residual binding after 1.5 hour of radioligand dissociation was still relatively high and equalled to approx. 40% of the uninhibited total binding (*N.B.* similar to the dissociation of [^{3}H]UR-DE257 at the gpH_2R-$G_{s\alpha S}$). At the same time, unspecific binding (determined by the addition of unlabelled competitors prior to equilibration with [^{3}H]HIS) equalled to only 4% of the uninhibited total binding.

Kinetic experiments at the hH_4R-GAIP+ $G_{i\alpha 2}$ + $G_{\beta 1\gamma 2}$ revealed the rate constant of [^{3}H]HIS dissociation of 0.0126 ± 0.0003 min^{-1} (95% CI of k_2: 0.0118 to 0.0135; data from 5 independent experiments, performed in duplicate with 10 µM HIS and/or 10-20 µM of the standard H_3R and H_4R antagonist THIO; cf. Fig. 5.3.8 B and Fig. 5.3.9 A), corresponding to the half-life time of radioligand dissociation of 55 min (95% CI of $t_{0.5}$: 51-59 min).

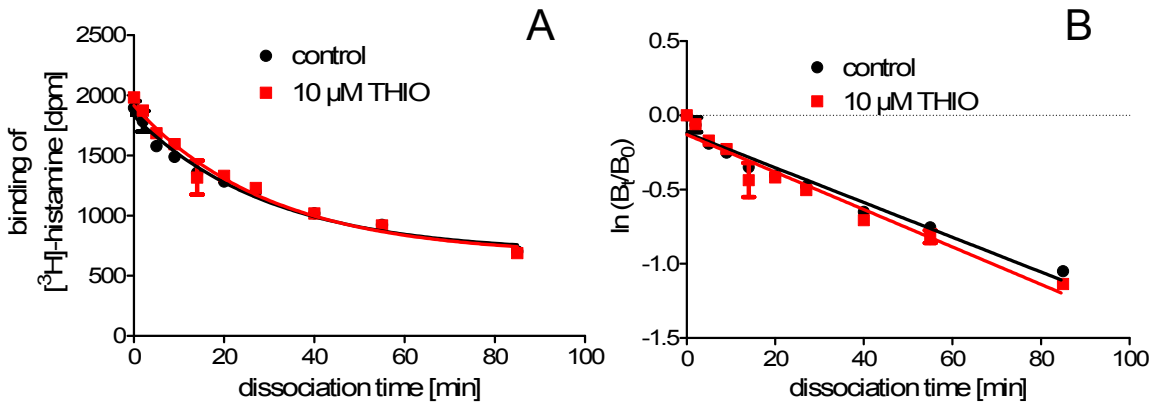

Fig. 5.3.8. *Dissociation of [^{3}H]HIS from the hH_4R-GAIP+ $G_{i\alpha 2}$ + $G_{\beta 1\gamma 2}$ after addition of 10 µM HIS in the absence (control) or in the presence of 10 µM THIO (K_i of HIS: 8 nM, K_i of THIO: 60 nM; cf. Thurmond et al., 2008): (A) uncorrected data of the radioligand residual binding fitted to the equation of one-phase exponential decay, (B) the same data after correction for unspecific binding and linearization. Results are means ± SEM of an experiment performed in duplicate.*

In this context it is indispensable to mention that so far the only published results for radioligand kinetics at the H_4R refer to [^{3}H]UR-PI294, a novel H_3R and H_4R radioligand developed recently in our research group (cf. Fig. 1.2.6; Igel *et al.*, 2009).

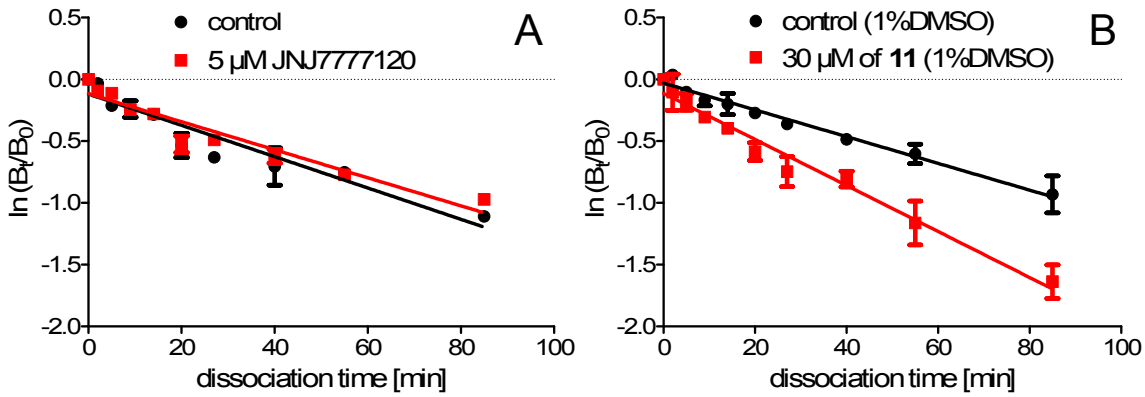

Fig. 5.3.9. *Dissociation of [^{3}H]HIS from the hH_4R-GAIP+ $G_{i\alpha 2}$ + $G_{\beta 1\gamma 2}$: after addition of 20 µM THIO in the absence (control) or in the presence of either (A) 5 µM JNJ7777120 or (B) 30 µM of the bivalent **11** (for better solubility, **11** and control contained 1% DMSO). Results in both panels are means ± SEM of an experiment performed in duplicate, respectively.*

As expected for an orthosteric ligand, 5 µM JNJ7777120 (K_i of approx. 4 nM; Thurmond *et al.*, 2008) did not change [^{3}H]HIS dissociation from the hH_4R (Fig. 5.3.9 A). Contrary to that, 30 µM of the homobivalent ligand **11** with a 20-atom spacer (500-fold K_i; cf. Fig. 4.3.21) induced the 1.7 times faster dissociation of the radioligand when compared with the control (k_2 for THIO alone: 0.0108 ± 0.0007 min^{-1}, 95% CI: 0.0094 to 0.0123 min^{-1}; k_2 for THIO with compound **11**: 0.0186 ± 0.0011 min^{-1}, 95% CI: 0.0163 to 0.0210 min^{-1}; $P < 0.0001$), resulting in the reduction of the half-life time of radioligand dissociation from 64 min to 37 min (Fig. 5.3.9 B). This finding was in line with the results obtained with [^{3}H]UR-DE257 at gpH_2R-$G_{s\alpha S}$ after addition of the bivalent ligand **11** (cf. Fig. 5.3.5).

5.3.1.4 Influence of bivalent ligands on the [^{3}H]histamine off-rate at the hH_4R

As the kinetic experiments at the hH_4R revealed monophasic dissociation curves for both mono- and bivalent ligands, it was possible to perform so called "two-point kinetic" assays (cf. subsection 5.1.1 and Table 5.2.2). This method, apart from being time- and material-saving, enables closer inspection of the effect of modulator concentration on the radioligand dissociation rate (Kostenis and Mohr, 1996).

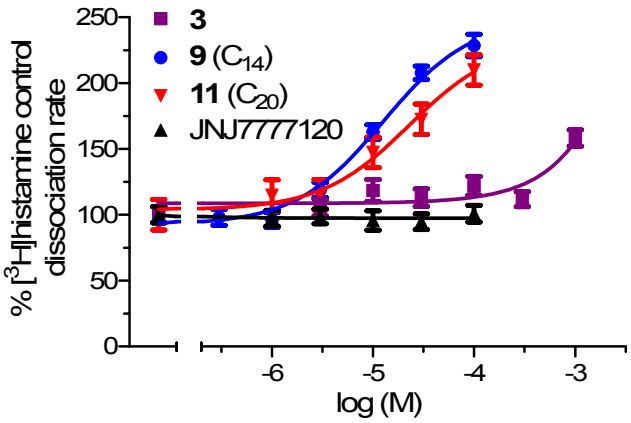

Fig. 5.3.10. *The effect of different mono- and bivalent ligands on [^{3}H]HIS dissociation from the hH_4R-GAIP+ $G_{i\alpha 2}$ + $G_{\beta 1\gamma 2}$ membranes. The linker lengths of the bivalent ligands **9** and **11** are indicated in parentheses as numbers of C-atoms. The acylguanidine **3** was tested as the monovalent counterpart. The results are means ± SEM of an experiment performed for each ligand in triplicate. The radioligand off-rate under control conditions was set to 100%.*

As shown in Fig. 5.3.10, two-point kinetic experiments confirmed that the selective H_4R ligand JNJ7777120 up to a concentration of 100 µM had no effect on the rate of [^{3}H]HIS dissociation from Sf9 cell membranes expressing the hH_4R-GAIP+ $G_{i\alpha 2}$ + $G_{\beta 1\gamma 2}$, as expected for the competitive mode of binding. Contrary to that, the bivalent N^G-acylated guanidines **9** and **11** induced significantly faster kinetics of the radioligand dissociation with $EC_{50,diss}$ values of approx. 10–20 µM, suggesting allosteric interactions with the hH_4R. However, their monovalent counterpart **3** did not exert any influence on the radioligand off-rate up to the concentration of 300 µM, contradicting rather the interaction with the allosteric binding site at the hH_4R.

Except for allosteric ligands possessing efficacy and true allosteric/orthosteric ligands, the effects of allosteric interactions could be observed only in the presence of an orthosteric ligand (May *et al.*, 2007; Smith and Milligan, 2010). Bivalent compounds could be considered as dualsteric ligands with one pharmacophore addressing the orthosteric and the other interacting with the allosteric binding site (Valant *et al.*, 2008). In that case, a mixture of monovalent orthosters and allosters should exhibit similar behaviour (in terms of allosterism) as would do a pure (hetero)bivalent ligand. In theory, non-linked pharmacophores should even more easily dock to their orthosteric and (putative) allosteric binding sites than two covalently bound pharmacophores. Indeed such *complementation* binding studies with a mixture of monovalent ligands were done previously at the human M_2 muscarinic receptor (Valant *et al.*, 2008). However, all pharmacophoric moieties of our bivalent N^G-acylated guanidines, being bioisosters, possess very similar structures. This means that the same compound might function concurrently as an orthosteric as well as an allosteric ligand. Therefore, complementation experiments could be actually performed, using an excess of a monovalent acylguanidine only. In theory, accelerated dissociation in the presence of a monovalent ligand **3** should be expected, as in the case of the bivalent compounds **9** and **11**. Nevertheless, a very weak effect of compound **3** showed that the bivalent ligands are not simply "doubled" pharmacophores, but rather new chemical entities with different pharmacological properties. Another interpretational difficulty resulted from the similar kinetic effects, observed at both the H_2R and the H_4R (cf. Fig. 5.3.5 and 5.3.7 B, respectively). Namely, for the putative allosteric binding sites, a higher subtype specificity of ligand-receptor interactions should be expected (May *et al.*, 2007).

5.3.1.5 Haemolytic properties of bivalent acylguanidines

Significant acceleration of radioligand off-rates, observed at both the H_2R and the H_4R in the presence of the bivalent N^G-acylated guanines, necessarily indicated some conformational changes of those receptors. However, aside from the apparent allosterism, this kinetic phenomenon could be simply caused by the toxicity of the bivalent ligands. Actually, polar character of both pharmacophoric groups and a hydrophobic alkanediyl linker (cf. Fig. 1.2.4) might be responsible for strong tensidic properties of these compounds. When used at high concentrations, such amphiphilic ligands could exert a range of unspecific effects (from the minor alterations of the receptor protein conformation to the significant destabilization of the cell membrane – haemolysis), only imitating an allosteric interaction. Noteworthy, 10 µM of the bivalent ligand **9** with a 14-membered linker caused 5% lysis of the exposed erythrocytes (increasing to about 45% at 100 µM), whereas the bivalent compounds **11** and **13** with 20-membered linkers induced approx. 25% haemolysis at concentrations as low as 10 µM. At the same time, four monovalent

and three bivalent ligands with octamethylene spacers possessed negligible haemolytic properties (0–10% haemolysis at 100 µM; Mr. Tobias Birnkammer and Ms. Melanie Kaske, Institute of Pharmacy, University of Regensburg, personal communication).

5.3.1.6 Allosteric ternary complex model

As shown schematically in Fig. 5.3.11 A, the addition of orthosteric competitors to radioligand-receptor complexes should not change the value of k_2 (Valant *et al.*, 2008). Therefore, any alteration of the radioligand off-rate in the presence of other unlabelled ligands (modulators) is unequivocally indicative of the adoption of another conformation by receptors. This might be, for example, an indication of the existence of different ligand-specific conformations of GPCRs (functional selectivity, cf. Rajagopal *et al.*, 2010). However, other authors hold the view that the radioligand and the unlabelled modulators have to bind simultaneously to the same receptor molecule, inevitably utilizing topographically distinct, but conformationally linked, recognition sites (Kostenis and Mohr, 1996; Kenakin, 2006; May *et al.*, 2007). According to this hypothesis, the orthosteric binding site can be occupied either by the radioligand or by another orthosteric competitor (e.g. the endogenous ligand), whereas the allosteric binding site is interacting with the modulators (Fig. 5.3.11 B). The formed allosteric ternary complexes (orthoster-receptor-alloster) are characterized by altered values of k_2: either increased, as shown for the α_{2A}-adrenoreceptor (Kenakin, 2006), or decreased with a prolonged half-life time of radioligand dissociation, which is valid e.g. for muscarinic receptors (Valant *et al.*, 2008).

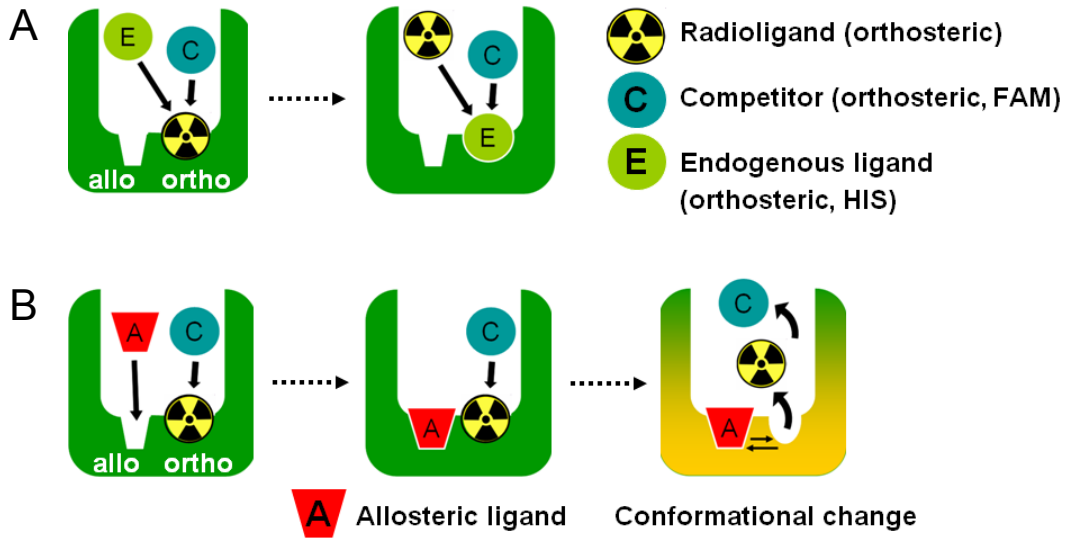

Fig. 5.3.11. *Radioligand dissociation commenced by the addition of an orthosteric competitor "C" in the presence of either (A) endogenous (orthosteric) ligand "E" or (B) an allosteric modulator "A".*

N.B. the hypothesis of the existence of ligand-specific receptor conformations (*functional selectivity*) at the H_2R and the H_4R will be discussed in chapter 6.

5.3.2 Association kinetics at the hH_4R

5.3.2.1 [^{3}H]Histamine association limited by a slowly dissociating competitor

Kinetics of unlabelled compounds might be roughly estimated by following the procedure proposed by Hulme and Birdsall (Hulme, 1992). According to this protocol, after incubation with a cold competitor (at a concentration saturating approx. 90% of receptors) and subsequent centrifugation, receptors were labeled with the radioligand, used in an excess (10-fold K_d). The measured association time-course was then compared with that of the untreated receptors (control) and shown in Fig. 5.3.12. Given, that an unlabelled ligand exerts slower kinetics than a radioligand, the apparent association rate of a radioligand is retarded in the presence of a slower ligand (Fig. 5.3.13).

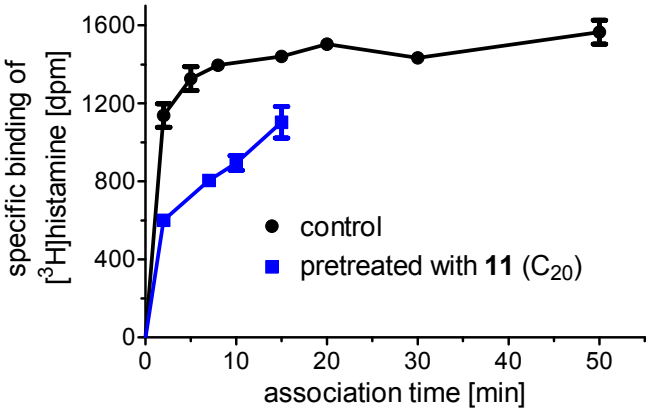

Fig. 5.3.12. *Association kinetics of 100 nM [^{3}H]HIS at the hH_4R-GAIP + $G_{i\alpha 2}$ + $G_{\beta 1\gamma 2}$. Membranes were not pretreated (control) or pretreated for 1 hour at 4° C with 150 nM of compound **11** (cf. IC_{50} value of 116 nM; Fig. 4.3.22 A) and washed. Results are means ± SEM of an experiment performed for each curve in duplicate.*

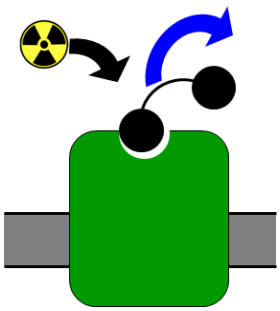

Fig. 5.3.13. *Interaction of a fast radioligand and a slow bivalent compound with a single receptor binding site. The association (black arrow) of a highly concentrated radioligand (10 K_d) is limited only by dissociation (blue arrow) of a slowly dissociating component.*

At the hH_4R membranes, pretreated with the bivalent **11** (containing a 20-atom linker), the apparent rate of [^{3}H]HIS association was slower than at the untreated membranes (Fig. 5.3.12 and 5.3.13), perhaps due to the limiting slow dissociation rate of ligand **11**.

5.3.2.2 Kinetics of [^{3}H]histamine association

Association of a radioligand is a reversible kinetic process, always accompanied by its dissociation from receptors. Therefore, performing this kind of kinetic experiments, it is possible to obtain both on- and off-rate constants for the used radioligand (cf. Eq. 1.3.5). As mentioned in subsection 5.1.2, association time-course could be also used to validate the test system by verifying if binding to receptors follows the law of mass action (cf. Motulsky and Christopoulos, 2004). The experiments were conducted on the Sf9 membranes expressing hH_4R-GAIP + $G_{i\alpha2}$ + $G_{\beta1\gamma2}$ with 10 and 30 nM of [^{3}H]HIS as the radioligand (cf. K_d of 9.8 ± 0.9 nM at the hH_4R + $G_{i\alpha2}$ + $G_{\beta1\gamma2}$ + GAIP; cf. Schnell *et al.*, 2011), as described under Material and methods (subsection 5.2.3).

Table 5.3.1. *Comparison of the k_2, $t_{0.5}$ and K_d values (cf. Eq. 1.3.1–5 and 5.1.1–2) determined for [^{3}H]HIS on Sf9 cell membranes expressing hH_4Rs.*

Parameters	Association kinetics best fit (95% CI)[a]	Other methods best fit (95% CI)
k_1	$7.6 \cdot 10^6$ $M^{-1} \cdot min^{-1}$ ($6.6–8.7 \cdot 10^6$ $M^{-1} \cdot min^{-1}$)	
k_2	**0.018 min^{-1} (0.009–0.027 min^{-1})**	**0.013 min^{-1} (0.012–0.014 min^{-1})[b]**
$t_{0.5}$	38 min (25–76 min)	55 min (51–59 min)[b]
K_d	**2.4 nM (1.2–3.6 nM)**	**9.8 nM (8.0–11.6 nM)[c]**

Data were determined either by association (2-3 experiments at the hH_4R-GAIP + $G_{i\alpha2}$ + $G_{\beta1\gamma2}$; cf. Fig. 5.3.14)[a] or dissociation (5 experiments at the hH_4R-GAIP + $G_{i\alpha2}$ + $G_{\beta1\gamma2}$; cf. Fig. 5.3.8 B and 5.3.9 A)[b] kinetics or by saturation binding (3 experiments at the hH_4R + $G_{i\alpha2}$ + $G_{\beta1\gamma2}$ + GAIP; cf. Schnell et al., 2011)[c].

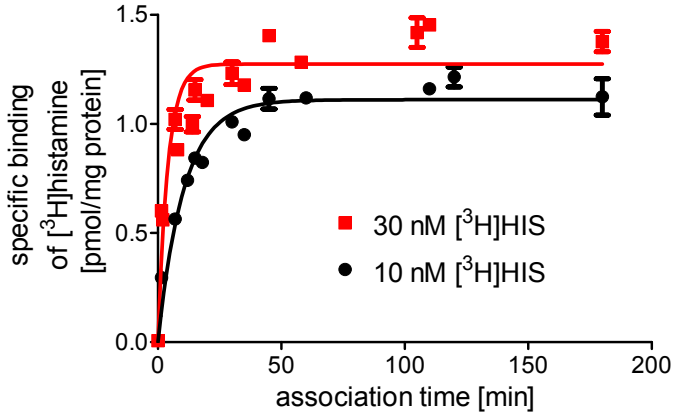

Fig. 5.3.14. *Association kinetics of [^{3}H]HIS on Sf9 cell membranes expressing hH_4R-GAIP + $G_{i\alpha2}$ + $G_{\beta1\gamma2}$. Data are mean values ± SEM of two (10 nM radioligand) or three (30 nM radioligand) independent experiments performed in triplicate. Best fit with the mass action model.*

As shown in Table 5.3.1, the k_2 and K_d constants of the tracer ligand calculated from association kinetics (Fig. 5.3.14) were in the same range as the values of k_2 from dissociation time-course and K_d from saturation binding of [^{3}H]HIS (K_d of 9.8 ± 0.9 nM; cf. Schnell *et al.*, 2011), supporting competitive nature of HIS binding at the hH_4R.

5.3.2.3 Kinetics of competitive binding

The on-rate and off-rate constants (k_3, k_4) of cold ligands might be determined by measurement of radioligand association kinetics in the presence of unlabelled compounds. Kinetics of competitive binding with 30 nM [^{3}H]HIS were performed at the hH_4R-GAIP + $G_{i\alpha 2}$ + $G_{\beta 1\gamma 2}$ after addition of 50–500 nM of the bivalent ligand **11** (K_i of 61 ± 4 nM; cf. Fig. 4.3.22 A).

Table 5.3.2. *Comparison of the k_4 and K_i values (cf. Eq. 5.1.3–6) of the bivalent compound **11**, determined with [^{3}H]HIS at the hH_4R-GAIP + $G_{i\alpha 2}$ + $G_{\beta 1\gamma 2}$ coexpressed in Sf9 cells.*

Parameters	Association kinetics best fit (95% CI)[a]	Other methods best fit (95% CI)
k_3	$5.3 \cdot 10^6$ M^{-1}·min^{-1} ($3.7–7.1 \cdot 10^6$ M^{-1}·min^{-1})	
k_4	**0.024 min^{-1} (0.019–0.029 min^{-1})**	**concentration-dependent[b]**
$t_{0.5}$	29 min (24–36 min)	
K_i	**4.5 nM (2.7–7.8 nM)**	**61 nM (47–74 nM)[c]**

Data determined either by association (cf. Fig. 5.3.15)[a] or "two-point" dissociation (cf. Fig. 5.3.10)[b] kinetics or by competition binding (4 experiments; cf. Fig. 4.3.22 A)[c].

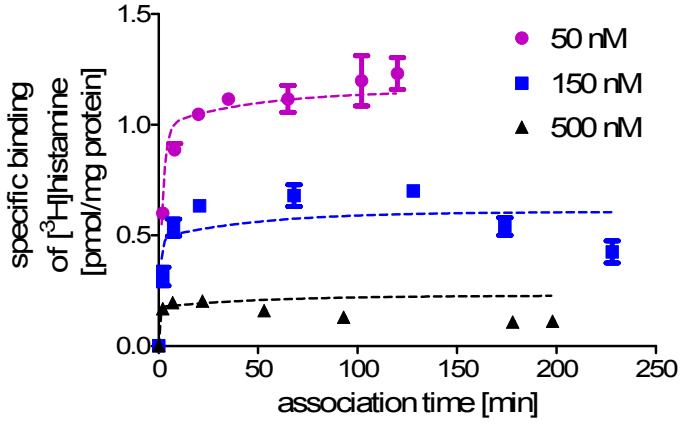

Fig. 5.3.15. *Association kinetics of 30 nM [^{3}H]HIS at the hH_4R-GAIP + $G_{i\alpha 2}$ + $G_{\beta 1\gamma 2}$ in presence of the indicated concentrations of the bivalent compound **11**. Data are mean values ± SEM of one (50 and 500 nM of compound **11**) or two (150 nM of compound **11**) independent experiments performed in triplicate. The dashed lines correspond to the best fit with the mass action model for kinetics of competitive binding.*

As shown in Fig. 5.3.15, fitting of the data points according to the mass action model for kinetics of competitive binding has not turned out satisfactory. Moreover, the comparison of the rate constants from Table 5.3.1 and 5.3.2 revealed that the bivalent ligand **11** associates more slowly, but dissociates more rapidly than [^{3}H]HIS, contrary to previous findings (cf. Fig. 5.3.12 and 5.3.13). Also the K_i value of compound **11**, calculated from kinetic rate constants according to Eq. 5.1.6, was approx. 10 times smaller than determined by competition binding at equilibrium. Thus, these findings did not support the competitive binding of the bivalent **11** at the hH_4R. Indeed, similar to the results from dissociation kinetics (cf. subsection 5.3.1), they might indicate rather an additional process following the binding to receptors (Motulsky and Christopoulos, 2004).

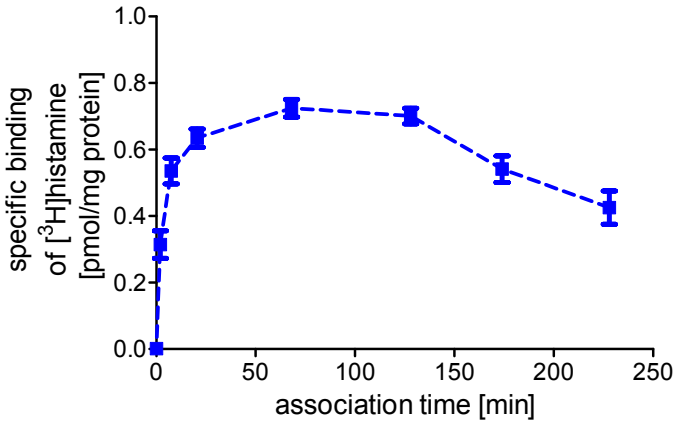

Fig. 5.3.16. *Association kinetics of 30 nM [^{3}H]HIS in the presence of 150 nM of the bivalent ligand **11** at the hH_4R-GAIP + $G_{i\alpha 2}$ + $G_{\beta 1\gamma 2}$. Data are mean values ± SEM of two independent experiments performed in triplicate.*

The kinetics of [^{3}H]HIS association in the presence of the bivalent compound **11** (Fig. 5.3.15–17) indicated an additional process that could not be explained by the simple model of competitive interaction with a single class of binding sites. As described in subsection 5.2.3, the experiments were carried out in reverse time order (first radioligand was added to the samples with longer association times and then to those with shorter association times). Thus, to find out if the reason for these peculiarities could be the adsorption of membranes to polypropylene test tubes, an additional experiment was performed with siliconized tubes (series C in Fig. 5.3.17). However, neither siliconization nor standard experimental conditions (usage of BSA and initial shaking) could solve the problem.

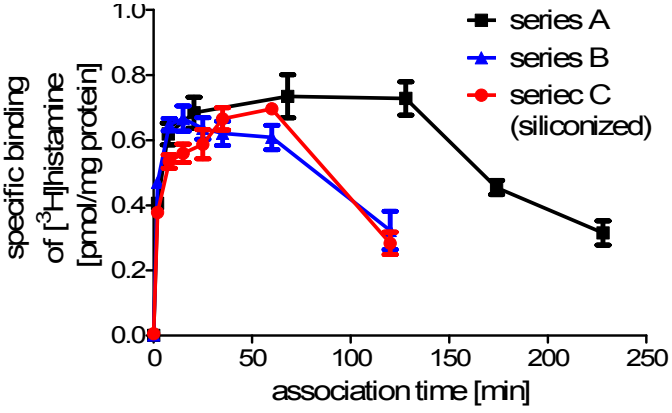

Fig. 5.3.17. *Association kinetics of 30 nM [^{3}H]HIS in the presence of 150 nM of the bivalent ligand **11** at the hH_4R-GAIP + $G_{i\alpha 2}$ + $G_{\beta 1\gamma 2}$. Data are mean values ± SEM of an experiment performed for each curve in triplicate.*

5.4 Summary and conclusion

As the tested monovalent and short bivalent H_2R ligands revealed Hill coefficients smaller than one after 90 min of incubation with [^{3}H]TIO (cf. Table 4.3.3), one could assume a negative cooperativity (allosterism) or the existence of a heterogenic population of the ligand binding sites at H_2R-$G_{s\alpha S}$ fusion proteins (Repke and Liebmann, 1987). Contrary to that the higher homologue **11**, a bivalent acylguanidine with a 20-membered linker, revealed steep competition curves (Hill slopes > 1) at both the gpH_2R-$G_{s\alpha S}$ (cf. Fig. 4.3.20 A) and the hH_4R-GAIP + $G_{i\alpha 2}$ + $G_{\beta 1\gamma 2}$ (cf. Fig. 4.3.21), indicating apparent positive cooperativity. However, after an extended incubation period, the slope of ligand **11** approximated unity (cf. Fig. 4.3.22 B). The latter might result from the premature termination of incubation, as time required for equilibration with the radioligand would be increased in the presence of both slowly and rapidly dissociating competitors (Hulme, 1992). Hence, in order to confirm or reject the hypothesis of allosteric interactions and to explain the peculiarities of the bivalent H_2R ligands, measurements of radioligand kinetics were performed:

1) The measurement of [^{3}H]TIO dissociation at the gpH_2R-$G_{s\alpha S}$ revealed the radioligand off-rate (k_2) of 0.076 ± 0.003 min^{-1}, which was in good agreement with data from the literature (Foreman *et al.*, 1985). No alteration of the [^{3}H]TIO dissociation rate constant (k_2) was found, when FAM was added in the presence of HIS (Fig. 5.3.2 A), indicating a competitive interaction with the orthosteric binding site (Valant *et al.*, 2008). However, a small but still significant increase in k_2 was shown in the presence of the bivalent compound **4** (Fig. 5.3.2 B), suggesting a weak allosteric interaction at the gpH_2R (Kostenis *et al.*, 1996).
2) Dissociation time-course of [^{3}H]UR-DE257 at the gpH_2R-$G_{s\alpha S}$ was accelerated by up to 7 times in the presence of the bivalent ligand **11** (Fig. 5.3.5), whereas no change of k_2 was found for the standard ligands HIS and RAN (Fig. 5.3.4).
3) The dissociation rate constant of [^{3}H]HIS at the hH_4R-GAIP+ $G_{i\alpha 2}$ + $G_{\beta 1\gamma 2}$ (k_2 of 0.0126 ± 0.0003 min^{-1}; half-life time of 55 min) was not altered by THIO and JNJ7777120 (Fig. 5.3.8 and 5.3.9 A, respectively), confirming the competitive binding behaviour. In contrast to these findings, the bivalent ligand **11** induced the 1.7 times faster dissociation of the radioligand (Fig. 5.3.9 B), unequivocally suggesting a conformational change of the hH_4R.
4) Similar results were obtained at the hH_4R-GAIP+ $G_{i\alpha 2}$ + $G_{\beta 1\gamma 2}$ in “two-point kinetic” experiments, where the homobivalent ligands **9** and **11** increased k_2 with $EC_{50,diss}$ values of approx. 10–20 µM (Fig. 5.3.10). However, the chemical nature of these

alterations of receptor conformation still remains unknown, as both ligands were able to induce haemolysis, perhaps due to their strong amphiphilic character (Birnkammer and Kaske, personal communications). Unexpectedly, in view of putative allosterism, the monovalent counterpart **3** did not change the radioligand off-rate up to 300 µM.

5) Association kinetics of [^{3}H]HIS at the hH_4R-GAIP+ $G_{i\alpha2}$ + $G_{\beta1\gamma2}$ revealed the k_2 value of 0.018 ± 0.005 min^{-1} and K_d of 2.4 ± 0.6 nM (Table 5.3.1 and Fig. 5.3.14), being in the same range as the values of k_2 from dissociation time-course and K_d from saturation binding (Schnell *et al.*, 2011), thus supporting competitive nature of HIS binding at the hH_4R.
6) As shown in Fig. 5.3.12, the bivalent compound **11** influenced [^{3}H]HIS association in a manner similar to slowly dissociating competitors (Motulsky and Mahan, 1984). However, the course of association curves in the presence of the bivalent compound **11** betrayed an additional process after ligand binding (Fig. 5.3.15), as the data could not be fitted by the simple mass action model (Motulsky and Christopoulos, 2004). The most probable explanations are either allosteric interactions or tensidic properties of ligand **11**, as the adsorption of membrane to the test tubes has to be excluded (Fig. 5.3.17).

The homobivalent acylguanidines **9** and **11** with pharmacophoric moieties, being derived from HIS by bioisosteric replacement, altered the dissociation of orthosteric radioligands at both the gpH_2R-$G_{s\alpha S}$ ([^{3}H]UR-DE257; Fig. 5.3.5) and the hH_4R-GAIP+ $G_{i\alpha2}$ + $G_{\beta1\gamma2}$ ([^{3}H]HIS; Fig. 5.3.9 B and 5.3.10) membranes. These findings contradicted the simple model of competitive interaction with a single class of binding sites (Kostenis and Mohr, 1996; Motulsky and Christopoulos, 2004). If artefacts could be excluded (e.g. unspecific changes of receptor conformation due to amphiphilic character of bivalent ligands), the results might be interpreted as a hint to allosterism at both the H_2R and the H_4R. Provided that the ortho- and the allosteric binding sites were occupied simultaneously by two pharmacophoric moieties, our bivalent compounds might act as true dualsteric ligands (Valant *et al.*, 2008; Antony *et al.*, 2009). However, there was no change of the radioligand off-rate in the presence of an excess of the monovalent acylguanidine (Fig. 5.3.10). This suggests that, apart from the pharmacophoric moiety, also the length of the hydrophobic alkanediyl linker may play an important role in ligand-receptor interactions.

5.5 References

Antony J *et al.*: Dualsteric GPCR targeting: a novel route to binding and signaling pathway selectivity, *FASEB J*, **2009**, *23*, 442–450.

Avlani V *et al.*: Application of a kinetic model to the apparently complex behavior of negative and positive allosteric modulators of muscarinic acetylcholine receptors, *J Pharmacol Exp Ther*, **2004**, *308*, 1062-1072.

Birnkammer T *et al.*: Structure-activity relationships of bivalent acylguanidine-type histamine H_2 receptor agonists, *5th Summer School "Medicinal Chemistry"*, University of Regensburg, **2010**, P4 (poster contribution).

Erdmann D: Histamine H_2 and H_3 receptor antagonists: Synthesis and characterization of radiolabelled and fluorescent pharmacological tools, Doctoral thesis, University of Regensburg, **2010**.

Foreman JC *et al.*: The binding of [^{3}H]-tiotidine to homogenates of guinea-pig lung parenchyma, *Br J Pharmacol*, **1985**, *86*, 475-482.

Hoare SR and Strange PG: Regulation of D_2 dopamine receptors by amiloride and amiloride analogs, *Mol Pharmacol*, **1996**, *50*, 1295–1308.

Hulme EC (ed.): Receptor-ligand interactions: A practical approach, *IRL Press/Oxford University Press*, New York, **1992**.

Igel P *et al.*: Tritium-labeled *N*^{1}-[3-(1*H*-imidazol-4-yl)propyl]-*N*^{2}-propionylguanidine ([^{3}H]UR-PI294), a high-affinity histamine H_3 and H_4 receptor radioligand, *ChemMedChem*, **2009**, *4*, 225–231.

Kenakin TP: A pharmacology primer: Theory, application, and methods, *Academic Press – Elsevier*, Amsterdam – Tokyo, **2006**.

Kostenis E and Mohr K: Two-point kinetic experiments to quantify allosteric effects on radioligand dissociation, *Trends Pharmacol Sci*, **1996**, *17*, 280–283.

Kostenis E *et al.*: Evidence for a multiple binding mode of bispyridinium-type allosteric modulators of muscarinic receptors, *Eur J Pharmacol*, **1996**, *314*, 385–392.

Leppik RA *et al.*: Characterization of the allosteric interactions between antagonists and amiloride analogues at the human α_{2A}-adrenergic receptor, *Mol Pharmacol*, **1998**, *53*, 916-925.

May LT *et al.*: Allosteric modulation of G protein-coupled receptors, *Annu Rev Pharmacol Toxicol*, **2007**, *47*, 1–51.

Motulsky HJ and Christopoulos A: Fitting models to biological data using linear and nonlinear regression: A practical guide to curve fitting, *GraphPad Software/Oxford University Press*, New York, **2004**.

Motulsky HJ and Mahan LC: The kinetics of competitive radioligand binding predicted by the law of mass action, *Mol Pharmacol*, **1984**, *25*, 1-9.

Rajagopal S *et al.*: Teaching old receptors new tricks: biasing seven-transmembrane receptors, Nat Rev Drug Discov, **2010**, *9*, 373-386.

Schnell D *et al.*: Expression and functional properties of canine, rat,and murine histamine H_4 receptors in Sf9 insect cells, *Naunyn Schmiedebergs Arch Pharmacol*, **2011**, *383*, 457–470.

Smith NJ and Milligan G: Allostery at G protein-coupled receptor homo- and heteromers: uncharted pharmacological landscapes, *Pharmacol Rev*, **2010**, *62*, 701–725.

Thurmond RL *et al.*: The role of histamine H_1 and H_4 receptors in allergic inflammation: the search for new antihistamines, *Nat Rev Drug Discov*, **2008**, *7*, 41-53.

Valant C *et al.*: A novel mechanism of G protein-coupled receptor functional selectivity: Muscarinic partial agonist McN-A-343 as a bitopic orthosteric/allosteric ligand, *J Biol Chem*, **2008**, *283*, 29312-29321.

Chapter 6

Investigations on histamine H_2 receptor internalization by confocal microscopy

6 Investigations on histamine H_2 receptor internalization by confocal microscopy

6.1 Introduction

Bivalent N^G-acylguanidines are highly potent H_2R ligands not only on the isolated guinea-pig right atrium, but also in steady-state GTPase assays on hH_2R- and gpH_2R-$G_{s\alpha S}$ fusion proteins expressed in Sf9 cells (Kraus, 2007; Birnkammer *et al.*, 2010). On the other hand these compounds reveal unusual binding behaviour (e.g. apparent positive cooperativity, equilibration period up to 3 hours, alteration of the radioligand off-rate; cf. chapters 4 and 5) and still very little is known about the intracellular fate of H_2Rs after exposure to the bivalent ligands. Therefore, in addition to radioligand binding studies (kinetic and at equilibrium), the influence of mono- and bivalent ligands on H_2R endocytosis was investigated.

6.1.1 Detection of hH_2R internalization by confocal microscopy

6.1.1.1 Endocytosis of fluorescently labelled H_2Rs

Confocal microscopy offers the unique opportunity to examine the internalization of receptors in living cells in response to various ligands. However, this technique requires the fluorescent labelling of the receptor of interest, e.g. by tagging it with fluorescent proteins (subsection 1.3.2). This implies the genetic manipulation of the receptor resulting in an artificial system. Nonetheless, as shown by Osawa and colleagues, the H_2R C-terminally tagged with GFPs could be functionally expressed in CHO cells, revealing the same affinity towards tritiated TIO as the wild-type receptors (Osawa *et al.*, 2005). Moreover, the same study demonstrated the internalization of the H_2R-GFP already after 30 min of stimulation with HIS, whereas high concentrations of CIM and FAM induced the recycling of the internalized receptors. Furthermore, colocalization studies revealed that the fluorescently labelled receptors were internalized into early endosomes (but not lysosomes) as shown in Fig. 6.1.1.

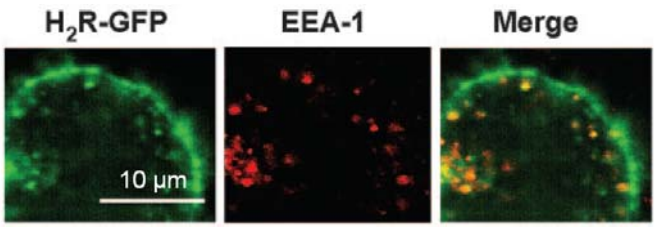

Fig. 6.1.1. *Colocalization studies in living cells revealed that H_2Rs (green) are translocated into early endosomes (stained with the red marker EEA-1) upon stimulation with 100 µM HIS (adopted from Osawa et al., 2005 with modifications).*

6.1.1.2 Towards the detection of functional selectivity

A previous study on transfected CHO cells suggests two distinct pathways for the down-regulation of the H_2R. Apart from the well known *G-protein-dependent* way, HIS concentration-dependently induced the down-regulation of the H_2R in a *G-protein-independent* manner (Smit *et al.*, 1996 a). Hence, in the light of the recent discovery of the first H_4R biased ligand, the antagonist JNJ7777120 (with respect to G-protein stimulation) inducing the recruitment of β-arrestins in a G-protein-independent manner (Rosethorne and Charlton, 2011; Seifert *et al.*, 2011), the question of the existence of biased ligands at the hH_2R was raised. A precondition for biased signalling is the existence of different ligand-induced GPCR conformations (cf. subsection 1.1.3.2). In the presence of biased ligands, distinct prevailing receptor conformations are assumed to be stabilized, triggering the coupling of receptors to different protein effectors (Kenakin and Miller, 2010). Indeed, Xie and colleagues found that new H_2R agonists are able to stabilize distinct ligand-specific H_2R conformations in steady-state GTPase assays both on hH_2R-$G_{s\alpha S}$ and gpH_2R-$G_{s\alpha S}$ fusion proteins expressed in Sf9 cells. IMP- and ARP-derived monovalent acylguanidines stabilized the ternary complex differently than the corresponding guanidines (Xie *et al.*, 2006). Moreover, some of the tested agonists revealed no GTPγS-dependent shift, indicating rather antagonistic properties (cf. Fig. 4.3.7).

In this context, it should be stressed that a very similar behaviour was observed in case of bivalent H_2R agonists at the gpH_2R-$G_{s\alpha S}$. As shown in chapter 4, the binding curves of these ligands were also found to be insensitive against guanine nucleotides, which is an attribute of antagonists. Interestingly, in GTPase assays on the hH_2R-$G_{s\alpha S}$ the bivalent compounds, containing 20-membered spacers between the carbonyl groups, turned out to be neutral antagonists with submicromolar activity (K_b values: compound **11**: 371 nM, compound **12**: 1679 nM, compound **13**: 770 nM; cf. Birnkammer *et al.*, 2010). Additionally, the bivalent H_2R agonists **4**, **9** and **11** induced detectable changes of the radioligand dissociation rate constant at gpH_2R-$G_{s\alpha S}$ fusion proteins (cf. chapter 5).

Motivated by the aforementioned results, the present investigation was focused on the visualization of receptor internalization in response to different H_2R ligands from our laboratory, to learn more about observed differences between monovalent and bivalent acylguanidines compared to the agonist histamine (cf. chapter 4 and 5). Experiments were performed on the CHO cells, expressing H_2Rs tagged with the monomeric far-red fluorescent protein mKate2, because of the significantly higher signal to noise ratio when compared with GFP (Shcherbo *et al.*, 2009).

6.2 Materials and methods

6.2.1 Materials

The pcDNA3.0-Neo-FLAG-hH_2R-HIS_6 plasmid was kindly provided by Prof. Dr. Roland Seifert (Institute of Pharmacology, Medical School of Hannover, Germany). The pcDNA3.1(+)Neo-hH_2R plasmid and the hH_2R sense(Kozak) primer were synthesized as described previously (Mosandl, 2009). The antisense (reverse) primer hH_2Rnostop-rev was purchased from Eurofins (Ebersberg, Germany). The pmKate2-N vector was from Evrogen (Moscow, Russia). Phusion DNA polymerase and the corresponding HF buffer were from Finnzymes (Espoo, Finland). Deoxynucleotide solution mix (dNTPs) was from New England Biolabs (Ipswich, MA, USA) and the thermal cycler for PCR (Mastercycler) was from Eppendorf (Hamburg, Germany). *Hind*III, *Nhe*I, *Xho*I, 6x Loading Dye, 10x Tango buffer and MassRuler DNA ladder mix were purchased from MBI Fermentas (St. Leon-Rot, Germany). *Apa*I and 10x BSA (0.1%) solution were from Amersham Pharmacia Biotech (Piscataway, NJ, USA). 1kb DNA ladder was from New England Biolabs, whereas PeqGOLD DNA ladder mix as well as gel chambers of the PerfectBlue Mini S gel system and agarose were from Peqlab (Erlangen, Germany). Ethidium bromide solution was obtained from Janssen Chimica (Beerse, Belgium). Tris base was from USB (Cleveland, OH, USA). Glacial acetic acid and EDTA (obtained as Titriplex III) were from Merck (Darmstadt, Germany). T4 DNA ligase and buffer for T4 DNA ligase (with 10 mM ATP) were from New England Biolabs. Kanamycin was from Sigma-Aldrich (Steinheim, Germany). QIAquick gel extraction, QIAprep spin miniprep and QIAGEN plasmid maxi kits were from QIAGEN (Hilden, Germany).

U-87 MG Katushka cells clone 3 (Kühnle, 2010) was a generous gift from Dr. Matthias Kühnle (Institute of Pharmacy, University of Regensburg). Cary Eclipse spectrofluorimeter was from Varian Inc. (Mulgrave, Victoria, Australia). CHO cells were from the DSMZ (Deutsche Sammlung für Mikroorganismen und Zellkulturen, Braunschweig, Germany). FuGENE HD transfection reagent was from Roche (Indianapolis, IN, USA). EMEM and Ham's F12 nutrient mixtures were purchased from Sigma-Aldrich. FCS and geneticin (G418) were from Biochrom (Berlin, Germany). Trypsin-EDTA (10x) was from PAA Laboratories (Pasching, Austria). The 8-well µ-slide chambers were from Ibidi (Martinsried, Germany). Leibovitz's L-15 medium without phenol red was from Invitrogen (Karlsruhe, Germany) and LysoTracker Green DND-26 was from Invitrogen (Molecular Probes; Eugene, OR, USA). The synthesis of the mono- and bivalent H_2R ligands (Fig. 1.2.4)

was described before (Kraus *et al.*, 2009). UR-DE74 was synthesized as described elsewhere (Erdmann, 2010). HIS was from Acros Organics (Geel, Belgium). FAM, RAN and concanavalin A type IV were from Sigma (St. Louis, MO, USA). Microscopic images were acquired with an inverted Carl Zeiss Axiovert 200M confocal laser-scanning microscope, equipped with a LSM510 scanning unit and the Zeiss Meta system.

6.2.2 Construction of the hH_2R-pmKate2-N plasmid

The human H_2R gene was in the pcDNA3.0-Neo-FLAG-hH_2R-HIS_6 plasmid, flanked with the sequences of a signal peptide and a FLAG epitope at the N-terminus and a hexahistidine tag at the C-terminus as shown in Fig. 6.2.1 (Schneider, 2005; Mosandl, 2009). In order to restore the native sequence of the receptor, the hH_2R cDNA was subcloned into the pmKate2-N vector (Fig. 6.2.2). The removal of a stop codon at the end of the hH_2R cDNA enabled the transcription of the hH_2R-mKate2 fusion protein.

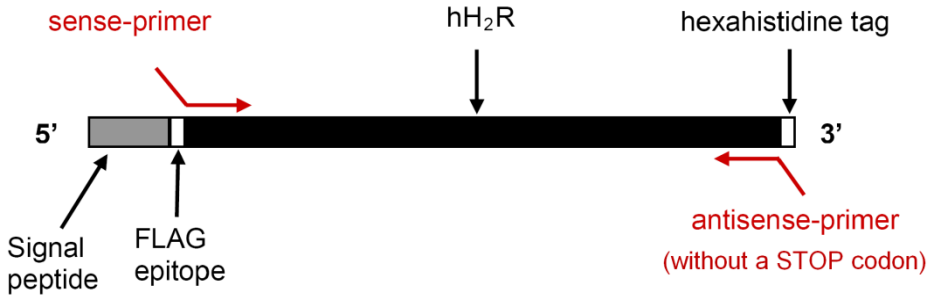

Fig. 6.2.1. *Fragment of the pcDNA3.0-Neo-FLAG-hH_2R-HIS_6 plasmid encoding the hH_2R. The annealing regions of the primers used for PCR are indicated by the red arrows.*

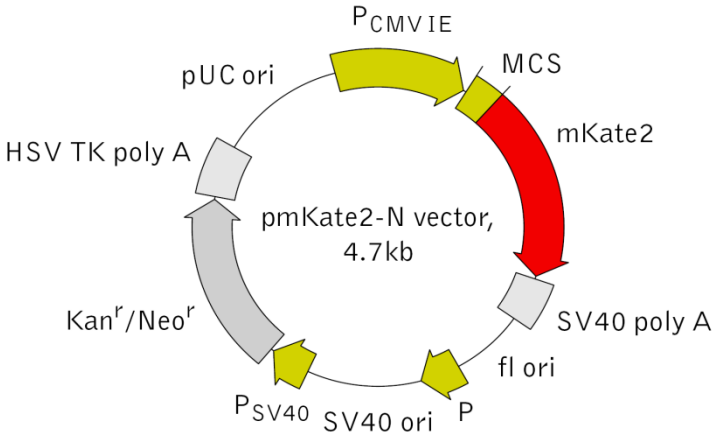

Fig. 6.2.2. *Schematic representation of the pmKate2-N vector. The hH_2R cDNA was subcloned into the multiple cloning site (MCS), upstream of the mKate-2 sequence.*

6.2.2.1 PCR

The sequence of the hH_2R gene was amplified by PCR from the pcDNA3.0-Neo-FLAG-hH_2R-HIS_6 plasmid template (Schneider, 2005; Mosandl, 2009). A 32-nucleotide forward primer contained: an overhang (lower case letters), a *Hind*III recognition site (AAGCTT) and a triplet **ATT** in front of a start codon ATG. As the first base downstream of the start codon is **G**, a Kozak consensus translation initiation site for an improved protein expression level in mammalian cells could be created (G/A NN ATG G, where N stands for any DNA base). A reverse primer was composed of 30 nucleotides, including a short overhang and an *Apa*I recognition site (GGGCCC), followed by an additional base **G**. This was inserted to avoid a shift of the open reading frame in the sequence of the red fluorescent protein (mKate2). As the H_2R (approx. 1100 bp) and mKate2 (approx. 700 bp) should be expressed as a fusion protein, the stop codon TAA had to be removed from the receptor sequence (the triplet TTA was missing in the reverse primer).

Sense (forward) primer – hH_2Rsense(Kozak):

5'-gc.gcg.AAG.CTT.**ATT.**ATG.**G**CA.CCC.AAT.GGC.ACA-3'

Antisense (reverse) primer – hH_2Rnostop-rev:

5'-ata.taG.GGC.CC**G**.CCT.GTC.TGT.GGC.TCC.CTG-3'

PCR amplification was performed in a thermal cycler in a final volume of 50 µL, containing: 1 µL of 5 ng/µL plasmid template solution, 2.5 µL of each primer (10 µM), 10 µL of the 5-fold HF buffer, 1 µL of 10 mM dNTP mix, 0.5 µL of 2 U/µL Phusion DNA polymerase and Millipore water, according to the following conditions (respecting the Finnzymes guidelines):

(1) initial denaturation: 98 °C, 30 s
(2) denaturation: 98 °C, 10 s
(3) annealing: 68 °C (65 + 3 °C), 30 s
(4) extension: 72 °C, 25 s
(5) steps (2) to (4) were repeated 30 times
(6) final extension: 72 °C, 10 min
(7) hold: 4 °C

To determinine the *annealing temperature* for PCR, the on-line T_m calculator from the website of Finnzymes was used: http://www.finnzymes.fi/tm_determination.html. The calculated T_m values were 65 °C and 69 °C for the overlapping sequences of hH_2R-rev and hH_2Rsense(Kozak), respectively. According to the DNA polymerase manufacturer's

instruction, for primers longer than 20 bases, annealing should be carried at a Tm + 3 °C of the lower T_m primer. Analytic agarose gel electrophoresis (150 V, 30 min) revealed the proper length of the PCR product, corresponding to the hH_2R (Fig. 6.2.3).

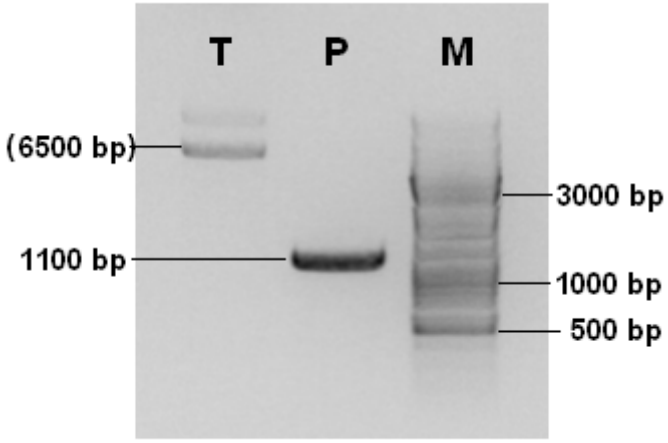

Fig. 6.2.3. *Agarose gel electrophoresis of the PCR product (P). Uncut plasmid (T). For reference the peqGOLD DNA ladder mix marker (M) was used.*

6.2.2.2 Agarose gel electrophoresis

Agarose gel electrophoresis was performed as described before by Dr. Johannes Mosandl (Mosandl, 2009) with some modifications: 100 mL of the 50-fold concentrated TAE buffer were prepared by dissolving 24.2 g of tris base, 5.7 mL of glacial acetic acid and 10 mL of 0.5 M EDTA (pH 8.0) in Millipore water (Mülhardt, 2009). 1x TAE buffer was prepared by dilution of the concentrated buffer with Millipore water. For the preparation of the 1% agarose gel, 0.5 g of agarose were dissolved in 50 mL of 1x TAE buffer under heating (approx. 200 °C) and continuous stirring. The obtained solution was cooled to approx. 60 °C and 2 µL of 10 mg/mL ethidium bromide solution were added. The warm mixture was poured into the gel chamber and supplied with a comb to create pockets of an appropriate size for the application of the DNA samples. After gel solidification, the comb was removed with caution and the chamber was filled with the 1x TAE buffer. Then 20 µL of each DNA sample (the PCR product and the template plasmid) were mixed with 4 µL of 6x loading dye solution. The stained DNA samples and 6 µL of the ready-to-use peqGOLD DNA ladder mix (for reference) were pipetted to separate pockets of the gel. Finally the voltage (150 V) was supplied and the gel was running for approx. 30 min. The separated DNA bands were visualized by transillumination at 254 nm while using the Quantity One software (Gel Doc 2000; Bio-Rad Laboratories, Munich, Germany).

6.2.2.3 Double digestion

Double digestion of the PCR product (the H_2R) and the pmKate2-N vector (400 ng/µL) was performed in a final volume of 50 µL under following conditions: 28 µL of each DNA sample were supplied with 5 µL of 10x Tango buffer, 5 µL of 10x BSA solution, 4 µL of 10 U/µL *Hind*III (a 2-fold excess) and 8 µL of 10 U/µL *Apa*I (a 4-fold excess). The amounts of restriction enzymes for *preparative* digestion were dictated by lower enzymatic activity in 1x Tango buffer. The samples were thoroughly mixed, shortly centrifuged and incubated for 2 hours at 37 °C. The addition of a calf intestinal phosphorylase (for protection of the digested plasmid against a possible self-ligation) was omitted and agarose gel electrophoresis was performed as described above (with an adjusted pocket size). The illumination of the gel revealed the expected lengths of the digested *Hind*III-hH_2R-*Apa*I (1100 bp) and the pmKate2-N vector (4700 bp) as shown in Fig. 6.2.4.

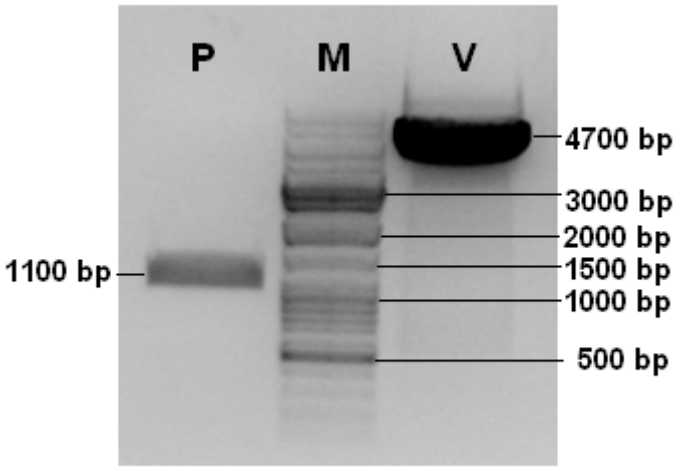

Fig. 6.2.4. *Analysis of the digested DNA fragments after agarose gel electrophoresis: the PCR product (P) and the linearized pmKate2-N vector (V). For reference the peqGOLD DNA ladder mix marker (M) was used.*

The gel fragments containing the *Hind*III-hH_2R-*Apa*I DNA and the pmKate2-N vector were quickly excised from the gel under UV light control (254 nm) and weighted. DNA was extracted using the QIAquick gel extraction kit and a microcentrifuge. The samples were eluted by addition of 20 µl of buffer EB (10 mM tris-HCl, pH 8.5) and DNA concentration was measured by UV spectroscopy.

6.2.2.4 Ligation

Ligation of the digested DNA fragments was performed in a thermal cycler as follows: 50 ng of the pmKate2-N vector, 59 ng of *Hind*III-hH_2R-*Apa*I (the insert in a 5-fold excess over the vector regarding to molar concentrations) and 2 µL of the 10x buffer for T4 DNA ligase (with 10 mM ATP) were diluted with Millipore water up to 19 µL, thoroughly mixed

and shortly centrifuged. After an incubation period of 5 min at 45 °C, 1 µL of T4 DNA ligase (400 U/µL) was added. The sample was thoroughly mixed, shortly centrifuged and incubated at 15 °C overnight (16 hours), before the mixture was heated up to 65 °C for 10 min in order to inactivate the enzyme and stored at -20 °C.

6.2.3 Transformation of bacteria and preparation of the plasmid

6.2.3.1 Transformation of bacteria

LB and SOC media, selective agar plates and competent bacteria *E. coli* (TOP10 strain) were prepared as described before (Mosandl, 2009). A 1.5 mL reaction vessel with 100 µL of competent bacteria (stored at -80 °C) was thawed on ice. After 10 min, 5 µL of the ligation mixture were added and the vessel was put on ice for the next 30 min. To allow the DNA to enter the bacterial cells, the sample was briefly heat shocked (90 s at 42 °C and then put on ice again for 3 min). Then, 900 µL of sterile SOC medium were added and the mixture was incubated at 37 °C for 1 hour under shaking at 150 rpm. The suspension was centrifuged for 5 min at 3000 rpm and approx. 950 µL of the supernatant were removed. The bacterial pellet was resuspended in the residual medium and plated on an agar plate containing kanamycin (30 µg/mL) for selection, as the pmKate2-N vector incorporates a *kanamycin/neomycin resistance gene*. After the agar plate was incubated overnight at 37 °C, it was stored at 4 °C for a period of 4 weeks.

6.2.3.2 Mini-Prep

From the bacteria grown on the selective agar plate 9 colonies were picked to inoculate LB medium, containing 30 µg/mL kanamycin. For each colony, 5 mL of the selective medium were used. After overnight incubation at 37 °C under shaking at 250 rpm, the suspensions were centrifuged for 1 min at 13000 rpm. The DNA samples were purified using a QIAprep spin miniprep kit and the respective concentrations were estimated by UV spectroscopy, all yielding approx. 300 ng/µL. *Analytical* digestion of DNA with restriction enzymes was performed as described above with minor modifications: 3 µL of a particular Mini-Prep product (approx. 1 µg DNA), 2 µL of 10x BSA solution, 2 µL of 10x Tango buffer, 2 µL of 10 U/µL *Hind*III (a 2-fold excess) and 4 µL of 10 U/µL *Apa*I (a 4-fold excess) were diluted in Millipore water up to a total volume of 20 µL. The samples were thoroughly mixed, shortly centrifuged and incubated for 1 hour at 37 °C. *Analytical* agarose gel electrophoresis was performed, as described above, with 10 µL of ready-to-use

1 kb DNA ladder used for reference. The transillumination of the agarose gel revealed a DNA band, corresponding to *Hind*III-hH$_2$R-*Apa*I (1100 bp), only for the clone 9 (Fig. 6.2.5).

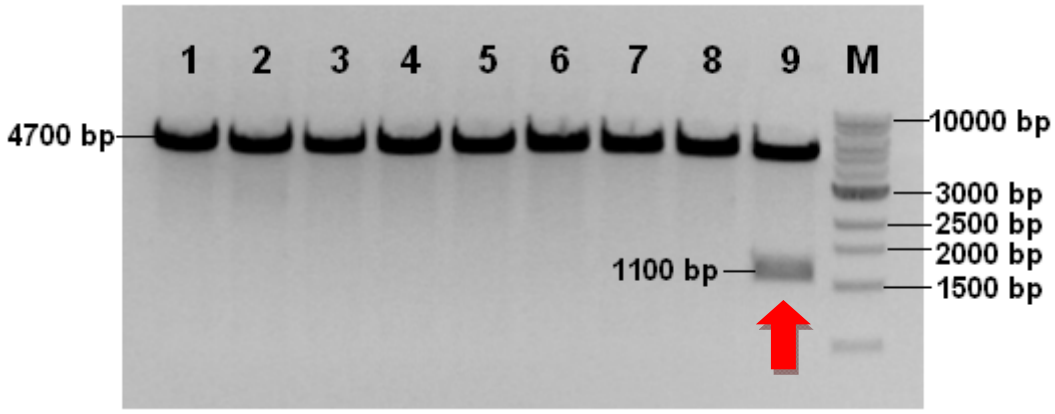

Fig. 6.2.5. *Agarose gel electrophoresis of the digested Mini-Prep products 1–9. The 1 kb DNA ladder was used as a DNA marker (M). A DNA band, corresponding to the HindIII-hH$_2$R-ApaI (1100 bp), was found only for the clone 9 (red arrow).*

6.2.3.3 Maxi-Prep

2 x 100 mL of selective LB medium (with 30 µg/mL kanamycin) were inoculated with 2 x 200 µL of bacterial suspension of clone 9 and incubated overnight at 37 °C under vigorous shaking at 300 rpm. Bacterial pellets were harvested by centrifugation at 6000 rpm for 15 min at 4 °C and processed with a QIAGEN plasmid maxi kit. DNA concentration was determined by UV spectroscopy. *Analytical* digestion of the isolated DNA with *Hind*III and *Apa*I restriction enzymes and *analytical* agarose gel electrophoresis was performed as described for the Mini-Prep product. The transillumination of the agarose gel confirmed the presence of the *Hind*III-hH$_2$R-*Apa*I construct in the Maxi-Prep product (Fig. 6.2.6).

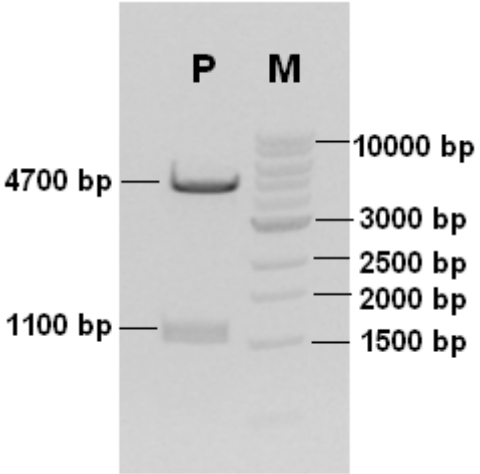

Fig. 6.2.6. *The digested Maxi-Prep product (P) contained the linearized pmKate2-N vector (4700 bp) and the HindIII-hH$_2$R-ApaI fragment (1100 bp). The 1 kb DNA ladder was used as a DNA marker (M).*

6.2.3.4 Sequencing

Sequencing of the Maxi-Prep product was performed by Entelechon (Regensburg, Germany) using the following primers:

reverse primer – ML_mKate2_rev1 (annealing at the beginning of the mKate2 gene):

5'-CCCTCGGATGTGCACTTGAAG-3'

reverse primer – ML_mKate2_rev2 (annealing in the middle of the hH_2R gene):

5´-CAAATTAAGACCAGAGAGATGG-3´

The alignment of the obtained sequences with the hH_2R sequence from the National Center for Biotechnology Information data base (available on-line at http://www.ncbi.nlm.nih.gov/nuccore/NM_022304.2) was done with the Serial Cloner 2.1 software. It revealed two point mutations (G→A and C→T at the positions 894 and 897 from the ATG start codon), which does not change the amino acid sequence of the receptor (Gly^{298} and Tyr^{299}). The isolated plasmid DNA was stored at -20 °C until used for transfection experiments.

6.2.4 Construction and preparation of the hH_2R-STOP-pmKate2-N plasmid

In order to obtain the cells, expressing the hH_2R and the mKate2 separately as a control for further microscopic studies, the hH_2R-STOP-pmKate2-N plasmid was constructed. For this purpose the hH_2R gene (including a stop codon) was subcloned from the pcDNA3.1(+)Neo-hH_2R plasmid (Fig. 6.2.7) into the pmKate2-N vector *via Nhe*I and *Xho*I restriction sites.

The construction and preparation of the hH_2R-STOP-pmKate2-N plasmid were performed as described in the paragraphs 6.2.2 and 6.2.3. Briefly, 10 µg of the pcDNA3.1(+)Neo-hH_2R plasmid and the pmKate2-N vector were digested, using 2 µL of 10 U/µL solution of *Nhe*I and 8 µL of 10 U/µL solution of *Xho*I (a 4-fold excess) for each sample. After agarose gel electrophoresis, the DNA fragments (the digested H_2R DNA containing a stop codon and the pmKate2-N vector) were extracted and DNA concentration was measured by UV spectroscopy. For the subsequent ligation with T4 DNA ligase, 50 ng of the digested pmKate2-N vector and 59 ng of the *Nhe*I-hH_2R-STOP-*Xho*I insert were used. After successful transformation with the ligation mixture, 10 bacterial colonies were picked from the selective agar plate for the Mini-Prep.

However, *analytical* digestion of the Mini-Prep products with the restriction enzymes (1 µL of 10 U/µL *Nhe*I and 4 µL of 10 U/µL *Xho*I (a 4-fold excess) for each clone) revealed a DNA band corresponding to the hH_2R gene only for one clone. This was successfully used for the Maxi-Prep, as shown by an *analytical* agarose gel in Fig. 6.2.8. By the UV illumination of the digested insert *Nhe*I-hH_2R-STOP-*Xho*I and the undigested hH_2R-STOP-pmKate2-N plasmid, 10 µL of ready-to-use MassRuler DNA ladder mix was used. After the estimation of DNA concentration by UV spectroscopy, the plasmid DNA was stored at -20 °C until used for transfection experiments.

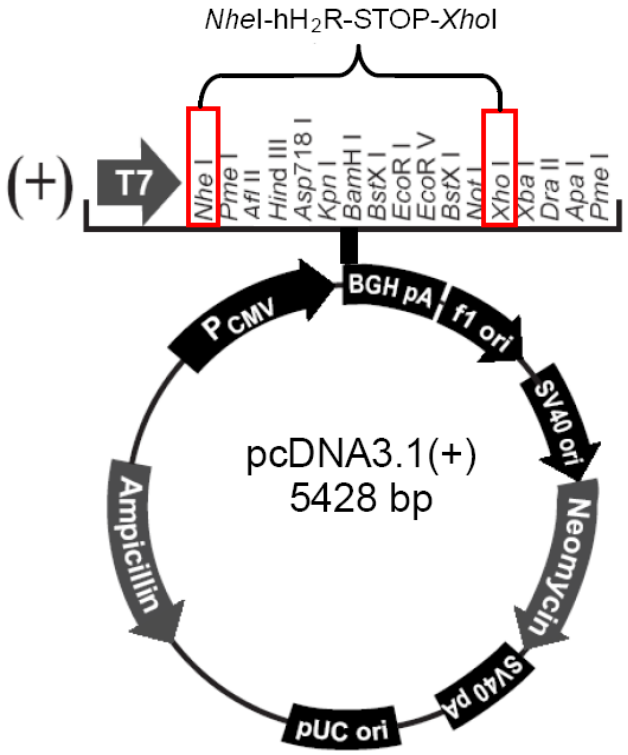

Fig. 6.2.7. *Schematic representation of the pcDNA3.1(+)Neo-hH_2R plasmid (Mosandl, 2009). The hH_2R cDNA with a stop codon was subcloned via NheI and XhoI restriction sites (marked up in red) into the multiple cloning site of the pmKate2-N vector (cf. Fig. 6.2.2) upstream of the sequence of mKate2).*

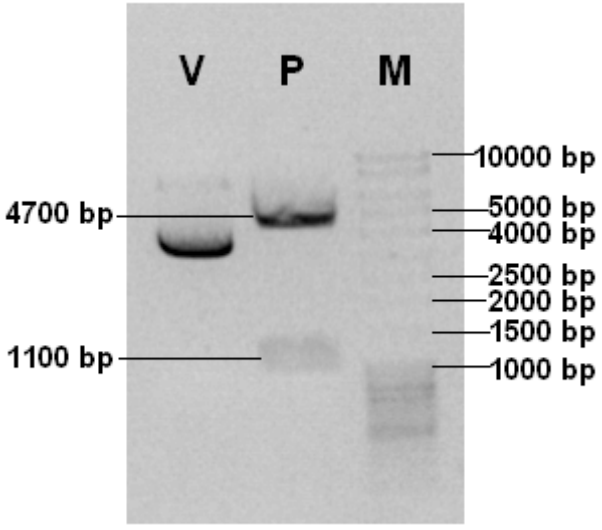

Fig. 6.2.8. *The digested Maxi-Prep product (P) contained the pmKate2-N vector (4700 bp) and the NheI-hH_2R-STOP-XhoI fragment (1100 bp). Different forms of the uncut hH_2R-STOP-pmKate2-N plasmid (supercoiled, nicked circle, V). The MassRuler DNA ladder mix was used as a DNA marker (M).*

6.2.5 Cell culture and transfection

Wild-type CHO-K1 cells were maintained in Ham's F12 medium suplemented with 10% FCS at 37 °C in the humidified atmosphere containing 5% CO_2. Every 4–7 days cells were trypsinized and passaged by 1:10 dilution with fresh medium to a 25-cm^2 culture flask. Prior to transfection with the hH_2R-pmKate2-N and the hH_2R-STOP-pmKate2-N plasmids, cells were seeded in 24-well plates and in µ-slide chambers, respectively. Transfection was performed with the FuGENE HD reagent according to the manufacturer's instructions, using 3:2, 5:2 and 8:2 (µL FuGENE HD to µg plasmid DNA) ratios. After 2 days, the expression of the mKate2 or the hH_2R-mKate2 fusion protein in transiently transfected cells, growing in the µ-slide chambers, was controlled by confocal microscopy. For the establishment of a cell line *stably expressing* the hH_2R-mKate2, the transfected and the wild-type CHO cells were passaged from the 24-well plate to a 6-well plate and grown in the culture medium supplemented with 400 µg/mL geneticin. The pmKate2-N vector confers resistance to the aminoglycoside antibiotic geneticin (as well as kanamycin and neomycin) to the transfected mammalian cells (cf. Fig. 6.2.2 and the plasmid brochure from Evrogen). After the next 2 days the transfected CHO cells survived and were passaged to a 25-cm^2 culture flask, whereas all CHO-K1 cells underwent apoptosis. The stably transfected CHO-hH_2R-mKate2 cells were further cultivated in the *selective* Ham's F12 medium, suplemented with 10% FCS and freshly added 400 µg/mL geneticin, and passaged 1:10 approx. every 4–7 days. As the clone of the CHO-hH_2R-mKate2 cells with the 5:2 (transfection reagent-to-DNA) ratio showed the highest transfection efficiency (30–50% cells revealed proper membranal expression of the hH_2R-mKate2), it was used for further experiments. However, as determined by confocal microscopy, the percentage of the CHO cells expressing the hH_2R-mKate2 predominantly in the cell membrane was dropping with increasing passage number, reaching circa 10% in the 15th passage.

6.2.6 Confocal microscopy

6.2.6.1 Preparation of specimens

2 days before microscopy, CHO cells were seeded in a µ-slide chamber and cultivated without geneticin at 37 °C in the humidified atmosphere containing 5% CO_2 (Gross, 2006). It is noteworthy that 3 days after seeding the cells would be too old for imaging. On the day of the experiment the cells were carefully washed with L-15 medium and

200 µL of L-15 medium were placed in each cavity of the µ-slide chamber. At the beginning of each experiment, untreated cells were imaged and the exact position of the chamber (without a lid) was stored. If not otherwise stated, 50 µL of the L-15 medium were used for total binding, whereas for unspecific binding 50 µL of an antagonist solution were pipetted with caution before the addition of a ligand tested. The labelled and unlabelled compounds were added as 6-fold concentrated feed solutions in the L-15 medium to the final volume of 300 µL per well. In the case of bivalent ligands, 80 µL of 4-fold feed solutions and the total volume of 320 µL per well were used. Incubation was performed at room temperature (20 °C) in the dark.

For experiments with concanavalin A (Con A), cells were incubated with 180 µL of the L-15 medium and 60 µL of 1 mg/mL Con A prior to addition of 60 µL of a feed solution of a compound to be tested.

Staining with the LysoTracker Green was performed according to manufacturer's instructions as follows: on the day of the experiment, the culture medium was replaced with the serum-free Ham's F12 medium containing 25 or 50 nM of the LysoTracker Green. After 15–150 min of incubation at 37 °C in the humidified atmosphere containing 5% CO_2, the cells were carefully washed with L-15 medium and 200 µL of L-15 medium were placed in each cavity of the µ-slide chamber. Thereafter, the cells were processed as described above.

6.2.6.2 Microscope settings

Specimens were illuminated using an inverted Carl Zeiss LSM 510 confocal laser scanning microscope. For image collection, a Plan Apochromat ×63 oil immersion objective was used. The monomeric far-red fluorescent mKate2 was detected with Texas red filter sets as reported elsewhere (Shcherbo *et al.*, 2009). In this work an excitation line of a helium-neon (HeNe) ion laser of 543 nm was used (transmission of 87–90%) and fluorescence emission was recorded with a UV/488/543/633 main dichroic beam splitter (HauptFarbTeiler, HFT), a 545 nm secondary dichroic beam splitter (NebenFarbTeiler, NFT) and a 650 nm long pass (LP) filter (cf. Fig. 6.2.10). If not otherwise stated, for the imaging of the LysoTracker Green an excitation line of an argon (Ar) ion laser of 488 nm, a 488 nm HFT and a 505–550 nm band pass (BP) filter were used (cf. the excitation and emission spectra in Fig. 6.2.9). For image acquisition of double-stained samples, the excitation lines of the Ar and HeNe lasers were switched after scanning of each plane. This multi-tracking facility of the LSM 510 software enabled the separate collection of

fluorescence signals. Fluorescence emission spectra of the transfected and the wild-type CHO cells were acquired in the lambda mode with a META detector, collecting the signal in series of 10 nm bands.

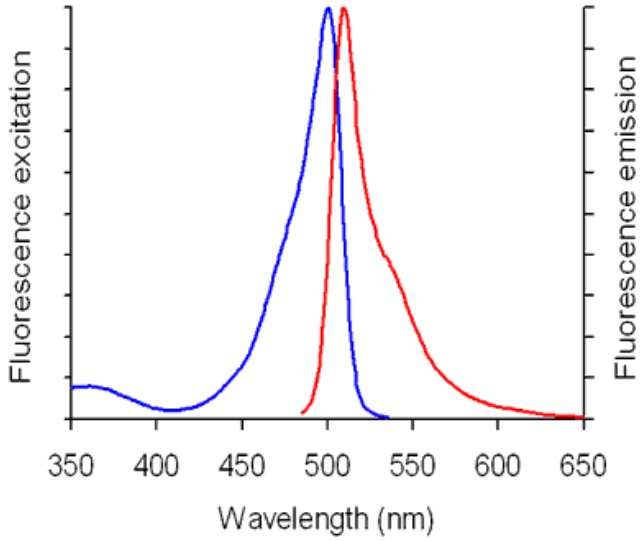

Fig. 6.2.9. *Fluorescence excitation (blue) and emission (red) spectra of LysoTracker Green DND-26 in buffer at pH 5.2 (redrawn from http://products.invitrogen.com/ivgn/product/L7526).*

6.2.7 Fluorimetry of the far-red fluorescent protein

Katushka, mKate and mKate2 proteins belong to the family of bright far-red fluorescent proteins developed by Evrogen with the same mechanism of chromophore formation and very similar spectral properties. Among them, the monomeric mKate2 is specially adapted for fusions with cellular proteins allowing the subcellular localization of the targeted protein (Shcherbo *et al.*, 2009).

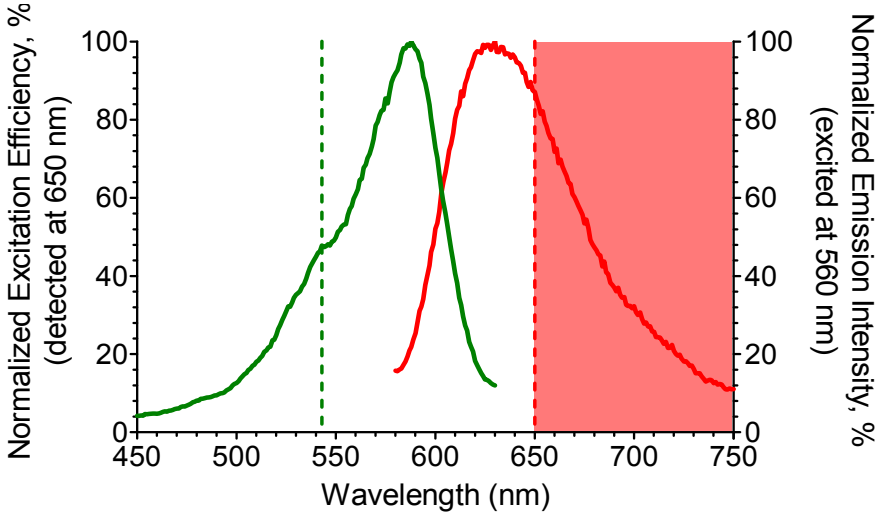

Fig. 6.2.10. *Spectral properties of the far-red fluorescent protein Katushka, expressed in human glioblastoma U-87 MG cells: The solid lines present the excitation (green) and the emission (red) spectra of the U-87 MG Katushka cells suspended in PBS buffer. The excitation and emission spectra of PBS were substracted, than the spectra were corrected. The dashed lines indicate the confocal microscope settings for the mKate2 channel: a 543 nm excitation line of a HeNe laser (green) and fluorescence emission detected beyond 650 nm (red).*

Since human glioblastoma U-87 MG cell clone 3, expressing the Katushka protein in the cytosol, were already used in our research group, they were chosen as a model system for later microscopic studies with the mKate2. The cells were cultivated in the EMEM medium supplemented with 5% FCS and 750 µg/mL geneticin (G418) for selection as described before (Kühnle, 2010). On the day of the experiment, the cells were trypsinized, washed and suspended in PBS. The excitation and emission spectra of the cell suspension were acquired at room temperature (20-23 ºC) using a Cary Eclipse spectrofluorimeter. The excitation and emission spectra of PBS buffer were substracted, than the spectra were corrected (Fig. 6.2.10).

6.3 Results and discussion

6.3.1 Membranal localization of the hH_2R-mKate2 in CHO cells

6.3.1.1 Membranal localization of the mKate2

CHO cells were transiently and stably transfected with the hH_2R-pmKate2-N plasmid as described under Materials and methods (section 6.2). On the basis of sequencing and agarose gel electrophoresis of the plasmid DNA, it was presumed that the hH_2R will be expressed as a fusion protein with the (C-terminally bound) monomeric mKate2 protein. In order to confirm that there was no shift of the open reading frame of mKate2 after the insertion of the hH_2R into the MCS of the pmKate2-N plasmid, the cells were visualized by means of confocal microscopy (Fig. 6.3.1).

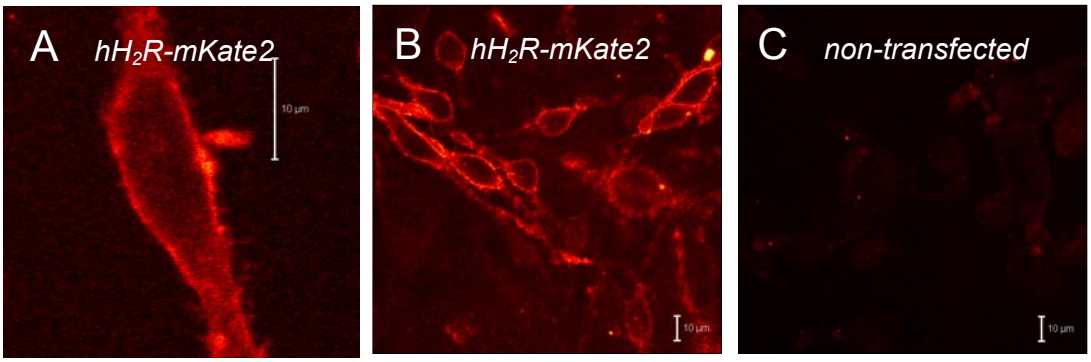

Fig. 6.3.1. *Membranal localization of the far-red fluorescent protein in CHO cells, transiently (A) and stably (B) transfected with the hH_2R-mKate2-N plasmid. There was hardly any autofluorescence of the non-transfected wild-type CHO-K1 cells (C). Plan Apochromat 63x/1.4 oil, HeNe 543 (87%), HFT UV/488/543/633, NFT 545, LP 650, pinhole <1.8 µm (2 a.u.).*

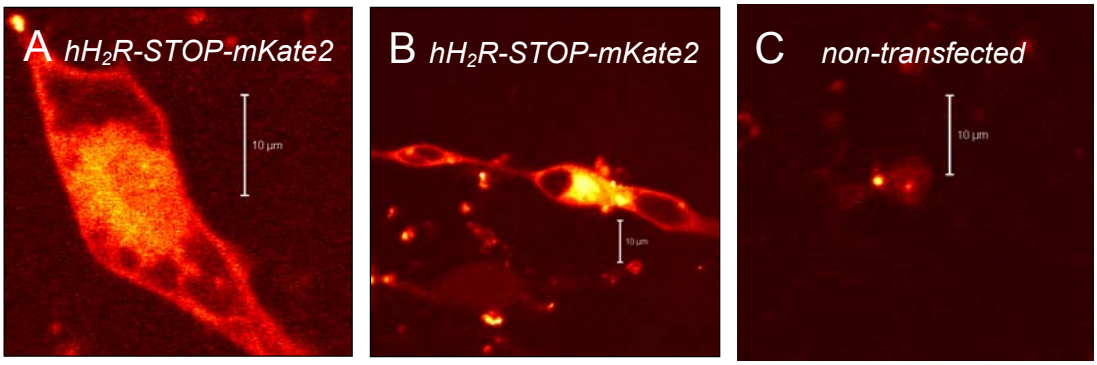

Fig. 6.3.2. *Predominantly cytosolic localization of the mKate2 in the CHO cells, transiently transfected with the hH_2R-STOP-mKate2-N plasmid (A and B). Negligible autofluorescence of CHO-K1 cells (C). Plan Apochromat 63x/1.4 oil, HeNe 543 (87%), HFT UV/488/543/633, NFT 545, LP 650, pinhole 3 a.u.*

The far-red fluorescence signal of hH_2R-mKate2 fusion proteins, detected in the cell membranes of the transfected CHO cells, confirmed the proper expression of the fluorescently labelled receptors (Fig. 6.3.1). Contrary to that, in the CHO cells transiently transfected with the hH_2R-STOP-pmKate2-N plasmid, the fluorescent signal came predominantly from the cytosol, suggesting the separate expression of the hH_2R and the far-red mKate2 fluorescent protein (Fig. 6.3.2).

6.3.1.2 Binding studies with a fluorescent H_2R ligand

In order to confirm the membranal expression of hH_2Rs in the transfected CHO cells, binding experiments with a fluorescent H_2R ligand were performed by means of confocal microscopy. As reported before, a series of green fluorescent ligands with the high affinity towards the H_2R (pA_2 up to 8.0 at the guinea-pig atrium) have been developed in our research group (Li *et al.*, 2003). Nevertheless, in this study a new red fluorescent H_2R ligand (UR-DE74) with a 633 nm laser line excitation was used, as the autofluorescence of CHO cells is marginal at this wavelength.

After 30–60 min of incubation with 200 nM of the fluorescent H_2R ligand UR-DE74 ($K_{b'}$ of 162 ± 51 nM in GTPase assay at hH_2R-$G_{s\alpha S}$; Erdmann, 2010), pronounced total binding as well as low unspecific binding and autofluorescence were detected in the CHO cells expressing hH_2R-mKate2 fusion proteins. This enabled a reliable estimation of the specific binding of UR-DE74 and confirmed the membranal localization of hH_2Rs (Fig. 6.3.3).

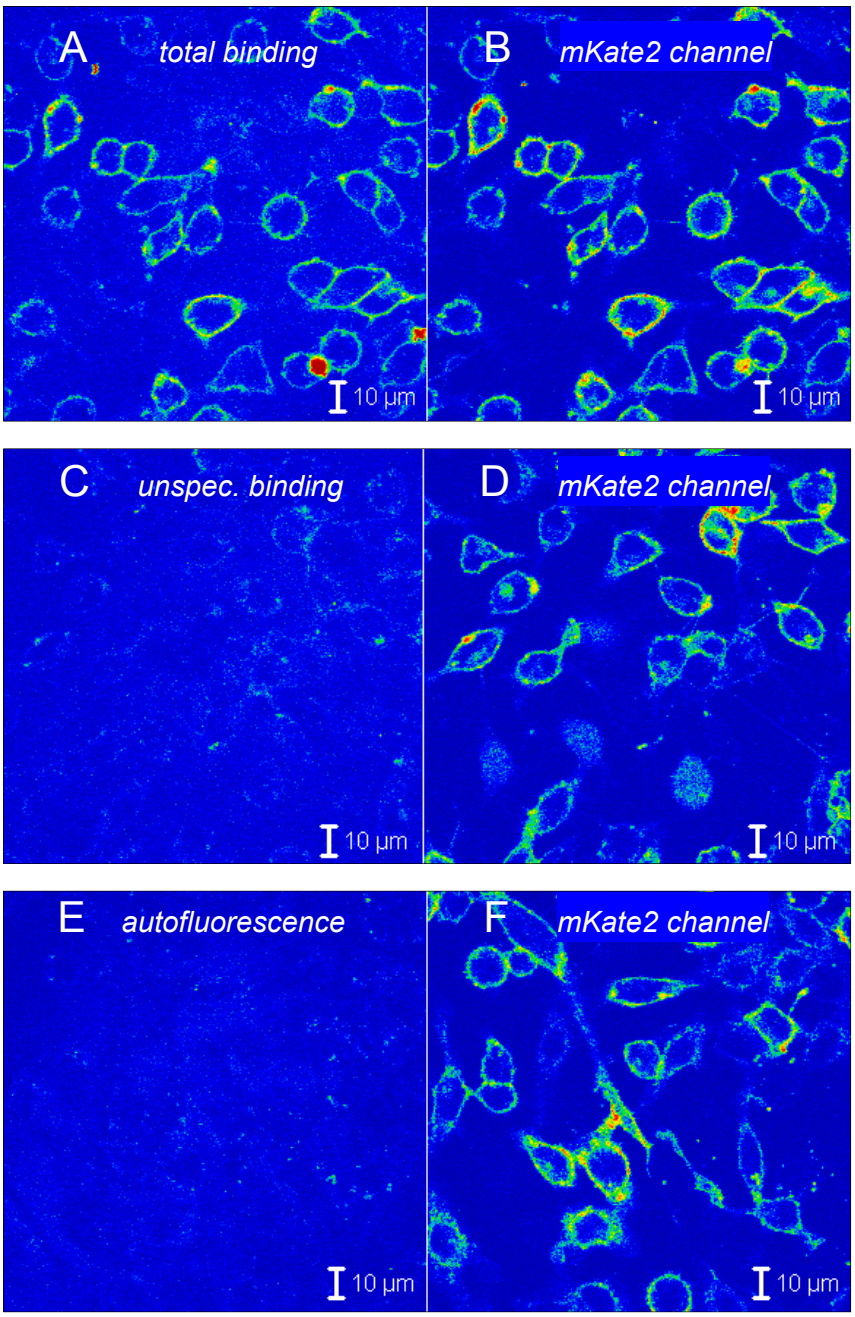

Fig. 6.3.3. *Binding of the red fluorescent H_2R ligand UR-DE74 to the CHO-hH_2R-mKate2 cells. The cells were preincubated for 50 min with 100 µM FAM (C and D) or L-15 medium (A, B, E and F). Confocal images (rainbow palette) were acquired 30 min after addition of 200 nM UR-DE74 (A–D) in a multi-track scanning mode. The unlabelled CHO-hH_2R-mKate2 cells (E and F) were used for reference. Fluorescence emission in the UR-DE74 channel (panels A, C and E: 8% HeNe 633, HFT UV/488/543/633, LP 650); fluorescence emission in the mKate2 channel (panels B, D and F: 90% HeNe 543, HFT UV/488/543/633, NFT 545, LP 650). Plan Apochromat 63x/1.4 oil, pinhole <1.5 µm (1.6 a.u.).*

6.3.2 Confocal microscopy imaging of agonist-induced H_2R internalization

6.3.2.1 Agonist-independent hH_2R-mKate2 internalization

CHO cells stably transfected with the hH_2R-pmKate2 plasmid were incubated for up to 4.5 hours with L-15 Leibovitz medium in the absence of H_2R agonists. As the transfected CHO cells presented a heterogenic population with respect to the level and the pattern of the hH_2R-mKate2 expression, only the cells with low cytosolic and high membranal expression of the fusion proteins were chosen for confocal imaging (the initial amount of approx. 30% of all transfected cells was systematically decreasing with the increasing number of passages). Otherwise, it would be impossible to estimate the effect of H_2R ligands in the cellular system, where receptor internalization was considered as the actual read-out, even though it enabled only a qualitative evaluation of the efficacy of a respective ligand. As shown in Fig. 6.3.4, receptor endocytosis did not appear up to approx. 90 min of incubation without H_2R ligands. However, after longer incubation periods (up to 270 min) with L-15 medium alone, the hH_2R-mKate2 fusion proteins were partially internalized. The internalized receptors formed predominantly diffuse areas. Only in a small fraction of the visualized cells, condensed and well defined “spots” were formed after receptor endocytosis (Fig. 6.3.4 F).

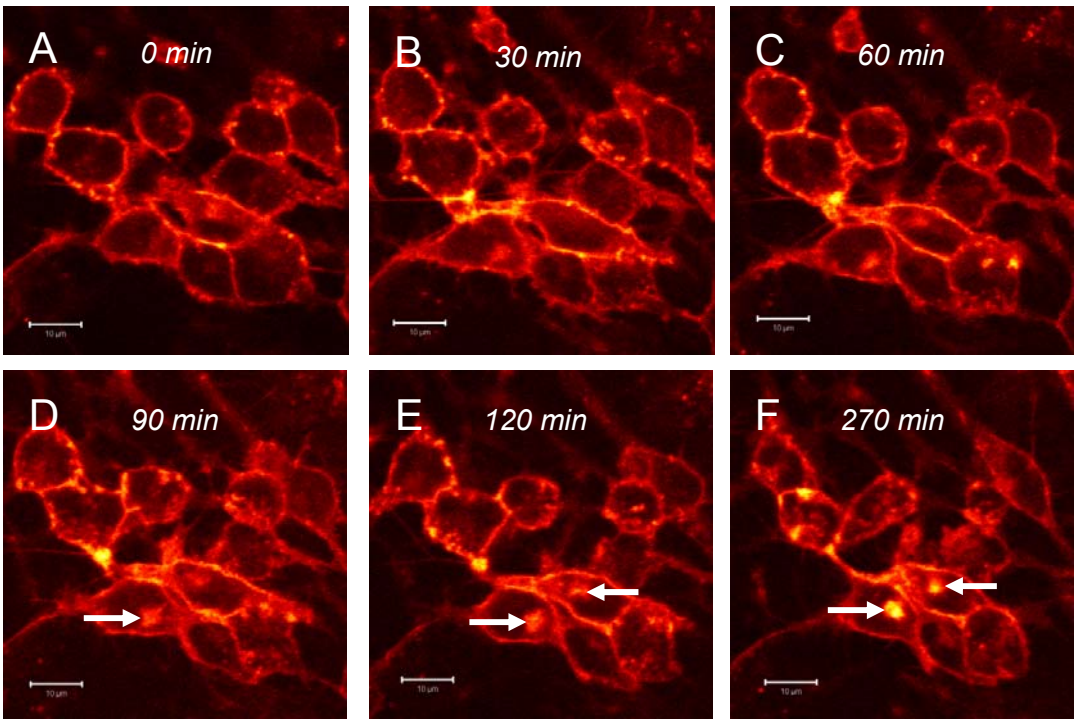

Fig. 6.3.4. *Agonist-independent internalization of the hH_2R-mKate2 in CHO cells. Images were acquired at 0 min (A), 30 min (B), 60 min (C), 90 min (D), 120 min (E) and 270 min (F) of incubation with medium alone. Arrows indicate the internalized fusion proteins. Plan Apochromat 63x/1.4 oil, HeNe 543 (90%), HFT UV/488/543/633, NFT 545, LP 650, pinhole <1.5 µm (1.6 a.u.).*

In order to check, if H_2R antagonists could inhibit this agonist-independent endocytosis, the cells were incubated with 100 µM FAM only. The translocation of the receptors did not occur during the first 120 min of incubation (Fig. 6.3.5), but later this process of internalization could not be completely blocked. The reason for that might be increased constitutive activity due to oxidative stress (after removal of culture medium and long incubation at 20 °C). A certain degree of the constitutive activity was reported before for the wild-type hH_2R as well as the hH_2R-GFP and the hH_2R-$G_{s\alpha S}$ fusion proteins expressed in recombinant systems (Monczor *et al.*, 2003; Osawa *et al.*, 2005; Preuss *et al.*, 2007).

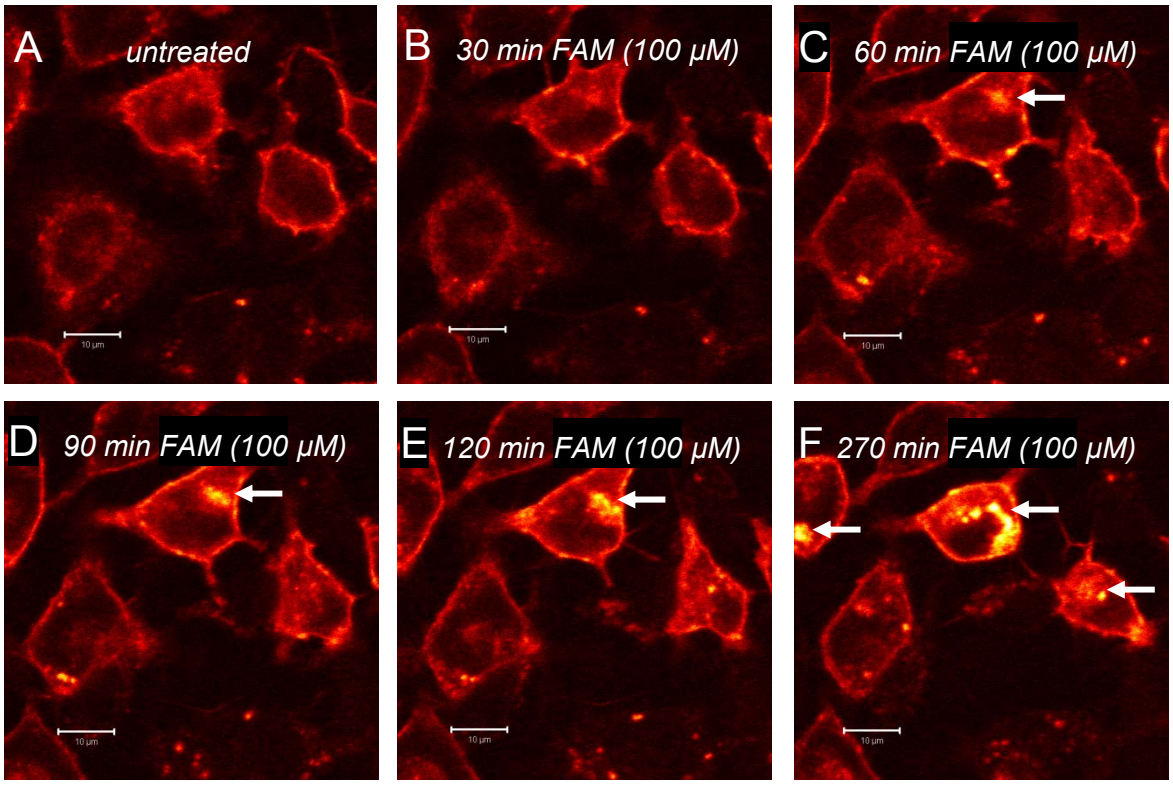

Fig. 6.3.5. *Ligand-independent internalization of the hH_2R-mKate2 in CHO cells. Confocal images were acquired before (A) and 30 min (B), 60 min (C), 90 min (D), 120 min (E) and 270 min (F) after addition of 100 µM FAM. Arrows indicate the perinuclear localization of internalized hH_2R-mKate2 fusion proteins. Plan Apochromat 63x/1.4 oil, HeNe 543 (90%), HFT UV/488/543/633, NFT 545, LP 650, pinhole <1.5 µm (1.6 a.u.).*

No internalization of hH_2R-mKate2 fusion proteins could be observed within the first 90 min of incubation in the absence of agonists. However, after longer incubation periods, there was a detectable degree of receptor endocytosis, which could not be blocked by 100 µM FAM. Because of the ligand-independent redistribution of receptors, the investigation of H_2R internalization in response to agonists should be limited to an initial time period of 90 min.

6.3.2.2 Effect of histamine on hH_2R internalization

Confocal imaging of CHO cells, expressing the hH_2R-mKate2, revealed receptor internalization after 30–60 min of incubation with 10–100 µM HIS. Upon 60-90 min of incubation, far-red fluorescence was localized in the perinuclear region of each cell as a single (clearly distinguishable) round "spot" (Fig. 6.3.6 and 6.3.7 A–B). At the same time the cells became slightly rounded. These findings were in agreement with previously published results for hH_2Rs C-terminally tagged with green fluorescent proteins (Osawa *et al.*, 2005).

The transfected CHO cells showed endocytosis of the hH_2R-mKate2 fusion protein within 90 min of incubation with 10–100 µM HIS (Fig. 6.3.6 and 6.3.7 A–B), as expected for a full H_2R agonist (Osawa *et al.*, 2005).

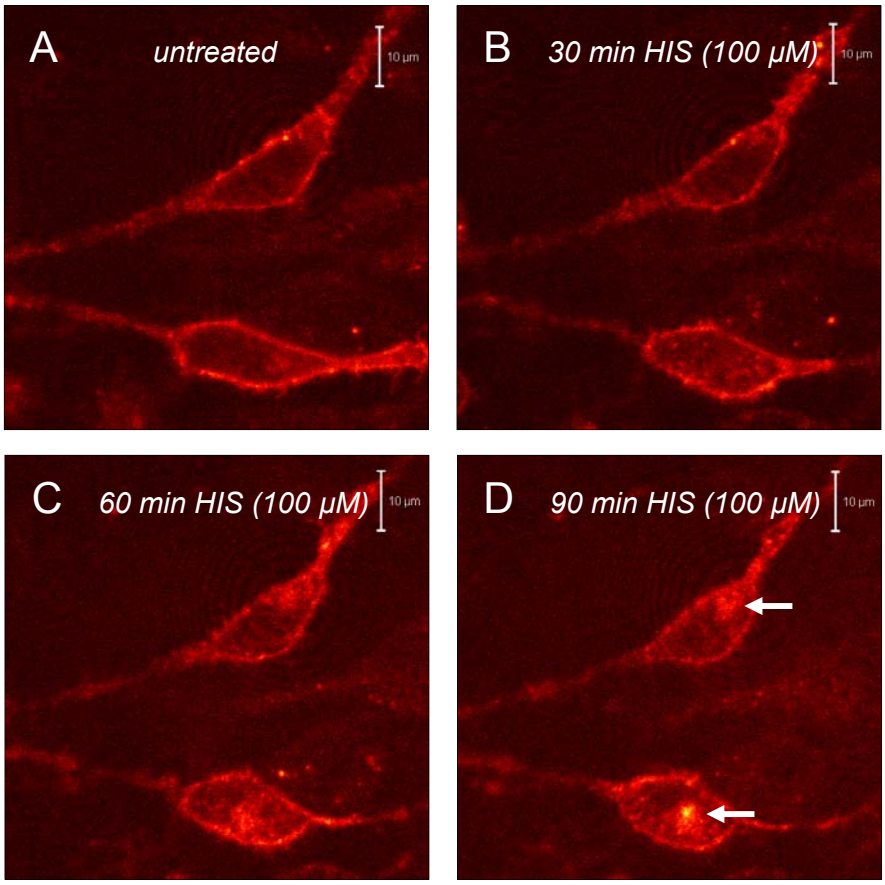

Fig. 6.3.6. *HIS-induced internalization of the hH_2R-mKate2 in CHO cells. Confocal images were acquired before (A) as well as 30 min (B), 60 min (C) and 90 min (D) after addition of 100 µM HIS. Arrows indicate the perinuclear localization of internalized hH_2R-mKate2 fusion proteins. Plan Apochromat 63x/1.4 oil, HeNe 543 (90%), HFT UV/488/543/633, NFT 545, LP 650, pinhole <1.8 µm (2 a.u.).*

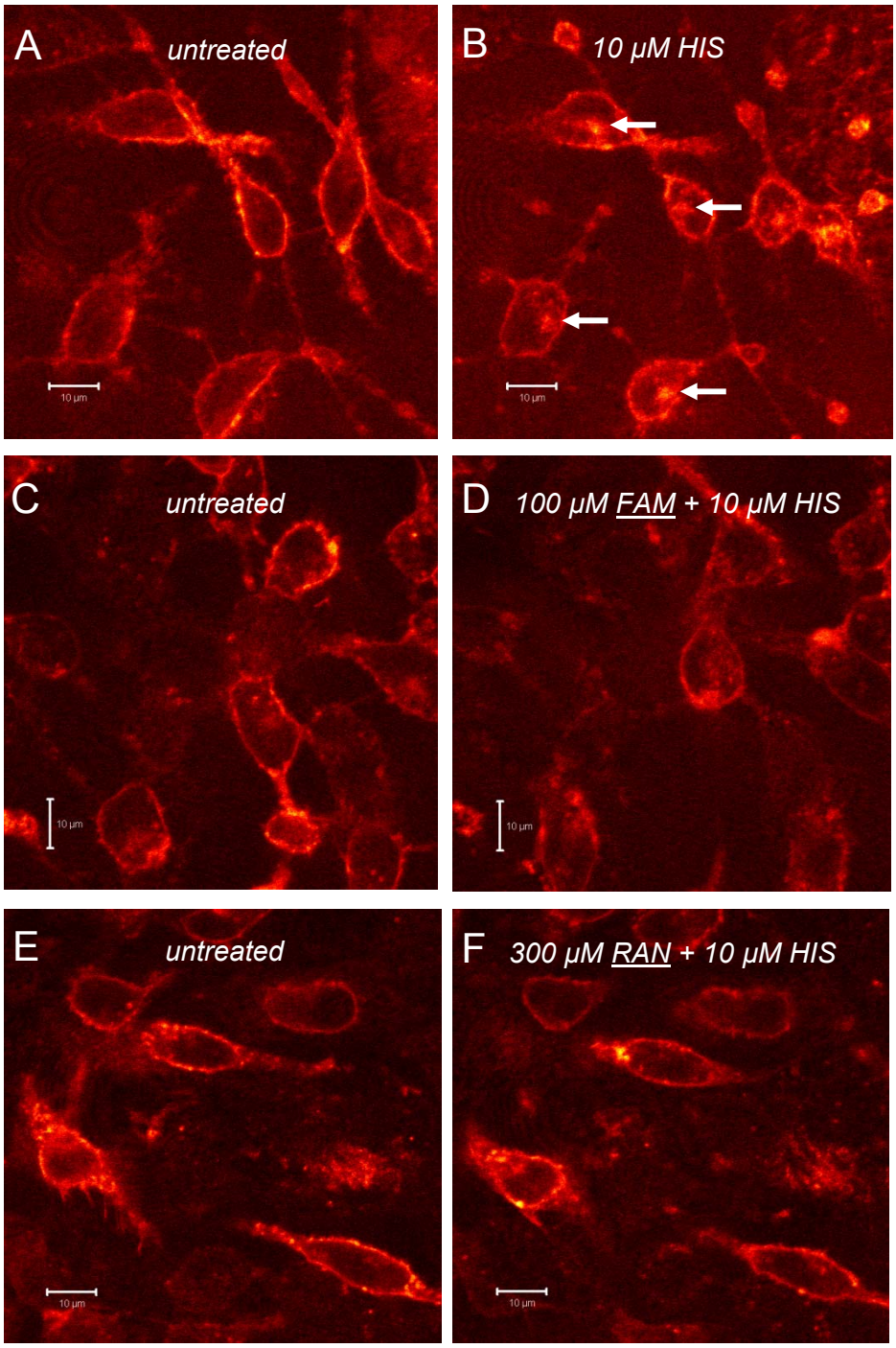

Fig. 6.3.7. *Effect of H_2R antagonists on HIS-induced internalization of the hH_2R-mKate2. Cells were preincubated for 15 min with 100 µM FAM (D) or 300 µM RAN (F). Confocal images were acquired before (A, C, E) and 90 min (B, D, F) after addition of 10 µM HIS. Arrows indicate the perinuclear localization of internalized hH_2R-mKate2 fusion proteins. Plan Apochromat 63x/1.4 oil, HeNe 543 (90%), HFT UV/488/543/633, NFT 545, LP 650, pinhole <1.8 µm (2 a.u.).*

6.3.2.3 Effect of antagonists on the histamine-induced hH_2R internalization

In order to prove a receptor-mediated mechanism of internalization, the transfected CHO cells expressing hH_2R-mKate2 fusion proteins were incubated with H_2R antagonists prior to the addition of HIS. Similarly to the determination of the unspecific binding in radiochemical studies (Kenakin, 2006), the antagonists were used at concentrations providing an approx. 200-fold excess relatively to HIS (cf. HIS: EC_{50} of 830 ± 290 nM, FAM: K_b of 50 ± 10 nM in calcium assay with fura-2 dye, RAN: K_i of 172 ± 11 nM in radioligand competition binding assay on whole cells; Mosandl, 2009).

As shown in Fig. 6.3.7, receptor internalization caused by 10 µM of the endogenous ligand could be blocked by H_2R antagonists FAM (100 µM) and RAN (300 µM), confirming a *receptor-mediated mechanism* of endocytosis. Remarkably, the CHO-hH_2R-mKate2 cells pretreated with H_2R antagonists stayed spindle-shaped.

In theory, H_2R antagonists (actually inverse agonists in systems with constitutive activity; cf. Fig. 1.1.6; Preuss *et al.*, 2007) should be able to up-regulate the spontaneously active H_2Rs (as shown by an increase in [^{125}I]APT binding; Smit *et al.*, 1996 b). Moreover, earlier studies reported that addition of 100 µM FAM induced the recycling of the H_2R-GFP fusion proteins internalized upon preincubation with 100 µM HIS to the cell membranes within 2 hours (Osawa *et al.*, 2005). However, recycling of the receptor was not observed in CHO cells expressing the H_2Rs tagged with far-red fluorescent proteins. There was no up-regulation of the internalized hH_2R-mKate2 fusion protein when cells were treated with 100 µM FAM (Fig. 6.3.8).

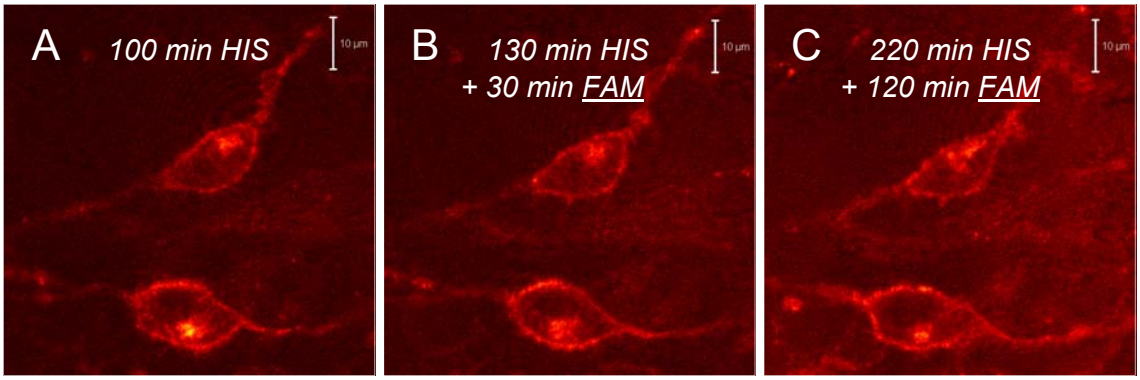

Fig. 6.3.8. *Effect of FAM on the HIS-induced internalization of the hH_2R-mKate2 fusion protein. Cells were preincubated for 100 min with 100 µM HIS (the same sample as in Fig. 6.3.6). Confocal images were acquired before (A), 30 min (B) and 120 min (C) after addition of 100 µM FAM. Plan Apochromat 63x/1.4 oil, HeNe 543 (90%), HFT UV/488/543/633, NFT 545, LP 650, pinhole <1.8 µm (2 a.u.).*

6.3.2.4 Effect of other agonists on hH_2R internalization

The partial H_2R agonist dimaprit (DIM), used at a concentration of 30 µM (cf. EC_{50} of 14.00 ± 4.14 µM, efficacy of 0.88 ± 0.03 in calcium assay with fura-2 dye; Mosandl, 2009; K_i of 25 ± 5 µM in [^{125}I]APT competition binding assay on transfected CHO cells; Leurs *et al.*, 1994), induced the translocation of hH_2R-mKate2 fusion proteins as shown in Fig. 6.3.9. However, the effect was not as pronounced as in case of HIS. The DIM-induced receptor internalization could be blocked by 100 µM FAM.

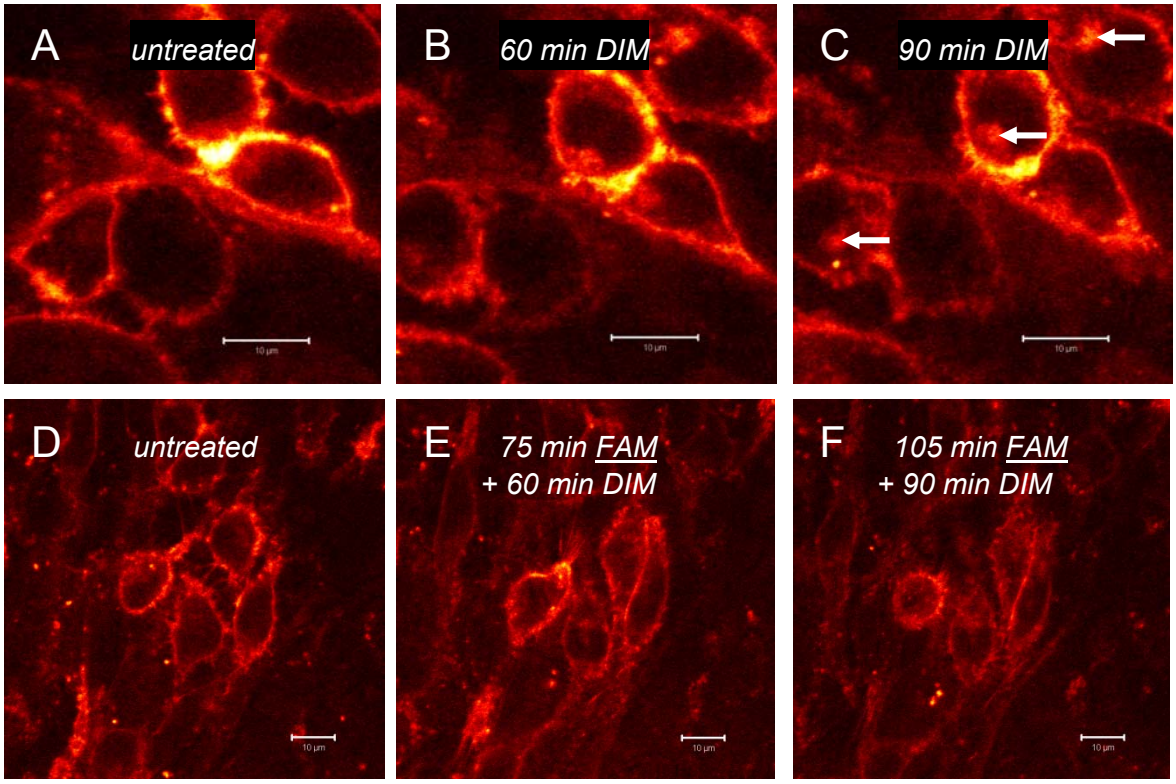

Fig. 6.3.9. *DIM-induced internalization of the hH_2R-mKate2 in CHO cells. The cells in panels E and F were preincubated for 15 min with 100 µM FAM. The images were acquired before (A, D) as well as 60 min (B, E) and 90 min (C, F) after addition of 30 µM DIM. Arrows indicate the perinuclear localization of internalized hH_2R-mKate2 fusion proteins. Plan Apochromat 63x/ 1.4 oil, HeNe 543 (90%), HFT UV/488/543/633, NFT 545, LP 650, pinhole <1.8 µm (2 a.u.).*

Similar observations were made for 10 µM arpromidine (ARP), a prototypical H_2R partial agonist (cf. K_i of 12 ± 2 µM in the flow cytometric and 5.4 ± 1.3 µM in the [^{3}H]TIO competition binding assay on whole cells; Mosandl, 2009). However, in contrast to DIM, the ARP-induced internalization was not completely antagonized by FAM (Fig. 6.3.10).

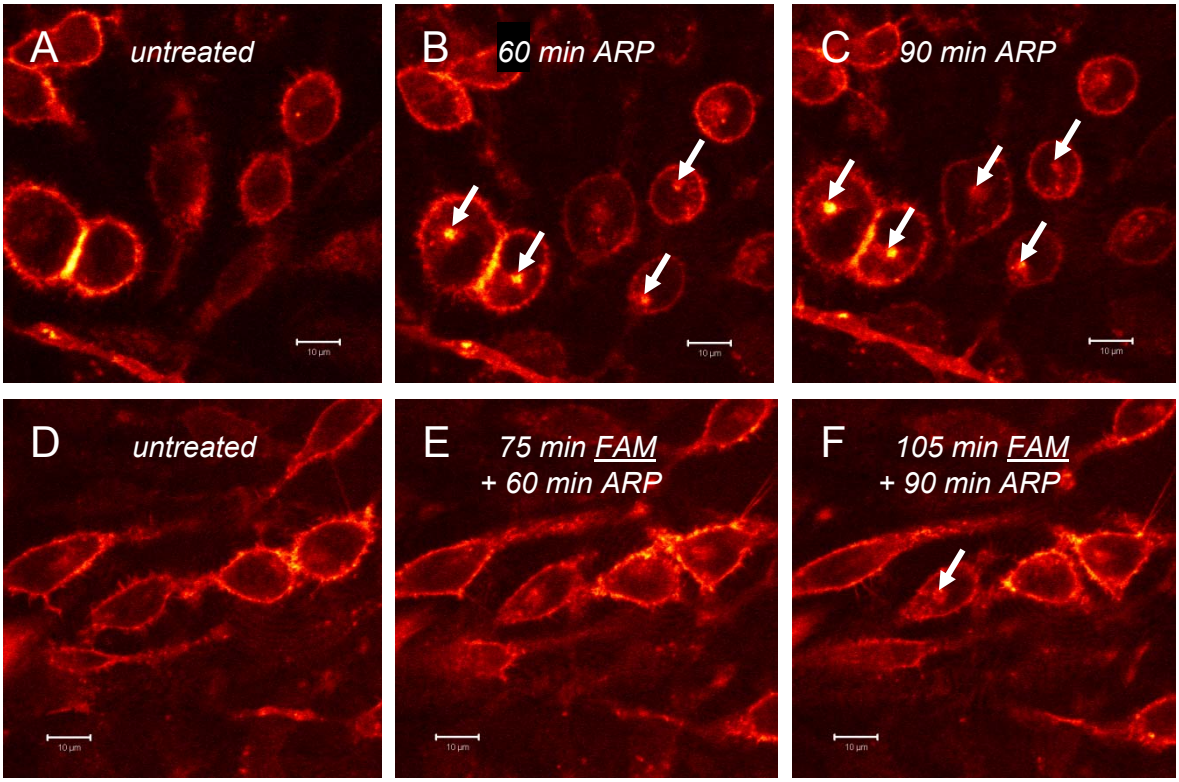

Fig. 6.3.10. *ARP-induced internalization of the hH_2R-mKate2 in CHO cells. The cells in panels E and F were preincubated for 15 min with 100 µM FAM. The images were acquired before (A, D) as well as 60 min (B, E) and 90 min (C, F) after addition of 10 µM ARP. Arrows indicate the perinuclear localization of internalized hH_2R-mKate2 fusion proteins. Plan Apochromat 63x/1.4 oil, HeNe 543 (90%), HFT UV/488/543/633, NFT 545, LP 650, pinhole <1.8 µm (2 a.u.).*

The pattern of H_2R internalization in the presence of standard agonists not only confirms published imaging results (Osawa *et al.*, 2005), but is also in agreement with radioligand binding studies, where H_2R agonists reduced the number of receptors in the cell membrane (Fig. 6.3.11; cf. Smit *et al.*, 1996 b). For example, HIS induced 44% down-regulation of H_2Rs in a concentration- (EC_{50} = 18 nM) and time-dependent ($t_{1/2}$ = 7 h) manner (Smit *et al.*, 1996 a). Also BU-E-75, an ARP-like agonist, caused the internalization of the H_2R (Legnazzi *et al.*, 2000). However, the present study did not confirm the receptor up-regulation in response to antagonists (inverse agonists).

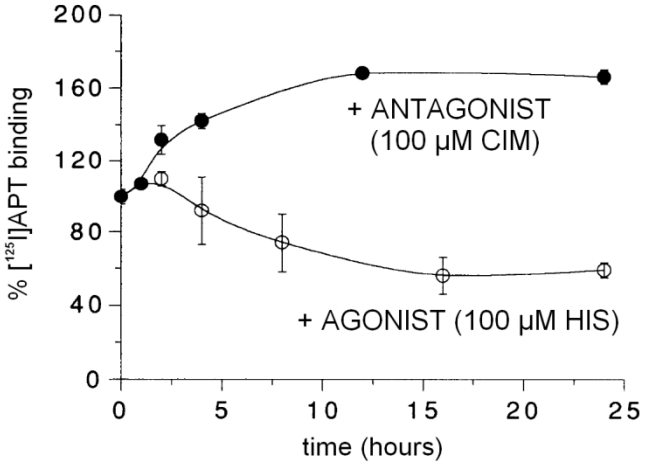

Fig. 6.3.11. *Prolonged incubation with a H_2R antagonist (100 µM CIM) leads to an increase in receptor number, while 100 µM HIS accounts for receptor internalization, measured as [^{125}I]APT binding on transfected CHO cells expressing rat H_2Rs (adopted from Smit et al., 1996 (b) with modifications).*

6.3.2.5 Influence of mono- and bivalent acylguanidines on hH_2R internalization

Usually, binding of (balanced) H_2R agonists leads to receptor internalization, because receptor conformation stabilized by agonists activates both G-protein-dependent signalling and recruitment of β-arrestins. However, it is still the mater of debate if the same receptor conformations, resulting in β-arrestin-dependent signalling, also lead to desensitization of receptors (Rajagopal *et al.*, 2010). Nevertheless, as mentioned in chapter 4, the binding curves of some bivalent acylguanidines revealed no GTPγS-dependent shift in competition binding assays at the gpH_2R-$G_{s\alpha S}$ (compounds **4** and **11** in experiments with [^{3}H]TIO and [^{3}H]UR-DE257, respectively). Although this could indicate rather antagonistism, most of the bivalent acylguanidines were found to be agonists in steady-state GTPase assays both on hH_2R-$G_{s\alpha S}$ and gpH_2R-$G_{s\alpha S}$ fusion proteins and spontaneously beating guinea-pig right atrium (Kraus, 2007). Only bivalent compounds, containing a 20-membered spacer between the carbonyl groups, were neutral antagonists at the hH_2R-$G_{s\alpha S}$ (Birnkammer *et al.*, 2010).

In light of the aforementioned results, the question of the existence of biased ligands at the hH_2R was raised. Therefore, influence of the bivalent H_2R ligands on receptor internalization was investigated, in order to compare ligand efficacy with the previous results on H_2R agonism (from steady-state GTPase assays on hH_2R-$G_{s\alpha S}$ fusion proteins expressed in Sf9 cells; cf. Birnkammer *et al.*, 2010). As shown in Fig. 6.3.12, the bivalent acylguanidine **4** was found to induce redistribution of the fluorescently labelled H_2Rs at a concentration of 1 µM. It is noteworthy that the same concentration was sufficient to alter the radioligand dissociation rate constant at gpH_2R-$G_{s\alpha S}$ fusion proteins expressed in Sf9 cells (cf. Fig. 5.3.2 B and 5.3.3 B). The bivalent agonist **5** also induced the translocation of hH_2R-mKate2 fusion proteins, as depicted in Fig. 6.3.13. Despite the fact that the internalization after a 90-min exposure to compound **5** was less pronounced than that induced by HIS (cf. Fig. 6.3.7 B), it was easily distinguishable from that in the untreated control (cf. Fig. 6.3.4 D and F). Moreover, the observed endocytosis could not result from ligand toxicity, because the used concentration of agonist **5** was 120 nM only (cf. EC_{50} of 60 ± 10 nM, efficacy of 0.42 ± 0.01 in calcium assays on intact cells; Mosandl, 2009).

Confocal microscopy imaging revealed that the incubation with the symmetric bivalent ligands **4** and **5**, containing octamethylene spacers, led to the internalization of the fluorescently labelled H_2R (Fig. 6.3.12 and 6.3.13, respectively), thus being in line with their agonistic properties with respect to G-protein activation (Kraus, 2007). However, it has to be noted that the observation of hH_2R-mKate2 internalization does not enable the (quantitative) determination of ligand efficacy for β-arrestin-mediated signalling.

These microscopic observations confirmed agonistic properties of the bivalent ligands **4** and **5**, being in agreement also with preliminary results obtained in our research group from the β-arrestin recruitment assay on the CHO cells expressing hH_2Rs as well as the cAMP assay on human neutrophils (Mr. Johannes Felixberger and Ms. Irena Brunskole, Institute of Pharmacy, University of Regensburg, personal communications). In both types of experiments, compounds **4** and **5** were tested up to a concentration of 1 μM, showing weak partial agonism (ligand **4** revealed higher efficacy than ligand **5**).

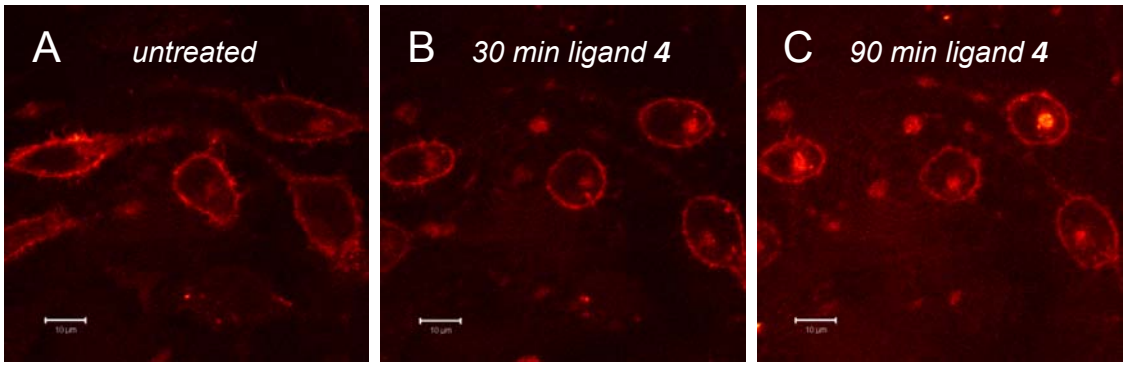

Fig. 6.3.12. *Internalization of the hH_2R-mKate2 in CHO cells induced by the bivalent agonist **4**. Confocal images were acquired before (A) as well as 30 min (B) and 90 min (C) after addition of 1 μM of compound **4**. Plan Apochromat 63x/1.4 oil, HeNe 543 (90%), HFT UV/488/543/633, NFT 545, LP 650, pinhole 2 a.u.*

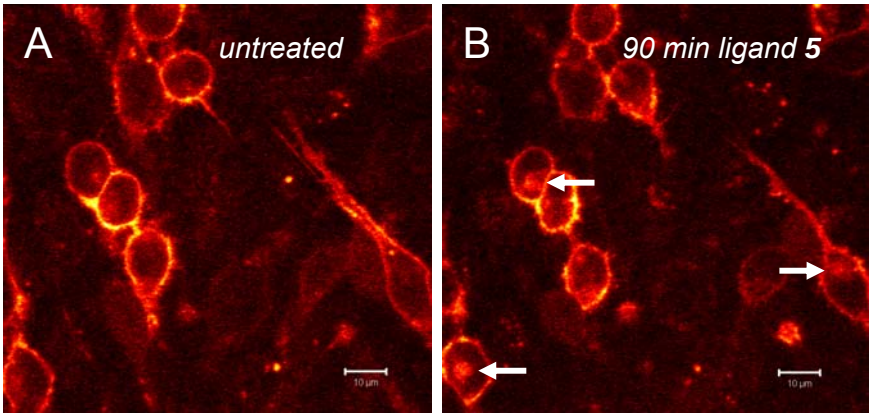

Fig. 6.3.13. *Internalization of the hH_2R-mKate2 in CHO cells induced by the bivalent agonist **5**. Confocal images were acquired before (A) and 90 min (B) after addition of 120 nM of compound **5**. Arrows indicate the perinuclear localization of internalized hH_2R-mKate2 fusion proteins. Plan Apochromat 63x/1.4 oil, HeNe 543 (90%), HFT UV/488/543/633, NFT 545, LP 650, pinhole 2 a.u.*

In contrast, an experiment with a 140-min exposure to 1 µM of compound **1** revealed no significant internalization of the hH_2R-mKate2. This was rather unexpected, since the monovalent ligand **1** behaved as an agonist in GTPase assays on the hH_2R-$G_{s\alpha S}$ (EC_{50} of 22 ± 5 nM, efficacy of 0.79 ± 0.02; Kraus *et al.*, 2009) as well as in [^{3}H]TIO competition binding assays, showing typical GTPγS-dependent shifts at both hH_2R-$G_{s\alpha S}$ (K_i of 39 ± 5 nM; cf. Table 4.3.3; cf. Fig. 4.3.5 E) and gpH_2R-$G_{s\alpha S}$ fusion proteins (cf. Fig. 4.3.5 F).

The monovalent H_2R agonist **1** did not induce hH_2R-mKate2 internalization at a concentration up to 300 nM upon 90-min exposure (Fig. 6.3.14 A–B). A prolonged incubation (110 min) with 1 µM of compound **1** led to marginal H_2R internalization (Fig. 6.3.14 C–D), which was, however, similar to the aforementioned ligand-independent receptor endocytosis (cf. Fig. 6.3.4 E).

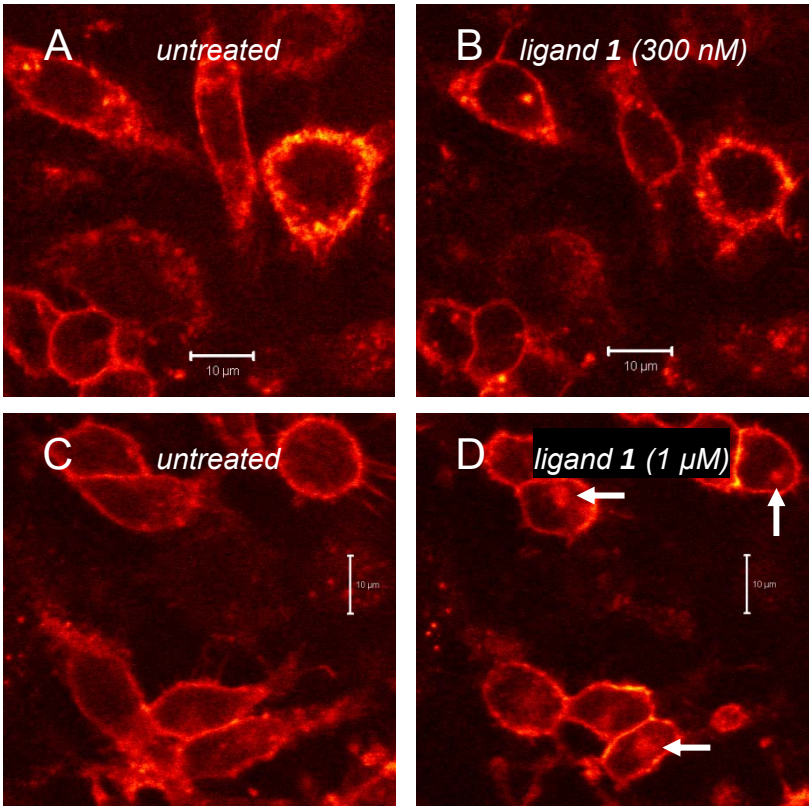

Fig. 6.3.14. *Influence of the monovalent ligand **1** on the internalization of the hH_2R-mKate2 in CHO cells. Upper panel: confocal images were acquired before (A) and 90 min (B) after addition of 300 nM of compound **1**; pinhole <1.8 µm (2 a.u.). Lower panel: confocal images were acquired before (C) and 110 min (D) after addition of 1 µM of compound **1**; pinhole <1.5 µm (1.6 a.u.). Arrows indicate the perinuclear localization of internalized hH_2R-mKate2 fusion proteins. Plan Apochromat 63x/1.4 oil, HeNe 543 (90%), HFT UV/488/543/633, NFT 545, LP 650.*

Also for the bivalent ligands **12** and **13** containing 20-membered spacers between the carbonyl groups no internalization within 90 min was observed. These compounds were previously reported to be also neutral antagonists in steady-state GTPase assays on the hH_2R-$G_{s\alpha S}$ (K_b values: compound **12**: 1679 nM, compound **13**: 770 nM; cf. Birnkammer *et al.*, 2010).

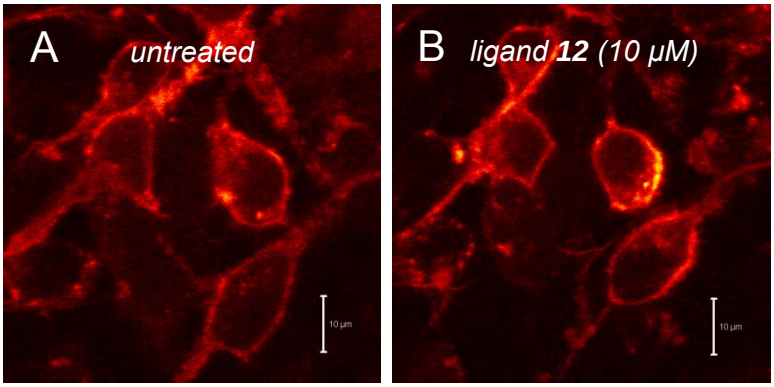

Fig. 6.3.15. *Effect of **12** on the internalization of the hH_2R-mKate2 in CHO cells. Confocal images were acquired before (A) and 100 min (B) after addition of 10 µM of compound **12**. Plan Apochromat 63x/1.4 oil, HeNe 543 (90%), HFT UV/488/543/633, NFT 545, LP 650, pinhole <1.5 µm (1.6 a.u.).*

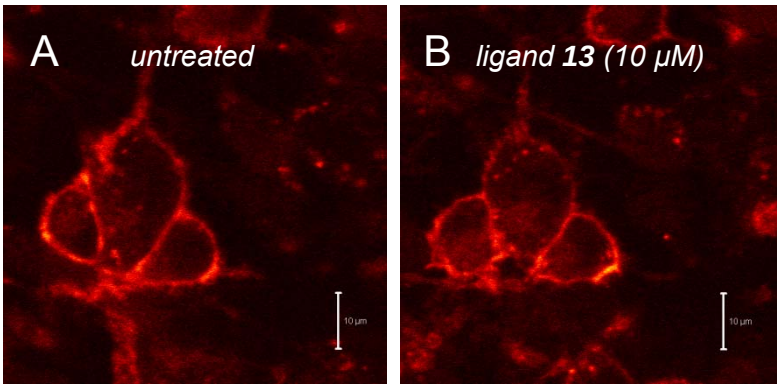

Fig. 6.3.16. *Influence of **13** on the internalization of the hH_2R-mKate2 in CHO cells. Confocal images were acquired before (A) and 90 min (B) after addition of 10 µM of compound **13**. Plan Apochromat 63x/1.4 oil, HeNe 543 (90%), HFT UV/488/543/633, NFT 545, LP 650, pinhole <1.5 µm (1.6 a.u.).*

Table 6.3.1. *Comparison of the effects of the bivalent H_2R ligands observed in GTPase assays ([a]Kraus, 2007; Birnkammer et al., 2010) and [b]confocal microscopy.*

Observed effects	Ligands 4 and 5	Ligands 12 and13
G-protein activation	yes[a]	no[a]
Receptor internalization	yes[b]	no[b]
Putative bias	**no**	**no**

In two independent experiments, the incubation with 10 µM of the bivalent ligand **12** (containing a 20-membered spacer) did not induce the H_2R internalization up to 90 min (Fig. 6.3.15), similar to the negative control (cf. Fig. 6.3.4). Also another bivalent compound **13** with a 20-carbon atom linker did not induce the internalization of the hH_2R-mKate2, when used at a concentration of 10 µM (Fig. 6.3.16). This was in line with the previously obtained functional data from GTPase assays, demonstrating antagonistic properties of these bivalent compounds (Table 6.3.1).

6.3.2.6 Ligand-specific conformations (functional selectivity) at the hH_2R

As described so far, at least in the case of the H_2R, binding experiments can be best explained by classical pharmacology, allowing a competitive interaction between one pharmacophore and a single independent binding site at the receptor (Baker, 2008; Kenakin, 2008). Baker demonstrated namely that affinities of standard H_2R antagonists are independent of the used agonists, providing a strong argument for the absence of multiple ligand-induced conformations at the hH_2R. However, this traditional concept, completed by the (extended) ternary complex model, cannot explain the aforementioned results, including the insensitivity of bivalent agonists **4** and **11** to GTPγS at the gpH_2R-$G_{s\alpha S}$ (chapter 4; Fig. 4.3.5 D and 4.3.17; cf. Kelley *et al.*, 2001; Xie *et al.*, 2006) as well as the slow changes of the Hill slope and altered kinetics of radioligand dissociation at Sf9 membranes, expressing both gpH_2R-$G_{s\alpha S}$ and hH_4R-GAIP + $G_{i\alpha 2}$ + $G_{\beta 1\gamma 2}$ (chapter 5).

To investigate if bivalent ligands bind to H_2Rs in a manner, postulated by classical pharmacology, additional functional studies (GTPase assays) were performed in our research group according to previously described procedures (Wenzel-Seifert *et al.*, 2001). The results were not consistent with those obtained previously by Baker (Baker, 2008), as K_b values of the tested H_2R antagonist depended strongly on the used agonist. Antagonistic activities of the monovalent (FAM, RAN, TIO, UR-DE257; Erdmann, 2010) and bivalent (**11**) compounds measured in presence of the bivalent agonist **4** at the hH_2R-$G_{s\alpha S}$ were significantly different from those assessed in presence of HIS (Table 6.3.2 and Fig. 6.3.17 A). Additionally, the detrimental effect of agonist **4** on the antagonistic activity was found at the gpH_2R-$G_{s\alpha S}$ for TIO and UR-DE257 (Table 6.3.2 and Fig. 6.3.17 B).

Indeed, such behaviour could be expected if each agonist induced/stabilized a unique receptor conformation. Ligands stabilizing distinct conformations would be able to bias the coupling of receptors to different protein effectors (Kenakin and Miller, 2010). Nevertheless, the action of compound **4** might be only an exception as two other bivalent H_2R agonists, compound **8** (containing a 2-amino-4-methylthiazole and a 2-aminothiazole ring with an octamethylene linker) and compound **11** (symmetric, imidazole-type, with a 20-membered linker), behaved as predicted by the classical model.

Table 6.3.2. *Antagonistic activities (pK_b ± SEM) of different H_2R ligands at hH_2R-$G_{s\alpha S}$ and gpH_2R-$G_{s\alpha S}$ fusion proteins as determined in GTPase assays in the presence of HIS and the bivalent agonists. The bivalent ligand **11** was an agonist at the gpH_2R-$G_{s\alpha S}$, but it turned out to be an antagonist at the hH_2R-$G_{s\alpha S}$ (Birnkammer et al., 2010). K_b values (mean ± SEM of N independent experiments preformed in duplicate) were calculated from IC_{50} values using the Cheng-Prusoff equation (Cheng and Prusoff, 1973) and compared using one-way ANOVA analysis – Dunnett's multiple comparison test (for 3 or more unmatched data sets) or unpaired t test (for 2 unmatched sets of measurements; Motulsky and Christopoulos, 2004). [a]The pK_b value for RAN at the hH_2R-$G_{s\alpha S}$ was from previous studies (Preuss et al., 2007).*

pK_b at hH_2R-$G_{s\alpha S}$					
Antagonist	**HIS**	**N**	**Agonist 4**	**N**	**Diff. significant**
FAM	6.83 ± 0.03	3	4.70 ± 0.21	4	yes (P<0.0001)
RAN	6.08 ± 0.03[a]	3	3.81 ± 0.22	3	yes (P=0.0006)
TIO	6.56 ± 0.04	4	4.57 ± 0.13	4	yes (P<0.0001)
Ligand 11	6.63 ± 0.02	3	6.00 ± 0.08	4	yes (P=0.0012)
UR-DE257	7.49 ± 0.03	3	4.92 ± 0.47	2	yes (P=0.0052)

pK_b at gpH_2R-$G_{s\alpha S}$							
Antagonist	**HIS**	**N**	**Agonist 4**	**N**	**Agonist 11**	**N**	**Diff. signific.**
FAM	7.22 ± 0.07	3	6.35 ± 0.77	4	6.91 ± 0.10	3	no
RAN	5.82 ± 0.02	3	5.63 ± 0.53	3	5.44 ± 0.03	3	no
TIO	6.90 ± 0.09	3	3.43 ± 0.48	2	-	-	yes (P=0.0027)
UR-DE257	7.34 ± 0.04	3	4.35	1	6.84	1	-

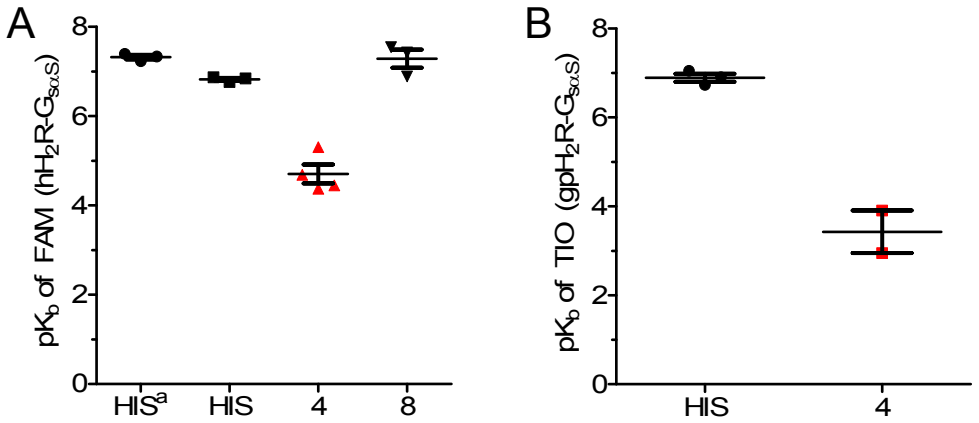

Fig. 6.3.17. *Antagonistic activities (pK_b) of: (A) FAM at hH_2R-$G_{s\alpha S}$ and (B) TIO at gpH_2R-$G_{s\alpha S}$ fusion proteins as determined in GTPase assays in the presence of different H_2R agonists (HIS and the bivalent agonists **4** and **8**), indicated on the abscissa. K_b values were calculated from IC_{50} values using the Cheng-Prusoff equation. The values for FAM (HIS^a) were from Preuss et al., 2007. The pK_b values obtained in presence of different agonists were compared using (A) one-way ANOVA analysis – Dunnett's multiple comparison test (HIS^a used as control) or (B) unpaired t test. Only the differences found for the bivalent agonist **4** (in red) are significant (P<0.05 and P=0.0027, respectively).*

6.3.3 Subcellular localization of the internalized hH_2R-mKate2

6.3.3.1 Spectral interference of the LysoTracker Green

In order to identify the subcellular compartment containing the internalized hH_2R, the CHO-hH_2R-mKate2 cells were incubated with the green fluorescent dye LysoTracker Green, staining preferably lysosomes. The untransfected CHO-K1 cells were used as negative controls. It was assumed that the *colocalization* of the both used fluorophores indicated the *lysosomal pathway* of the hH_2R-mKate2 fusion proteins undergoing agonist-induced internalization (cf. LysoTracker Red; Osawa *et al.*, 2005). However, detectable far-red emission was found already for the wild type CHO-K1 cells stained with the LysoTracker Green (Fig. 6.3.18 A), although spectral properties of this dye (cf. Fig. 6.2.9) should exclude both the excitation with a 543 nm line and the detection with a LP 650 filter set. Spectral interference (pretending a colocalization) appeared, although the concentration of the LysoTracker Green was reduced to 25 nM and the incubation time was shortened to 15 min to avoid problems by over-staining (cf. manufacturer's recommendation: incubation with 50–75 nM of the dye for 30-120 min).

The CHO-K1 cells stained with LysoTracker Green revealed a weak but still detectable signal in the far-red channel, pretending a colocalization (Fig. 6.3.18 A). This resulted from the *spectral bleed through* of the green dye. As expected, no colocalization was detected by the unstained CHO-K1 (Fig. 6.3.18 B) and CHO-hH_2R-mKate2 (Fig. 6.3.19 C) cells, used as negative controls.

Theoretically, multi-tracking should provide complete separation of signals in case of *emission cross-talk*, where emission signals of fluorescent dyes overlap, but excitation spectra differ. Also *excitation cross-talk* (simultaneous excitation of a few dyes by the same laser line without overlapping emission spectra) could be simply avoided by the acquisition of signals in separate PMT channels (course materials, Carl Zeiss, 2005). Unfortunately, all these precautions taken to avoid spectral interference were not helpful in case of the samples stained with the LysoTracker Green. Probably, the reason of this phenomenon was a strong excitation (90% transmission of a HeNe laser), used due to a very weak fluorescence signal of the membranally expressed hH_2R-mKate2 fusion protein. This could also explain a relatively high level of the autofluorescence of CHO-K1 cells in the far-red channel (not shown). The found spectral interference would lead to false positive results in case of the CHO-hH_2R-mKate2 cells stained with the LysoTracker Green, when analyzing the images with the colocalization facility of the LSM 510 software.

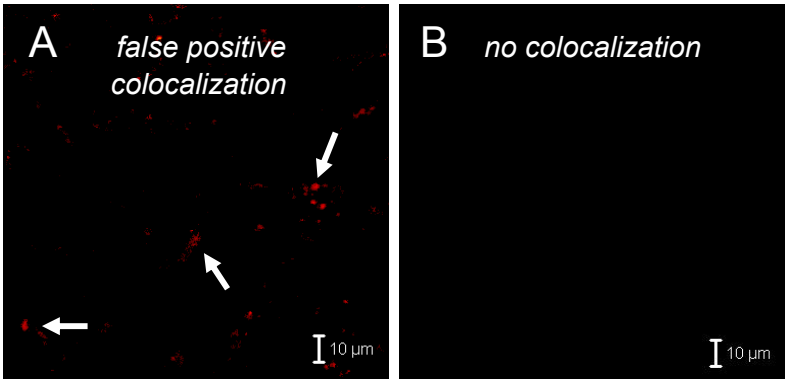

Fig. 6.3.18. *Colocalized images of the CHO-K1 wild-type cells: (A) a weak signal pretending colocalization in the cells stained with 25 nM of the LysoTracker Green. Arrows indicate the lysosomes. (B) No colocalization could be observed in the unstained cells. Images were acquired in the far-red (90% HeNe 543, HFT488/UV/488/543/633, NFT 545, LP 650) and the LysoTracker Green channel (5% Ar 488, HFT488, BP 505-530) and colocalized using Zeiss microscope software. Plan Apochromat 63x/1.4 oil, pinhole <1.6 µm (1.5 a.u.).*

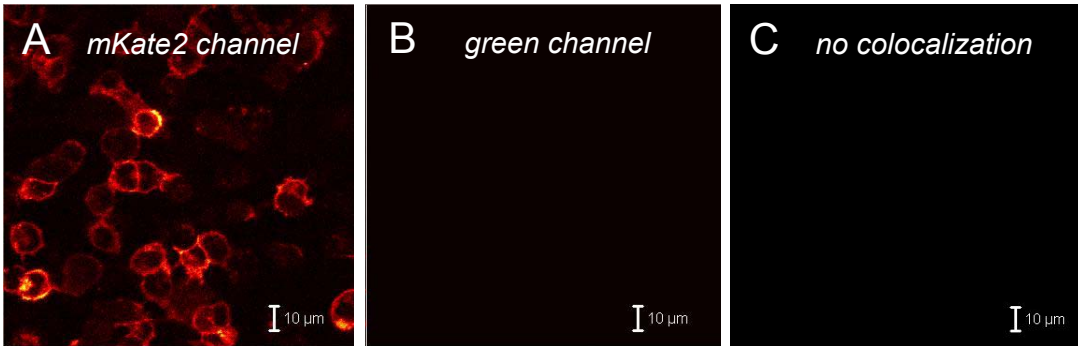

Fig. 6.3.19. *CHO-hH_2R-mKate2 cells (multi-track, glow scale): (A) fluorescence in the mKate2 channel (90% HeNe 543, HFT488/UV/488/543/633, NFT 545, LP 650), (B) lacking fluorescence emission in the LysoTracker Green channel (5% Ar 488, HFT488, BP 505-530). (C) No colocalization could be observed. Plan Apochromat 63x/1.4 oil, pinhole <1.6 µm (1.5 a.u.).*

In order to solve the problem with the spectral interference of the LysoTracker Green (*combined excitation and emission cross-talk*), prior to the colocalization, confocal images had to be processed using *emission fingerprinting* and *linear unmixing* (cross-talk removal by automatic component extraction). As these facilities of the LSM 510 software required the acquisition of images in the *lambda mode* (course materials, Carl Zeiss, 2005), emission spectra of the stained and unstained CHO-K1 and CHO-hH_2R-mKate2 cells were collected with a META detector (involving a 543 nm excitation line of a HeNe laser, exactly as used in the multi-track mode). However, green fluorescence signals collected by the META detector had lower intensities than in case of a usual PMT and the used excitation wavelength (543 nm) was distant from the excitation maximum of the green fluorescent dye (cf. Fig. 6.2.9). These both factors resulted in a merely detectable emission spectrum of the CHO-K1 cells stained with the LysoTracker Green (Fig. 6.3.20 C). For comparison, the spectrum of the same sample collected by the META detector at a 488 nm excitation line (as the green channel in the multi-tracking mode) using a 499-

585 nm band-pass filter for the detection is shown in Fig. 6.3.20 B. Also the mKate2 signal collected by the META detector was very weak, even when excited with a 100% laser transmission (Fig. 6.3.21).

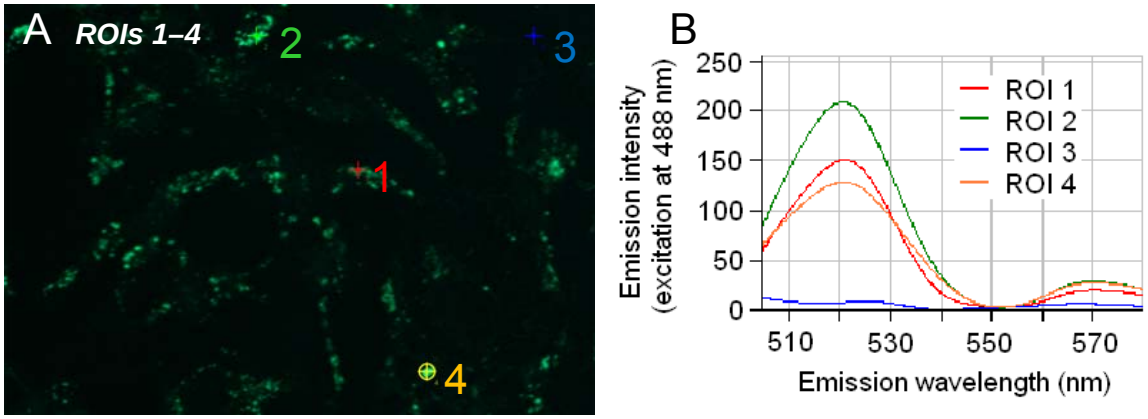

Fig. 6.3.20. *Images and spectra collected with a META detector. (A) Overlaid series of confocal images of the CHO-K1 cells stained with 25 nM of the LysoTracker Green, acquired by the excitation with a 488 nm line (7%) of an Ar laser. The image ROIs: 1 (red), 2 (green) and 4 (yellow) included lysosomes, whereas ROI 3 (blue) was the background and (B) the corresponding emission spectra. (C) Emission spectra (LP 650) of the same green-labelled CHO-K1 cells and the unlabelled CHO-K1 cells (autofluorescence), collected using a 543 nm excitation line (90%) of a HeNe laser. Plan Apochromat 63x/1.4 oil, HFT UV/488/543/633, pinhole 1.6 a.u.*

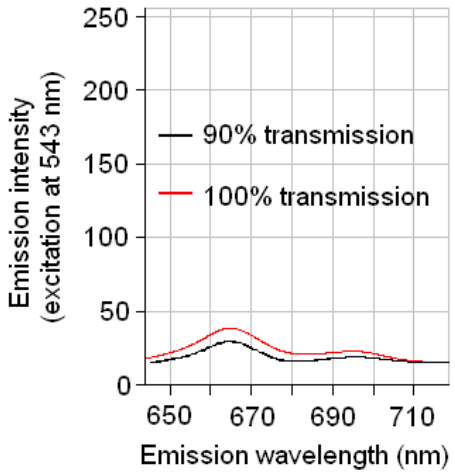

Fig. 6.3.21. *Far-red emission spectra of the CHO-hH_2R-mKate2 cells labelled with 25 nM of the LysoTracker Green, collected with a META detector: (A) 543 nm excitation line (90%) of a HeNe laser, pinhole 1.6 a.u. (as used in Fig. 6.3.20 A); (B) the same cells at 100% transmission of the HeNe laser, pinhole 3 a.u. Plan Apochromat 63x/1.4 oil, HFT UV/488/543/633.*

Low sensitivity of the META detector (excitation at a 543 nm) precluded separation of the interfering signal of the LysoTracker Green (Fig. 6.3.20 C and 6.3.21). Thus, the analysis of subcellular localization of the internalized H_2Rs could not be done by the colocalization facility of the LSM 510 software.

6.3.3.2 Subcellular localization of hH_2Rs in the double-staining specimens

The CHO-hH_2R-mKate2 cells were stained with 25–50 nM of the LysoTracker Green for the visualization of lysosomes and incubated with different agonists. Before addition of ligands, hH_2Rs tagged with the mKate2 were located mostly in the cell membranes, whereas the green labelled lysosomes were in the cytosol (Fig. 6.3.22 as well as Fig. 6.3.23 A and C).

Within 90 min of incubation with 100 µM HIS, the fluorescently labelled H_2 receptors were translocated from the membranes (Fig. 6.3.22) to the perinuclear region of the cells (cf. Fig. 6.3.6), but still no overlapping with the lysosomes could be detected (Fig. 6.3.23 B). Similar results were obtained for the bivalent agonist **4** as shown in Fig. 6.3.25 B (cf. Fig. 6.3.12). This supported the previous findings that upon a short exposure to an H_2R agonist the receptors undergo the rapid internalization, but not the trafficking to lysosomes for enzymatic degradation (Osawa *et al.*, 2005).

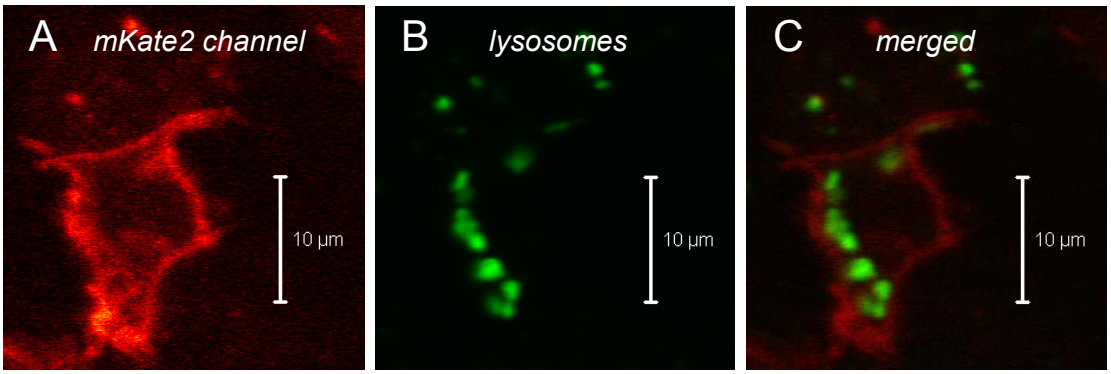

Fig. 6.3.22. *Subcellular localization of the fluorescently labelled H_2Rs (red) and the lysosomes stained with 25 nM LysoTracker Green in the non-stimulated CHO-hH_2R-mKate2 cells. Confocal images in a multi-track scanning mode: (A) fluorescence emission in the mKate2 channel (90% HeNe 543, HFT488/UV/488/543/633, NFT 545, LP 650), (B) fluorescence emission in the Lyso-Tracker Green channel (5% Ar 488, HFT488, BP 505-530), (C) merged images. Plan Apochromat 63x/1.4 oil, pinhole <1.6 µm (1.5 a.u.).*

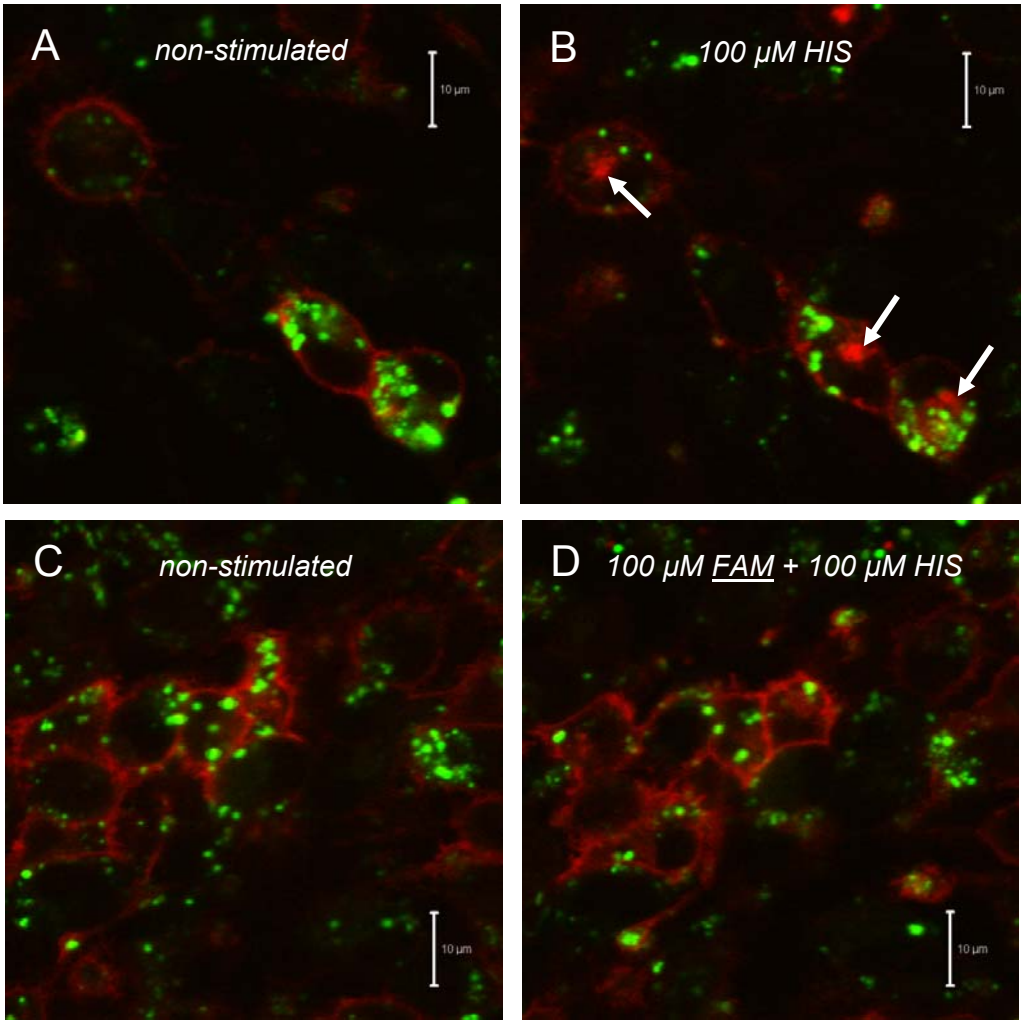

Fig. 6.3.23. *HIS-induced H_2R internalization in the CHO-hH_2R-mKate2 cells labelled with 50 nM LysoTracker Green. The cells in panel D were preincubated for 15 min with 100 µM FAM. Confocal images were acquired before (A and C) and 90 min (B and D) after addition of 100 µM HIS. Arrows indicate the perinuclear localization of the internalized hH_2R-mKate2 fusion proteins. Merged confocal images acquired in a multi-track scanning mode: the mKate2 channel (90% HeNe 543, HFT488/UV/488/543/633, NFT 545, LP 650), the LysoTracker Green channel (5% Ar 488, HFT488, BP 505-530). Plan Apochromat 63x/1.4 oil, pinhole <1.6 µm (1.5 a.u.).*

6.3.3.3 Inhibition of the hH_2R endocytosis

Receptor redistribution in the CHO-hH_2R-mKate2 cells was shown to be agonist-induced (upon 60-90 min of incubation). In order to learn more about this process, the single- and double-stained living cells were preincubated with an inhibitor of the receptor internalization, the plant lectin concanavalin A (Con A). The lectin is known to block extracellularly the *clathrin-mediated receptor endocytosis* by binding to cell membrane glycoproteins. At the same time it does not impede the G-protein-dependent signal transduction, as reported e.g. for the β_2-adrenergic (Wang and Liu, 2003) and angiotensin II receptor AT_1 (Tang *et al.*, 2000).

As shown in Fig. 6.3.24 C–D, the agonist-promoted receptor endocytosis was inhibited by Con A (250 µg/mL), as the hH_2R-mKate2 fusion proteins were found in the cell membranes still after 2.5 hours of incubation with 10 µM HIS. Similar results were obtained also for 2 µM of the bivalent agonist **4** (Fig. 6.3.25 C–D), indicating receptor internalization *via* clathrin-coated pits for both monovalent and bivalent H_2R agonists.

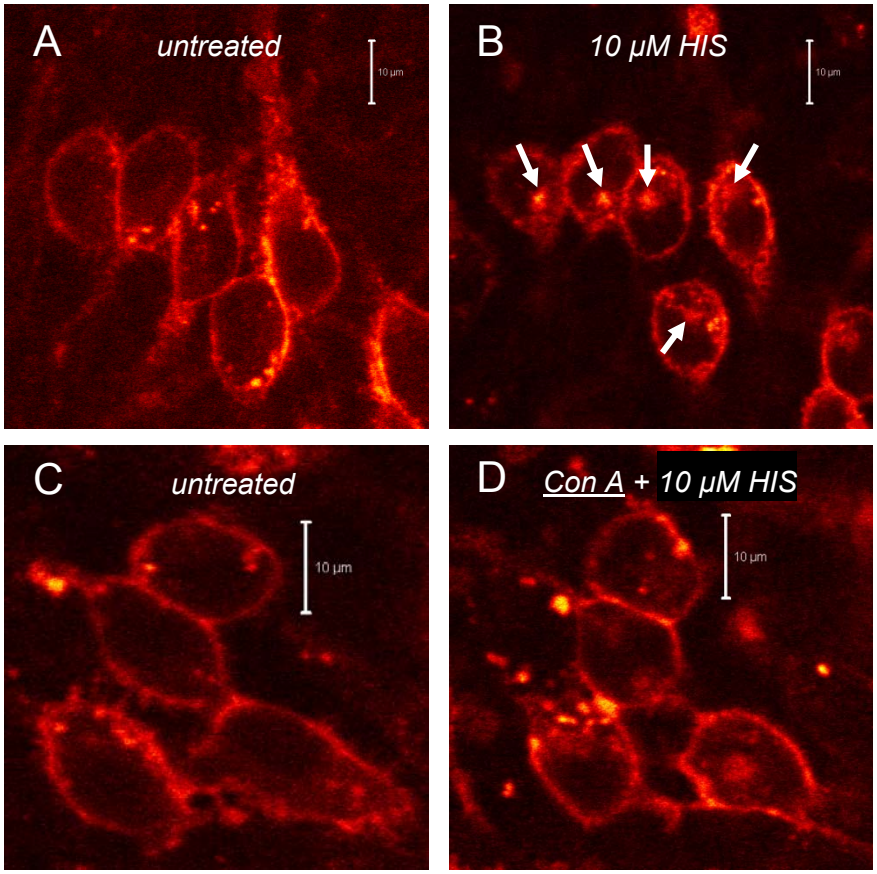

Fig. 6.3.24. *HIS-induced H_2R internalization in the CHO-hH_2R-mKate2 cells. The cells in panel D were preincubated for 30 min with 250 µg/mL Con A. Confocal images were acquired before (A and C) and 100 min (B and D) after addition of 10 µM HIS. Arrows indicate the perinuclear localization of internalized hH_2R-mKate2 fusion proteins. Plan Apochromat 63x/1.4 oil, 90% HeNe 543, HFT488/UV/488/543/633, NFT 545, LP 650, pinhole <1.6 µm (1.5 a.u.).*

The observed inhibitory effect of Con A on receptor endocytosis confirmed previous findings, suggesting that the H_2R belongs to class A GPCRs (in terms of internalization). This means that, upon agonist stimulation, receptors are internalized *via clathrin-coated pits* (cf. Fig. 1.1.7) and then, in the absence of agonists, rapidly recycled to the cell membrane (Fernandez *et al.*, 2008). Additionally, the endocytosis of the H_2R should be at least partially *dynamin-dependent* (Xu *et al.*, 2008).

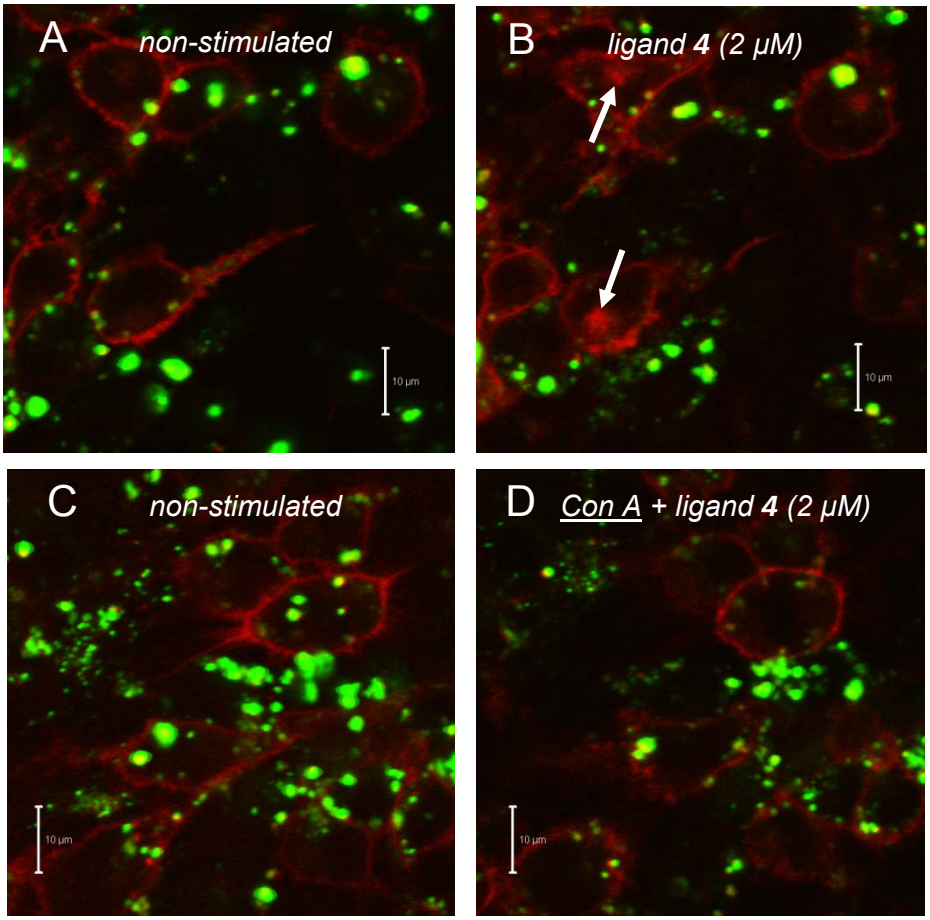

Fig. 6.3.25. *Agonist-induced H_2R internalization in the CHO-hH_2R-mKate2 cells labelled with 50 nM of LysoTracker Green. The cells in panel D were preincubated for 30 min with 250 µg/mL Con A. Confocal images were acquired before (A and C) and 60 min (B and D) after addition of 2 µM of the bivalent ligand* ***4****. Arrows indicate the perinuclear localization of internalized hH_2R-mKate2 fusion proteins. Merged confocal images acquired in a multi-track scanning mode: fluorescence emission in the mKate2 channel (90% HeNe 543, HFT488/UV/488/543/633, NFT 545, LP 650), fluorescence emission in the LysoTracker Green channel (5% Ar 488, HFT488, BP 505-530). Plan Apochromat 63x/1.4 oil, pinhole <1.6 µm (1.5 a.u.).*

6.4 Summary and conclusion

The H_4R antagonist JNJ7777120 (with respect to G-protein stimulation) was reported to induce the recruitment of β-arrestins in a G-protein-independent manner (Rosethorne and Charlton, 2011; Seifert *et al.*, 2011). As reported by Smit and colleagues, two distinct pathways for the down-regulation of the H_2R (*G-protein-dependent* and *G-protein-independent*) were found in the transfected CHO cells (Smit *et al.*, 1996 a), indicating a second, *cAMP-independent* mechanism of the agonist-induced H_2R translocation. This raised the question, if functional selectivity might also occur at H_2R. However, such investigations are not routine for the H_2R so far due to the lack of both appropriated assays and reference ligands. This prompted us to explore the H_2R internalization in the presence of structurally diverse agonists using genetically engineered fluorescent hH_2R fusion protein expressing CHO cells. The results of the confocal microscopy were consistent with the following conclusions:

1) The hH_2R was successfully subcloned into the pmKate2-N vector, encoding the monomeric far-red fluorescent protein mKate2 (Shcherbo *et al.*, 2009), and stably expressed in CHO cells. In contrast to the CHO cells expressing both the hH_2R and the mKate2 separately (Fig. 6.3.2), the far-red fluorescence signal of the hH_2R-mKate2 fusion protein was detected in the cell membranes (Fig. 6.3.1). Additionally, the membranal localisation of the H_2R was confirmed by using a selective fluorescent H_2R antagonist (Erdmann, 2010) as shown in Fig. 6.3.3.
2) The incubation with monovalent H_2R agonists (HIS, DIM and ARP, but not the monovalent ligand **1**) led to the fast internalization of the hH_2R-mKate2 (Fig. 6.3.6–10), as expected (Osawa *et al.*, 2005). For the first time, it was possible to visualize the intracellular fate of receptors after exposure to the bivalent H_2R ligands. As listed in Table 6.3.1, the bivalent H_2R agonists **4** and **5** with 8-membered linkers induced endocytosis (Fig. 6.3.12–13), whereas the bivalent H_2R antagonists **12** and **13** with 20-membered linkers had no influence on the receptor internalization (Fig. 6.3.15–16), hence being in line with the previous results on H_2R agonism, e.g. from steady-state GTPase assays on hH_2R-$G_{s\alpha S}$ fusion proteins expressed in Sf9 cells (Birnkammer *et al.*, 2010). However, it should be noted that microscopic imaging of the CHO cells expressing mKate-tagged H_2Rs could be carried out only within the first 90 min of incubation, because of the subsequent ligand-independent redistribution of receptors (Fig. 6.3.4–5).

3) Due to the weak spectral bleed through between the lysosomal fluorescent dye LysoTracker Green and the far-red florescence emission channel (Fig. 6.3.18 A), colocalization studies on the CHO-hH2R-mKate2 cells were discontinued. Nonetheless, confocal imaging of the agonist-induced H_2R internalization (Fig. 6.3.23–25) supported previous finding that these receptors do not undergo the lysosomal degradation pathway after short exposure to an agonist (Osawa *et al.*, 2005). In doing so, the receptor internalization pattern in the presence of the bivalent H_2R agonists was very similar to that in the presence of HIS. The preincubation with an inhibitor of the clathrin-mediated receptor internalization, concanavalin A resulted in the complete blockage of the agonist-induced endocytosis of the hH_2R-mKate2 fusion protein (Fig. 6.3.24–25). This finding confirmed that mono- and bivalent H_2R agonists release the receptor internalization *via* clathrin-coated pits.

Confocal microscopy studies on the living CHO cells, expressing the hH_2R fused to the monomeric far-red fluorescent protein mKate2 (Shcherbo *et al.*, 2009), revealed that both mono- and bivalent H_2R agonists (with respect to G-protein activation) induced clathrin-mediated receptor internalization (Fig. 6.3.6–10 and 6.3.12–13). Moreover, bivalent ligands known to be neutral antagonists in steady-state GTPase assays on hH_2R-$G_{s\alpha S}$ fusion proteins (Birnkammer *et al.*, 2010) did not influence the endocytosis of hH_2Rs (Fig. 6.3. 15–16). It is important to emphasize that the observation of hH_2R-mKate2 internalization does not enable the (quantitative) determination of ligand efficacy for β-arrestin-mediated signalling. Additionally, it is still the mater of debate if the same receptor conformations, resulting in β-arrestin-dependent signalling, also lead to desensitization of receptors (Rajagopal *et al.*, 2010). Nevertheless, in consideration of the results from systems with different read-outs (Table 6.3.1; receptor internalization requires β-arrestin, whereas the measurement of GTPase activity is limited to the receptor-dependent G protein activation), there is no hint to unconventional (biased) signalling of the hH_2R in the presence of the investigated ligands. Future work in this field should be focused on the development of assays for direct quantification of β-arrestin-mediated signalling at the H_2R and the H_2R. Additionally, a Schild plot analysis should be performed to examine if the bivalent ligands bind competitively and to uncover possible non-equilibrium steady states (Kenakin, 2006).

6.5 References

Baker JG: A study of antagonist affinities for the human histamine H_2 receptor, *Br J Pharmacol*, **2008**, *153*, 1011–1021.

Birnkammer T *et al.*: Bivalent acylguanidine-type ligands as potent and selective histamine H_2 receptor agonists, *Drugs Fut*, **2008**, *33* (Suppl. A), 127-128 (P205).

Birnkammer T *et al.*: Structure-activity relationships of bivalent acylguanidine-type histamine H_2 receptor agonists, *5th Summer School "Medicinal Chemistry"*, University of Regensburg, **2010**, P4 (poster contribution).

Carl Zeiss (course materials): Multi FL Imaging and Quantitative Colocalization, Jena, May **2005**.

Cheng Y-C and Prusoff WH: Relationship between the inhibition constant (K_i) and the concentration of inhibitor which causes 50 per cent inhibition (IC_{50}) of an enzymatic reaction, *Biochem Pharmacol*, **1973**, *22*, 3099–3108.

Erdmann D: Histamine H_2 and H_3 receptor antagonists: Synthesis and characterization of radiolabelled and fluorescent pharmacological tools: Doctoral thesis, University of Regensburg, **2010**.

Fernandez N *et al.*: Histamine H_2 receptor trafficking: Role of arrestin, dynamin and clathrin in histamine H_2 receptor internalization, *Mol Pharmacol*, **2008**, *74*, 1109–1118.

Gross D: New approaches to the chemotherapy of glioblastoma: investigations on doxorubicin nanoparticles, inhibition of PDGF receptors and kinesin Eg5, with emphasis on confocal laser-scanning microscopy, Doctoral thesis, University of Regensburg, **2006**.

Kelley MT *et al.*: Distinct interaction of human and guinea pig histamine H_2-receptor with guanidine-type agonists, *Mol Pharmacol*, **2001**, *60*, 1210–1225.

Kenakin T and Miller LJ: Seven transmembrane receptors as shapeshifting proteins: The impact of allosteric modulation and functional selectivity on new drug discovery, *Pharmacol Rev*, **2010**, *62*, 265–304.

Kenakin T: What systems can and can't do, *Br J Pharmacol*, **2008**, *153*, 841–843.

Kenakin TP: A pharmacology primer: Theory, application, and methods, *Academic Press – Elsevier*, Amsterdam – Tokyo, **2006**.

Kraus A *et al.*: N^G-acylated aminothiazolylpropylguanidines as potent and selective histamine H_2 receptor agonists, *ChemMedChem*, **2009**, *4*, 232-240.

Kraus A: Highly potent, selective acylguanidine-type histamine H_2 receptor agonists: Synthesis and structure-activity relationships, Doctoral thesis, University of Regensburg, **2007**.

Kühnle M: Experimental therapy and detection of glioblastoma: investigation of nanoparticles, ABCG2 modulators and optical imaging of intracerebral xenografts, Doctoral thesis, University of Regensburg, **2010**.

Legnazzi BL *et al.*: Rapid desensitization and slow recovery of the cyclic AMP response mediated by histamine H_2 receptors in the U937 cell line, *Biochem Pharmacol*, **2000**, *60*, 159–166.

Leurs R *et al.*: Pharmacological characterization of the human histamine H_2 receptor stably expressed in Chinese hamster ovary cells, *Br J Pharmacol*, **1994**, *112*, 847-854.

Li L *et al.*: Synthesis and pharmacological activity of fluorescent histamine H_2 receptor antagonists related to potentidine, *Bioorg Med Chem Lett*, **2003**, *13*, 1717–1720.

Monczor F *et al.*: Tiotidine, a histamine H_2 receptor inverse agonist that binds with high affinity to an inactive G-protein–coupled form of the receptor: Experimental support for the cubic ternary complex model, *Mol Pharmacol,* **2003**, *64*, 512–520.

Mosandl J: Radiochemical and luminescence-based binding and functional assays for human histamine receptors using genetically engineered cells, Doctoral thesis, University of Regensburg, **2009**.

Motulsky HJ and Christopoulos A: Fitting models to biological data using linear and non-linear regression: A practical guide to curve fitting, *GraphPad Software/Oxford University Press*, New York, **2004**.

Mülhardt C: Der Experimentator: Molekularbiologie/Genomics, *Spektrum Akademischer Verlag*, Heidelberg, **2009**.

Osawa S *et al.*: Alteration of intracellular histamine H_2 receptor cycling precedes antagonist-induced upregulation, *Am J Physiol Gastrointest Liver Physiol*, **2005**, *289*, G880-G889.

Preuss H *et al.*: Mutations of Cys-17 and Ala-271 in the human histamine H_2 receptor determine the species selectivity of guanidine-type agonists and increase constitutive activity, *J Pharmacol Exp Ther*, **2007**, *321*, 975–982.

Rajagopal S *et al.*: Teaching old receptors new tricks: biasing seven-transmembrane receptors (review), *Nat Rev Drug Discov*, **2010**, *9*, 373-386.

Rosethorne EM and Charlton SJ: Agonist-biased signalling at the histamine H_4 receptor: JNJ7777120 recruits beta-arrestin without activating G proteins, *Mol Pharmacol*, **2011**, *79*, 749-757.

Schneider E: Development of fluorescence-based methods for the determination of ligand affinity, selectivity and activity at G-protein coupled receptors, Doctoral thesis, University of Regensburg, **2005**.

Seifert R *et al.*: Paradoxical stimulatory effects of the “standard” histamine H_4-receptor antagonist JNJ7777120: The H_4-receptor joins the club of 7TM receptors exhibiting functional selectivity, *Mol Pharmacol*, **2011**, *79*, 631–638.

Shcherbo D *et al.*: Far-red fluorescent tags for protein imaging in living tissues, *Biochem J*, **2009**, *418*, 567–574.

Smit MJ *et al.* (a): Two distinct pathways for histamine H_2 receptor down-regulation: H_2 Leu^{124} → Ala receptor mutant provides evidence for a cAMP-independent action of H_2 agonists, *J Biol Chem*, **1996**, *271*, 7574-7582.

Smit MJ *et al.* (b): Inverse agonism of histamine H_2 antagonists accounts for upregulation of spontaneously active histamine H_2 receptors, *Proc Natl Acad Sci USA*, **1996**, *93*, 6802-6807.

Tang H *et al.*: Inhibition of AT_1 receptor internalization by concanavalin A blocks angiotensin II-induced ERK activation in vascular smooth muscle cells, *J Biol Chem*, **2000**, *275*, 13420–13426.

Wang J and Liu XJ: A G protein-coupled receptor kinase induces *Xenopus* oocyte maturation. *J Biol Chem*, **2003**, *278*, 15809–15814.

Wenzel-Seifert K *et al.*: Similar apparent constitutive activity of human histamine H_2-receptor fused to long and short splice variants of $G_{s\alpha}$, *J Pharmacol Exp Ther*, **2001**, *299*, 1013-1020.

Xie Sh-X *et al.*: Probing ligand-specific histamine H_1- and H_2-receptor conformations with N^G-acylated imidazolylpropylguanidines, *J Pharmacol Exp Ther*, **2006**, *317*, 139–146.

Xu A-J *et al.*: Agonist-induced internalization of histamine H_2 receptor and activation of extracellular signal-regulated kinases are dynamin-dependent, *J Neurochem*, **2008**, *107*, 208–217.

Chapter 7

Summary

7 Summary

In the last three decades, a large amount of experimental data (for example Förster resonance energy transfer (FRET) at fluorescently labelled receptors) supported the hypothesis of the dimerization of G-protein-coupled receptors (GPCR), including neuropeptide Y (NPY Y_xR) and histamine (H_xR) receptors. Targeting GPCR dimers could be helpful to understand (patho)physiological processes and may be applied therapeutically.

This work aimed at the exploration of the applicability of FRET-based and ligand-based approaches to the investigation of NPY Y_1R and histamine H_2R dimers. Special attention was paid to bivalent N^G-acylated hetarylpropylguanidines, the most potent H_2R agonists, known so far, which were initially designed to bind to the orthosteric recognition sites of dimerized H_2R protomers. Surprisingly, agonists having octamethylene linkers, insufficient in length to bridge two adjacent receptor molecules, proved to be most active. Thus, the intent of this thesis was to investigate the assumed mode of binding of such "twin compounds", e.g. with respect to the ternary complex model, allosterism and functional selectivity.

Fluorescently labelled NPY Y_1 receptors

Human Y_1Rs, tagged either with enhanced cyan (ECFP) or with yellow fluorescent proteins (EYFP), were stably expressed in human U-373 MG glioblastoma cells (plasmids from Prof. Dr. A. Beck-Sickinger, University of Leipzig). Membranal localization of the labelled receptors was confirmed by radioligand and flow cytometric binding assays. However, imaging of the transfected U-373 MG and CHO cells by means of confocal microscopy (CLSM) revealed primarily intracellular distribution of the fusion proteins, precluding prospective FRET-based investigations of receptor dimerization. Additionally, bivalent argininamide-type Y_1R antagonists, developed in our group, did not support the hypothesis of receptor dimerization. Thus, all further work was focused on bivalent H_2R/H_4R ligands.

Hill slopes of bivalent H_2R/H_4R ligands

Radioligand binding assays were performed on Sf9 membranes, expressing either the human (h) or guinea-pig (gp) H_2R-$G_{s\alpha S}$ fusion protein or the hH_4R, because the imidazolylpropylguanidine moiety turned out to be a privileged structure with respect to histamine receptors (cooperation with Prof. Dr. Roland Seifert, Medical School of Hannover). Satu-

ration binding experiments confirmed that tiotidine is an inverse agonist of H_2R, and that fusing of the H_2Rs and $G_{s\alpha S}$ proteins did not alter ligand-receptor interactions. GTPγS-dependent shifts of the competition binding curves, predicted by the ternary complex model, were found for monovalent H_2R agonists, but not for the bivalent ligands, tested at the gpH_2R-$G_{s\alpha S}$, suggesting antagonism rather than agonism. Additionally, Hill coefficients (n_H) < 1 (negative cooperativity) observed for short bivalent compounds (gpH_2R-$G_{s\alpha S}$), as well as n_H > 1 (positive cooperativity) for the bivalent compound with a 20-membered linker, approximated unity after very long periods of incubation (gpH_2R-$G_{s\alpha S}$ and hH_4R), disclosing the failure of having reached equilibrium.

Radioligand off-rate (k_2)

Radioligand dissociation kinetics at the gpH_2R-$G_{s\alpha S}$ and the hH_4R (k_2 of [^{3}H]histamine at hH_4R: 0.0108 ± 0.0007 $min^{-1,}$ reported for the first time) revealed a concentration-dependent increase in k_2 in the presence of bivalent ligands. This could result from amphiphilic properties (for the “longer” bivalent compounds) or from an existence of the allosteric binding site either at the same protomer or at a neighboring receptor.

H_2R internalization

Clathrin-mediated receptor endocytosis was visualized in transfected CHO cells by confocal microscopy (CLSM). Both mono- and bivalent H_2R agonists, but not bivalent antagonists (with respect to G-protein activation), induced the internalization of human H_2Rs fused to the monomeric far-red fluorescent protein mKate2. These observations were in line with previously obtained functional data from GTPase assays, and there is no evidence for unconventional (biased) signalling of the hH_2R. By contrast, agonist-dependent activities of standard antagonists were found in GTPase assays at the hH_2R-$G_{s\alpha S}$ in presence of a bivalent agonist with an 8-membered linker.

In conclusion, the obtained results cannot be solely explained by the competitive binding model. Considering the size of the bivalent H_2R/H_4R ligands, additional temporary interactions with the extracellular domains of the receptors seem to be inevitable. Provided that the ortho- and the allosteric binding sites were occupied by two pharmacophoric moieties simultaneously, these bivalent compounds might act as true dualsteric ligands. Future work at the H_2R and the H_4R should be focused on the differentiation between G-protein-dependent and β-arrestin-mediated signalling. Additionally, the preparation of a bivalent radioligand is suggested to determine the ligand-receptor stoichiometry.

Ich erkläre hiermit an Eides statt, dass ich die vorliegende Arbeit ohne unzulässige Hilfe Dritter und ohne Benutzung anderer als der angegebenen Hilfsmittel angefertigt habe; die aus anderen Quellen direkt oder indirekt übernommenen Daten und Konzepte sind unter Angabe des Literaturzitats gekennzeichnet.

Regensburg,

Miroslaw Lopuch